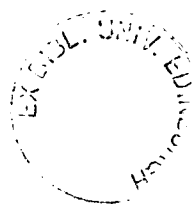


# A Lattice Study of Semi-Leptonic B Decay

Gary Douglas



**Doctor of Philosophy**  
The University of Edinburgh  
1999



To Mum, Dad, Craig, Ben and Susan

## Abstract

This thesis describes a lattice study of matrix elements relevant to the semi-leptonic decay of B mesons. The simulation was performed on two lattices, the first with a volume of  $16^3 \times 48$  at  $\beta = 6.0$  and the second with a volume of  $24^3 \times 48$  at  $\beta = 6.2$ . Both lattices employ an  $\mathcal{O}(a)$  non-perturbatively improved fermion action in the quenched approximation.

The thesis describes fully the theoretical tools required to analyse such a process on the lattice, in particular Lattice QCD and Heavy Quark Effective Theory.

The two form factors relevant to the decay  $\overline{B} \rightarrow D l \overline{\nu}$  are extracted using these theoretical tools and their dependence on the various kinematical quantities is studied.

The Isgur Wise function is obtained from the heavy quark limit of these form factors and its slope is extracted. From a comparison of this Isgur Wise function and the experimental analysis of the decay, the Cabibbo-Kobayashi-Maskawa matrix element  $V_{cb}$  is obtained.

# Declaration

This thesis has been wholly composed by me and presents work carried out as part of the UKQCD collaboration.

The calculation used previously generated gauge configurations and light quark propagators. The routines to generate the heavy-light two point functions and the three point functions was adapted from existing UKQCD code. The  $\beta = 6.2$  dataset was previously generated by UKQCD and the  $\beta = 6.0$  dataset was generated by me. The code used in the statistical analysis was developed from an existing set of basic routines.

The results presented in chapters 5 and 6 are to appear in

- The Isgur Wise function from the Lattice.  
(Talk presented at Lattice '99).  
hep-lat/9909126.  
Edinburgh Preprint 99/13.

Gary Douglas

# Acknowledgements

I would first of all like to thank my parents for their constant support throughout my seven years at University. I would not have been able complete my studies without their financial help.

I would like to thank Richard Kenway, Ken Bowler, David Richards and Laurent Lellouch for their advice, support and encouragement over the past three years. In particular I would like to thank Richard and Ken for their careful scrutiny of this thesis.

Thanks go to all the members of the PPT group, especially to Joyce with whom I shared an office and many laughs over the past three years.

Thanks also to all my friends outside JCMB (yes I have some!) Richard, Scott, Albert, Graeme and many others - you know who you are! Thanks guys for the great holiday in Aviemore!

Special thanks to Craig, not least for all the F1 sundays and games of 'Track and Field'. Finally, special thanks go to Susan for all her love and support and putting up with me while I wrote this thesis!

# Contents

<b>1</b>	<b>Introduction</b>	<b>1</b>
1.1	Overview of QCD and Weak Physics	2
1.1.1	Weak Lagrangian	3
1.1.2	The CKM matrix	7
1.1.3	Weak Matrix Elements	11
<b>2</b>	<b>Lattice QCD</b>	<b>12</b>
2.1	Lattice Formulation	13
2.1.1	Gauge Invariance	15
2.1.2	Lattice Gauge Action	16
2.2	Lattice Fermionic actions	17
2.2.1	Naive Fermions	18
2.2.2	Fermion Doubling	18
2.2.3	Wilson Fermions	20
2.3	Improved Fermion Actions	23
2.3.1	Sheikholeslami-Wohlert Action	24
2.3.2	Non-Perturbative Improvement	24
2.4	Numerical Simulation	27
2.4.1	Partition Function for Lattice QCD	27
2.4.2	Grassmann Algebra	29
2.4.3	Numerical Techniques	31
2.5	Finite Size Effects	33
<b>3</b>	<b>Heavy Quark Effective Field Theory</b>	<b>34</b>
3.1	Heavy Quark Symmetry	34
3.2	Heavy Quark Effective Theory	36
3.3	Series Expansion in $\frac{1}{m_Q}$	39
3.4	Renormalisation	41
3.5	Mesonic Form Factors	42
3.6	The Isgur Wise function	45

<b>4</b>	<b>Lattice Correlation Functions</b>	<b>50</b>
4.1	Interpolating Operators	50
4.2	Two Point Functions	51
4.2.1	Mesonic Observables	52
4.3	Three Point Functions	53
4.3.1	Extended Propagator	55
4.3.2	Explicit time dependence	56
4.4	Smearing	57
4.4.1	Jacobi Smearing	57
4.4.2	Fuzzing	58
4.4.3	Gauge Invariant Smearing for Heavy Quarks	58
4.5	Statistical Analysis	60
<b>5</b>	<b>Meson Spectrum</b>	<b>62</b>
5.1	Simulation Details	62
5.2	Meson Spectrum	62
5.2.1	Fit Procedure	64
5.3	Vector Mesons	65
5.4	Chiral Extrapolation	67
5.5	Strange extrapolation	70
5.6	Heavy-Light Mesons	72
<b>6</b>	<b>Semi-leptonic Decay <math>\bar{B} \rightarrow D l \bar{\nu}</math></b>	<b>78</b>
6.1	Isolating the weak matrix element	78
6.2	Lattice Details	79
6.2.1	Improved Vector Current	81
6.2.2	Extended Propagator Source	82
6.3	Calculation of $Z_{\text{eff}}^{\text{v}}$	82
6.3.1	Radiative Corrections	86
6.3.2	Lattice results for $Z_{\text{eff}}^{\text{v}}$	86
6.4	Calculation of Form Factors	87
6.4.1	Results for $h_-(\omega)$	91

6.4.2	Results for $h_+(\omega)$	92
6.5	Power Corrections	104
6.6	Lattice Isgur Wise functions	114
6.7	Spectator Quark Mass Dependence	120
6.7.1	Chiral Extrapolation	120
6.7.2	Interpolation to Strange Quark Mass	121
6.8	Extracting $\rho^2$	121
6.8.1	Systematic error	127
6.8.2	Discussion of results for $\rho^2$	128
6.9	Extracting $V_{cb}$	130
<b>7</b>	<b>Summary and Conclusions</b>	<b>134</b>
<b>A</b>	<b>Appendix – Radiative Corrections</b>	<b>136</b>
<b>B</b>	<b>Appendix – Meson Spectrum</b>	<b>140</b>
<b>C</b>	<b>Appendix – Form Factor Results</b>	<b>145</b>
	<b>References</b>	<b>170</b>

# Chapter 1

## Introduction

The Standard Model [1, 2, 3] is a remarkable construction which for the past 25 years has attempted to describe particle interactions in terms of three of the four fundamental forces of nature. It has survived countless tests of its validity from many experiments around the world. There are however some unsatisfactory aspects of this model. Crucially, gravity is not included in the framework of the Standard Model. Clearly any fundamental model governing high energy physics should describe and predict the effects of gravity [4]. There are also far too many free parameters in the Standard Model. These parameters are illustrated in table 1.1. The fact that these parameters are not calculable directly from this model and instead obtained indirectly from experiment is a clear indication that the Standard Model is some subset of a larger theory. Indeed tests of the Standard Model have focussed on the determination of these parameters in the search for a hint of this larger theory.

Amongst the most poorly determined parameters in the Standard Model are the weak mixing angles. These quantities correspond to the mixing of quark flavour from weak decay. However only the weak decays of hadrons are observed experimentally and so in order to establish a theoretical understanding of these decays it is necessary to concentrate on the long distance region of QCD.

Unlike QED where the effective coupling constant increases as the momentum scale increases, QCD exhibits asymptotic freedom as a consequence of the underlying non-Abelian group structure [5, 6] and thus as the quark separation

<b>Masses</b>	
6 quarks u d s c b t 2 gauge vector bosons $W^\pm Z^0$	6 leptons e $\mu$ $\tau$ $\nu_e$ $\nu_\mu$ $\nu_\tau$ Higgs Boson $H$
<b>Weak Sector</b>	
3 mixing angles $\theta_1$ $\theta_2$ $\theta_3$	CP violating phase $\delta$
<b>Coupling Constants</b>	
Strong $\alpha_s$ Fermi $G_F$	Fine structure $\alpha$

Table 1.1: The free parameters of the Standard Model. There is some evidence for more parameters, in particular from the recent discovery of massive neutrinos there will be mixing angles for leptons.

increases, so the coupling increases. Thus in order to probe large range physics at the hadron scale where the coupling constant is  $\mathcal{O}(1)$  a methodology other than perturbation theory is required. There are several such methods which deal with the non-perturbative aspects of QCD, most notably quark models, QCD sum rules and low energy effective theories [7]. It is Lattice QCD [8, 9, 10] however, which provides the only systematically improvable, model independent framework for exploring this low-energy sector.

## 1.1 Overview of QCD and Weak Physics

Although the Standard Model represents a coalescence of many complex aspects of high energy physics, the basic constituents of matter are surprisingly simple to classify. There exist two types of fundamental constituent, fermions and bosons. The (spin  $\frac{1}{2}$ ) fermions are the building blocks of matter and fall into two classifications. The *quarks* carry a fractional electric charge and are subject to the strong interaction whilst the *leptons* carry integral electric charge and are not subject to the strong interaction. Both leptons and quarks appear in three doublets or *generations*. The bosons are spin 1 particles and are responsible for the mediation of the forces in the Standard Model.

The Standard Model is based on a simple product of three groups,

$$SU(3) \otimes SU(2)_L \otimes U(1)_Y \quad (1.1)$$

where  $SU(3)$  corresponds to the (colour) symmetry group of strong interactions,  $SU(2)_L$  corresponds to the weak isospin group acting on left-handed fermions and  $U(1)_Y$  is the hypercharge group.

The QCD Lagrangian density is given by

$$L_{\text{QCD}} = -\frac{1}{4}F_{\mu\nu}^a F^{a\mu\nu} + \bar{\psi}[(i\partial_\mu + gA_\mu^a T^a)\gamma^\mu - m]\psi \quad (1.2)$$

where  $T^a$  is a traceless, hermitian  $3 \times 3$  matrix corresponding to the eight generators of  $SU(3)$  satisfying the properties

$$[T_x, T_y] = if_{xyz}T_z, \quad \text{Tr}[T_x T_y] = 2\delta^{xy} \quad (1.3)$$

with  $f_{xyz}$ , the structure constants, antisymmetric and real. The field strength tensor for the gauge sector (corresponding to the 8 vector fields  $A_\mu^a$ ) is given by

$$F_{\mu\nu}^a = \partial_\mu A_\nu^a - \partial_\nu A_\mu^a + gf^{abc}A_\mu^b A_\nu^c. \quad (1.4)$$

### 1.1.1 Weak Lagrangian

Weak decays can be described by the following Lagrangian

$$L = \frac{G_F}{\sqrt{2}} J_\mu^\dagger J^\mu \quad (1.5)$$

where the current  $J_\mu$  contains both a leptonic and hadronic part,

$$J_\mu^L = \bar{\psi}_e \gamma_\mu (1 - \gamma_5) \psi_{\nu_e} + \bar{\psi}_\mu \gamma_\mu (1 - \gamma_5) \psi_{\nu_\mu} + \dots \quad (1.6)$$

$$J_\mu^H = \bar{\psi}_u \gamma_\mu (1 - \gamma_5) \psi_d + \bar{\psi}_c \gamma_\mu (1 - \gamma_5) \psi_s + \dots \quad (1.7)$$

Given this structure for the weak interaction, it is prudent to distinguish between the handedness of the fermion fields. Decomposing the fields as

$$\psi = \psi_L + \psi_R \quad (1.8)$$

with

$$\psi_L = \frac{1}{2}(1 - \gamma_5)\psi \quad (1.9)$$

$$\psi_R = \frac{1}{2}(1 + \gamma_5)\psi \quad (1.10)$$

it is clear that, for massless fields, it is the left handed fermions alone which are susceptible to the weak interaction. For one generation of fermions the lepton part is

$$\psi_{e_L} = \begin{pmatrix} \nu_e \\ e_L \end{pmatrix}, \quad \psi_{e_R} = e_R, \quad (1.11)$$

and the quark part is

$$\psi_{q_L} = \begin{pmatrix} u_L \\ d_L \end{pmatrix}, \quad \psi_{q_R} = q_R. \quad (1.12)$$

In order to construct a weak Lagrangian it is necessary to impose  $SU(2)$  local gauge invariance on the left handed sector. The result of this condition is to introduce (as in the case of  $SU(3)$  gauge invariance) a set of gauge vector fields  $W_b^\mu$ , ( $b = 1, 2, 3$ ) with an  $SU(2)$  field strength defined through the tensor

$$F_b^{\mu\nu} = \partial^\mu W_b^\nu - \partial^\nu W_b^\mu + g\epsilon_{bcd}W_c^\mu W_d^\nu. \quad (1.13)$$

The familiar charged vector bosons are then defined to be linear combinations of the above gauge vector fields  $W_b^\mu$ ,

$$W^{+\mu} = \frac{1}{\sqrt{2}}(W_1^\mu - iW_2^\mu) \quad (1.14)$$

$$W^{-\mu} = \frac{1}{\sqrt{2}}(W_1^\mu + iW_2^\mu). \quad (1.15)$$

The application of the  $SU(2)_L$  gauge invariance leads to a conserved current  $J_3^\mu$ . The electromagnetic current  $J_e^\mu$  is also conserved. The hypercharge current is related to these two currents by,

$$J_Y^\mu = 2(J_e^\mu + J_3^\mu) \quad (1.16)$$

and is also therefore a conserved quantity. The corresponding hypercharge is then given by

$$Y = 2(Q - t_3) \quad (1.17)$$

where  $Q$  is the electromagnetic charge and  $t_3$ , one of the eigenvalue components of the weak isospin is  $+\frac{1}{2}$  for  $\nu_L$  and  $u_L$ ,  $-\frac{1}{2}$  for  $e_L$  and  $d_L$ , and zero for the right handed sector as discussed above.

The next stage in construction of a weak Lagrangian is to impose  $U(1)$  local gauge invariance. In doing so, another gauge boson  $B_\mu$ , the weak hypercharge gauge field, is introduced. This gauge field, unlike the isospin fields, couples to both left and right handed components. The fermionic Lagrangian is then given by the following form,

$$L_F^{\text{weak}} = i [\bar{\psi}_L \not{D} \psi_L + \bar{\psi}_R \not{D} \psi_R] \quad (1.18)$$

where the right hand covariant derivative is given by,

$$D_R^\mu = \partial^\mu - \frac{i}{2} g_Y Y B^\mu \quad (1.19)$$

and the left hand derivative is,

$$D_L^\mu = \partial^\mu - \frac{i}{2} g_Y Y B^\mu - \frac{i}{2} g \vec{\tau} \cdot \vec{W}^\mu. \quad (1.20)$$

Under this  $SU(2) \otimes U(1)$  model, the fermions, like the vector bosons are massless since a mass term would render the Lagrangian gauge dependent. The introduction of massive particles is realised through spontaneous symmetry breaking. In order to implement this mechanism, the Lagrangian has to be extended to

account for the scalar fields,

$$L \rightarrow L + L_{\text{scalar}} + L_{\text{Yukawa}}. \quad (1.21)$$

The physical vacuum may be defined by

$$\langle \Phi \rangle = \begin{pmatrix} 0 \\ \frac{\alpha}{\sqrt{2}} \end{pmatrix} \quad (1.22)$$

obtained from the minimisation of the potential

$$V(\Phi) = -\mu^2 \Phi^\dagger \Phi + \rho (\Phi^\dagger \Phi)^2 \quad (1.23)$$

so that

$$\alpha^2 = \frac{\mu^2}{\rho}. \quad (1.24)$$

Following the form of the left hand covariant derivative, the scalar Lagrangian is given by

$$L_{\text{scalar}} = \left| (\partial^\mu - \frac{i}{2} g_Y B^\mu - \frac{i}{2} g \vec{\tau} \cdot \vec{W}^\mu) \Phi \right|^2 - V(\Phi) \quad (1.25)$$

Working in terms of physical fields related to the unphysical ones through,

$$\begin{pmatrix} Z^\mu \\ A^\mu \end{pmatrix} = \begin{pmatrix} \cos \theta_W & -\sin \theta_W \\ \sin \theta_W & \cos \theta_W \end{pmatrix} \begin{pmatrix} W_3^\mu \\ B^\mu \end{pmatrix} \quad (1.26)$$

where  $\theta_W$  is the Weinberg weak mixing angle ( $g \sin \theta_W = g_Y \cos \theta_W = e$ ), the  $W^\pm$  bosons acquire a mass given by

$$M_W = \frac{e\alpha}{2 \sin \theta_W} \quad (1.27)$$

and the  $Z$  boson acquires a mass given by

$$M_Z = \frac{e\alpha}{\sin 2\theta_W} \quad (1.28)$$

Similarly by considering the Yukawa interaction and perturbations about the

vacuum the fermions can be shown to acquire mass.

### 1.1.2 The CKM matrix

It is found that the charged weak interactions discussed above are not diagonal in flavour space. There exists some mixing between the weak basis of the electroweak interaction and the physical mass basis.

The six flavours of quark may be neatly divided into two categories,

$$U = (u, c, t), \quad D = (d, s, b) \quad (1.29)$$

Under spontaneous symmetry breaking, the Yukawa part of the electroweak Lagrangian is of the form,

$$L_{\text{Yukawa}} = \frac{\alpha}{\sqrt{2}}(U_L r_U U_R + D_L r_D D_R + h.c.) \quad (1.30)$$

where  $r_U$  and  $r_D$  are  $3 \times 3$  matrices corresponding to the generalised Yukawa couplings. In general these matrices are the products of a Hermitian and unitary matrix. Under a particular unitary transformation, these Yukawa matrices may be diagonalised,

$$m_U = v_{U_L}^\dagger r_U v_{U_R} \quad (1.31)$$

$$m_D = v_{D_L}^\dagger r_D v_{D_R} \quad (1.32)$$

where  $m_U$  and  $m_D$  given by

$$m_U = \begin{pmatrix} m_u & 0 & 0 \\ 0 & m_c & 0 \\ 0 & 0 & m_t \end{pmatrix}, \quad m_D = \begin{pmatrix} m_d & 0 & 0 \\ 0 & m_s & 0 \\ 0 & 0 & m_b \end{pmatrix} \quad (1.33)$$

define the mass matrices. This diagonalisation may be achieved through a transformation of the quark flavour basis

$$U' = v_{U_L} U, \quad D' = v_{D_L} D. \quad (1.34)$$

The quark sector of the electroweak Lagrangian can therefore be written as

$$L = \frac{g}{\sqrt{2}} [U_L \gamma^\mu v_{U_L} v_{D_L}^\dagger D_L W_\mu^+ + D_L \gamma^\mu v_{D_L} v_{U_L}^\dagger U_L W_\mu^-]. \quad (1.35)$$

The matrix  $v_{U_L} v_{D_L}^\dagger$  is the Cabibbo-Kobayashi-Maskawa matrix [11, 12] denoted by

$$V_{\text{CKM}} = \begin{pmatrix} V_{ud} & V_{us} & V_{ub} \\ V_{cd} & V_{cs} & V_{cb} \\ V_{td} & V_{ts} & V_{tb} \end{pmatrix} \quad (1.36)$$

From its construction, the CKM matrix is unitary. This condition reduces the number of parameters required to describe this matrix; three real numbers and six complex phases. Through a redefinition of the quark fields, five of these phases may be removed since they are unphysical. The final phase cannot be removed. Therefore only four parameters are required to describe the CKM matrix. The original representation uses the four parameters detailed in table 1.1

$$V_{\text{CKM}} = \begin{pmatrix} c_1 & -s_1 c_3 & -s_1 s_3 \\ s_1 c_2 & c_1 c_2 c_3 - s_2 s_3 e^{i\delta} & c_1 c_2 s_3 + s_2 c_3 e^{i\delta} \\ s_1 s_2 & c_1 s_2 c_3 + c_2 s_3 e^{i\delta} & c_1 s_2 s_3 - c_2 c_3 e^{i\delta} \end{pmatrix} \quad (1.37)$$

where  $c_i = \cos \theta_i$  and  $s_i = \sin \theta_i$ . Since the dominant transitions between flavours occur within the generations, it is prudent to re-express the CKM matrix in a parametrisation which highlights this. One such representation is given by Wolfenstein in which the element  $V_{us} = \lambda$  (the Cabibbo angle  $\sin \theta_c$ ) acts as an expansion parameter. To  $\mathcal{O}(\lambda^3)$  the Wolfenstein parametrisation [13] is

$$V_{\text{CKM}} = \begin{pmatrix} 1 - \frac{\lambda^2}{2} & \lambda & A\lambda^3(\rho - i\eta) \\ -\lambda & 1 - \frac{\lambda^2}{2} & A\lambda^2 \\ A\lambda^3(1 - \rho - i\eta) & -A\lambda^2 & 1 \end{pmatrix}. \quad (1.38)$$

In this case,  $\eta$  corresponds to the CP violating phase.

Of the nine entries in the matrix, seven are measured directly from experiment,

the other two may be obtained from neutral meson mixing as shown in table 1.2.

Mixing Element	Physical Process
$V_{ud}$	$\pi \rightarrow \mu\nu$
$V_{us}$	$K \rightarrow \pi\nu e$
$V_{ub}$	$B \rightarrow \pi\nu e, B \rightarrow \rho\nu e$
$V_{cd}$	$D \rightarrow \pi\nu e, D \rightarrow \rho\nu e$
$V_{cs}$	$D \rightarrow K\nu e, D \rightarrow K^*\nu e$
$V_{cb}$	$B \rightarrow D\nu e, B \rightarrow D^*\nu e$
$V_{td}$	$B_d^0 \leftrightarrow \bar{B}_d^0$
$V_{ts}$	$B_s^0 \leftrightarrow \bar{B}_s^0$
$V_{tb}$	$t \rightarrow b\nu$

Table 1.2: Physical processes from which the nine CKM elements may be derived.

Assuming unitarity, the entries in the CKM matrix at the 90% confidence level [14] are

$$\begin{pmatrix} 0.9745 \Leftrightarrow 0.9760 & 0.217 \Leftrightarrow 0.224 & 0.0018 \Leftrightarrow 0.0045 \\ 0.217 \Leftrightarrow 0.224 & 0.9737 \Leftrightarrow 0.9753 & 0.036 \Leftrightarrow 0.042 \\ 0.004 \Leftrightarrow 0.013 & 0.035 \Leftrightarrow 0.042 & 0.9991 \Leftrightarrow 0.9994 \end{pmatrix} \quad (1.39)$$

It is clear from these values that as the Wolfenstein parametrisation suggests, there is a hierarchical structure associated with the flavour transitions, with a clear domination by the diagonal terms.

The apparent unitarity of the CKM matrix has important implications for the Standard Model. For such a  $3 \times 3$  matrix, unitarity simply corresponds to the following conditions,

$$\sum_x V_{xy} V_{xz}^* = 0 \quad (1.40)$$

for  $y \neq z$ , and

$$\sum_x |V_{xy}|^2 = \sum_y |V_{xy}|^2 = 1. \quad (1.41)$$

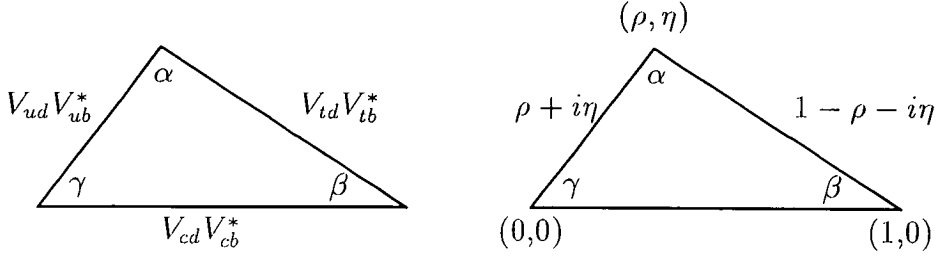


Figure 1.1: The unitarity triangle for equation 1.44 and the rescaled version.

Violations of this last result would imply the following

- $\sum_x |V_{xy}|^2 > 1 \rightarrow$  physics beyond SM
- $\sum_x |V_{xy}|^2 < 1 \rightarrow$  new generation(s)

Consider the off-diagonal unitarity constraints. For the columns the orthogonality condition gives

$$V_{ud}V_{us}^* + V_{cd}V_{cs}^* + V_{td}V_{ts}^* = 0 \quad (1.42)$$

$$V_{us}V_{ub}^* + V_{cs}V_{cb}^* + V_{ts}V_{tb}^* = 0 \quad (1.43)$$

$$V_{ud}V_{ub}^* + V_{cd}V_{cb}^* + V_{td}V_{tb}^* = 0 \quad (1.44)$$

These conditions can be conveniently expressed in a geometric context as triangles in the complex plane as shown in figure 1.1.

In order to describe physical effects such as CP violation (which has only been measured experimentally in neutral K-meson decays) the expansion of the Wolfenstein parametrisation has to be extended to include terms of  $\mathcal{O}(\lambda^5)$  [15].

$$V_{\text{CKM}} = \begin{pmatrix} 1 - \frac{\lambda^2}{2} & \lambda & A\lambda^3(\rho - i\eta) \\ -\lambda - iA^2\lambda^5\eta & 1 - \frac{\lambda^2}{2} & A\lambda^2 \\ A\lambda^3(1 - \rho(1 - \frac{\lambda^2}{2}) - i\eta(1 - \frac{\lambda^2}{2})) & -A\lambda^2 - iA\lambda^4\eta & 1 \end{pmatrix}. \quad (1.45)$$

Then by rescaling the unitarity triangle in figure 1.1 the parameters of the Wolfenstein parametrisation may be determined, allowing tests of unitarity and CP violation. Different models exist which suggest that in fact, the CP violating phase  $\eta$  is zero and therefore the CKM matrix is entirely real [16, 17, 18]. A current best estimate of the vertex is  $(\rho, \eta) = (0.160, 0.381)$  suggesting that this is not the case although it is not ruled out [19].

### 1.1.3 Weak Matrix Elements

In order to calculate transition amplitudes, the above weak current must be considered between two physical states. This is a straightforward calculation for leptons, yielding an expression in terms of Dirac spinors. Due to the confinement of quarks within bound states, the hadronic sector is therefore less tractable. For low energy processes (using the  $W^\pm$  mass as a scale), an effective Lagrangian may be used to describe the decay (equation 1.5),

$$L_{\text{eff}} = -\frac{G_F}{\sqrt{2}} J_\mu^\dagger J^\mu \quad (1.46)$$

where  $G_F$  the Fermi constant is related to the coupling,  $g$ , by

$$G_F = \frac{\sqrt{2}g^2}{8M_W^2}. \quad (1.47)$$

The amplitude for a given semi-leptonic decay can therefore be shown to be

$$-i\frac{G_F}{\sqrt{2}} V_{xy} J_\mu^L J_\mu^H \quad (1.48)$$

where  $J_\mu^L$  and  $J_\mu^H$  are the leptonic and hadronic currents respectively and the quark transition is  $y \rightarrow x$ .  $J_\mu^H$  is given by the matrix element,

$$J_\mu^H = \langle B | \bar{x} \gamma_\mu (1 - \gamma_5) y | A \rangle. \quad (1.49)$$

All the non-perturbative physics is embedded within this matrix element and its calculation is the subject of this thesis.

## Chapter 2

### Lattice QCD

The path integral formulation [20] is the calculational tool employed in lattice simulations. Consider a scalar field theory for simplicity. The Greens functions are given by

$$G^{(n)}(x_1, \dots, x_n) = \frac{1}{Z} \int d\phi(\phi(x_1) \cdots \phi(x_n)) e^{iS[\phi]} \quad (2.1)$$

where

$$Z = \int d\phi e^{iS[\phi]} \quad (2.2)$$

is the partition function. Clearly if a numerical simulation is to be attempted, the exponential in the above integrand must be real. This is accomplished by transforming from Minkowski to Euclidean space-time through a Wick rotation,

$$t \rightarrow \tau = it. \quad (2.3)$$

$$E \rightarrow ip_4 \quad (2.4)$$

$$S \rightarrow iS_E \quad (2.5)$$

which is equivalent to a change of space-time metric from  $g^{\mu\nu}$  to  $\delta^{\mu\nu}$ . The Euclidean Dirac matrices are related to the Minkowski matrices through

$$\gamma^i = i\gamma_E^i \quad (2.6)$$

$$\gamma^0 = \gamma_E^4. \quad (2.7)$$

The QCD Lagrangian (equation 1.2) is now given by

$$L_{\text{QCD}} = -\frac{1}{4}F_{\mu\nu}F^{\mu\nu} + \bar{\psi}(\not{D} + m)\psi \quad (2.8)$$

Hence now the integrand in equation 2.1 is real and therefore the theory is suitable for computer simulation. Through rotation to Euclidean space-time, the theory is analogous to classical statistical mechanics with the action equivalent to the statistical Hamiltonian and the Green functions equivalent to correlation functions.

## 2.1 Lattice Formulation

There are many geometries which may be employed to discretise continuum physics. By far the most popular method used today, and the one employed throughout this thesis, is a hypercubic representation. This geometry is extremely amenable to large scale numerical calculation ie computer simulation. Under such a geometry, the discretisation is realised through the introduction of a minimum length scale  $a$ , the lattice spacing which is the same for both temporal and spatial extents of the lattice. Integrals over space-time are therefore replaced by finite summations

$$\int d^4x \rightarrow a^4 \sum_{\vec{x}} \quad (2.9)$$

For non-Abelian gauge theories such as QCD, asymptotic freedom provides a connection between the lattice spacing (in effect, a measure of the scale) and the coupling  $g_0$ .

$$g_0^2 \approx \frac{1}{\beta_0 \log(a^{-2}/\Lambda^2)} \quad (2.10)$$

Rearranging this to get the lattice spacing as a function of the coupling yields

$$a \approx \frac{1}{\Lambda} e^{-\frac{1}{2\beta_0 g_0^2}} \quad (2.11)$$

The lattice spacing can be thought of as a maximum energy-momentum cutoff defining an ultra-violet regularisation for the theory.

The geometry of the lattice reduces the symmetry of the theory. The symmetries are now discrete and in particular only rotations in multiples of  $\frac{\pi}{2}$  are symmetry operations. Combined with a minimum distance scale, the momenta of simulated hadrons are forced to become discretised. The allowed values are given by

$$p = \pm \frac{2\pi r}{aN_s}, \quad r = 0, 1, \dots, \frac{N_s}{2} \quad (2.12)$$

where  $aN_s$  is the spatial dimension.

Having established the geometry of the discretisation procedure, the discretisation of the Euclidean Field Theory can be established. This analysis was first realised by Wilson [21, 22] in 1974, enabling the introduction of large scale numerical simulation of non-perturbative QCD.

Under the presence of a gauge field, a fermion (in the continuum) moving from space-time site  $a$  to  $b$  picks up a path dependent phase factor given by

$$U(b, a) = \mathcal{P} e^{\int_a^b igA_\mu(x)dx_\mu} \quad (2.13)$$

where  $\mathcal{P}$  is a path ordering operator. In effect, the fermion field is rescaled as it moves from one site to another. This is an important geometrical result known as parallel transporting, a hint of the underlying differential geometry inexorably linked to the formulation of any gauge theory.

It is trivial to show that this phase factor is an element of  $SU(3)$ . This motivates the assertion that the gauge fields in the discretised theory be represented by links between fermion sites,

$$U(x + \hat{\mu}, x) \equiv U_\mu(x) = e^{igaA_\mu(x + \frac{a}{2}\hat{\mu})} \quad (2.14)$$

where a unit lattice vector  $\hat{\mu}$  has been introduced. The gauge field  $A_\mu$  is defined at the middle of the link. Clearly  $U_\mu(x)$  is an approximation to a parallel transporter between two adjacent lattice (fermion) sites and is represented by an  $SU(3)$  matrix.

### 2.1.1 Gauge Invariance

In order to construct a discretised theory of QCD, quantities which preserve gauge invariance must be derived. To achieve this, it is useful to study the effect of a local gauge transformation. For QCD such a gauge transformation may be described by  $G(x) \in SU(3)$  such that the fermions transform as

$$\psi(x) \rightarrow G(x)\psi(x) \quad (2.15)$$

$$\bar{\psi}(x) \rightarrow \bar{\psi}(x)G^\dagger(x) \quad (2.16)$$

And hence trivially, the parallel transport transforms as

$$U_\mu(x) \rightarrow G(x)U_\mu(x)G^\dagger(x + a\hat{\mu}) \quad (2.17)$$

By considering the above transformation properties of the link variable  $U_\mu(x)$  and by noting that for  $SU(3)$  it follows that  $G^\dagger(x) = G^{-1}(x)$  it is readily apparent that a gauge invariant quantity can be constructed by considering a product of link variables for which the factors of  $G(x)$  and  $G^\dagger(x)$  combine at each site. Exclusively this can occur only for traces of products around closed paths called *Wilson Loops*. The simplest such loop is called the plaquette

$$P_{\mu\nu} = Tr[U_{\mu\nu}^\square(x)] \quad (2.18)$$

where

$$U_{\mu\nu}^\square(x) = U_\mu(x)U_\nu(x + a\hat{\mu})U_\mu^\dagger(x + a\hat{\nu})U_\nu^\dagger(x) \quad (2.19)$$

is the loop of link variables over a closed path spanned by lattice vectors  $\hat{\mu}$  and  $\hat{\nu}$ . There is in fact one other gauge invariant quantity which may be derived by considering the above transformation laws. Consider an unclosed product of link

variables,

$$S(x, y) \equiv U_\mu(x)U_\nu(x + a\hat{\mu}) \cdots \cdots U_\rho(y - a\hat{\rho} - a\hat{\delta})U_\delta(y - a\hat{\delta}) \quad (2.20)$$

Then under a local transformation

$$S(x, y) \rightarrow G(x)S(x, y)G^\dagger(y) \quad (2.21)$$

and hence by introducing a fermion and an anti-fermion at the ends of the path a gauge invariant quantity is obtained.

$$\bar{\psi}(x)S(x, y)\psi(y) \rightarrow [\bar{\psi}(x)G^\dagger(x)][G(x)S(x, y)G^\dagger(y)][G(y)\psi(y)] \quad (2.22)$$

This object is called a *string*.

### 2.1.2 Lattice Gauge Action

Having established two gauge invariant discretised objects a Lattice QCD action may now be constructed. In order to establish the discretised version of the Yang-Mills action it is worth noting the following result

$$F_{\mu\nu} \equiv \partial_\mu A_\nu - \partial_\nu A_\mu + g[A_\mu, A_\nu] \quad (2.23)$$

which states that the field strength is associated with the curvature of the gauge field.

Consider  $U^\square$  as defined in equation 2.19. Identifying the lattice difference operator with the central difference approximation to replace the continuum derivative

$$\lim_{a \rightarrow 0} \frac{f(x + a\hat{\mu}) - f(x - a\hat{\mu})}{2a} = \partial_\mu f(x) + \mathcal{O}(a^2) \quad (2.24)$$

and by expanding the gauge fields in terms of the lattice spacing

$$A_\nu(x \pm a\hat{\mu}) = A_\nu(x) \pm a \frac{\partial}{\partial x_\mu} A_\nu + \mathcal{O}(a^2) \quad (2.25)$$

it can be shown that the continuum limit of  $U^\square$  is given by

$$e^{ia^2g[F_{\mu\nu}+\mathcal{O}(a)]} \quad (2.26)$$

By performing an expansion in powers of the lattice spacing the above result may be written as

$$U_{\mu\nu}^\square = e^{ia^2g[F_{\mu\nu}+aF'_{\mu\nu}+a^2F''_{\mu\nu}+\dots]} \quad (2.27)$$

where due to the unitarity of  $U_{\mu\nu}^\square$  the quantities  $F'_{\mu\nu}$  and  $F''_{\mu\nu}$  are Hermitian. Hence by taking the real part of the trace

$$\Re Tr U_{\mu\nu}^\square = Tr(1 - g^2 \frac{a^4}{2} F_{\mu\nu}^2) + \mathcal{O}(a^6) \quad (2.28)$$

where the exponential in equation 2.27 has been expanded explicitly to  $\mathcal{O}(a^4)$ . In order to make the connection with the Yang-Mills part of the QCD action

$$\int \frac{1}{4} F_{\mu\nu} F^{\mu\nu} d^4x \quad (2.29)$$

the relevant summation required to approximate the above space-time integral is required. Noting that there are 6 *positively* oriented plaquettes ( $\mu < \nu$ ) associated with each site, Wilson arrived at the famous action

$$S_G = \beta \sum_x \sum_{(\mu < \nu)} [1 - \frac{1}{3} \Re Tr U_{\mu\nu}^\square(x)] \quad (2.30)$$

where

$$\beta = \frac{6}{g^2} \quad (2.31)$$

is the inverse coupling.

The discretisation error inherent to the Wilson action [23] can readily be seen from equation 2.28 to be  $\mathcal{O}(a^2)$  and will be discussed further in section 2.3.

## 2.2 Lattice Fermionic actions

### 2.2.1 Naive Fermions

In Euclidean space, the fermionic part of the QCD action is given by

$$S_{\text{EF}} = \int \bar{\psi}(x)(\gamma_\mu D_\mu + m)\psi(x)d^4x \quad (2.32)$$

for a Dirac field  $\psi(x)$  with the  $\gamma$  matrices satisfying the following relations

$$\{\gamma^\mu, \gamma^\nu\} = 2\delta^{\mu\nu} \quad (2.33)$$

$$\gamma_\mu = \delta_{\mu\nu}\gamma^\nu. \quad (2.34)$$

The discretisation of the above action is instigated by application of the following:

- The Dirac field  $\psi(x)$  is replaced by fermionic variables representing quarks at the sites of the lattice
- The covariant derivative is replaced by a central difference (c.f. equation 2.24)
- The integral is replaced by a sum over lattice sites

Thus the following (naive) fermion action is obtained.

$$S_{\text{N}} = \sum_x \left( \frac{a^3}{2} \sum_{\mu=1}^4 \bar{\psi}(x)\gamma_\mu[U_\mu(x)\psi(x + a\hat{\mu}) - U_\mu^\dagger(x - a\hat{\mu})\psi(x - a\hat{\mu})] + a^4 m \bar{\psi}(x)\psi(x) \right) \quad (2.35)$$

Surprisingly there are important problems with this (naive) action. Although constructed in a completely analogous way to the gauge action in the previous section, this prescription fails dramatically for fermions as discussed below.

### 2.2.2 Fermion Doubling

Consider the 1 dimensional free fermion Hamiltonian corresponding to the above (naive) massless fermion action,

$$H_N = -\frac{i}{2} \sum_x \psi^\dagger(x) \gamma_0 \gamma_1 (\psi(x+a) - \psi(x-a)) \quad (2.36)$$

which corresponds in the continuum to

$$H_N^{\text{cont}} = -i \int \psi^\dagger(x) \gamma_0 \gamma_1 \partial_x \psi(x) \quad (2.37)$$

It is prudent now to re-express the Hamiltonian in momentum space. The Dirac fields are transformed by virtue of the following Fourier sum

$$\psi(x) = \frac{1}{aL} \sum_{k=-\frac{\pi}{a}}^{+\frac{\pi}{a}} \psi_k e^{ikx} \quad (2.38)$$

where  $L$  is the spatial extent of the lattice in the  $x$  direction and for convenience the momenta are bounded in the first Brillouin zone  $(-\frac{\pi}{a}, \frac{\pi}{a})$ , cf equation 2.12). Then the Hamiltonian may be written as

$$H_N = \sum_{k=-\frac{\pi}{a}}^{+\frac{\pi}{a}} \psi_k^\dagger \gamma_0 \gamma_1 \frac{\sin(ka)}{a} \psi_k \quad (2.39)$$

Hence the eigenvalue spectrum for this particular action is given by

$$E_k = \pm \frac{\sin(ka)}{a} \quad (2.40)$$

This is to be compared with the continuum spectrum for a *massless* Dirac particle

$$E_k^{\text{cont}} = \pm k \quad (2.41)$$

Clearly when  $k \rightarrow 0$ , the lattice fermion state corresponds to the continuum Dirac particle of interest. However when  $k \rightarrow \frac{\pi}{a}$ , ie when the limit of the Brillouin

zone is reached another fermion state is obtained. This is known as 'doubling', for each Euclidean dimension the (naive) fermion action yields two degenerate fermion states and hence for a hypercubic lattice 16 states are obtained. In fact this doubling problem is a systematic effect of certain lattice actions. The No-Go theorem of Nielsen and Ninomiya [24] states that it is not possible to define a local, translationally invariant hermitian lattice fermion action which does not break chiral symmetry and does not reproduce degenerate fermion species.

### 2.2.3 Wilson Fermions

In order to work around the No-Go theorem, several prescriptions have been realised so that fermions can successfully be implemented in lattice calculations. The three most popular techniques used in current simulations are briefly outlined below:

- The naive fermion action is modified so that it explicitly breaks chiral symmetry by introduction of terms raising the mass of the spurious fermion states [21].
- The fermionic degrees of freedom are re-distributed around the lattice such that they observe a larger effective lattice spacing and hence the Brillouin Zone is reduced. This is achieved through Kogut-Susskind fermions [25] where using spin diagonalisation, only 3 extra fermions states are created.
- Free Wilson-like fermions are introduced in  $d+1$  dimensions. A mass term is included in the Lagrangian with a defect along the extra dimension resulting in a single chiral fermion bound to the ( $d$  dimensional) defect. Then a low energy effective theory can be employed to study chiral fermions on the defect [26].

The most popular method (and the one employed in this thesis) is the first one which was developed by Wilson and involves adding a term to the naive fermion

action. The Wilson fermion action is given by

$$S_F = S_N + S_W \quad (2.42)$$

where the extra term  $S_W$  is

$$S_W = -\frac{ar}{2} \sum_x \bar{\psi}(x) \square \psi(x) \quad (2.43)$$

with

$$\square \psi(x) = \frac{1}{a^2} \sum_{\mu} [U_{\mu}(x) \psi(x + a\hat{\mu}) + U_{\mu}^{\dagger}(x) \psi(x - a\hat{\mu}) - 2\psi(x)] \quad (2.44)$$

representing the lattice second derivative. The coefficient  $r$  is dimensionless. The effect of the addition of this extra term can be seen by consideration of the corresponding Hamiltonian. In one spatial dimension the Wilson Hamiltonian is

$$H_W = -ia \sum_x \psi^{\dagger}(x) \left[ \gamma_0 \gamma_1 \frac{(\psi(x+a) - \psi(x-a))}{2a} - \frac{ar\gamma_0}{2} \frac{(\psi(x+a) + \psi(x-a) - 2\psi(x))}{a^2} \right] \quad (2.45)$$

which reduces in momentum space to

$$\sum_k \psi_k^{\dagger} \left[ \gamma_0 \gamma_1 \frac{\sin(ak)}{a} + ir\gamma_0 \frac{\cos(ak) - 1}{a} \right] \psi_k. \quad (2.46)$$

Hence the energy eigenvalue spectrum for this action is given by

$$E_k^2 = \frac{\sin^2(ak)}{a^2} + \frac{r^2(\cos(ak) - 1)^2}{a^2} \quad (2.47)$$

This spectrum has the following limits

$$\lim_{k \rightarrow 0} E_k = \pm k \left( 1 - \left( \frac{r^2}{8} - \frac{1}{6} \right) a^2 k^2 \right) \quad (2.48)$$

$$\lim_{k \rightarrow \frac{\pi}{2}} E_k = \pm \frac{2r}{a} \quad (2.49)$$

Thus as the continuum limit ( $a \rightarrow 0$ ) is approached, for  $k \approx 0$  the correct continuum fermion state is reproduced whilst for momenta at the edge of the Brillouin zone the spurious state picks up an infinite effective mass (for a fixed non-zero value of the Wilson coefficient  $r$ ). Thus the Wilson fermion action (equation 2.42) given explicitly by

$$S_F = \sum_x \frac{a^3}{2} \left[ - \sum_{\mu=1}^4 \bar{\psi}(x) ((r - \gamma_\mu) U_\mu(x) \psi(x + a\hat{\mu}) + (r + \gamma_\mu) U_\mu^\dagger(x) \psi(x - a\hat{\mu})) + (8r + 2am) \bar{\psi}(x) \psi(x) \right] \quad (2.50)$$

satisfies the No-Go theorem by breaking chiral symmetry

$$\psi \rightarrow e^{i\alpha\gamma_5} \psi \quad (2.51)$$

through the final term. This final term motivates the introduction of a hopping parameter  $\kappa$  (so named since it gives an indication of the strength of the nearest neighbour coupling) ,

$$\kappa = \frac{1}{8r + 2am} \quad (2.52)$$

which will act as an input parameter for the bare quark mass. It also serves as a scaling factor (helpful for computational requirements) implying the following redefinition of the quark fields,

$$\psi \rightarrow \psi' = \sqrt{2\kappa} \psi. \quad (2.53)$$

$$\bar{\psi}(x) \rightarrow \bar{\psi}(x) \sqrt{2\kappa} \quad (2.54)$$

The effect of the chiral symmetry breaking is that the fermion mass is additively renormalised, and thus the bare quark mass in the presence of gauge fields is denoted by

$$m_q = \frac{1}{2} \left( \frac{1}{\kappa} - \frac{1}{\kappa_c} \right) \quad (2.55)$$

where  $\kappa_c$  represents the hopping parameter at which the pion mass vanishes.

The Wilson Fermion action is often re-expressed in terms of the lattice Dirac operator

$$\mathcal{D}(x, y) = \sum_{\mu} [(r - \gamma_{\mu})U_{\mu}(x)\delta(x + a\hat{\mu}, y) + (r + \gamma_{\mu})U_{\mu}^{\dagger}(x)\delta(x - a\hat{\mu}, y)] \quad (2.56)$$

where  $\delta(x, y)$  is the Kronecker delta symbol. Hence equation 2.50 may now be written as

$$S_F = \bar{\psi}(x)M_F(x, y)\psi(y) \quad (2.57)$$

where

$$M_F(x, y) = \delta(x, y) - \kappa\mathcal{D}(x, y) \quad (2.58)$$

is the Wilson Fermion matrix and is the subject of some discussion in the next section. The Wilson coefficient  $r$  is usually set to one in simulation. It can be shown, by a Taylor expansion with respect to the lattice spacing, that the Wilson Fermion action has the following form in the continuum

$$S_F = \int \bar{\psi}(x)(\gamma_{\mu}D_{\mu} + m)\psi(x)d^4x + \mathcal{O}(a) \quad (2.59)$$

and hence this action suffers from larger discretisation errors than the gauge action discussed above.

### 2.3 Improved Fermion Actions

A clear fundamental goal of lattice simulation is the accurate calculation of physical observables. It is prudent therefore to strive to reduce where possible all systematic errors. Recall from the previous two sections the continuum properties of the gauge and fermion actions. Clearly, the QCD action is simply the sum of these two actions,

$$S_{\text{QCD}}^{\text{W}} = S_F + S_G \quad (2.60)$$

and hence the above action suffers from  $\mathcal{O}(a)$  discretisation errors coming from the fermionic part. The goal then is to introduce a term to the fermion action

as before such that the continuum limit is unchanged, the Dirac eigenvalue spectrum is maintained in the continuum limit and the terms contributing to the discretisation errors start as a higher power of the lattice spacing.

### 2.3.1 Sheikholeslami-Wohlert Action

By adding the following term to the Wilson fermion action,

$$S_{\text{SW}} = -a^4 \sum_{x,\mu,\nu} \frac{iga}{4} \bar{\psi}(x) \sigma_{\mu\nu} F^{\mu\nu}(x) \psi(x) \quad (2.61)$$

where

$$\sigma_{\mu\nu} = \frac{1}{2} [\gamma_\mu, \gamma_\nu] \quad (2.62)$$

an improved action is created which destroys the  $\mathcal{O}(a^2)$  artifact in  $S_{\text{F}}$ [27, 28]. The term  $F^{\mu\nu}(x)$  is a lattice definition of the field strength tensor and is defined

$$F^{\mu\nu}(x) = \frac{1}{4} \sum_{\square=1}^4 \frac{1}{i2a^2g} [U_{\mu\nu}^\square + U_{\mu\nu}^{\square\dagger}]. \quad (2.63)$$

where the sum runs over the four plaquettes in the  $\{\mu, \nu\}$  plane centred around a lattice site. By virtue of this choice of the field strength tensor, the Sheikholeslami-Wohlert action is colloquially known as the clover action as can be seen schematically in figure 2.1. Hence the lattice QCD action is defined to be

$$S_{\text{QCD}}^{\text{L}} = S_{\text{G}} + S_{\text{F}} - \frac{ia^5 c_{\text{sw}}}{4} \sum_{x,\mu,\nu} \bar{\psi}(x) \sigma_{\mu\nu} F^{\mu\nu}(x) \psi(x) \quad (2.64)$$

and on-shell Green functions calculated using this action contain no discretisation errors of  $\mathcal{O}(a)$ . The coefficient  $c_{\text{sw}}$  has to be determined and at tree level is unity.

### 2.3.2 Non-Perturbative Improvement

As the continuum limit is reached, the lattice theory can be parametrised in terms of a local effective theory [29, 30] whose action may be written as

$$S_{\text{eff}} = S_0 + aS_1 + a^2S_2 + a^3S_3 + \dots \quad (2.65)$$

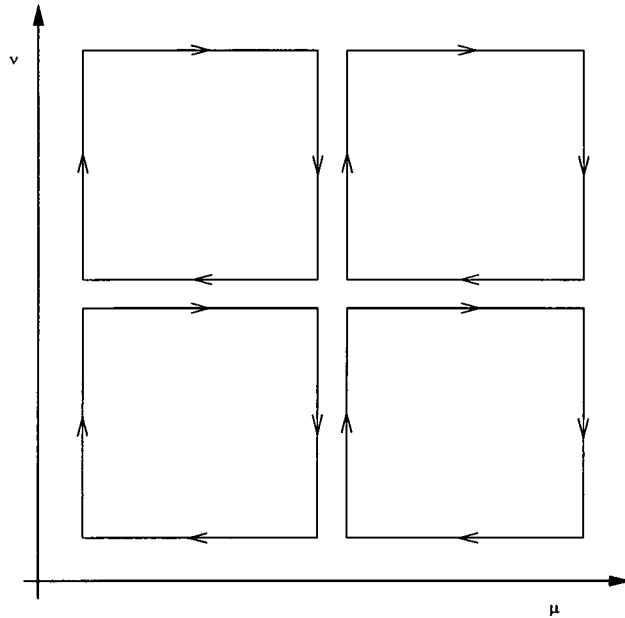


Figure 2.1: Geometric representation of the clover term.

where clearly the term  $S_0$  is representative of the continuum limit ( and hence in this context a lattice theory with an extremely small spacing). The other terms in the effective action may be expressed as

$$S_d = \int L_d(x) d^4x \quad (2.66)$$

where the Lagrangians  $L_d(x)$  are expressed as linear combinations of local composite fields. These fields must then obey the following properties,

- They must be invariant under  $U(1) \otimes SU(N_f)$
- They must respect space-time lattice symmetry
- They must be invariant under charge conjugation.

Using these conditions, the Lagrangian  $L_1(x)$  is constructed from some linear combination of the following five fields,

$$G_1 = \bar{\psi} \sigma_{\mu\nu} F_{\mu\nu} \psi, \quad (2.67)$$

$$G_2 = \bar{\psi} D_\mu D_\nu \psi + \bar{\psi} \overleftarrow{D}_\mu \overleftarrow{D}_\nu \psi \quad (2.68)$$

$$G_3 = m \text{Tr}(F_{\mu\nu} F_{\mu\nu}) \quad (2.69)$$

$$G_4 = m(\bar{\psi} \gamma_\mu D_\mu \psi - \bar{\psi} \overleftarrow{D}_\mu \gamma_\mu \psi) \quad (2.70)$$

$$G_5 = m^2 \bar{\psi} \psi. \quad (2.71)$$

This basis of fields may be reduced by application of the classical field equations of motion and by exclusively considering on-shell quantities. Under such a procedure,  $G_2$  and  $G_4$  vanish and hence the counter-term is given by

$$\Delta S = a^5 \sum_x (c_1 g_1(x) + c_2 g_3(x) + c_3 g_5(x)) \quad (2.72)$$

where  $g_i(x)$  is the lattice representation of  $G_i$ . By comparison with the gauge action discussed earlier it may be deduced that the basis may be further reduced. If the field  $G_3$  is chosen to be represented by the plaquette and  $G_5$  is represented by the local scalar density then it is clear that these two fields can be eliminated from the possible basis. In effect, these two terms then represent a renormalisation of the bare coupling and mass respectively [31]. Hence the relevant counter term is given by equation 2.61, the clover term.

The coefficient  $c_{\text{sw}}$  is therefore critical in establishing a fully  $\mathcal{O}(a)$  improved QCD action. In particular it is necessary to evaluate this coefficient in a non-perturbative scheme. Such a scheme has been devised by the ALPHA collaboration [32]. By imposing the PCAC relation,

$$\partial_\mu A_\mu = 2mP \quad (2.73)$$

where  $A_\mu$  and  $P$  are the axial current and density respectively, and its lattice counterpart,

$$\partial_\mu \langle A_\mu^R(\lambda)\Theta \rangle = 2m_R \langle P_\mu^R(\lambda)\Theta \rangle + \mathcal{O}(a^2) \quad (2.74)$$

where  $\Theta$  is a product of fields excluded from the point  $\lambda$ , and employing the Schrödinger functional [33, 34] as a calculational tool (periodic spatial boundary conditions and Dirichlet boundary conditions in the temporal extent), the improvement coefficient  $c_{\text{sw}}$  is extracted in a non-perturbative fashion. For values of  $\beta \geq 6.0$ ,  $c_{\text{sw}}$  has the following functional dependence on the bare coupling [32],

$$c_{\text{sw}} = \frac{1 - 0.656g^2 - 0.152g^4 - 0.054g^6}{1 - 0.992g^2}. \quad (2.75)$$

## 2.4 Numerical Simulation

Having established the action used to represent the discretised version of QCD amenable to numerical simulation, relevant physical quantities may now be extracted. This is done by application of the path integral formulation.

### 2.4.1 Partition Function for Lattice QCD

Before explicitly calculating the partition function for lattice QCD it is useful to re-express the Sheikholeslami-Wohlert fermion action in terms of the fermion matrix,

$$S_{\text{SW}} = \sum_{x,y} \bar{\psi}(x) M(x, y, U) \psi(y), \quad (2.76)$$

where  $M(x, y, U)$ , the fermion matrix is represented by,

$$M(x, y, U) = B(x) \partial_{x,y} - \kappa \sum_{\mu} \left[ (1 - \gamma_{\mu}) U_{\mu}(x) \delta(x + a\hat{\mu}, y) + (1 + \gamma_{\mu}) U_{\mu}^{\dagger}(x) \delta(x - a\hat{\mu}, y) \right] \quad (2.77)$$

where

$$B(x) = 1 - \frac{i}{2} c_{\text{sw}} \sigma_{\mu\nu} F_{\mu\nu}. \quad (2.78)$$

As for the fermion matrix corresponding to the unimproved fermion action, this fermion matrix obeys the hermiticity relation,

$$M(x, y) = \gamma_5 M^\dagger(y, x) \gamma_5. \quad (2.79)$$

The generating functional given by

$$Z = \int D\bar{\psi} D\psi DU e^{-S_{\text{QCD}}^{\text{L}}} \quad (2.80)$$

may be written as

$$Z = \int D\bar{\psi} D\psi DU \exp[-S_{\text{G}} - \bar{\psi} M(x, y, U) \psi]. \quad (2.81)$$

with the integration defined as

$$\int DU = \prod_{x, \mu} \int dU_\mu(x), \quad (2.82)$$

$$\int D\bar{\psi} D\psi = \prod_x \int d\bar{\psi}(x) d\psi(x) \quad (2.83)$$

Since the gluonic sector of QCD is, in the context of lattice field theory, represented by  $SU(3)$  matrices, the integration of this sector requires more careful thought. Clearly, a requirement for this integration is the introduction of a gauge invariant group measure. Wilson employed such a measure (the Haar measure) [35] with the following properties:

$$\int dU f(U) = \int dU f(UV) = \int dU f(WU) \quad (2.84)$$

$$\int dU = 1 \quad (2.85)$$

From equation 2.88 it is clear that any generalised functional form for an element of this Grassmann algebra is given by a finite power series of the elements since the set is finite,

$$\zeta(\psi) = \zeta_0 + \sum_j \zeta_j \psi_j + \sum_{j \neq k} \zeta_{jk} \psi_j \psi_k + \cdots + \zeta_{12 \dots N} \psi_1 \cdots \psi_N. \quad (2.91)$$

Clearly these generalised functions will form part of the integrand of the partition function. Therefore integrals of the form

$$\int \prod_j d\psi_j \zeta(\psi) \quad (2.92)$$

will have to be computed. From the above results it is clear that

$$\int d\psi_j = 0 \quad (2.93)$$

$$\int d\psi_j \psi_j = 1 \quad (2.94)$$

where like the original elements  $\psi_j$ , the integration measures anti-commute amongst themselves

$$\{d\psi_j, d\psi_k\} = \{d\psi_j, \psi_k\} = 0. \quad (2.95)$$

Introducing another set of  $N$  Grassmann variables  $\{\alpha_j\}$ , the function

$$\zeta(\psi, \alpha) = \exp[\alpha_j \Upsilon_{jk} \psi_k] \quad (2.96)$$

has an expansion given by

$$(1 - \alpha_1 \Upsilon_{1j_1} \psi_{j_1}) \cdots (1 - \alpha_N \Upsilon_{Nj_N} \psi_{j_N}). \quad (2.97)$$

Under an integration such as given by equation 2.92, then from the rules of integration, only the term which contains a product of all the Grassmann variables will survive. Such a term will clearly be antisymmetric under the exchange of

where  $f(U)$  is an arbitrary function over  $SU(3)$  and  $U, V$  and  $W$  are all elements of  $SU(3)$ . This construction is such that the functional integral is gauge invariant and no gauge fixing terms are required.

Using the above partition function, the vacuum expectation value of an observable  $\theta$  is then given by

$$\langle \theta \rangle = \frac{1}{Z} \int D\bar{\psi} D\psi DU \theta \exp [-S_G - \bar{\psi} M(x, y, U) \psi]. \quad (2.86)$$

This cannot however be calculated stochastically in a numerical process due to the nature of the fermionic degrees of freedom. These fields representing the quarks (spin  $\frac{1}{2}$ ) are elements of a Grassmann algebra with the following properties.

### 2.4.2 Grassmann Algebra

Consider a set of  $N$  anti-commuting Grassmann variables  $\{\psi_1, \psi_2, \dots, \psi_N\}$ . These elements then have the property

$$\{\psi_i, \psi_j\} = \psi_i \psi_j + \psi_j \psi_i = 0 \quad (2.87)$$

which for  $i = j$  reduces to

$$\psi_j^2 = 0. \quad (2.88)$$

This result allows certain functions of the elements  $\psi_j$  to be reduced to more trivial forms. In particular, consider the following function of the elements,

$$\zeta = \prod_{j,k} e^{-\psi_j \Upsilon_{jk} \psi_k} \quad (2.89)$$

which using equation 2.88 becomes

$$\zeta = \prod_{j \neq k} (1 - \psi_j \Upsilon_{jk} \psi_k). \quad (2.90)$$

labels  $j_a, j_b$  and hence may be written as

$$\alpha_1 \psi_1 \cdots \alpha_N \psi_N \sum_{j_1 \cdots j_N} \epsilon_{j_1 \cdots j_N} \Upsilon_{1j_1} \cdots \Upsilon_{Nj_N} \quad (2.98)$$

where  $\epsilon_{j_1 \cdots j_N}$  is the N-dimensional anti-symmetric tensor. The above result may be written in the more compact form

$$(\det \Upsilon) \sum_j \alpha_j \psi_j. \quad (2.99)$$

By making the following assignments

$$\alpha_j \rightarrow \bar{\psi}_j \quad (2.100)$$

$$\Upsilon_{jk} \rightarrow M_{jk} \quad (2.101)$$

and using equation 2.99 the integration over the fermionic sector in the partition function simplifies it to the following

$$Z = \int DU \det M e^{-S_g(U)} \quad (2.102)$$

and hence the vacuum expectation value of an observable  $\theta$  is expressed as

$$\langle \theta \rangle = \frac{1}{Z} \int DU \det M \theta e^{-S_g(U)}. \quad (2.103)$$

### 2.4.3 Numerical Techniques

By choosing a lattice with a finite temporal and spatial extent the number of degrees of freedom present in the generating functional becomes finite allowing the extraction of physics from the lattice QCD action using numerical techniques. The finite range of the temporal extent may be thought of as introducing a temperature to the lattice given by  $\frac{1}{aN_t}$ . This quantity may be chosen small enough that the lattice is effectively at zero temperature. In order to calculate the lat-

tice action for a particular gauge and fermion field configuration, it is necessary to impose boundary conditions on these fields. It is standard to impose periodic boundary conditions on the gluonic sector. Due to the anti-commutation properties of the fermion sector, periodic boundaries are imposed on the spatial directions whilst an anti-periodic boundary condition is imposed on the temporal extent.

In order to evaluate the path integral it is necessary to calculate the gluonic configurations. Perhaps the simplest technique is the Metropolis algorithm [36]. This method works by starting with some configuration  $U$  and transforming the link variables in a prescribed way to obtain a new configuration  $U'$ . The actions  $S, S'$  corresponding to each configuration are calculated and the new configuration is accepted if  $\exp(-S'(U')) > \exp(-S(U))$  otherwise it is accepted with a probability given by  $\exp(S(U) - S'(U'))$ . Thus this Markov process by obeying detailed balance converges to the correct probability distribution. All these methods use importance sampling, in other words they move through the space of possible configurations such that the resulting distribution is weighted according to  $\det M e^{-S_g[U]}$ . In such a way, a finite ensemble of configurations is constructed allowing the integral to be approximated by a sum over the ensemble. For  $W$  configurations,

$$\langle \theta \rangle \simeq \bar{\theta} = \frac{1}{W} \sum_i^W \theta[U_i]. \quad (2.104)$$

It is worth noting that successive configurations generated by the Markov process are highly correlated. Clearly the configurations employed in simulations should be uncorrelated, ie observables on one configuration should be independent of the starting configuration. Hence the only configurations which are saved are those which are separated by a sufficient distance along the Markov chain. Inherent correlations however will still be present and this issue will be discussed later in section 4.5.1.

Consider the form of the measure used in the Markov process. The hardest task numerically is to calculate  $\det M$  since in general  $M$  is a very large, sparse

and non-local matrix. With computing technology only recently rendering the calculation of this determinant affordable, this quantity has historically been set to a constant. The physical effect of this is to ignore internal quark loops. This *quenched* approximation [37, 38] has proven to be highly successful and calculations employing this simplification have been shown to be qualitatively very close to those of experiment.

## 2.5 Finite Size Effects

Thus far, various errors inherent to the lattice method have been discussed such as quenching errors and discretisation errors. Another important consideration in lattice QCD is the effect of the spatial extent of the lattice. Clearly, the size of the box approximating spacetime should be large enough to accommodate the relevant mesons and baryons of interest. A typical length scale for a heavy light meson is  $\frac{1}{\Lambda_{\text{QCD}}}$  and hence this means that for a lattice with  $N_s$  sites in a spatial direction  $aN_s \gg \frac{1}{\Lambda_{\text{QCD}}}$ .

Using periodic boundary conditions implies there will exist many copies of the hadron of interest [39]. Therefore it is a requirement that the lattice be larger than the range of the strong interaction so that there is negligible interaction between the copies. The range of such interactions is given by the pion Compton wavelength. This is a difficult requirement to overcome and therefore as a work-around, the lattice simulation is done with unphysically large masses for the light quarks. In order to achieve errors from this effect at less than the 5% level, the copies should be three pion Compton wavelengths apart. Thus the lightest pseudoscalar meson has a mass  $m$  constrained by

$$\frac{3}{m} \leq aN_s - \frac{1}{\Lambda_{\text{QCD}}} \quad (2.105)$$

for unquenched QCD (since in fact a virtual pion cannot be created from the vacuum in quenched QCD). Therefore the observables have to be extrapolated to the chiral limit, using the quark mass dependence given by chiral perturbation theory. This is discussed in section 5.4.

## Chapter 3

### Heavy Quark Effective Field Theory

In order to accurately test the flavour sector of the Standard Model and probe for a theory beyond, one clear goal is a more precise knowledge and understanding of  $b$  physics. To achieve this it is necessary to understand the experimentally observed confinement of quarks into colour neutral hadrons such as the  $B$  meson arising from the non-Abelian group structure of QCD. Unlike short distance physics such as Drell-Yan processes and deep inelastic scattering [40] which have been phenomenologically and qualitatively well understood for some time now, long distance physics proves more difficult to disentangle.

In many aspects of physics often it is useful to strip the theory down to a simpler theory. In doing so, new symmetries emerge which when exploited yield a framework for the extraction of the physics sought in a controlled and predictive manner synonymous with perturbative calculations. A familiar example of the power of an effective field theory is that of Chiral Perturbation Theory (ChPT) [41]. In ChPT, the chiral symmetry  $SU(3)_L \otimes SU(3)_R$  (which arises because the masses of the lightest three quarks  $m_u, m_d$  and  $m_s$  are considered small compared to the intrinsic mass scale of the strong interactions) is spontaneously broken, generating a set of massless Goldstone bosons. The quarks are not massless in reality and this approximation to the symmetry results in the Goldstone bosons acquiring a small mass. The Goldstone bosons are identified as light pseudoscalar particles, in particular the pion, and ChPT allows exact predictions for the emission and absorption of soft pions. The salient point here is that it is not the coupling constant of QCD which is relevant but the ratio of mass scales involved.

### 3.1 Heavy Quark Symmetry

The difference in mass scales for  $B$  physics allows a similar effective theory to be constructed. The six quarks divide naturally into two classes, light and heavy and have the following measured masses [14].

Quark Flavour	Mass (MeV)
$u$	$1.5 \Leftrightarrow 5$
$d$	$3 \Leftrightarrow 9$
$s$	$60 \Leftrightarrow 170$
$c$	$1100 \Leftrightarrow 1400$
$b$	$4100 \Leftrightarrow 4400$
$t$	$168600 \Leftrightarrow 179000$

Table 3.1: Listing of the quark masses

It is clear therefore that for heavy light systems, involving one of  $c$  or  $b$  ( $t$  decays too fast) and one of  $u$ ,  $d$  or  $s$  then the mass scales are indeed completely different. This is exploited to form the Heavy Quark Symmetry [42, 43, 44, 45].

Consider a heavy light meson containing a heavy quark, henceforth denoted  $Q$ . This quark is surrounded by a complicated ‘cloud’ consisting of quarks, anti-quarks and gluons. These are then the light degrees of freedom. The mass of the heavy quark is much greater than the scale of QCD,  $m_Q \gg \Lambda_{QCD}$ . As this quark becomes more massive, its Compton wavelength will naturally be much smaller than the typical size of the meson,  $\lambda_Q \ll R_{\text{meson}}$ . The consequence of this simple observation is that in order to resolve the internal structure of the heavy quark a very sensitive probe is required. However, the light degrees of freedom by their very nature are unable to probe at such short length scales because of their relatively small momenta and hence are in some sense blind to the quantum properties of the heavy quark. In fact, the light degrees of freedom are characterised by momenta of  $\mathcal{O}(\Lambda_{QCD})$  and their Compton wavelength is much larger than that of the heavy quark. The light degrees of freedom are unable to resolve the flavour (and thus mass) and spin of the heavy quark. The heavy

quark does not recoil against the emission and absorption of soft gluons and is then almost on shell acting as an electric and chromo-electric static source. In the limit of infinite heavy quark mass, its velocity is equal to that of the meson itself. Also, in this limit the binding of the two components is independent of the flavour of the heavy quark. The heavy quark is carrying most of the mass of the meson and in the limit  $m_Q \rightarrow \infty$  the relation  $M_{\text{meson}} = m_Q + \mathcal{O}(\Lambda_{QCD})$  may then be re-expressed in terms of  $\bar{\Lambda} = M_{\text{meson}} - m_Q$ , a universal, flavour independent constant. The Heavy Quark symmetry is summarised as follows. The configuration of the light degrees of freedom (and hence meson) is independent of the flavour (mass) and spin of the constituent heavy quark [46]. It is important to note that this symmetry does not extend to the velocity of the heavy quark.

### 3.2 Heavy Quark Effective Theory

Motivated by the above discussion of the symmetries inherent to a heavy light system, an effective theory which reproduces the low energy behaviour of such systems can be introduced, allowing the extraction of hadronic quantities such as matrix elements and decay constants. This is achieved by making the dependence of all quantities on  $m_Q$  explicit and then developing the Lagrangian in a power series in the inverse heavy quark mass.

The starting point for this analysis is the momentum of the heavy quark. As discussed above, the heavy quark is almost on shell and moves with almost the same velocity as the meson itself. Thus, its momentum is given by

$$P_Q^\mu = m_Q v^\mu + k^\mu \quad (3.1)$$

where  $m_Q v^\mu$  represents the on-shell condition and  $k^\mu$  is some residual momentum. Clearly, in accordance with the above discussion  $k^\mu$  is  $\mathcal{O}(\Lambda_{QCD})$  and is due to the exchange of soft gluons. To illustrate the fact that in the heavy quark symmetry, the velocity of the heavy quark is conserved, consider some scattering of the above

meson. The new momentum will be given by

$$P_Q^\mu = m_Q v'^\mu + k'^\mu. \quad (3.2)$$

Hence the momentum transfer is

$$\Delta P_Q^\mu = m_Q (v - v')^\mu + (k - k')^\mu. \quad (3.3)$$

Therefore it is clear that exchange of soft gluons cannot alter the velocity of the meson, and therefore the assertion  $v^\mu = v'^\mu$  is made explicit.

In the heavy quark limit, the Feynman rules of QCD are greatly simplified [47, 48]. In particular, the heavy quark propagator may be expanded as,

$$\frac{i}{\not{P}_Q - m_Q} = \frac{i(1 + \not{v})}{2v \cdot k} + \mathcal{O}\left(\frac{k}{m_Q}\right) \quad (3.4)$$

where  $(1 + \not{v})/2$  is a positive energy projection operator. In the exact limit,

$$\lim_{m_Q \rightarrow \infty} \frac{i}{\not{P}_Q - m_Q} = \frac{i(1 + \not{v})}{2v \cdot k}. \quad (3.5)$$

and is independent of the heavy quark mass. The couplings between heavy quarks and gluons can also be simplified,

$$-ig\gamma^\mu \frac{\lambda^a}{2} \rightarrow -igv^\mu \frac{\lambda^a}{2}. \quad (3.6)$$

and hence these couplings are independent of the heavy quark spin by virtue of the fact there is no gamma matrix structure in the above expression. These Feynman rules may also be obtained from an HQET Lagrangian. The full QCD Lagrangian for a heavy quark field  $Q$  is given by

$$L = \bar{Q}(i\not{D} - m_Q)Q. \quad (3.7)$$

An effective quark field  $h_v$  is defined in terms of the original quark field [43],

$$h_v = \frac{1 + \not{v}}{2} e^{im_Q v \cdot x} Q \quad (3.8)$$

and is subject to the on-shell constraint,

$$\not{v} h_v = \frac{1 + \not{v}}{2} h_v = h_v. \quad (3.9)$$

Hence the effective field  $h_v$  annihilates a heavy quark but does not create an anti-quark. Substitution into the above Lagrangian yields,

$$L_v = \bar{h}_v [m_Q (\not{v} - 1) + i \not{D}] h_v \quad (3.10)$$

Using equation 3.9 this reduces to

$$L_v = \bar{h}_v i \not{D} h_v. \quad (3.11)$$

Making use of the relation

$$\frac{1 + \not{v}}{2} \gamma^\mu \frac{1 - \not{v}}{2} = \frac{1 + \not{v}}{2} v^\mu \frac{1 - \not{v}}{2} \quad (3.12)$$

the effective Lagrangian becomes

$$L_v = \bar{h}_v i v \cdot D h_v. \quad (3.13)$$

From this Lagrangian, the Feynman rules discussed above are naturally produced. The spin and mass dependencies have been eradicated from this Lagrangian as required. The development of the Lagrangian to incorporate more than one heavy quark moving at the same velocity is trivial and amounts to simply adding the individual Lagrangians. For example for  $N$  heavy quarks moving with velocity  $v_k$ , the Lagrangian for the system is,

$$L_{\text{sys}} = \sum_{j=1}^N \bar{h}_{v_k}^j i v_k \cdot D h_{v_k}^j. \quad (3.14)$$

For the particular case of a decay  $Q(v) \rightarrow Q'(v')$  the Lagrangian is then

$$L_{\text{decay}} = \bar{h}_v i v \cdot D h_v + \bar{h}'_{v'} i v' \cdot D h'_{v'}. \quad (3.15)$$

### 3.3 Series Expansion in $\frac{1}{m_Q}$

The above analysis is correct only for a meson which contains an on-shell heavy quark. In order to correct the theory and allow for slightly off-shell quarks, another decomposition of the heavy quark field similar to equation 3.8 is required. To satisfy the off-shell physics, the field  $H_v$  is introduced such that

$$H_v = e^{im_Q v \cdot x} \frac{1 - \not{v}}{2} Q. \quad (3.16)$$

It is clear that the original heavy quark field  $Q$  may be expressed as a linear combination of the two new quark fields,

$$Q = e^{-im_Q v \cdot x} [h_v + H_v] \quad (3.17)$$

with

$$\not{v} H_v = -H_v \quad (3.18)$$

by virtue of the projection operator. In its rest frame, the spinor decomposition for the heavy quark field may be written as

$$Q_{r.f} = e^{-im_Q v \cdot x} \begin{pmatrix} h_v \\ H_v \end{pmatrix} \quad (3.19)$$

Hence  $h_v$ , which annihilates a heavy quark with velocity  $v$  corresponds to the upper two components of  $Q$ , whilst  $H_v$ , which creates a heavy anti-quark with velocity  $v$  corresponds to the lower two components of  $Q$ . Substituting equation 3.17 into the heavy quark QCD Lagrangian gives,

$$L_{\text{eff}} = \bar{h}_v i v \cdot D h_v + \bar{h}_v i \not{D}_\perp H_v - \bar{H}_v (i v \cdot D + 2m_Q) H_v + \bar{H}_v i \not{D}_\perp h_v \quad (3.20)$$

where the covariant derivative has been decomposed to reveal the longitudinal and transverse components with respect to the heavy quark velocity,

$$v \cdot D_{\perp} = 0, \quad D^{\mu} = v^{\mu}(v \cdot D) + D_{\perp}^{\mu}. \quad (3.21)$$

The effective Lagrangian reflects the fact that the mixing between the quark and anti-quark components of the Dirac spinor is suppressed by powers of  $2m_Q$ , the mass gap between the positive and negative energy parts of the wavefunction. The field  $H_v$  corresponds to the heavy degrees of freedom that must be integrated out to construct the heavy quark effective theory. This can be achieved by exploiting the equation of motion to expand  $H_v$  in terms of  $h_v$  [49]. The relation,

$$(m_Q(\not{v} - 1) + i\not{D})[H_v + h_v] = 0 \quad (3.22)$$

gives

$$H_v = \left( \frac{2m_Q - i\not{D}}{2m_Q} \right)^{-1} \frac{i\not{D}h_v}{2m_Q} \quad (3.23)$$

which is built up from a non-local object. An expansion in powers of the inverse heavy quark mass alleviates this problem, and to leading order,

$$H_v = \frac{i}{2m_Q} \not{D}_{\perp} h_v + \dots \quad (3.24)$$

Hence the original heavy quark field is given by

$$Q = e^{-im_Q v \cdot x} \left( \frac{2m_Q + i\not{D}_{\perp}}{2m_Q} \right) h_v + \dots \quad (3.25)$$

Substituting this form of the field into the heavy quark Lagrangian yields,

$$L_{\text{eff}} = \bar{h}_v i v \cdot D h_v + \frac{\bar{h}_v}{2m_Q} \left( -D_{\perp}^2 - \frac{1}{2} \alpha_s \sigma_{\mu\nu} F^{\mu\nu} \right) h_v + \dots \quad (3.26)$$

where  $F^{\mu\nu}$  is the field strength tensor,

$$F^{\mu\nu} = \frac{i}{\alpha_s} [D^{\mu}, D^{\nu}]. \quad (3.27)$$

The first term which is proportional to  $\frac{1}{m_Q}$  in the above Lagrangian is a gauge covariant form of the kinetic energy due to the off shell motion of the heavy quark inside the meson and violates the flavour symmetry. The final term can be shown to contain components of the colour magnetic gluon field and this term can therefore be interpreted as a chromo-magnetic interaction, violating both flavour and spin symmetries. Hence now any operator (at tree level) may be constructed. For example the vector current for a heavy light system is given by

$$V^\mu = \bar{q}\gamma^\mu Q = e^{-im_Q v \cdot x} \bar{q}\gamma^\mu \left(1 + \frac{i \not{D}_\perp}{2m_Q}\right) h_v + \dots \quad (3.28)$$

### 3.4 Renormalisation

The effective theory describes well the long distance regime of QCD. The symmetry was provoked by the realisation that the soft gluons were unable to resolve quantum structure. Clearly then, there are problems for this effective theory when the short distance regime is considered. At this high energy scale the virtual momenta of the gluons may be substantially greater than the confinement scale  $\Lambda_{\text{QCD}}$  and hence these hard gluons have the property of decoding the quantum numbers of the heavy quark. There is therefore a problem in matching operators in full QCD with that of the effective theory due to the emission and absorption of hard gluons. In this regime, the renormalisation of the coefficients of the operators in the effective theory is achieved by a perturbative expansion. An example of this renormalisation issue comes from considering the vector current. In full QCD this current is conserved but matrix elements involving this current yield a logarithmic dependence on  $m_Q$  and in the heavy quark limit of the effective theory renormalisation is unavoidable. The expansion in terms of local operators in the HQET is

$$J_{\text{QCD}} \cong \sum_i C_i(\mu) J_i(\mu)_{\text{HQET}} + \mathcal{O}\left(\frac{1}{m_Q}\right) \quad (3.29)$$

where the quantities  $C_i(\mu)$  are the Wilson coefficients and the operators  $\{J_i\}$  are constructed thus

$$J_i = \bar{h}_Q \Gamma_i h_Q \quad (3.30)$$

where

$$\Gamma_i = \{\gamma^\mu, v^\mu, v'^\mu\} \quad (3.31)$$

for the vector current and

$$\Gamma_i = \{\gamma^\mu \gamma^5, v^\mu \gamma^5, v'^\mu \gamma^5\} \quad (3.32)$$

for the axial current. In the HQET, since the heavy quark velocity  $v$  is not a dynamical degree of freedom, it appears explicitly in the definition of the effective current operators. The expansion of the heavy quark currents is complicated by the fact that there are two heavy quark scales :  $m_b$  and  $m_c$ . Neubert [50, 51] has calculated these Wilson coefficients as a function of the heavy quark masses by comparing the effective and full theories at  $\mathcal{O}(\alpha_s)$ .

### 3.5 Mesonic Form Factors

From the above discussion of Heavy Quark Symmetry, it is apparent that the dynamical quantity with which matrix elements may be parametrised is the heavy quark velocity. By considering the Lorentz properties of the matrix elements for the three spin configurations for a flavour changing weak current, it is found that these currents are expressed in terms of 20 form factors

$$\begin{aligned} \langle \sigma(v') | V^\mu | \bar{\alpha}(v) \rangle &= h_+(w) (v + v')^\mu + h_-(w) (v - v')^\mu, \\ \langle \sigma^*(v', \varepsilon') | V^\mu | \bar{\alpha}(v) \rangle &= i h_V(w) \epsilon^{\mu\nu\alpha\beta} \varepsilon'_\nu v'_\alpha v_\beta, \\ \langle \sigma(v') | V^\mu | \bar{\alpha}^*(v, \varepsilon) \rangle &= i h_{\bar{V}}(w) \epsilon^{\mu\nu\alpha\beta} \varepsilon_\nu v'_\alpha v_\beta, \\ \langle \sigma^*(v', \varepsilon') | V^\mu | \bar{\alpha}^*(v, \varepsilon) \rangle &= - \left[ h_1(w) (v + v')^\mu + h_2(w) (v - v')^\mu \right] \varepsilon'^* \cdot \varepsilon \\ &\quad + h_3(w) \varepsilon'^* \cdot v \varepsilon^\mu + h_4(w) \varepsilon \cdot v' \varepsilon'^*{}^\mu \\ &\quad - \left[ h_5(w) v^\mu + h_6(w) v'^\mu \right] \varepsilon'^* \cdot v \varepsilon \cdot v', \end{aligned} \quad (3.33)$$

for the vector current, and

$$\begin{aligned}
\langle \sigma^*(v', \varepsilon') | A^\mu | \bar{\alpha}(v) \rangle &= h_{A_1}(\omega) (\omega + 1) \varepsilon'^{* \mu} - \left[ h_{A_2}(\omega) v^\mu + h_{A_3}(\omega) v'^\mu \right] \varepsilon^* \cdot v, \\
\langle \sigma(v') | A^\mu | \bar{\alpha}^*(v, \varepsilon) \rangle &= h_{\bar{A}_1}(\omega) (\omega + 1) \varepsilon^\mu - \left[ h_{\bar{A}_2}(\omega) v'^\mu + h_{\bar{A}_3}(\omega) v^\mu \right] \varepsilon \cdot v', \\
\langle \sigma^*(v', \varepsilon') | A^\mu | \bar{\alpha}^*(v, \varepsilon) \rangle &= i \varepsilon^{\mu\nu\alpha\beta} \left\{ \left[ h_7(\omega) (v + v')^\mu + h_8(\omega) (v - v')^\mu \right] \varepsilon_\alpha \varepsilon'_\beta \right. \\
&\quad \left. + \left[ h_9(\omega) \varepsilon'^* \cdot v \varepsilon_\nu + h_{10}(\omega) \varepsilon \cdot v' \varepsilon'_\nu \right] v'_\alpha v_\beta \right\}, \quad (3.34)
\end{aligned}$$

for the axial current and where  $\varepsilon^\mu$  and  $\varepsilon'^\mu$  are the polarisation vectors of the final and initial meson respectively. As introduced above,  $\omega$  is the product of the four velocities and is related to the momentum transfer  $q$ ,

$$\omega \stackrel{def}{=} v \cdot v' = \frac{m_\alpha^2 + m_\sigma^2 - q^2}{2m_\alpha m_\sigma} \quad (3.35)$$

such that  $\omega$  is bounded

$$1 \leq \omega \leq \frac{m_\alpha^2 + m_\sigma^2}{2m_\alpha m_\sigma} \quad (3.36)$$

This can be compared with the pole dominance model used in heavy-light to light-light decays in which the maximum momentum transfer,  $q_{\max}^2$ , is important

$$\omega = \frac{q_{\max}^2 - q^2}{2m_\alpha m_\sigma} + 1. \quad (3.37)$$

Indeed for the heavy-light to heavy-light decays, the range of the recoil is very small in comparison to that of, for example  $B \rightarrow \pi l \nu$ . Typically  $\delta\omega = 0.5$  so there is only a relatively mild variation in the form factors.

The above meson states have been normalised in terms of their velocities. As will be revealed in the following chapter, the normalisation used in the construction of lattice correlation functions is the conventional relativistic normalisation. The two are trivially related

$$|\Theta(v)\rangle = \frac{1}{\sqrt{m_\Theta}} |\Theta(p)\rangle. \quad (3.38)$$

In the infinitely heavy quark limit, an important simplification occurs; the above twenty form factors are reduced to a single universal function [44]. In particular

for the case of a pseudoscalar initial meson,

$$\langle \sigma(v') | V^\mu | \bar{\alpha}(v) \rangle = \xi(\omega, \mu)(v + v')^\mu \quad (3.39)$$

$$\langle \sigma^*(v', \varepsilon') | V^\mu | \bar{\alpha}(v) \rangle = i\xi(\omega, \mu)\varepsilon^{\mu\nu\alpha\beta}\varepsilon_\nu^*v'_\alpha v_\beta \quad (3.40)$$

$$\langle \sigma^*(v', \varepsilon') | A^\mu | \bar{\alpha}(v) \rangle = \xi(\omega, \mu)((\omega + 1)\varepsilon^* - v'\varepsilon^* \cdot v)^\mu \quad (3.41)$$

Therefore in the exact symmetry limit, the nine form factors are related to the universal form factor,

$$h_\Delta(\omega) = (\alpha_\Delta + \beta_\Delta + \gamma_\Delta)\xi(\omega, \mu) \quad (3.42)$$

where

$$\alpha_\Delta = 1 \quad (3.43)$$

when

$$\Delta = +, V, A_1, A_3 \quad (3.44)$$

and

$$\alpha_\Delta = 0 \quad (3.45)$$

when

$$\Delta = -, A_2. \quad (3.46)$$

The quantities  $\beta_\Delta$  correspond to the previously discussed radiative corrections. The remaining quantities  $\gamma_\Delta$  represent power corrections to the currents. These power corrections occur from the consideration of higher dimensional operators manifest in the effective theory. These corrections are clearly non-perturbative in nature. However their effect is much less severe than the radiative corrections imposing a correction on  $h_+$  and  $h_{A_1}$  of only a few percent.

A renormalisation group invariant universal form factor may be defined through

$$\xi(\omega) = \xi(\omega, \mu)K(\omega, \mu) \quad (3.47)$$

where  $K(\omega, \mu)$  contains all the dependence on  $\mu$ , is independent of the spin structure and is normalised at zero recoil,

$$K(1, \mu) = 1 \quad (3.48)$$

and  $\xi(\omega)$  is the famous Isgur-Wise function. The radiative corrections to the naive relations between the form factors and the Isgur Wise function are given in terms of the Wilson coefficients [50] (omitting terms proportional to powers of inverse heavy quark mass),

$$h_+ = \left( C_1 + \frac{\omega + 1}{2}(C_2 + C_3) \right) \xi(\omega) \quad (3.49)$$

$$h_- = \frac{\omega + 1}{2}(C_2 - C_3)\xi(\omega) \quad (3.50)$$

$$h_V = C_1\xi(\omega) \quad (3.51)$$

for the vector current and

$$h_{A_1} = C_1\xi(\omega) \quad (3.52)$$

$$h_{A_2} = C_2\xi(\omega) \quad (3.53)$$

$$h_{A_3} = (C_1 + C_3)\xi(\omega) \quad (3.54)$$

for the axial current.

### 3.6 The Isgur Wise function

The Isgur Wise function encodes all the long distance physics attributed to the interaction through the strong force of the light degrees of freedom. It is a fundamentally non-perturbative quantity and its functional form is not predicted from HQET. However there are some constraints which may be imposed on it. In particular, the Isgur Wise function is found to be normalised to unity at zero recoil. For pseudoscalar to pseudoscalar decay and in terms of the current in the

effective theory [44],

$$\langle X'(v') | \bar{h}_{v'} \gamma^\mu h_v | X(v) \rangle = (v + v')^\mu \xi(\omega) \quad (3.55)$$

From the equations of motion of the effective Lagrangian

$$L_{\text{eff}} = \bar{h}_v i v \cdot D h_v \quad (3.56)$$

it may be shown that

$$i \partial_\mu J^\mu = \bar{h}'_v i v \cdot D h_v + \bar{h}'_v i v \cdot \overleftarrow{D} h_v = 0 \quad (3.57)$$

and hence irrespective of the flavour of the heavy quarks, if the velocities are identical then the vector current is a conserved quantity. The corresponding conserved charges are given by

$$C_{Q'Q} = \int d^3x J^0(x) = \int d^3x h_v'^{\dagger}(x) h_v(x) \quad (3.58)$$

It may be shown that

$$\langle X'(v) | C_{Q'Q} | X(v) \rangle = \langle X(v) | X(v) \rangle \quad (3.59)$$

Comparison with equation 3.55 leads to the conclusion

$$\xi(1) = 1. \quad (3.60)$$

Thus there is no form factor suppression when there is no velocity transfer. Many attempts have been made to parametrise the Isgur Wise function in terms of the velocity transfer. Conventionally the choice has been to introduce a charge radius  $\rho$  such that

$$-\frac{d\xi(\omega)}{d\omega} = \rho^2. \quad (3.61)$$

The simplest such parametrisation of the Isgur Wise function is

$$\xi_{\text{linear}}(\omega) = 1 - \rho^2(\omega - 1) \quad (3.62)$$

Evolved from this is a quadratic form

$$\xi_{\text{QUAD}}(\omega) = 1 - \rho^2(\omega - 1) + c(\omega - 1)^2 \quad (3.63)$$

where the coefficient  $c$  is the curvature at zero recoil. Derived from Stech's oscillator model, Neubert and Rieckert [52] suggested the following as a form for the Isgur Wise function,

$$\xi_{\text{NR}}(\omega) = \frac{2}{\omega + 1} \exp \left[ -\frac{(2\rho^2 - 1)(\omega - 1)}{\omega + 1} \right] \quad (3.64)$$

Similar to the quadratic form, Isgur et al [53] suggest

$$\xi_{\text{ISGW}}(\omega) = \exp [-\rho^2(\omega - 1)]. \quad (3.65)$$

A pole type antatz [45] yields

$$\xi_{\text{POLE}}(\omega) = \left[ \frac{2}{\omega + 1} \right]^{2\rho^2}. \quad (3.66)$$

As discussed above, for heavy light to heavy light decays, the range of recoil is comparatively small. Indeed in the kinematically accessible region ( $1.0 < \omega < 1.6$ ) the above parametrisations for the Isgur Wise function are very similar and are plotted in figure 3.1. Thus in order to establish the correct form of the Isgur Wise function in nature, the precise value of the slope at zero recoil must be determined. Constraints on  $\rho^2$  in the literature are quite spread out. The sum rules of Bjorken [54] and Voloshin [55] give the following lower and upper bound,

$$\frac{1}{4} < \rho^2 < \frac{1}{4} + \frac{m_M - m_Q}{E_{\text{min}}} \quad (3.67)$$

where  $E_{min}$  is the minimum excitation energy relative to the ground state heavy meson and the masses are those of the meson and heavy quark. A more complete discussion of the Isgur Wise function is postponed until chapter 6 where it is used to extract the CKM element  $V_{cb}$ .

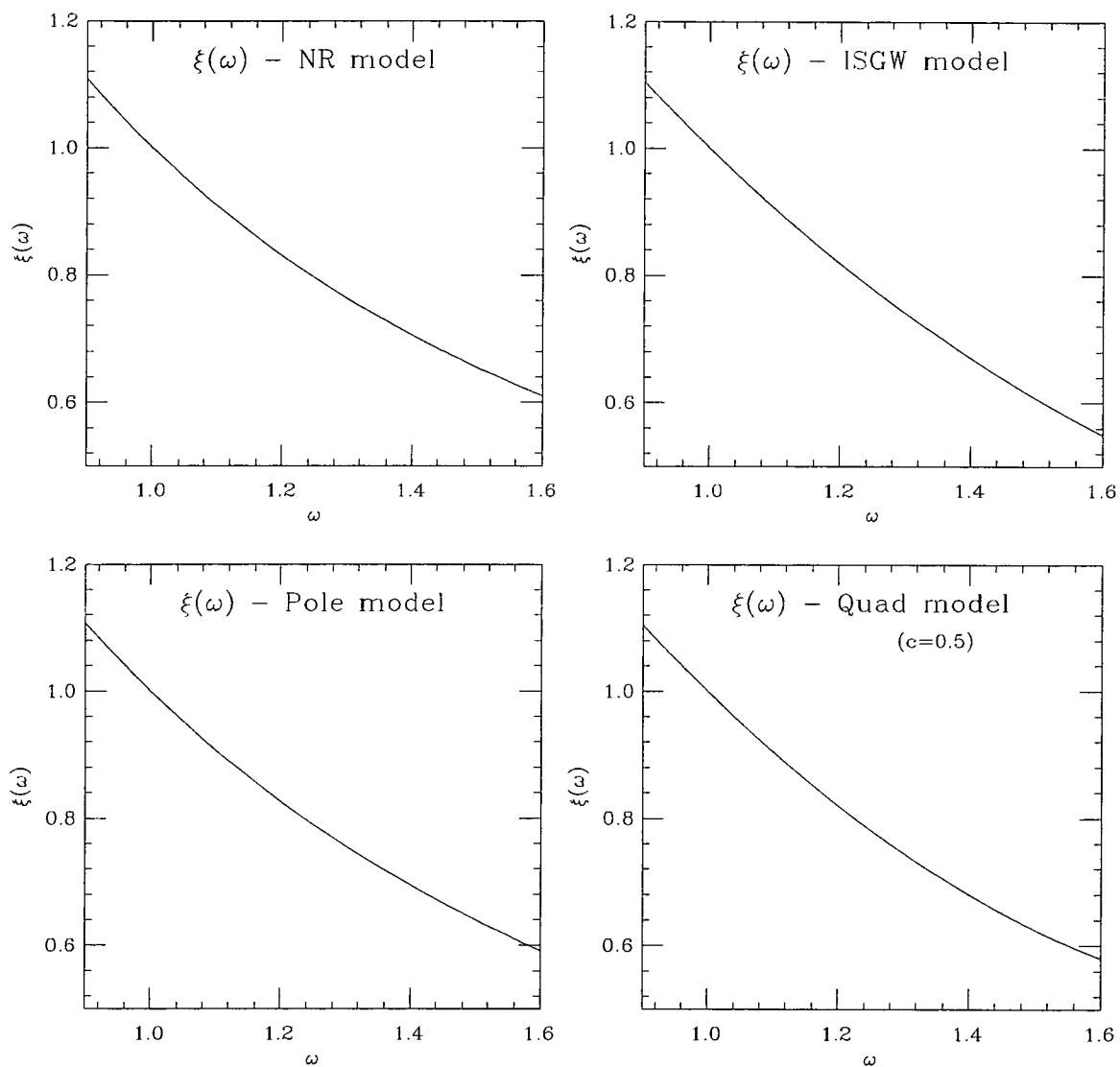


Figure 3.1: Plots of the Isgur Wise function for four different parametrisations as described in the text; for each plot  $\rho^2 = 1$ .

## Chapter 4

### Lattice Correlation Functions

On the lattice, spectroscopic quantities such as meson and baryon masses are calculated from the large Euclidean time behaviour of correlation functions computed from quark propagators. This chapter describes the particular correlation functions required in order to simulate semileptonic decay on the lattice.

#### 4.1 Interpolating Operators

Clearly, in order to correctly simulate the physical spectrum, the field operators used to construct the correlation functions must be chosen such that the quantum numbers of the hadronic state match those of the operators. So for a given hadronic state  $\Theta$  and a corresponding field operator  $\eta$  the requirement is simply expressed through the condition

$$\langle 0|\eta|\Theta\rangle \neq 0. \tag{4.1}$$

For a mesonic state, the simplest choice for the interpolating operator is given by

$$\eta = \bar{q}\Gamma q \tag{4.2}$$

This quantity remains gauge invariant through the implicit assertion that the quark fields  $q$  are at the same point in space-time. The quantity  $\Gamma$  represents one of the sixteen independent Dirac matrices,

$$\Gamma = 1, \gamma^5, \gamma^\mu, \gamma^\mu\gamma^5, \sigma^{\mu\nu}. \tag{4.3}$$

## 4.2 Two Point Functions

The propagation of a meson from one point in space-time to another is defined

$$C_{\text{meson}}(x, 0) = \langle 0 | T \{ \eta(x) \eta^\dagger(0) \} | 0 \rangle \quad (4.4)$$

where  $\eta(x)$  as defined in equation 4.2 is the operator which annihilates the meson at point  $x$ , and correspondingly  $\eta^\dagger(0)$  is the operator which creates the state at the origin. Consequently, it is defined by

$$\eta^\dagger = -\bar{q} \bar{\Gamma} q. \quad (4.5)$$

A generic two point function can be decomposed into its constituent quark and anti-quark propagators, by means of a Wick contraction. Writing the correlator in terms of the path integral formulation,

$$C_{\text{meson}} = \frac{1}{Z} \int D U \text{Tr} \{ C_{q_1}(0, x; U) \Gamma_1 C_{q_2}(x, 0; U) \Gamma_2 \} \quad (4.6)$$

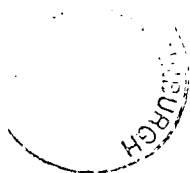
where the trace is taken over the colour and spin indices. Combining this result with the lattice Hermiticity relation for the quark propagators,

$$C_{\alpha\beta}^\dagger(x, 0; U) = \gamma_{\alpha\rho}^5 C_{\rho\delta}(0, x; U) \gamma_{\delta\beta}^5 \quad (4.7)$$

yields the following result,

$$\langle 0 | T \{ \eta(x) \eta^\dagger(0) \} | 0 \rangle = \left\langle \text{Tr} \{ \gamma^5 \Gamma_1 C_{q_1}(x, 0) \Gamma_2 \gamma^5 C_{q_2}^\dagger(x, 0) \} \right\rangle_U \quad (4.8)$$

where the result is averaged over each gauge configuration. Therefore the reproduction of the hadronic spectrum on the lattice reduces to the problem of calculating the quark propagator for each gauge configuration and the use of the Hermiticity relation ensures that the propagator need only be computed from the



origin to all space points. The lattice quark propagator,

$$C(x, y) = \langle 0 | T \{ q(x) \bar{q}(y) | 0 \rangle \quad (4.9)$$

is related to the fermion matrix (equation 2.77) through

$$M_{\alpha\beta}^{ab}(x, y, U) C_{\beta\gamma}^{bc}(y, 0, U) = \delta_{\alpha\gamma} \delta^{ac} \delta(x, 0) \quad (4.10)$$

where the upper indices correspond to colour and the lower ones spin. The average over the gauge configurations is achieved as discussed in section 2.4.3 through a Monte Carlo estimate. The inversion of the fermion matrix may be realised from a number of iterative techniques [56, 57].

#### 4.2.1 Mesonic Observables

The goal of the computation of the meson correlators is to enable the extraction of the mesonic properties of interest, in particular the energies and masses of meson states. This is achieved by looking at the functional dependence of the large Euclidean time correlators. For a given meson with three momentum  $\vec{k}$ , the Fourier transform of equation 4.4 yields

$$C_{\text{meson}}(\vec{k}, t) = \sum_{\vec{x}} C_{\text{meson}}(x, 0) e^{-i\vec{k}\cdot\vec{x}} \sum_{\vec{x}} \langle 0 | \eta(x) \eta^\dagger(0) | 0 \rangle e^{-i\vec{k}\cdot\vec{x}} \quad (4.11)$$

with specific time ordering. This may be rewritten as

$$C_{\text{meson}}(\vec{k}, t) = \sum_{\vec{x}} \langle 0 | e^{(\hat{E}t + i\vec{k}\cdot\vec{x})} \eta(0) e^{-(\hat{E}t + i\vec{k}\cdot\vec{x})} \eta^\dagger(0) | 0 \rangle e^{-i\vec{k}\cdot\vec{x}} \quad (4.12)$$

by making use of translational operator invariance,

$$\Theta(\vec{x}, t) = e^{(\hat{E}t + i\vec{k}\cdot\vec{x})} \Theta(0) e^{-(\hat{E}t + i\vec{k}\cdot\vec{x})} \quad (4.13)$$

Inserting a complete set of states  $|n\rangle$  through the completeness relation,

$$\sum_n \int \frac{d^3 q_n}{8\pi^3} \frac{1}{2E_n} |n\rangle \langle n| = 1 \quad (4.14)$$

gives,

$$\begin{aligned} C_{\text{meson}}(\vec{k}, t) &= \sum_{\vec{x}} \sum_n \int \frac{d^3 q_n}{8\pi^3} \frac{1}{2E_n} \langle 0 | e^{(\hat{E}t + i\vec{\alpha}\cdot\vec{x})} \eta(0) e^{-(\hat{E}t + i\vec{\alpha}\cdot\vec{x})} |n\rangle \langle n | \eta^\dagger(0) | 0 \rangle e^{-i\vec{k}\cdot\vec{x}} \\ &= \sum_{\vec{x}} \sum_n \int \frac{d^3 q_n}{8\pi^3} \frac{1}{2E_n} e^{i(\vec{q}_n\cdot\vec{x} - \vec{k}\cdot\vec{x})} |\langle 0 | \eta(0) | n \rangle|^2 e^{-E_n t} \end{aligned} \quad (4.15)$$

Using a particular definition of the delta function,

$$\sum_{\vec{x}} e^{-i\vec{z}\cdot\vec{x}} = 8\pi^3 \delta^3(\vec{z}) \quad (4.16)$$

the above result reduces neatly to

$$C_{\text{meson}}(\vec{k}, t) = \sum_n \int \frac{1}{2E_n} |\langle 0 | \eta(0) | n \rangle|^2 e^{-E_n t} \delta^3(\vec{k} - \vec{q}_n) d^3 q_n \quad (4.17)$$

Performing the integral over the momenta  $q_n$  leads to the final result,

$$C_{\text{meson}}(\vec{k}, t) = \sum_n \frac{|\langle 0 | \eta(0) | n \rangle|^2}{2E_n} e^{-E_n t}. \quad (4.18)$$

Clearly as  $t \rightarrow \infty$  the ground state will dominate the above expression and then the ground state energy is in principle calculable. If the momentum of the particle is zero then from the dispersion relation, the ground state mass governs the decay of the Fourier transformed correlator.

### 4.3 Three Point Functions

The simulation of a weak matrix element is analogous to that for the hadron spectrum. For a transition from one meson to another mediated by a weak current then clearly three operators are required to describe the physical process,

a meson annihilation operator, a meson creation operator and a current operator. Extending the analysis of the previous section, the relevant three point function is defined as,

$$C_{3pt}^\mu(t_x, t_y, \vec{p}, \vec{q}) = \sum_{\vec{x}, \vec{y}} \langle 0 | T \{ \eta'(x) J^\mu(y) \eta^\dagger(0) \} | 0 \rangle e^{-i\vec{q}\cdot\vec{y}} e^{-i\vec{p}\cdot\vec{x}} \quad (4.19)$$

where  $\eta^\dagger$  creates the final meson,  $\eta'$  annihilates the initial meson and  $J^\mu$  represents the weak current. The notation is such that the initial state has three momentum  $\vec{p}$  while the momentum recoil is denoted by  $\vec{q}$ , resulting in a final state with a momentum of  $(\vec{p} + \vec{q})$ . The time reversed three point function is calculated and in this convention  $t_x < t_y < 0$ . A schematic representation of the weak decay is illustrated in figure 4.1.

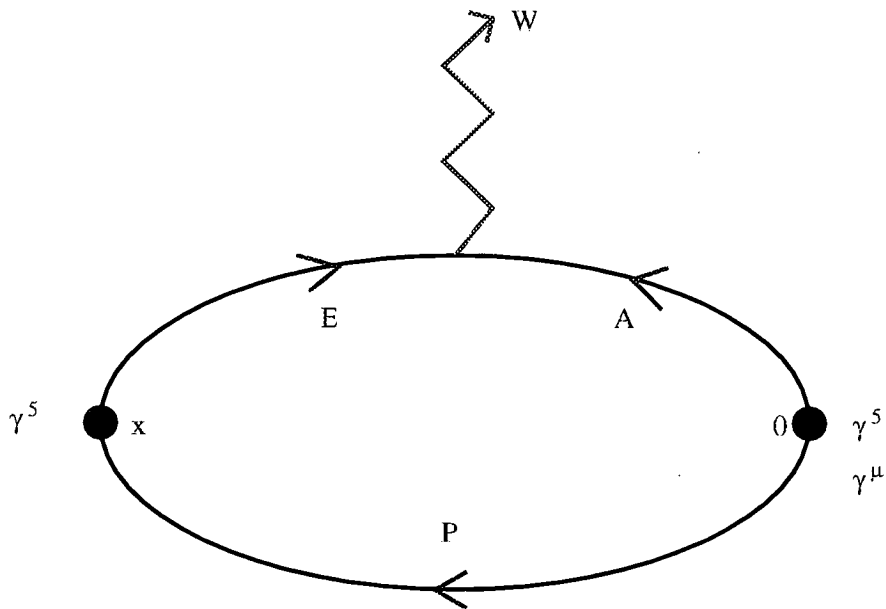


Figure 4.1: Schematic representation of a weak decay.  $E$  denotes the extended quark line,  $A$  the active and  $P$  the passive (which is assumed to take no role in the decay).

For a complete study of the processes listed in equations 3.39-3.41 it is sufficient to consider the following representations for the three current operators

$$\Gamma_E = \gamma^5, \gamma^\mu \quad (4.20)$$

corresponding to a pseudoscalar or vector *initial* meson,

$$J^\mu = \gamma^\mu(1 - \gamma^5) \quad (4.21)$$

corresponding to the vector and axial vector currents and

$$\Gamma_A = \gamma^5, \gamma^\mu \quad (4.22)$$

for a pseudoscalar or vector *final* meson, where in this notation the quark fields have been suppressed. The labels  $A$ ,  $E$  and  $P$  refer to the active (final heavy), extended (initial heavy) and passive (spectator light) quarks.

In terms of the path integral, equation 4.19 may be rewritten as

$$C_{3\text{pt}}^\mu(t_x, t_y, \vec{p}, \vec{q}) = \frac{1}{Z} \sum_{\vec{x}, \vec{y}} e^{-i\vec{p}\cdot\vec{x}} e^{-i\vec{q}\cdot\vec{y}} \int DU D\psi D\bar{\psi} \eta'(x) J^\mu(y) \eta^\dagger(0) e^{-S_{QC D}}. \quad (4.23)$$

Performing the Wick contractions and using the Hermiticity relation, the three point correlation function can be written explicitly in terms of the bare quark propagators and the Dirac structure of the current and interpolating operators,

$$C_{3\text{pt}}^\mu(t_x, t_y, \vec{p}, \vec{q}) = \sum_{\vec{x}, \vec{y}} e^{-i(\vec{p}\cdot\vec{x} + \vec{q}\cdot\vec{y})} \langle \text{Tr}[C_E(y, x; U) \Gamma^E C_P(x, 0; U) \Gamma^A C_A(0, y; U) J^\mu] \rangle_U \quad (4.24)$$

where as for the case of the two point functions, the average is taken over all gauge configurations. There is an implicit difficulty in calculating the above correlator. It requires the costly production of a heavy propagator from all space time points to all space time points. It is therefore prudent to construct this correlator via some other technique.

### 4.3.1 Extended Propagator

The extended propagator is simply defined as,

$$\chi(y, 0, t_x, \vec{p}; U) = \sum_{\vec{x}} e^{-i\vec{p}\cdot\vec{x}} C_E(y, x; U) \Gamma^E C_P(x, 0; U) \quad (4.25)$$

The construction of a quark propagator involves the inversion of the fermion matrix (equation 2.77). Motivated by this, the operation of the inverse heavy propagator on the extended propagator yields,

$$G_E^{-1}(z, y; U) \chi(y, 0, t_x, \vec{p}; U) = \delta(t_z, t_x) e^{i\vec{p}\cdot\vec{z}} \Gamma^E C_P(z, 0; U) \quad (4.26)$$

so then the calculation of the extended propagator is analogous to that of a regular propagator with the particular distinction that the source is in effect the timesliced light propagator.

### 4.3.2 Explicit time dependence

A functional form for the three point correlators in terms revealing the implicit time dependence may be realised in an analogous fashion to that for the meson correlators. Inserting two complete sets of states (denoted  $\alpha, \beta$ ) into equation 4.19 gives

$$\begin{aligned} C_{3\text{pt}}^\mu(t_x, t_y, \vec{p}, \vec{q}) &= \frac{1}{L^6} \sum_{\vec{x}, \vec{y}, \alpha, \beta, k_\alpha, k_\beta} \frac{1}{4a^2} e^{-i(\vec{p}\cdot\vec{x} + \vec{q}\cdot\vec{y})} \frac{1}{E_\alpha(\vec{k}_\alpha)} \frac{1}{E_\beta(\vec{k}_\beta)} \\ &\times \langle 0 | \eta'(x) | \alpha, \vec{k}_\alpha \rangle \langle \beta, \vec{k}_\beta | \eta^\dagger(0) | 0 \rangle \\ &\times \langle \alpha, \vec{k}_\alpha | J^\mu(y) | \beta, \vec{k}_\beta \rangle \end{aligned} \quad (4.27)$$

Using the Euclidean translational invariance of the operators and applying the definition of the delta function (equation 4.16) to remove the summations over the space time points yields,

$$\begin{aligned}
C_{3\text{pt}}^\mu(t_x, t_y, \vec{p}, \vec{q}) &= \sum_{\alpha, \beta} \frac{e^{E_\alpha(t_x - t_y)}}{2E_\alpha(\vec{p})} \frac{e^{E_\beta(t_y)}}{2E_\beta(\vec{p} + \vec{q})} \\
&\quad \langle 0 | \eta'(0) | \alpha, \vec{p} \rangle \langle \beta, \vec{p} + \vec{q} | \eta^\dagger(0) | 0 \rangle \\
&\quad \langle \alpha, \vec{p} | J^\mu(0) | \beta, \vec{p} + \vec{q} \rangle
\end{aligned} \tag{4.28}$$

The Euclidean time dependence of the three point correlator is compared with that for a meson in chapter 6.

## 4.4 Smearing

Recall from section 4.1, the definition of a meson correlator (equation 4.4). To ensure that a numerical simulation of the hadron spectrum matches that of the continuum, it is clear that an interpolating field be chosen such that it maximises the overlap with the desired state (equation 4.1).

For such an operator with a non zero overlap on the required meson, this may be written,

$$\eta(0)|\Theta\rangle = \sum_{i=0} \beta_i |i\rangle \tag{4.29}$$

An obvious requirement for a suitable operator is therefore one in which the coefficient  $\beta_0$  dominates. As equation 4.18 suggests, although the ground state will dominate the analysis of the large Euclidean time correlator, contamination from the excited states will lead to a poorer signal. Quite obviously, the excited state contributions could be greatly diminished by increasing the extent of the temporal component of the lattice, however this is expensive. This section focuses on other techniques enabling the minimisation of this contamination.

### 4.4.1 Jacobi Smearing

An obvious idea to try to select only the ground state of the hadron, is to attempt to reproduce the wavefunction of the s-wave [58]. Such a wavefunction is spherically symmetric, and therefore on the lattice with its reduced geometry,

this may be realised in a number of ways.

The smearing of hadrons on the lattice is applied at the quark level. The quark propagators may be smeared at both source and sink. This is realised through modified definitions of the quark fields. In particular in the case of sink smearing,

$$\phi^s(\vec{x}, t) = \sum_{\vec{y}} S(\vec{x}, \vec{y}) \phi(\vec{y}, t) \quad (4.30)$$

for some smearing function  $S(\vec{x}, \vec{y})$ . The problem of introducing this smearing technique reduces neatly to the solution the following equations,

$$\sum_{\vec{y}} M(\vec{x}, \vec{y}) S(\vec{y}, 0) = \delta(\vec{x}, 0) \quad (4.31)$$

analogous to the generation of quark propagators. The most notable technique for this inversion is the Jacobi algorithm, in which the smearing manifests itself in the construction of an octahedral collection of gauge links.

#### 4.4.2 Fuzzing

The Fuzzing technique is a more advanced smearing algorithm [59]. The procedure is to create gluon flux tubes which connect a quark and an antiquark at some fixed distance. This is shown schematically in figure 4.2. These gluon flux tubes are developed through an iterative technique. Each gauge link is replaced by itself and a combination of spatial staples, so then

$$U_\mu(x) \rightarrow \mathcal{U}_\mu(x) = P_{SU(3)} \left[ cU_\mu(x) + \sum_{\mu \neq \nu} U_\nu(x) U_\mu(x + a\hat{\nu}) U_\nu^\dagger(x + a\hat{\mu}) \right] \quad (4.32)$$

As in the case of Jacobi smearing, it is the quark propagators which are fuzzed, although the computational cost of Fuzzing is much smaller than that required for Jacobi smearing. The spatial extent of the fuzzing is controlled through a parameter  $r$  (figure 4.2), which is chosen to minimise the contribution from the first excited state.

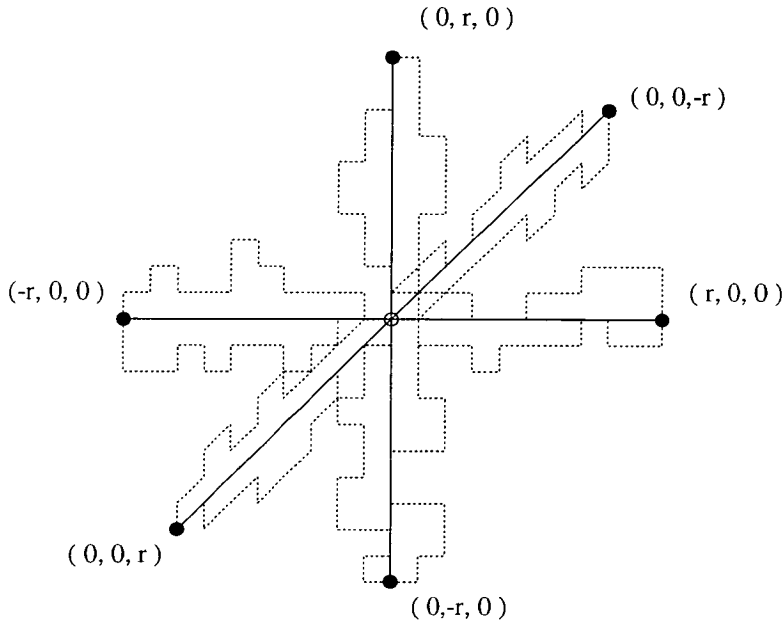


Figure 4.2: Schematic guide to the fuzzing prescription.

#### 4.4.3 Gauge Invariant Smearing for Heavy Quarks

As discussed in section 3.1, heavy light systems have the property that the light degrees of freedom are characterised by momenta of  $\mathcal{O}(\Lambda_{QCD})$ , with a Compton wavelength much larger than that of the heavy quark. In such a regime, it may be possible to describe the heavy quark in terms of non relativistic QCD. In such an approximation, non-relativistic wavefunctions may be used to describe the hadron [60]. The overlap of such a wavefunction with a smearing function may be given by

$$C_{nm} = \int d^3x \psi_m^*(\vec{x}) S_n(\vec{x}, 0). \quad (4.33)$$

The new gauge invariant smearing technique is defined,

$$\psi(x) \rightarrow \psi^{GIF}(x) = \frac{1}{4} \sum_{r=0}^N (2r+1)^2 \phi_n(r) \sum_{i=\pm x, \pm y, \pm z} \left[ \prod_{n=0}^r U_i(x+ni) \right] \psi(x+ri) \quad (4.34)$$

where the links  $U$  are simply the fuzzed links discussed in the previous section. The function  $\phi_m$  is chosen to approximate the true wavefunction  $\psi_m$ . This approximate wavefunction is a quantity which may be chosen so that the technique more effectively screens out the unwanted excited states. It is common, and indeed it is the choice for the work in this thesis, that the trial function is the hadronic wavefunction and the efficiency of the smearing technique is controlled through the Bohr radius,  $R_0$ , of the smearing function.

## 4.5 Statistical Analysis

The clear goal of hadronic physics on the lattice is the faithful reproduction of physical observables. This is achieved as previously indicated by studying the large Euclidean time behaviour of correlators. The expectation values of operators can be estimated from the average over an ensemble of gauge configurations. For  $N$  statistically independent configurations, the statistical error falls off only as  $\frac{1}{\sqrt{N}}$ . The aim is to get a reliable estimate of the error from a relatively small number of gauge configurations.

The method used to estimate the errors in the subsequent chapters of this thesis is the Bootstrap resampling technique [61]. This technique involves creating ensembles of configurations from the original set. For a given set of  $N$  configurations, the new ensembles are created, with the same number of configurations as the original, by randomly sampling from the set allowing repetitions. Then on each new ensemble the covariance matrix,

$$\sigma(t_i, t_j) = \frac{1}{N(N-1)} \sum_{k=1}^N (C_k(t_i) - \bar{C}(t_i))(C_k(t_j) - \bar{C}(t_j)) \quad (4.35)$$

may be calculated where  $C_k(t)$  is the value of the correlator at some time  $t$ , and  $\bar{C}$  is the average over all  $N$  configurations.

The data is fitted to some analytic model function. For a generic model function  $g(\rho_i)$ , the fit parameters  $\rho_i$  are obtained by performing a least  $\chi^2$  fit, tantamount

to minimising the function,

$$\chi^2 = \sum_{t_i, t_j} [g(t_i; \rho_k) - \bar{f}(C(t_i))] \sigma^{-1}(t_i, t_j) [g(t_j; \rho_k) - \bar{f}(C(t_j))] \quad (4.36)$$

where  $\sigma^{-1}(t_i, t_j)$  is the inverse of the covariance matrix. This minimisation procedure is achieved using a Marquardt-Levenberg numerical algorithm [62]. The errors in the fit parameters corresponds to a 68% confidence level on a bootstrap distribution containing 1000 ensembles. A measure of the quality of the fit is given by  $\frac{\chi^2}{dof}$ , where  $dof$  corresponds to the number of degrees of freedom which is defined as the difference between the number of data points in the fit and the number of parameters  $\rho_i$ . The result  $\frac{\chi^2}{dof} = 1$  is indicative that the fit has been of a high calibre.

# Chapter 5

## Meson Spectrum

### 5.1 Simulation Details

The simulation was performed on a Cray T3D housed at the Edinburgh Parallel Computing Centre using processor resources allocated to the UKQCD collaboration. The gauge configurations were created in the quenched approximation, using the standard Wilson gauge action described in section 2.1.2. at two different values of the coupling;  $\beta = 6.0$  and  $\beta = 6.2$ . The Cabibbo-Marinari [63] and over-relaxation [64] algorithms were employed to generate the Wilson glue, both using periodic boundary conditions.

Both the heavy and light quark propagators were generated using the  $\mathcal{O}(a)$  improved Sheikholeslami-Wohlert Wilson fermion action with a non-perturbatively determined value for the improvement coefficient  $c_{\text{sw}}$ . The inversion of the fermion matrix was achieved using the BiCGstab [57] algorithm, with periodic spatial and anti-periodic temporal boundary conditions. For each dataset there are three values of the light quark hopping parameter and four values of the heavy quark hopping parameter.

The light propagators are either fuzzed at source and sink or local (point) at source and sink. The heavy propagators are smeared using the gauge invariant technique discussed in section 4.4.3. The lattice details for both datasets are summarised in tables 5.1 and 5.2.

$\beta$	Volume	$a^{-1}(\sqrt{\sigma})$	$a^{-1}(\rho)$ (GeV)	$a^{-1}(r_0)$	$ N_s $ (fm)	Number of configurations
6.0	$16^3 \times 48$	1.89	1.86	2.20	1.674	305
6.2	$24^3 \times 48$	2.64	2.60	2.94	1.795	216

Table 5.1: Details of the two different lattices showing the difference in the lattice spacing using the string tension,  $\rho$  meson mass and  $r_0$  (the hadronic radius) to set the scale [65].

$\beta$	$c_{sw}$	$\kappa_q$	$\kappa_Q$	Fuzz Radius $r$	Bohr Radius $R_0$
6.0	1.769	0.13344	0.11230	6.0	2.2
		0.13417	0.11730		
		0.13455	0.12230		
			0.12730		
6.2	1.614	0.13460	0.12000	8.0	3.0
		0.13510	0.12330		
		0.13530	0.12660		
			0.12990		

Table 5.2: Details of the quark propagators for both datasets. As described in the text, the fuzz radius (in lattice units) corresponds to  $\kappa_q$  and the Bohr radius to  $\kappa_Q$ .

## 5.2 Meson Spectrum

In section 4.2.1, it was shown that the large Euclidean time behaviour of a meson with spatial momentum  $\vec{k}$  may be written as,

$$C_{\text{meson}}(\vec{k}, t) = \sum_n \frac{|\langle 0 | \eta(0) | n \rangle|^2}{2E_n} e^{-E_n t} \quad (5.1)$$

Periodic boundary conditions on the lattice ensure only a finite set of allowed momenta for the correlation functions, so that

$$\vec{k} = \frac{2\pi}{aL} (n_x, n_y, n_z) \quad (5.2)$$

with  $n_i$  integer. The momentum channels used in both datasets are tabulated below. Since the statistical noise inherent in the correlation functions increases with the magnitude of the momentum then the momentum  $\vec{k}$  is restricted such that

$$|\vec{k}| = 0, 1, \sqrt{2}, \sqrt{3}, 2 \quad (5.3)$$

in units of  $\frac{2\pi}{aL}$ .

Channel	$n_x$	$n_y$	$n_z$
0	0	0	0
1	1	0	0
2	0	1	0
3	0	0	1
4	1	1	0
5	1	0	1
6	0	1	1
7	1	1	1
8	2	0	0
9	0	2	0
10	0	0	2

Table 5.3: Momentum channels for the meson correlators.

### 5.2.1 Fit Procedure

Following the functional form of the meson correlator, an obvious choice for a corresponding fitting function would be,

$$C(t) = \alpha e^{-\beta t} \quad (5.4)$$

However a meson can propagate both forwards and backwards in the temporal direction from its creation point. From the (anti)periodic boundary condition imposed in this lattice direction, the extent of the propagation is half the temporal extent of the lattice. For an infinite number of gauge configurations and using time reversal symmetry ( $\gamma_4\gamma_5$ ) the meson propagator is symmetric about  $\frac{T}{2}$ . Therefore, the meson correlators may be *folded* about the mid-point of the

lattice, effectively increasing the statistics and improving the stability of the fit, by making the replacement,

$$C(t) \rightarrow \frac{C(t) + C(T-t)}{2} \quad (5.5)$$

The mesons are therefore fitted to the following form,

$$C(t) = \alpha(e^{-\beta t} + e^{\beta(t-T)}) \quad (5.6)$$

which may be re-written,

$$C(t) = 2\alpha e^{-\frac{\beta T}{2}} \cosh\left(\beta\left(t - \frac{T}{2}\right)\right). \quad (5.7)$$

Since it is the ground state that is required, it is imperative that the fit to the above functional form occurs for a time range when the effect of the excited states is negligible. This can be achieved by studying ratios of adjacent time-sliced correlator values. The *effective mass* function is defined to be

$$m_{\text{eff}}(t) = \log\left[\frac{C(t)}{C(t+1)}\right]. \quad (5.8)$$

In the large Euclidean time limit, this function will be asymptotic about the ground state mass. Therefore the fit range may be determined from the nature of the plateau of the effective mass function. Figures 5.1 and 5.2 show the effective mass functions for both a light-light and a heavy-light pseudoscalar meson for each dataset. Following analysis of the effective mass functions, the optimal fit range for the light-light mesons is found to be 8 – 22, and 12 – 22 for the heavy-light mesons. The plateaux are consistent for both datasets.

### 5.3 Vector Mesons

The vector meson interpolating field is given by,

$$\eta^\mu(x) = \bar{\psi}(x)\gamma^\mu\psi(x). \quad (5.9)$$

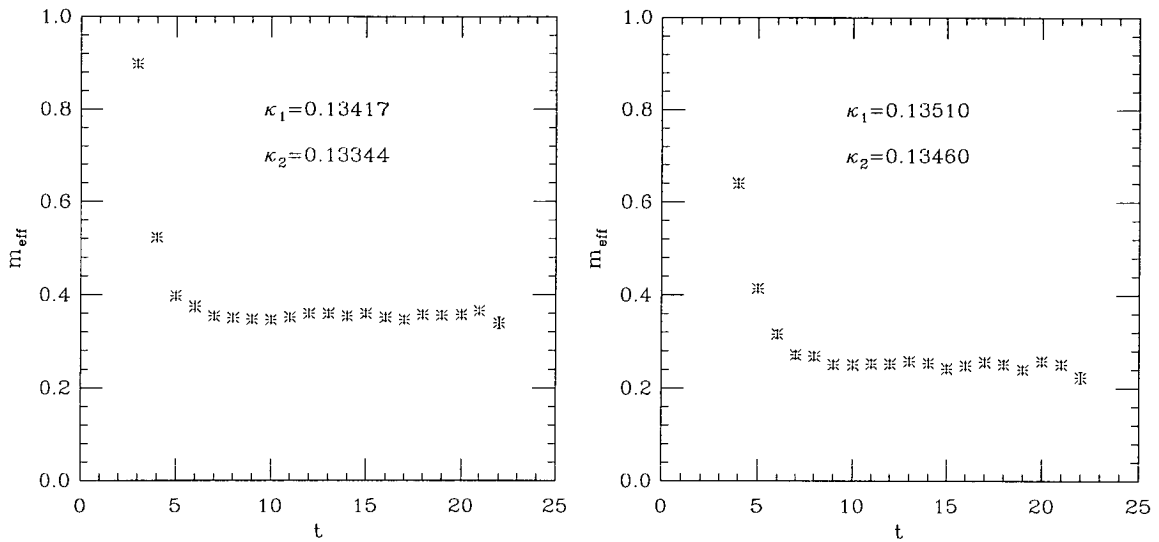


Figure 5.1: Effective mass plots for light-light pseudoscalar mesons (left  $\beta = 6.0$ , right  $\beta = 6, 2$ ). In both cases the propagator with  $\kappa_1$  is local at source and sink, and that with  $\kappa_2$  is fuzzed at source and sink.

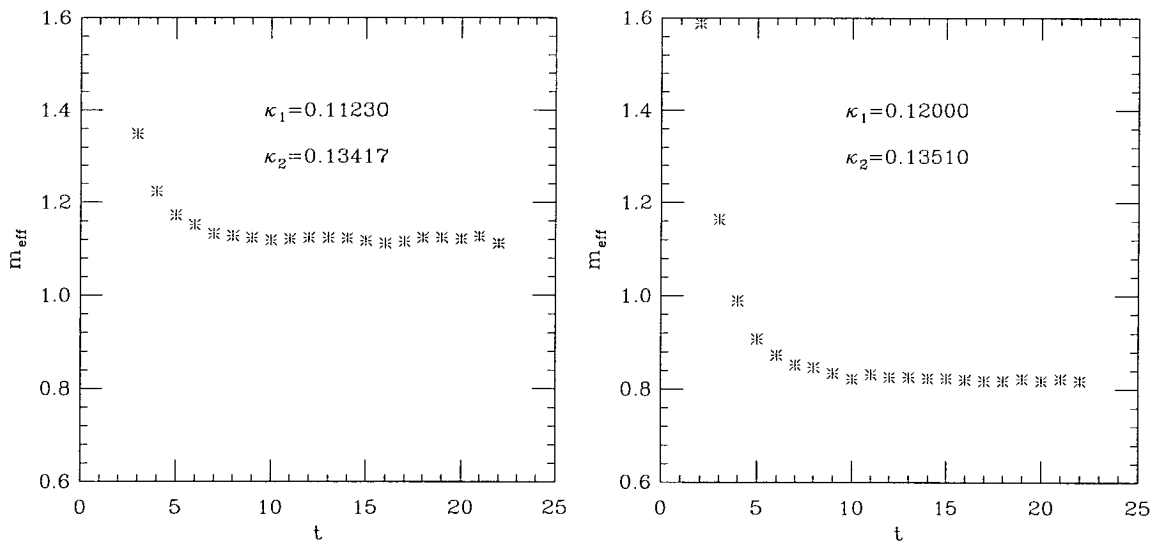


Figure 5.2: Effective mass plots for heavy-light pseudoscalar mesons (left  $\beta = 6.0$ , right  $\beta = 6, 2$ ). In both cases the propagator with  $\kappa_1$  is wavefunction smeared at source and sink, and that with  $\kappa_2$  is local at source and sink.

An analogous analysis to section 4.2.1, reveals the form of the large Euclidean time vector meson correlator,

$$C_{\text{meson}}^{\mu\nu}(\vec{k}, t) = \sum_{\tau=1}^3 \frac{e^{-E(\vec{k})t}}{2E(\vec{k})} \langle 0 | \eta^\mu(0) | V_\tau \rangle \langle V_\tau | \eta^{\nu\dagger}(0) | 0 \rangle \quad (5.10)$$

where the sum is over the polarisation states. The overlap of the interpolating field and the vector state can be written as

$$\epsilon_\tau^\mu Z(|\vec{k}|^2) = \langle 0 | \eta^\mu(0) | V_\tau \rangle. \quad (5.11)$$

The explicit polarisations can be removed using the polarisation sum,

$$\sum_{\tau=1}^3 \epsilon_\tau^\mu \epsilon_\tau^\nu = \frac{1}{m^2} k^\mu k^\nu - g^{\mu\nu}. \quad (5.12)$$

Hence the vector correlator is

$$C_{\text{vmeson}}^{\mu\nu}(\vec{k}, t) = \left[ \frac{1}{m^2} k^\mu k^\nu - g^{\mu\nu} \right] \frac{e^{-E(\vec{k})t}}{2E(\vec{k})} |Z(|\vec{k}|^2)|^2 \quad (5.13)$$

which, when assuming the on-shell condition, may be defined as

$$C_{\text{vmeson}}(\vec{k}, t) = \frac{-3e^{-E(\vec{k})t}}{2E(\vec{k})} |Z(|\vec{k}|^2)|^2. \quad (5.14)$$

The vector mesons are fitted in exactly the same way as the pseudoscalar mesons. Figures 5.3 and 5.4 show the effective mass plots for vector states with the same quark content as those shown in figures 5.1 and 5.2.

## 5.4 Chiral Extrapolation

In section 2.2.3, the bare unrenormalised quark mass was defined

$$m_q = \frac{1}{2} \left( \frac{1}{\kappa} - \frac{1}{\kappa_c} \right). \quad (5.15)$$

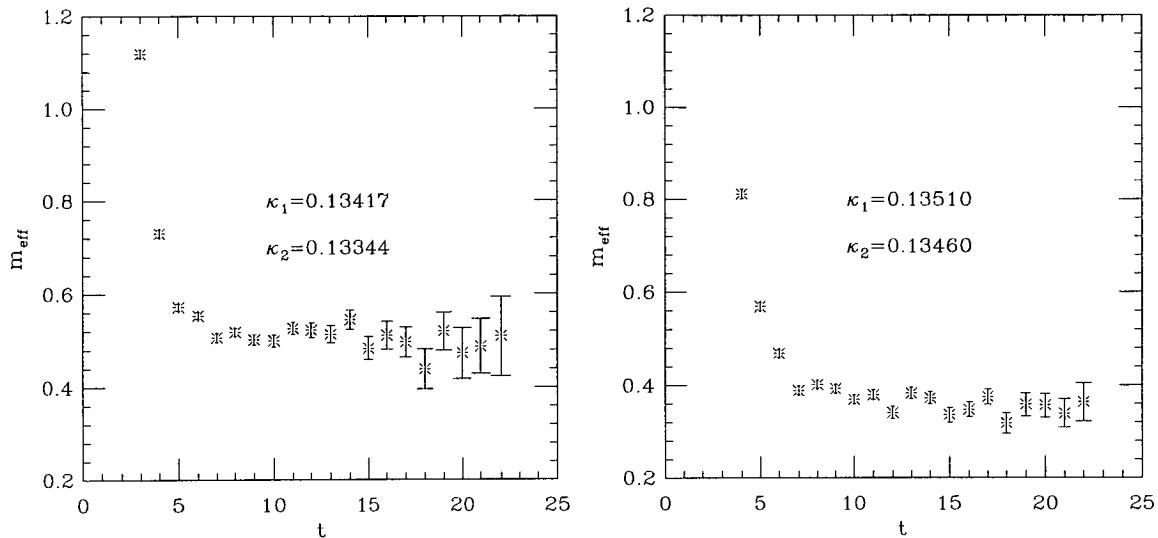


Figure 5.3: Effective mass plots for vector light-light mesons. In both cases the propagator with  $\kappa_1$  is local at source and sink, and that with  $\kappa_2$  is fuzzed at source and sink.

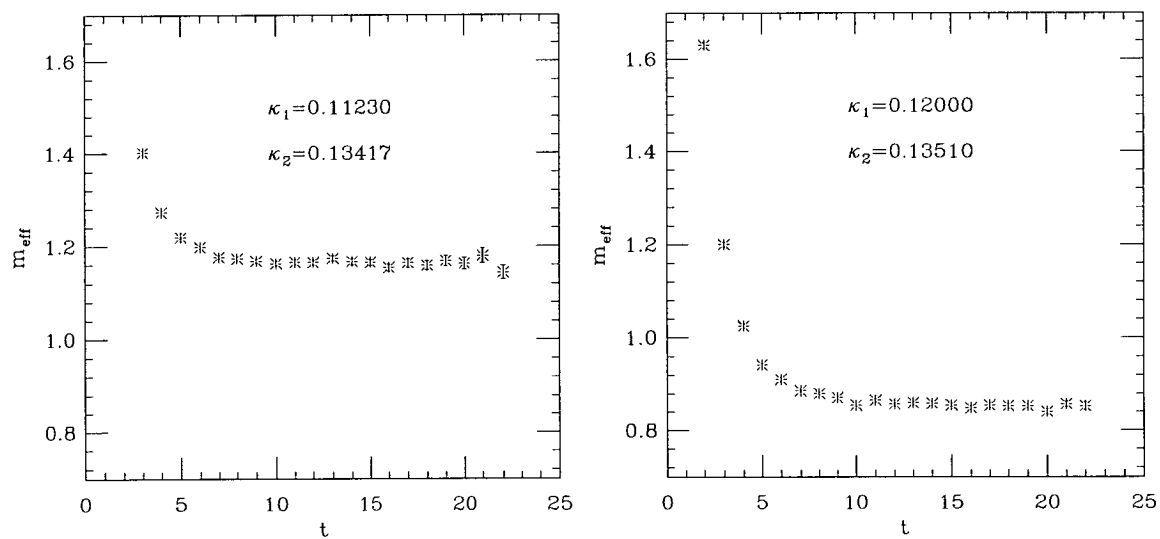


Figure 5.4: Effective mass plots for vector heavy-light mesons. In both cases the propagator with  $\kappa_1$  is wavefunction smeared at source and sink, and that with  $\kappa_2$  is local at source and sink.

The critical hopping parameter,  $\kappa_c$ , is an *a priori* unknown quantity. Therefore any lattice measurement of the hadronic spectrum necessarily requires an explicit calculation of  $\kappa_c$ . The dependence of light-light mesons on the quark masses is obtained from Quenched Chiral Perturbation Theory [66, 67]. It states that the pseudoscalar mass has the following functional dependence,

$$M_{\text{pseudo}}^2 = \alpha(m_1 + m_2)(1 + \beta \log(m_1 + m_2)) + \dots \quad (5.16)$$

where the ellipsis represent higher order terms in the quark masses. In the following analysis, the effect of the quenched chiral logarithms will be ignored so that

$$M_{\text{pseudo}}^2 = \tilde{\alpha}(m_1 + m_2). \quad (5.17)$$

In order to complete the improvement prescription, the bare quark mass is redefined [31],

$$a\tilde{m}_q = am_q(1 + b_m am_q) \quad (5.18)$$

The quantity  $b_m$  depends on the coupling and has been computed non-perturbatively only for  $\beta = 6.2$  [68]. Therefore in the current analysis, this coefficient is obtained from perturbation theory [69]. Defining the boosted coupling as the replacement,

$$\tilde{g}_0^2 \rightarrow \frac{g_0^2}{u_0^4} \quad (5.19)$$

where  $u_0$  is given by,

$$u_0^4 = \frac{1}{3} \langle \Re \text{Tr} U^\square \rangle. \quad (5.20)$$

then the boosted perturbation expansion for  $b_m$  to  $\mathcal{O}(\tilde{g}_0^2)$  is

$$b_m(\tilde{g}_0) = -\frac{1 + 0.1924\tilde{g}_0^2}{2} \quad (5.21)$$

which yields

$$\begin{aligned} b_m|_{\beta=6.0} &= -0.6620 \\ b_m|_{\beta=6.2} &= -0.5931 \end{aligned} \quad (5.22)$$

Inserting equation 5.18 into the result of quenched chiral perturbation theory leads to the following form for the dependence of pseudoscalar mass on the hopping parameters,

$$M_{\text{pseudo}}^2 = \rho + \sigma \left( \frac{1}{\kappa_1} + \frac{1}{\kappa_2} \right) + \eta \left( \frac{1}{\kappa_1^2} + \frac{1}{\kappa_2^2} \right) \quad (5.23)$$

where

$$\rho = \frac{\tilde{\alpha}}{2\kappa_c^2} (b_m - 2\kappa_c), \quad (5.24)$$

$$\sigma = \frac{\tilde{\alpha}}{2\kappa_c} (\kappa_c - b_m), \quad (5.25)$$

$$\eta = \frac{b_m \tilde{\alpha}}{4} \quad (5.26)$$

The light-light pseudoscalar correlators are fitted to this prescription and the results shown in table 5.4 for both datasets. Figure 5.5 shows the dependence of the pseudoscalar mass against the sum of the improved quark masses. The data adhere to the prediction of equation 5.17 and therefore the omission of chiral logarithms is justified. The masses and amplitudes of pseudoscalar (and vector) mesons for the six kappa combinations for  $\beta = 6.0$  and  $\beta = 6.2$  are listed in tables B.1 and B.2.

$\beta$	$\kappa_c$	$\tilde{\alpha}$	$\chi^2/dof$
6.0	0.13525 $\begin{smallmatrix} +6 \\ -4 \end{smallmatrix}$	1.640 $\begin{smallmatrix} +10 \\ -8 \end{smallmatrix}$	1.43692/4
6.2	0.13583 $\begin{smallmatrix} +3 \\ -1 \end{smallmatrix}$	1.216 $\begin{smallmatrix} +9 \\ -6 \end{smallmatrix}$	0.354463/4

Table 5.4: Results of light-light chiral extrapolation of pseudoscalar meson mass.

## 5.5 Strange extrapolation

The hopping parameter corresponding to the strange quark mass will be required in the following chapter to analyse the physical form factors. The lattice strange

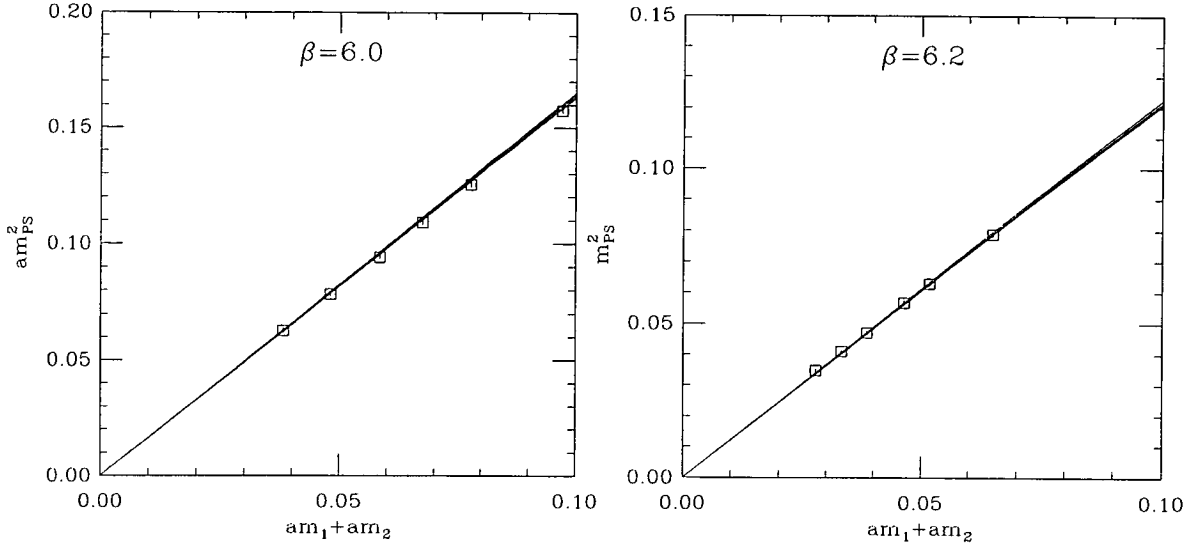


Figure 5.5: Linear plot of squared pseudoscalar mass against boosted perturbation theory improved quark mass

quark mass may be defined,

$$am_s = \left( \frac{a}{r_0} \right)_{\text{latt}}^2 \times (m_K r_0)_{\text{physical}}^2 \times \frac{1}{\tilde{\alpha}} \quad (5.27)$$

The physical product used in this analysis is [14],

$$(m_K r_0) = \frac{495.7 \text{MeV} \times 0.5 \text{fm}}{197.33 \text{MeVfm}} = 1.256 \quad (5.28)$$

The lattice ratio is derived from the analytic expression by Guagnelli et al. [70],

$$\log \left( \frac{a}{r_0} \right) = -1.6805 - 1.7139(\beta - 6) + 0.8155(\beta - 6)^2 - 0.6667(\beta - 6)^3. \quad (5.29)$$

Hence using the coefficient  $\tilde{\alpha}$  from table 5.4, the lattice strange quark masses are,

$$am_s|_{\beta=6.0} = 0.03338 \begin{matrix} +16 \\ -20 \end{matrix}$$

$$am_s|_{\beta=6.2} = 0.02396 \begin{matrix} +13 \\ -17 \end{matrix} \quad (5.30)$$

The hopping parameter  $\kappa_s$  corresponding to the strange quark mass, is found from the solution of

$$\frac{b_m}{2}\theta^2 + \left(1 - \frac{b_m}{\kappa_c}\right)\theta - \left(2(am_s) + \frac{1}{\kappa_c} \left[1 - \frac{b_m}{\kappa_c}\right]\right) = 0 \quad (5.31)$$

where  $\theta\kappa_s = 1$ . Hence the strange quark hopping parameter values are,

$$\begin{aligned} \kappa_s|_{\beta=6.0} &= 0.13400 \begin{matrix} +1 \\ -1 \end{matrix} \\ \kappa_s|_{\beta=6.2} &= 0.13493 \begin{matrix} +1 \\ -1 \end{matrix}. \end{aligned} \quad (5.32)$$

For both lattices, the strange quark hopping parameter has a value between the two heaviest of the light hopping parameters used in the simulation.

## 5.6 Heavy-Light Mesons

It is assumed that the dependence of the heavy-light meson masses on the heavy quark mass is negligible, whilst the dependence on the light quark mass is linear. So then, for both vector and pseudoscalar mesons,

$$m_{\text{PS}} = m_V = \alpha + \beta \left( \frac{1}{\kappa_l} - \frac{1}{\kappa_c} \right) \left( 1 + \frac{b_m}{2} \left[ \frac{1}{\kappa_l} - \frac{1}{\kappa_c} \right] \right) \quad (5.33)$$

The heavy-light mesons are fitted to the same prescription as for the light-light mesons. The results of the fits to extract the masses and amplitudes are given in tables B.3-B.4. Figures 5.6-5.9 show the chiral extrapolation for the heavy-light pseudoscalar and vector mesons for both datasets. It is clear from the plots that the form of the extrapolation is valid. Figure 5.10 shows the chirally extrapolated heavy-light masses for each of the heavy quarks. The solid horizontal lines represent the  $D^0$  mass and the  $D^{*+}$  mass in lattice units setting the lattice spacing with three different scales. From this it is clear that the second heaviest hopping parameter can be associated with the charm quark mass.

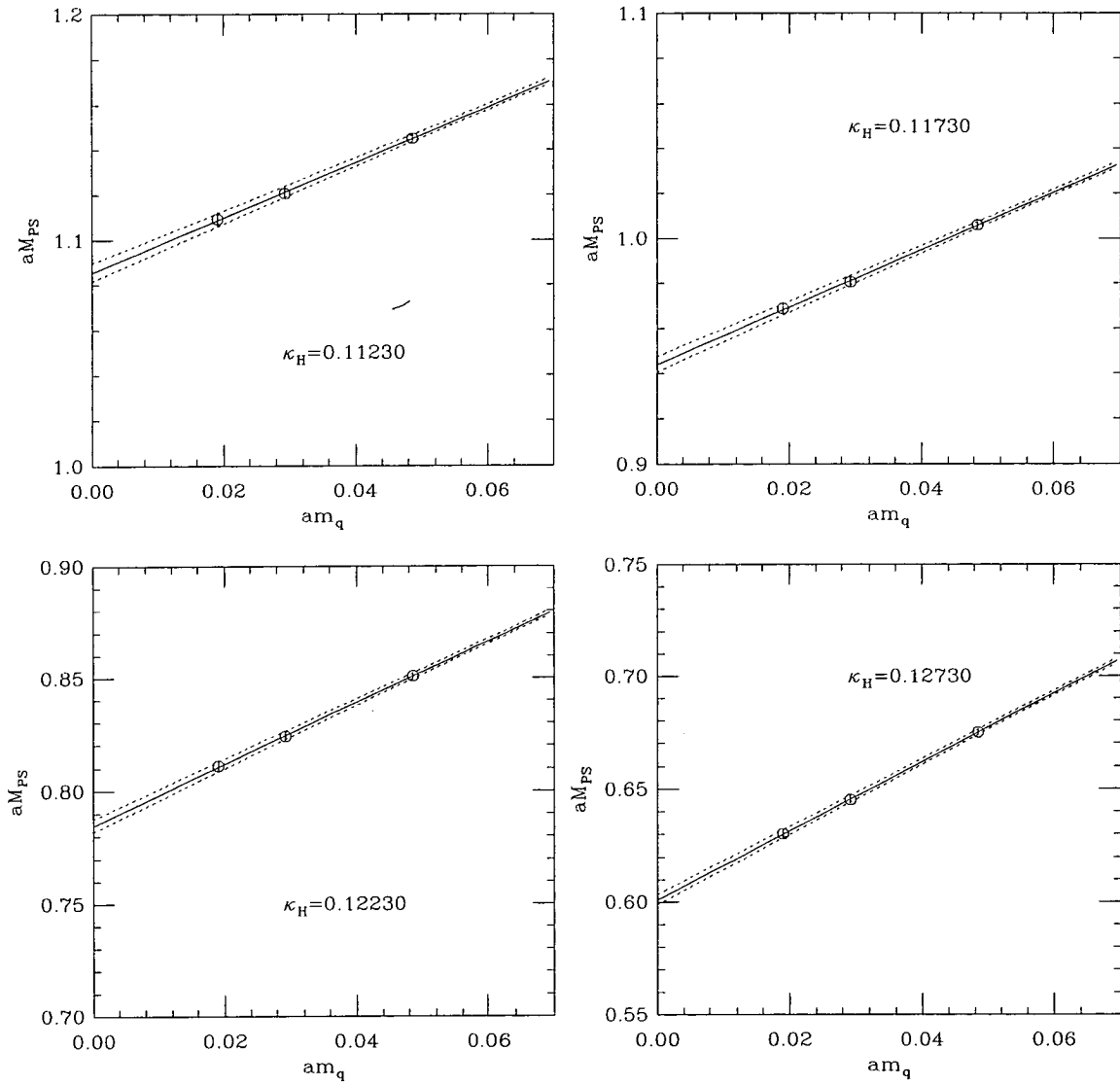


Figure 5.6: Linear chiral extrapolations for the heavy-light pseudoscalar mesons at  $\beta = 6.0$ .

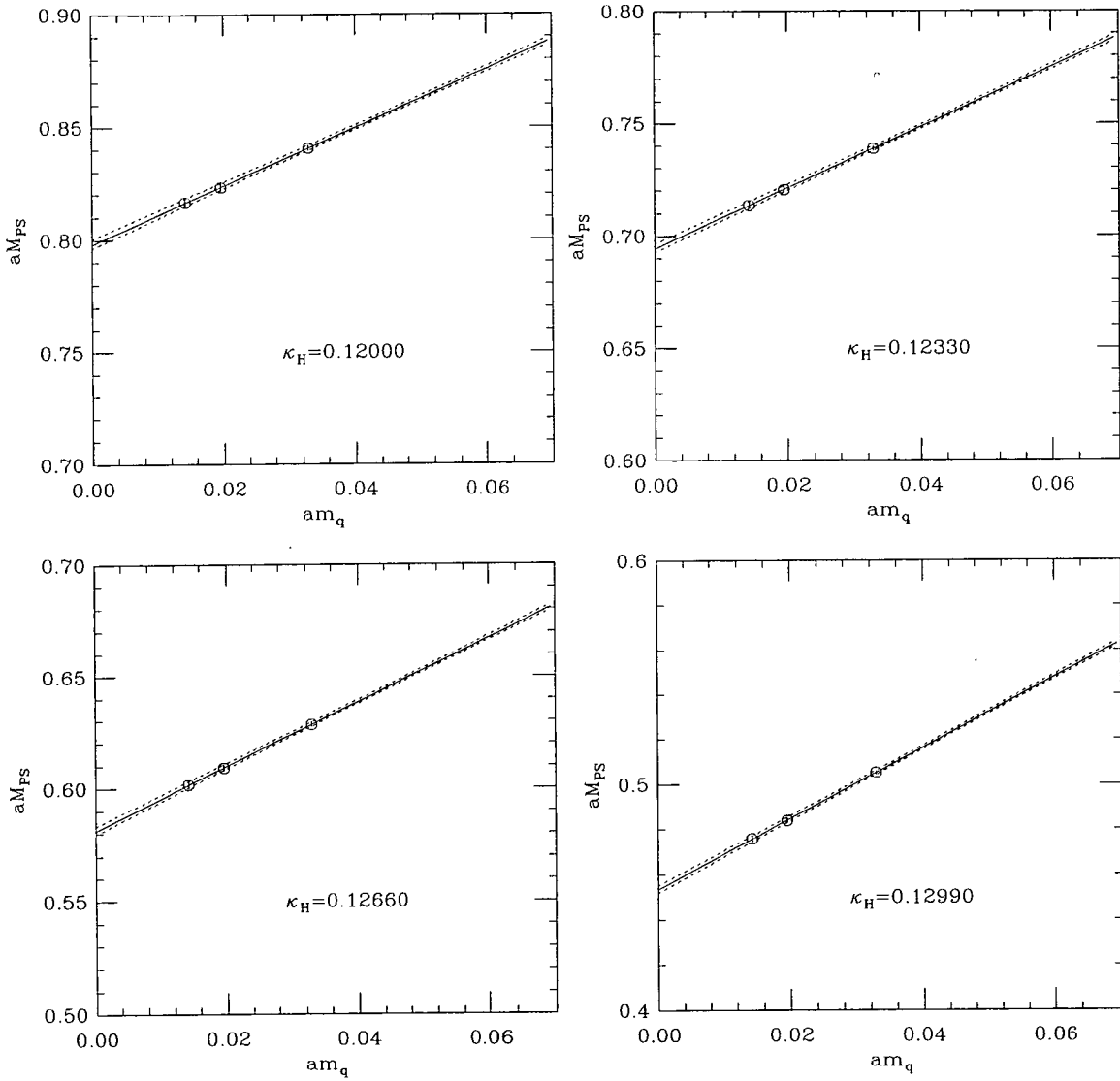


Figure 5.7: Linear chiral extrapolations for the heavy-light pseudoscalar mesons at  $\beta = 6.2$ .

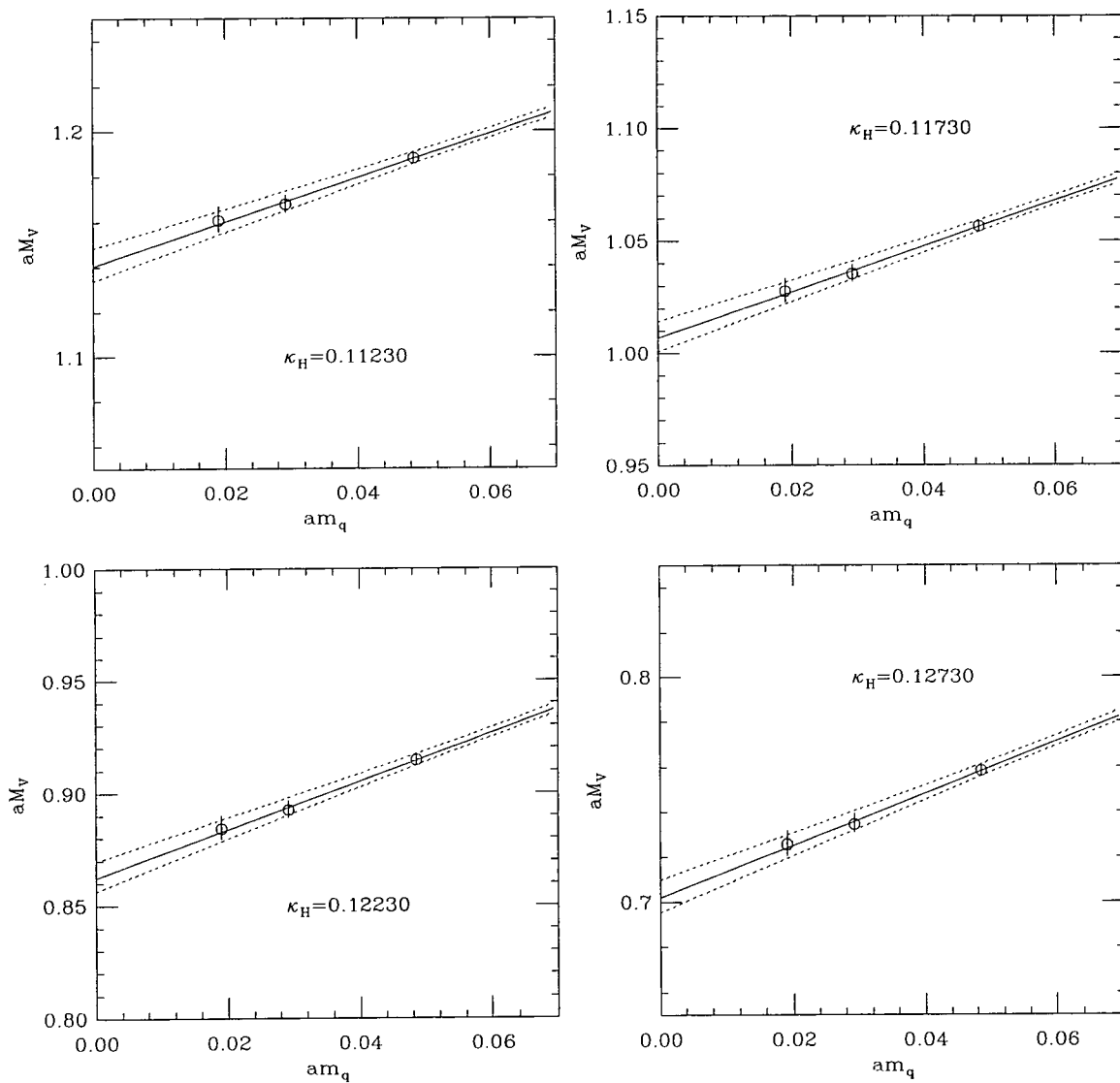


Figure 5.8: Linear chiral extrapolations for the heavy-light vector mesons at  $\beta = 6.0$ .

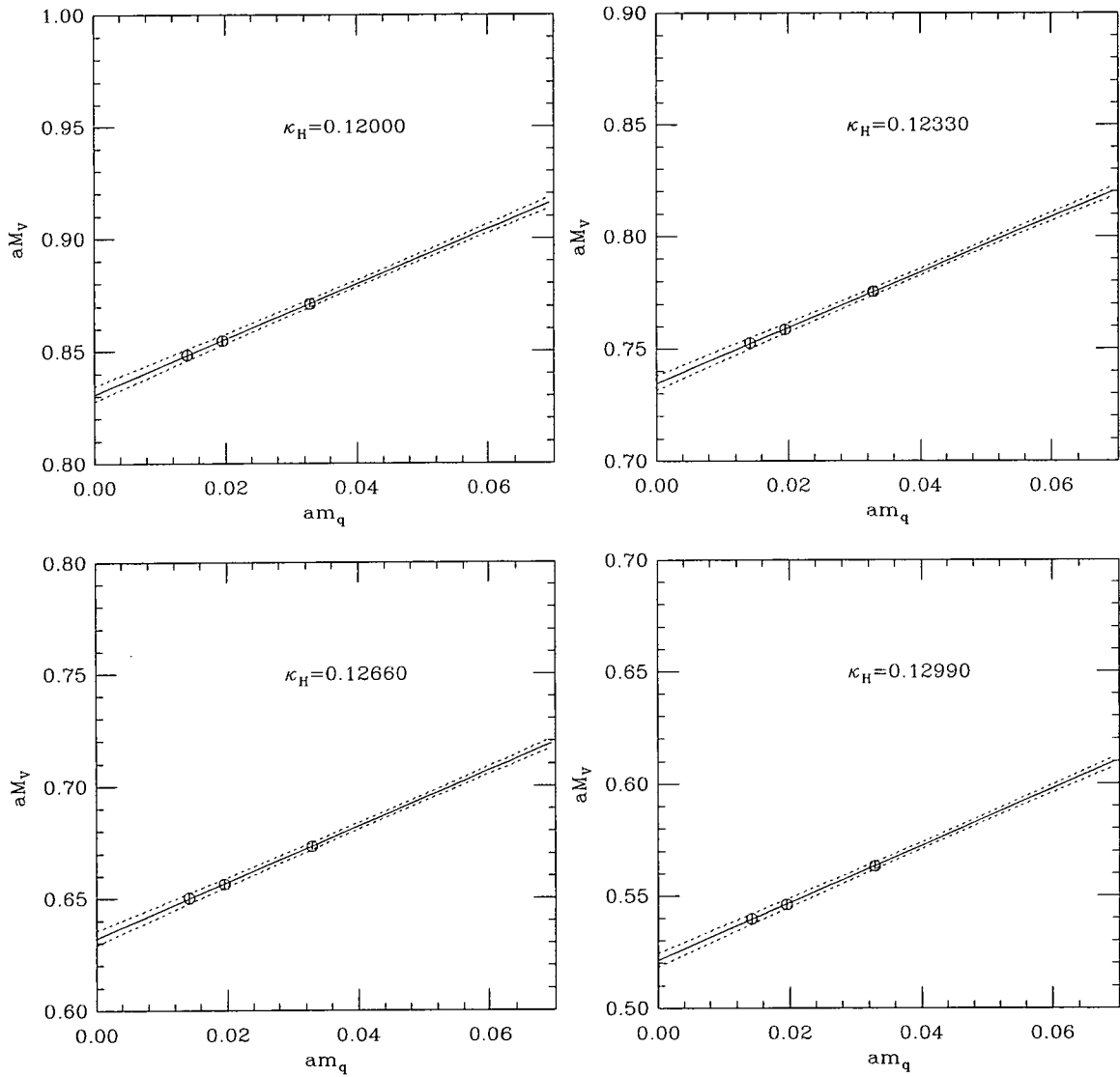


Figure 5.9: Linear chiral extrapolations for the heavy-light vector mesons at  $\beta = 6.2$ .

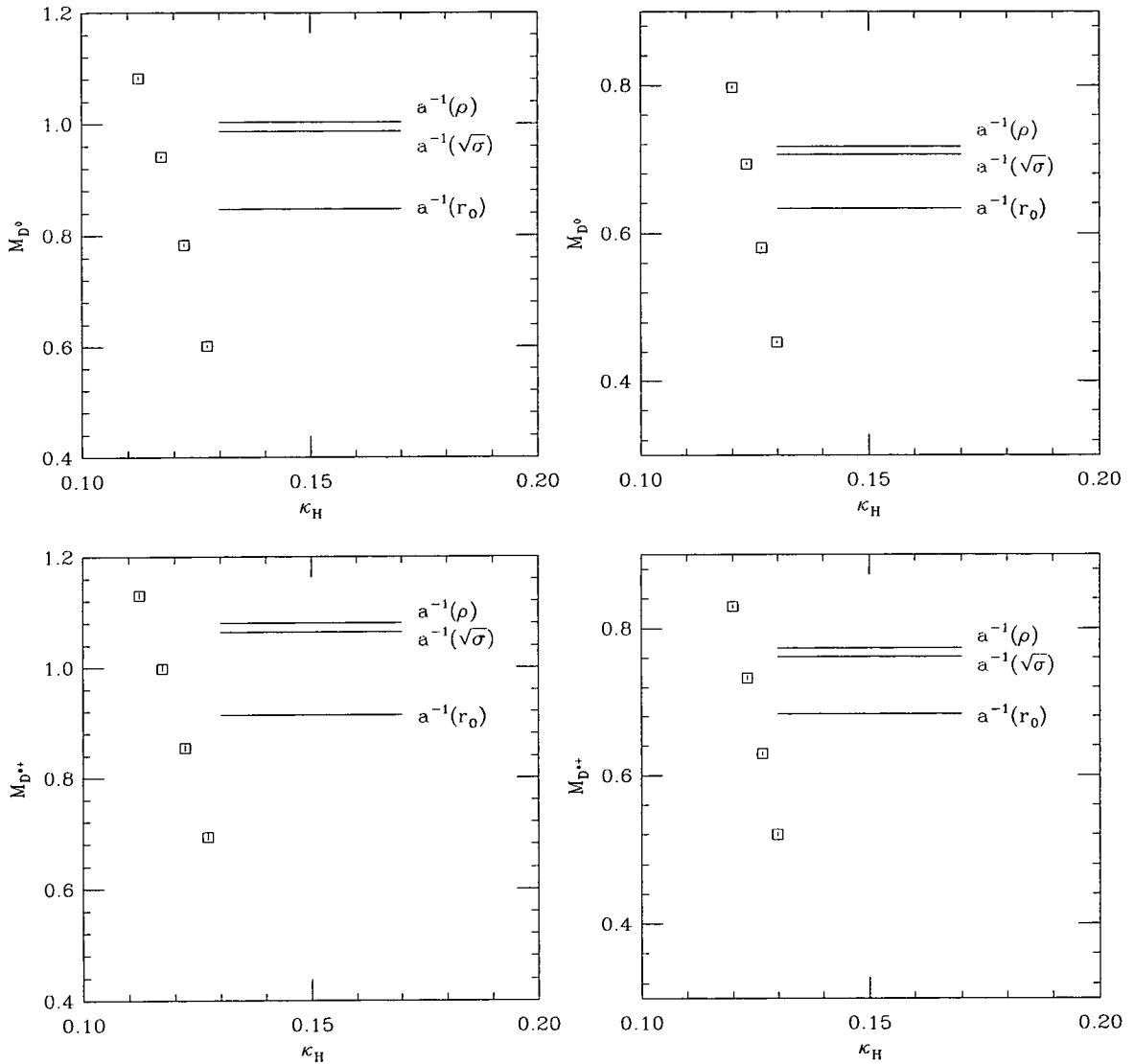


Figure 5.10: Top row : plot of the chirally extrapolated pseudoscalar mass compared with the experimental measured  $D^0$  meson mass (1864.6MeV). Bottom row: plot of the chirally extrapolated vector mass compared with the experimentally measured  $D^{*+}$  meson mass (2010MeV). For each plot the experimental mass is converted to a lattice mass using as a scale the  $\rho$  meson, the string tension and  $r_0$ .

## Chapter 6

### Semi-leptonic Decay $\bar{B} \rightarrow D l \bar{\nu}$

#### 6.1 Isolating the weak matrix element

The hadronic matrix element of equation 1.49 is the ultimate goal of this calculation. In order to extract this quantity, it is necessary to consider the Euclidean behaviour of the two and three point functions. Recall from section 4.2.1 the Euclidean form for a meson correlator,

$$C_{\text{meson}}(\vec{k}, t) = \sum_n \frac{|\langle 0 | \eta(0) | n \rangle|^2}{2E_n} e^{-E_n t}. \quad (6.1)$$

From section 4.3.2 the Euclidean form for a three point correlator was shown to be

$$\begin{aligned} C_{3\text{pt}}^\mu(t_x, t_y, \vec{p}, \vec{q}) &= \sum_{\alpha, \beta} \frac{e^{E_\alpha(t_x - t_y)}}{2E_\alpha(\vec{p})} \frac{e^{E_\beta t_y}}{2E_\beta(\vec{p} + \vec{q})} \\ &\quad \langle 0 | \eta'(0) | \alpha, \vec{p} \rangle \langle \beta, \vec{p} + \vec{q} | \eta^\dagger(0) | 0 \rangle \\ &\quad \langle \alpha, \vec{p} | J^\mu(0) | \beta, \vec{p} + \vec{q} \rangle \end{aligned} \quad (6.2)$$

The matrix element is thus obtained by taking the ratio of the three point correlator and the relevant two point correlators corresponding to the initial and final mesons,

$$R^\mu = \frac{C_{3\text{pt}}^\mu(t_x, t_y, \vec{p}, \vec{q})}{C_{\text{meson}}(\vec{p}, t_x - t_y) C_{\text{meson}}(\vec{p} + \vec{q}, t_y)}. \quad (6.3)$$

Hence

$$\langle 0 | \eta'(0) | \beta, \vec{p} + \vec{q} \rangle \langle 0 | \eta(0) | \alpha, \vec{p} \rangle R^\mu = \langle \alpha, \vec{p} | J^\mu(0) | \beta, \vec{p} + \vec{q} \rangle \quad (6.4)$$

## 6.2 Lattice Details

The three point function was computed using all four values of the heavy quark hopping parameters to simulate the initial heavy quark, with the two heaviest of the light quark hopping parameters used to simulate the passive (spectator) quark. The extended propagator is then correlated with all seven values of the hopping parameter to allow study of heavy-light to heavy-light decays as well as heavy-light to light-light. The initial meson, represented by the extended propagator, is always pseudoscalar, while the final meson is either pseudoscalar or vector. A total of 74 operators were used in the construction of the three point functions including operators to study penguin decay, and thus the following matrix elements are calculable from the dataset,

$$\begin{aligned} &\langle PS|V^\mu|PS\rangle, \\ &\langle V|(V - A)^\mu|PS\rangle, \\ &\langle V|T^{\mu\nu}|PS\rangle. \end{aligned} \tag{6.5}$$

In each case, the initial meson is injected with a spatial momentum  $\vec{p} = (0, 0, 0)$  or  $\vec{p} = (1, 0, 0)$ . The final meson has spatial momentum  $|\vec{p} + \vec{q}| \leq 2$ . The momentum channels used in the simulation are shown in tables 6.1 and 6.2.

In order to increase the quality of the statistics, the correlator data is averaged over equivalent momentum and Lorentz channels corresponding to the same matrix element. Due to the fact that the statistical noise increases rapidly with the momenta of the correlation functions, only momentum channels corresponding to a final meson momentum less than  $2\pi/aL$  are included in the analysis of the form factors. This leaves six momentum channels as illustrated in table 6.3.

For the  $\beta = 6.0$  lattice, all four heavy quark hopping parameters are used to simulate the initial (extended) heavy quark while for  $\beta = 6.2$  only  $\kappa_A = 0.1200$  and  $\kappa_A = 0.1266$  are used.

Channel	$\vec{q}$	$\vec{p} + \vec{q}$	Channel	$\vec{q}$	$\vec{p} + \vec{q}$
0	(0,0,0)	(0,0,0)	9	(0,1,-1)	(0,1,-1)
1	(1,0,0)	(1,0,0)	10	(1,1,1)	(1,1,1)
2	(0,1,0)	(0,1,0)	11	(-1,1,1)	(-1,1,1)
3	(0,0,1)	(0,0,1)	12	(1,-1,1)	(1,-1,1)
4	(1,1,0)	(1,1,0)	13	(1,1,-1)	(1,1,-1)
5	(1,0,1)	(1,0,1)	14	(2,0,0)	(2,0,0)
6	(0,1,1)	(0,1,1)	15	(0,2,0)	(0,2,0)
7	(1,-1,0)	(1,-1,0)	16	(0,0,2)	(0,0,2)
8	(-1,0,1)	(-1,0,1)			

Table 6.1: Momentum channels for three point correlators with  $\vec{p} = (0, 0, 0)$  in units of  $2\pi/aL$ .

Channel	$\vec{q}$	$\vec{p} + \vec{q}$	Channel	$\vec{q}$	$\vec{p} + \vec{q}$
0	(-1,0,0)	(0,0,0)	10	(0,0,-1)	(1,0,-1)
1	(0,0,0)	(1,0,0)	11	(-1,1,1)	(0,1,1)
2	(-2,0,0)	(-1,0,0)	12	(-1,1,-1)	(0,1,-1)
3	(-1,1,0)	(0,1,0)	13	(-1,-1,1)	(0,-1,1)
4	(-1,-1,0)	(0,-1,0)	14	(-1,-1,-1)	(0,-1,-1)
5	(-1,0,1)	(0,0,1)	15	(0,1,1)	(1,1,1)
6	(-1,0,-1)	(0,0,-1)	16	(0,-1,1)	(1,-1,1)
7	(0,1,0)	(1,1,0)	17	(0,1,-1)	(1,1,-1)
8	(0,0,1)	(1,0,1)	18	(0,-1,-1)	(1,-1,-1)
9	(0,-1,0)	(1,-1,0)	19	(1,0,0)	(2,0,0)

Table 6.2: Momentum channels for three point correlators with  $\vec{p} = (1, 0, 0)$  in units of  $2\pi/aL$ .

$\vec{p}$	$\vec{q}$	$\vec{p} + \vec{q}$
(0,0,0)	(0,0,0)	(0,0,0)
(0,0,0)	(1,0,0)	(1,0,0)
(1,0,0)	(0,0,0)	(1,0,0)
(1,0,0)	(-1,0,0)	(0,0,0)
(1,0,0)	(-1,1,0)	(0,1,0)
(1,0,0)	(-2,0,0)	(-1,0,0)

Table 6.3: The six momentum channels (with implicit permutation) used in the extraction of the form factors.

### 6.2.1 Improved Vector Current

In section 2.3.2 the improvement procedure used to remove cut-off effects was discussed. This is sufficient for the calculation of spectral quantities but not for matrix elements. By considering the transformation properties of the vector current under lattice symmetries [31, 71] it can be shown that the improved lattice vector current is given by

$$V_{\text{improved}}^{\mu} = V_{\text{bare}}^{\mu} + \frac{ac^{\nu}}{2} (\partial_{\nu}^{*} + \partial_{\nu}) \Sigma^{\mu\nu}. \quad (6.6)$$

There exists a non-perturbative evaluation for the improvement coefficient  $c^{\nu}$  [72]. However this result is only preliminary and yields a much larger value than the perturbative estimate [69] and therefore the perturbative estimate is used in this calculation,

$$c^{\nu} = -\frac{0.49}{3} g_0^2 + \mathcal{O}(g_0^4), \quad (6.7)$$

so that

$$c^{\nu}|_{\beta=6.0} = -0.016333, \quad c^{\nu}|_{\beta=6.2} = -0.015806 \quad (6.8)$$

The full set of operators used in the simulation is shown in table 6.4.

### 6.2.2 Extended Propagator Source

For both lattices, the extension time slice  $t_x$  does not occur at the mid-point ( $T/2$ ) of the lattice and hence unlike the two point correlators, the three point correlators cannot be folded about the mid-point to improve the quality of the fit procedure. In each case, the extension time slice  $t_x = 28$ . This choice allows for a study of certain systematic effects in the lattice calculation. By definition, the three point correlator contains an explicit time ordering,

$$C_{3\text{pt}}^\mu(t_x, t_y, \vec{p}, \vec{q}) = \sum_{\vec{x}, \vec{y}} \langle 0 | T \{ \eta'(x) J^\mu(y) \eta^\dagger(0) \} | 0 \rangle e^{-i\vec{q} \cdot \vec{y}} e^{-i\vec{p} \cdot \vec{x}}. \quad (6.9)$$

Recall from section 4.3 the implicit assumption that  $t_x > t_y > 0$ , which is the statement that the current intersects the mesons in the temporal direction. From the above equation it is clear that there can exist some alternative time orderings of the correlator,

$$C_{\text{alternative}}^{\prime\mu}(t_x, t_y, \vec{p}, \vec{q}) = \sum_{\vec{x}, \vec{y}} \langle 0 | \eta^\dagger(0) \eta'(x) J^\mu(y) | 0 \rangle e^{-i\vec{q} \cdot \vec{y}} e^{-i\vec{p} \cdot \vec{x}}. \quad (6.10)$$

where  $t_y > t_x > 0$ .

Figures 6.1 and 6.2 show the ratio  $R^\mu$  separately for the temporal ( $R^0$ ) and spatial components ( $R^i$ ). The different magnitudes in these quantities arises from the quantities from which they are constructed (energies for  $R^0$  and momenta for  $R^i$ ). For the  $\beta = 6.0$  lattice, the data is clearly less noisy for  $t > t_x$ . In this region the contamination from other time orderings is small. For the  $\beta = 6.2$  lattice the data is much quieter on both sides of the extension point. However a better, more extensive plateau is observed when  $t < t_x$ , although for the particular channel shown a fit for  $t > t_x$  produces an acceptable fit (although not as good as for  $t > t_x$ ). The analysis of the form factors on the  $\beta = 6.0$  lattice is done with  $t_y > t_x$  which is equivalent to considering the extension point  $t_x = 20$ . For both lattices it is clear that the chosen plateau region is one where the two point functions are asymptotic and hence there is no contamination from excited states.

Channel	$\Gamma^A$	$J^\mu$	Channel	$\Gamma^A$	$J^\mu$	Channel	$\Gamma^A$	$J^\mu$
1	$\gamma^5$	$\gamma^1$	26	$\gamma^4$	$\gamma^4$	51	$\gamma^1$	$\sigma^{23}$
2	$\gamma^5$	$\gamma^2$	27	$\gamma^1$	$\gamma^1\gamma^5$	52	$\gamma^2$	$\sigma^{23}$
3	$\gamma^5$	$\gamma^3$	28	$\gamma^2$	$\gamma^1\gamma^5$	53	$\gamma^2$	$\sigma^{23}$
4	$\gamma^5$	$\gamma^4$	29	$\gamma^3$	$\gamma^1\gamma^5$	54	$\gamma^3$	$\sigma^{23}$
5	$\gamma^5$	$\sigma^{34}$	30	$\gamma^4$	$\gamma^1\gamma^5$	55	$\gamma^1$	$\sigma^{14}$
6	$\gamma^5$	$\sigma^{24}$	31	$\gamma^1$	$\gamma^2\gamma^5$	56	$\gamma^2$	$\sigma^{14}$
7	$\gamma^5$	$\sigma^{23}$	32	$\gamma^2$	$\gamma^2\gamma^5$	57	$\gamma^3$	$\sigma^{14}$
8	$\gamma^5$	$\sigma^{14}$	33	$\gamma^3$	$\gamma^2\gamma^5$	58	$\gamma^4$	$\sigma^{14}$
9	$\gamma^5$	$\sigma^{13}$	34	$\gamma^4$	$\gamma^2\gamma^5$	59	$\gamma^1$	$\sigma^{13}$
10	$\gamma^5$	$\sigma^{12}$	35	$\gamma^1$	$\gamma^3\gamma^5$	60	$\gamma^2$	$\sigma^{13}$
11	$\gamma^1$	$\gamma^1$	36	$\gamma^2$	$\gamma^3\gamma^5$	61	$\gamma^3$	$\sigma^{13}$
12	$\gamma^2$	$\gamma^1$	37	$\gamma^3$	$\gamma^3\gamma^5$	62	$\gamma^4$	$\sigma^{13}$
13	$\gamma^3$	$\gamma^1$	38	$\gamma^4$	$\gamma^3\gamma^5$	63	$\gamma^1$	$\sigma^{12}$
14	$\gamma^4$	$\gamma^1$	39	$\gamma^1$	$\gamma^4\gamma^5$	64	$\gamma^2$	$\sigma^{12}$
15	$\gamma^1$	$\gamma^2$	40	$\gamma^2$	$\gamma^4\gamma^5$	65	$\gamma^3$	$\sigma^{12}$
16	$\gamma^2$	$\gamma^2$	41	$\gamma^3$	$\gamma^4\gamma^5$	66	$\gamma^4$	$\sigma^{12}$
17	$\gamma^3$	$\gamma^2$	42	$\gamma^4$	$\gamma^4\gamma^5$	67	$\gamma^1$	$I$
18	$\gamma^4$	$\gamma^2$	43	$\gamma^1$	$\sigma^{34}$	68	$\gamma^2$	$I$
19	$\gamma^1$	$\gamma^3$	44	$\gamma^2$	$\sigma^{34}$	69	$\gamma^3$	$I$
20	$\gamma^2$	$\gamma^3$	45	$\gamma^3$	$\sigma^{34}$	70	$\gamma^4$	$I$
21	$\gamma^3$	$\gamma^3$	46	$\gamma^4$	$\sigma^{34}$	71	$\gamma^1$	$\gamma^5$
22	$\gamma^4$	$\gamma^3$	47	$\gamma^1$	$\sigma^{24}$	72	$\gamma^2$	$\gamma^5$
23	$\gamma^1$	$\gamma^4$	48	$\gamma^2$	$\sigma^{24}$	73	$\gamma^3$	$\gamma^5$
24	$\gamma^2$	$\gamma^4$	49	$\gamma^3$	$\sigma^{24}$	74	$\gamma^4$	$\gamma^5$
25	$\gamma^3$	$\gamma^4$	50	$\gamma^4$	$\sigma^{24}$			

Table 6.4: Lorentz channels for the three point correlators. For the case of the vector current, channels 1-4 correspond to the bare operator and channels 5-10 to the improvement term.

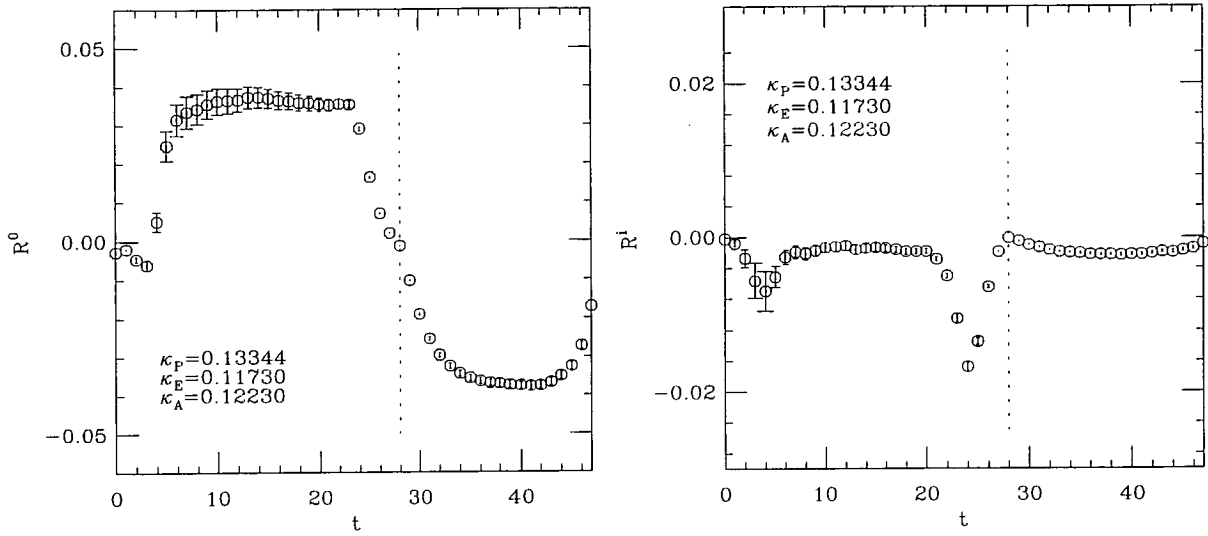


Figure 6.1: Temporal and spatial components of  $R^\mu$  for  $\beta = 6.0$ . Momentum channel is  $(1,0,0) \rightarrow (1,0,0)$ .

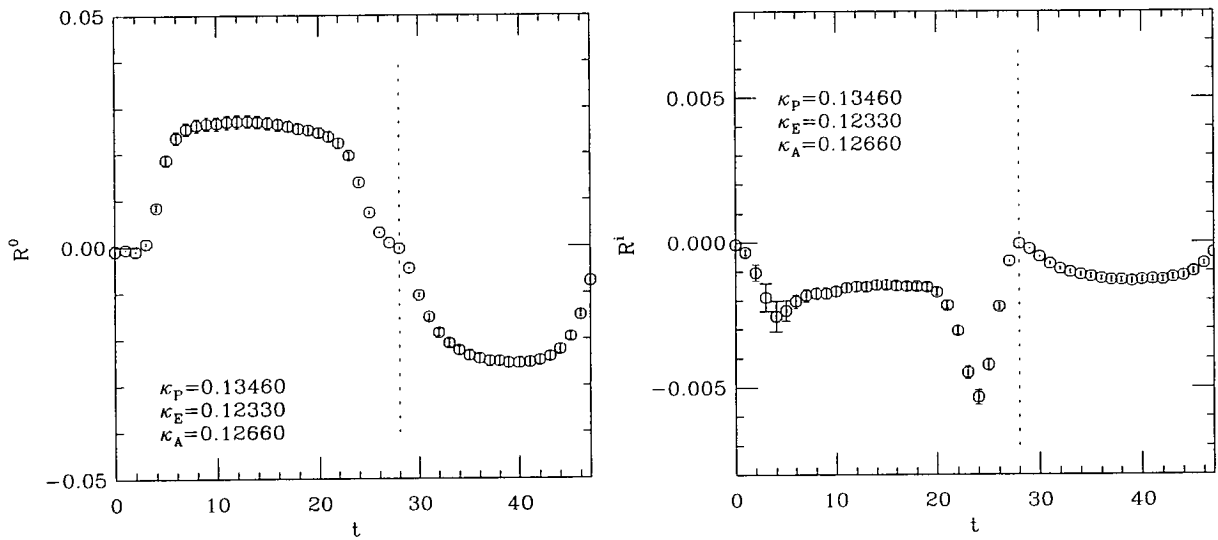


Figure 6.2: Temporal and spatial components of  $R^\mu$  for  $\beta = 6.2$ . Momentum channel is  $(1,0,0) \rightarrow (1,0,0)$ .

### 6.3 Calculation of $Z_{\text{eff}}^{\text{v}}$

The continuum vector current is related to the improved lattice vector current (equation 6.6) by a renormalisation constant  $Z_{\text{eff}}^{\text{v}}$ ,

$$V_{\text{cont}}^{\mu} = Z_{\text{eff}}^{\text{v}} V_{\text{improved}}^{\mu} \quad (6.11)$$

where

$$Z_{\text{eff}}^{\text{v}} = Z^{\text{v}}(1 + b^{\text{v}}(am_q + am_Q)). \quad (6.12)$$

The quantities  $Z^{\text{v}}$  and  $b^{\text{v}}$  are known non-perturbatively. An estimate of these quantities is given by a ratio of polynomials in terms of the bare coupling  $g_0$  [73],

$$Z^{\text{v}} = \frac{1 - 0.7663g_0^2 + 0.0488g_0^4}{1 - 0.6369g_0^2}, \quad (6.13)$$

$$b^{\text{v}} = \frac{1 - 0.8496g_0^2 + 0.0610g_0^4}{1 - 0.7332g_0^2}. \quad (6.14)$$

Recall from section 3.6 that when there is no velocity transfer in the weak decay, then the Isgur Wise function is normalised to unity. This condition can be exploited to formulate a lattice estimate of the effective renormalisation  $Z_{\text{eff}}^{\text{v}}$ . The matching of the lattice vector current to continuum vector current naturally follows through to the ratio  $R^{\mu}$ . Therefore using equation 3.33 which relates matrix elements to the relevant form factors,

$$h_{\pm}^{\text{cont}}(\omega) = Z_{\text{eff}}^{\text{v}} h_{\pm}^{\text{latt}}(\omega). \quad (6.15)$$

From equation 3.42,  $h_+(\omega)$  is related to  $\xi(\omega)$  by

$$h_+(\omega) = \left[ 1 + \beta_+(\omega) + \mathcal{O}\left(\frac{1}{m_Q}\right) \right] \xi(\omega). \quad (6.16)$$

Thus the renormalisation constant may be obtained from

$$Z_{\text{eff}}^{\text{v}} = \frac{\left[1 + \beta_+(1) + \mathcal{O}\left(\frac{1}{m_Q^2}\right)\right]}{h_+^{\text{latt}}(1)}. \quad (6.17)$$

where the power corrections are suppressed at  $\mathcal{O}\left(\frac{1}{m_Q}\right)$  at zero recoil as a result of Luke's Theorem [74].

For the case of degenerate transitions, the above is simplified greatly; current conservation implies

$$Z_{\text{eff}}^{\text{v}} = \frac{1}{h_+^{\text{latt}}(1)}. \quad (6.18)$$

### 6.3.1 Radiative Corrections

In order to implement equation 6.17 it is necessary to calculate the radiative correction  $\beta_+(\omega)$ . Neubert's short distance expansion is used for this purpose. Since the calculation is performed in quenched QCD, the quantity  $N_f$  representing the number of dynamical quark flavours is set to zero. There are then only three inputs required to obtain the function  $\beta_+$ ; the size of recoil  $\omega$  and the masses of the heavy quarks involved in the transition.

Recall from section 3.1 that heavy quark symmetry allows the mass of a heavy-light meson to be expressed in terms of the heavy quark mass and a universal constant,  $\bar{\Lambda}$ , the binding energy. Thus the heavy quark mass may be determined from the lattice as a function of the meson mass,

$$M_Q = \frac{a^{-1} [3(aM_{\text{vector}}^{\text{x}}) + (aM_{\text{pseudo}}^{\text{x}})]}{4} - \bar{\Lambda} \quad (6.19)$$

where  $(aM_{\text{vector}}^{\text{x}})$  and  $(aM_{\text{pseudo}}^{\text{x}})$  are the chirally extrapolated vector and pseudoscalar heavy-light meson masses in lattice units. The binding energy is set at 500 MeV [45]. Following the analysis of section 5.6, the heavy quark masses are listed in table 6.5.

$\kappa_Q$	$(aM_{\text{pseudo}}^X)$	$(aM_{\text{vector}}^X)$	$M_Q(\text{GeV})$
0.1123	1.0817	1.1301	1.6130
0.1173	0.9410	0.9980	1.3592
0.1223	0.7827	0.8534	1.0795
0.1273	0.6006	0.6925	0.7655
0.1200	0.7970	0.8295	1.6683
0.1233	0.6940	0.7328	1.4088
0.1266	0.5807	0.6299	1.1305
0.1299	0.4531	0.5200	0.8286

Table 6.5: Physical heavy quark masses. The value of the inverse lattice spacing used in the result is obtained from the string tension [65];  $a^{-1} = 1.89$  GeV at  $\beta = 6.0$ ,  $a^{-1} = 2.64$  GeV at  $\beta = 6.2$ .

### 6.3.2 Lattice results for $Z_{\text{eff}}^y$

Irrespective of the heavy quark mass, the momentum channel  $(0,0,0) \rightarrow (0,0,0)$  corresponds to a decay with zero recoil. For this particular channel, there is no spatial contribution to the three point correlator. Thus  $Z_{\text{eff}}^y$  is obtained from equation 6.17 from a two parameter fit to

$$\langle 0 | \eta'(0) | \beta, \vec{p} + \vec{q} \rangle \langle 0 | \eta(0) | \alpha, \vec{p} \rangle R^0 = \sqrt{M_\alpha M_\beta} [(v + v')^0 h_+(\omega) + (v - v')^0 h_-(\omega)] \quad (6.20)$$

The results of the fits are shown in figures 6.3, 6.4 and 6.5, both with radiative correction included (for the non-degenerate cases) and without. The results are compared to the non-perturbatively calculated values [73]. The agreement between the theoretical and lattice results is striking. The interpretation from this is that the higher order discretisation errors are indeed small. However since the power corrections to the form factors are ignored in this analysis, another conclusion is that these corrections are cancelling the discretisation errors. In section 6.5, the power corrections will be investigated and shown to be negligible.

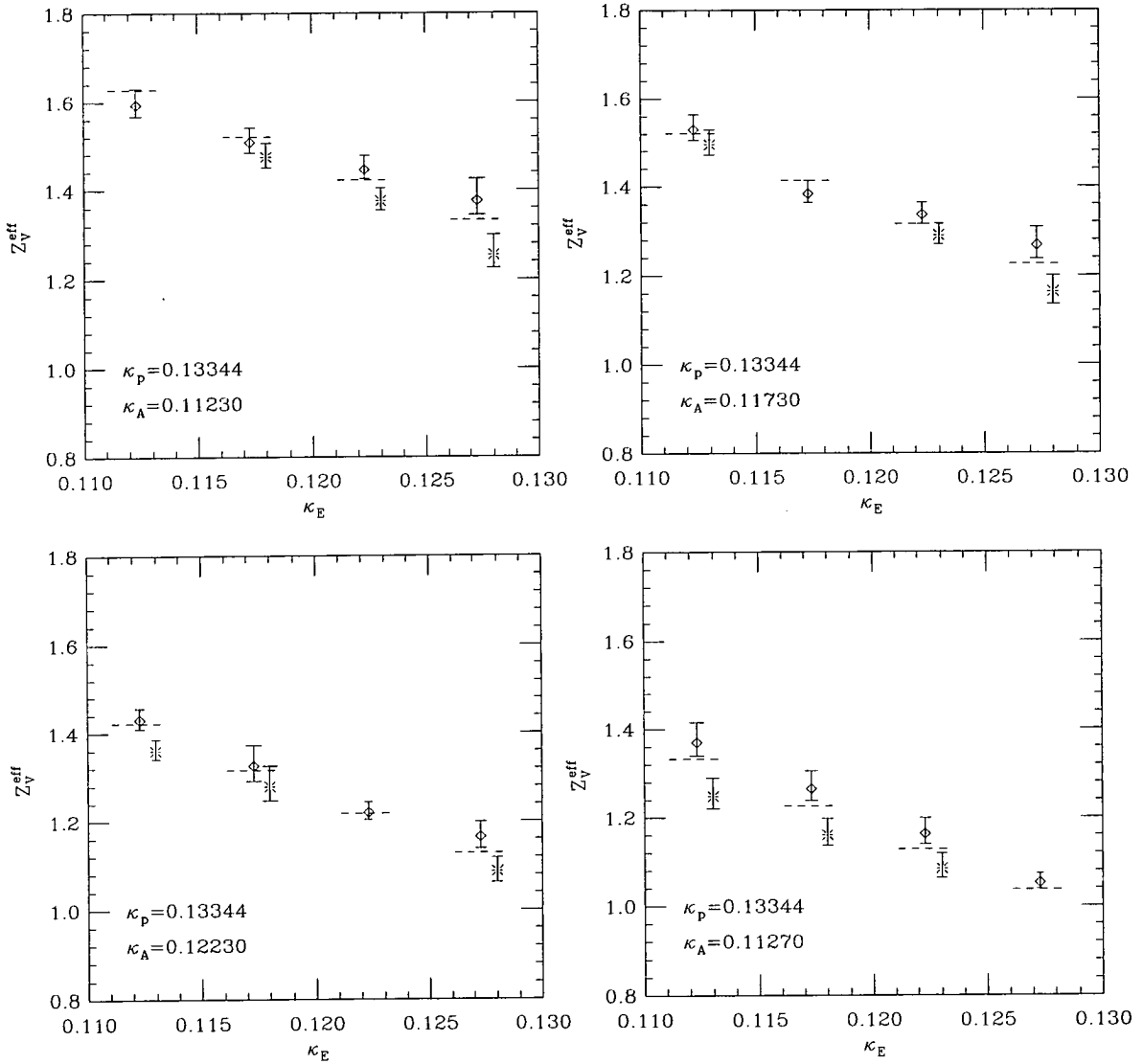


Figure 6.3: Lattice determination for  $Z_V^{\text{eff}}$  at  $\beta = 6.0$ . The diamonds correspond to including radiative corrections and the burst points to their exclusion. The non-perturbative estimates (equations 6.12-6.14) are shown as horizontal dotted lines.

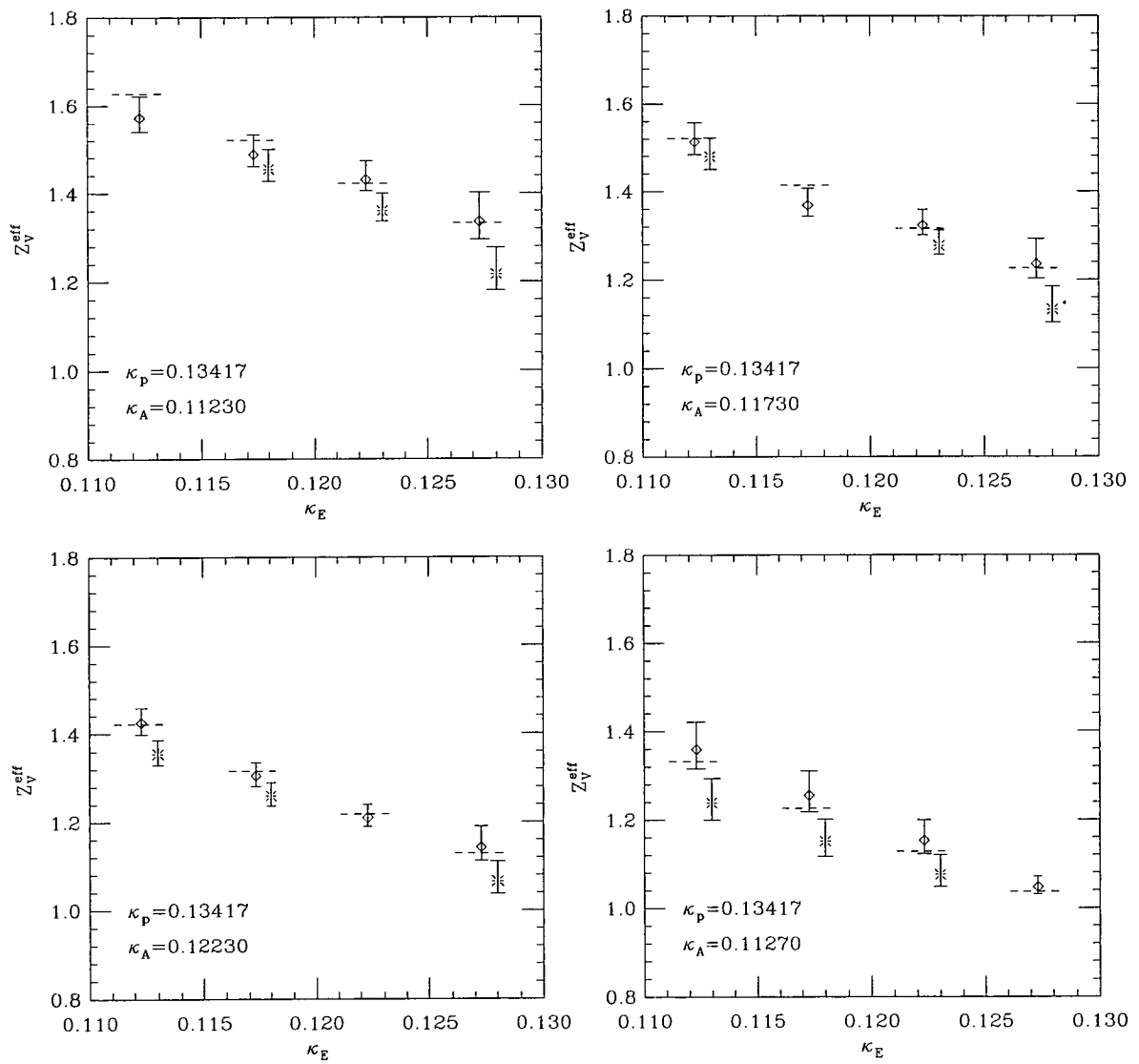
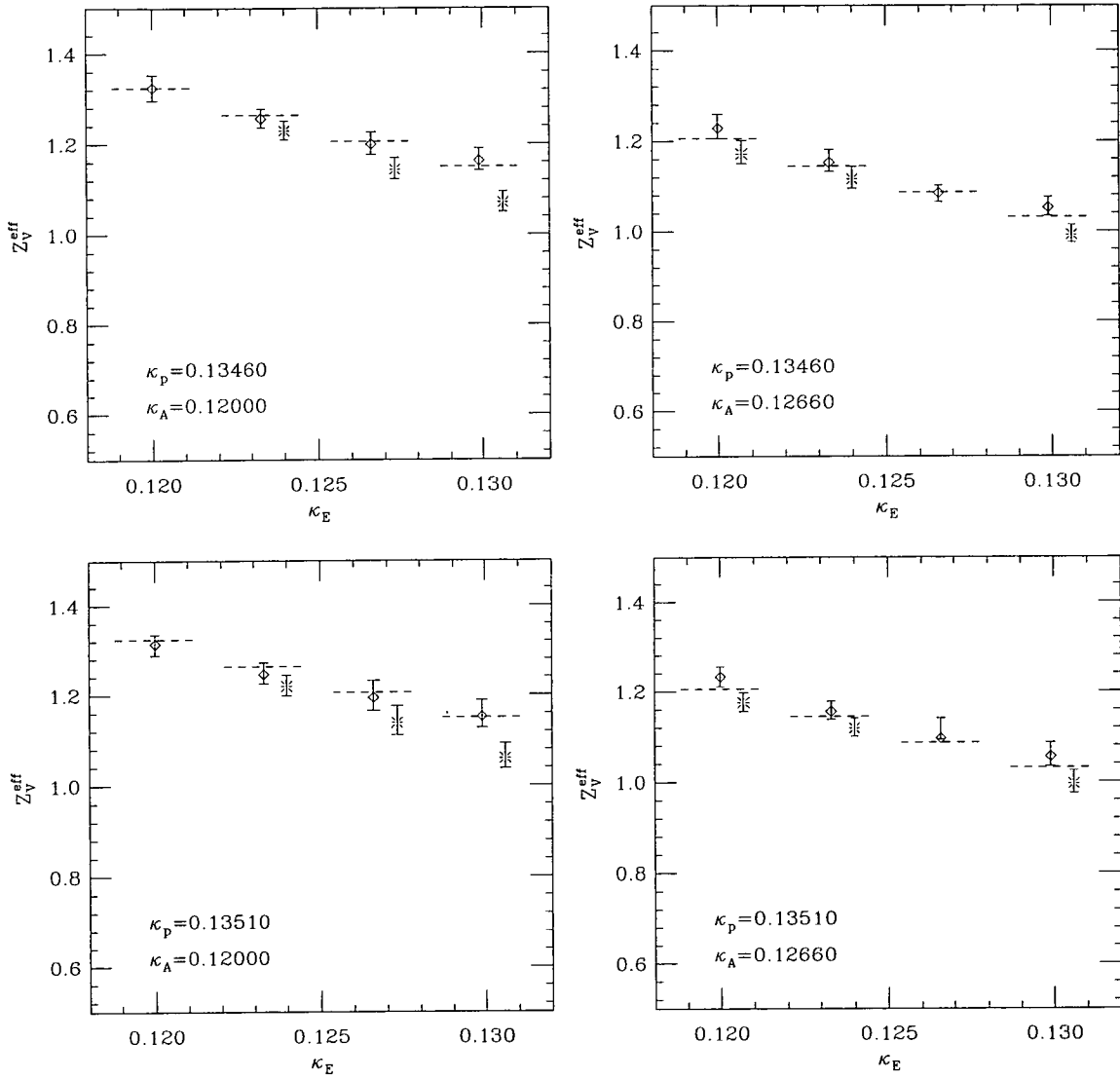


Figure 6.4: As for figure 6.3.

Figure 6.5: As for figure 6.3 with  $\beta = 6.2$ .

## 6.4 Calculation of Form Factors

The calculation for  $Z_{\text{eff}}^V$  used the lattice determination of the form factor  $h_+(\omega)$  for zero velocity transfer. This channel is unique in that there is no contribution from the spatial component of the ratio  $R^\mu$ . The remaining five momentum channels considered in this analysis (table 6.3) all have spatial contributions. The form factors  $h_\pm(\omega)$  are extracted by simultaneously fitting the spatial and temporal components of  $R^\mu$ . The energies of the mesons with non-zero spatial momenta are calculated using the dispersion relation for relativistic particles,

$$E^2(|\vec{k}|^2) = m^2 + |\vec{k}|^2 \quad (6.21)$$

where the mass is obtained from a fit to the zero momentum particle. Table B.5 lists the amplitudes and energies for the heavy-light pseudoscalar mesons with  $|\vec{k}|^2 = 1$ .

As for the zero transfer, zero recoil channel, the ratio is fitted for  $t_x > t_y$  when  $\beta = 6.2$  and  $t_x < t_y$  when  $\beta = 6.0$ . The timeslices used for the correlated fits are 11-15 for  $\beta = 6.2$  and 39-43 for  $\beta = 6.0$  (corresponding to 11-15 with  $t_x = 20$ ).

### 6.4.1 Results for $h_-(\omega)$

In the limit of infinitely heavy quarks, there is no analogue of  $h_-(\omega)$  and  $h_+(\omega)$  is identified as the Isgur Wise function. Away from this limit,  $h_-(\omega)$  is simply a collection of radiative and power corrections which multiply the Isgur Wise function,

$$h_-(\omega) = (\beta_-(\omega) + \gamma_-(\omega)) \xi(\omega) \quad (6.22)$$

Unlike  $h_+(\omega)$ , Luke's Theorem does not protect  $h_-(\omega)$  against power corrections proportional to the inverse heavy quark mass at zero recoil.

Figures 6.6, 6.7, 6.8 and 6.9 show the lattice determination for  $h_-(\omega)$ , computed for the five remaining momentum channels using all available hopping parameter combinations. Thus there are 80 points for each  $\beta = 6.0$  plot and 40 for each  $\beta = 6.2$  plot. The form factor is not radiatively corrected ( the corrections to

$h_-(\omega)$  are, in general terms, an order of magnitude smaller than those for  $h_+(\omega)$ . The figures clearly show that  $h_-(\omega)$  is consistent with zero. There are several anomalous points however, corresponding to the channel  $(1,0,0) \rightarrow (1,0,0)$ . For this particular channel, when  $m_{Q'} \neq m_Q$ , the coefficient  $(v - v')^\mu$  becomes very small and thus causes  $h_-(\omega)$  to be large with large errors. For the degenerate case there is no contribution for this particular channel since this coefficient is exactly zero. Reassuringly, for degenerate decays,  $h_-(\omega)$  is small; current conservation implies that for a degenerate decay,  $h_-(\omega) = 0, \forall \omega$ . The results indicate that  $h_-(\omega)$  is independent of spectator quark mass. Ignoring the anomalous points, then an upper bound of 0.08 can be placed on the magnitude of  $h_-(\omega)$ .

The results for  $h_-(\omega)$  are listed in appendix C, together with the results for  $h_+(\omega)$  and  $\chi^2/dof$  for the two parameter correlated fits.

#### 6.4.2 Results for $h_+(\omega)$

The form factor  $h_+(\omega)$  is related to the Isgur Wise function by

$$h_+(\omega) = [1 + \beta_+(\omega) + \gamma_+(\omega)] \xi(\omega), \quad (6.23)$$

where from Luke's theorem the power corrections  $\gamma_+(\omega)$  are suppressed at  $\mathcal{O}\left(\frac{1}{m_Q}\right)$  for  $\omega = 1$ . The radiative corrections are a function of the recoil and heavy quark masses. The masses are obtained as described in section 6.3.1. The recoil,  $\omega$ , is obtained from the masses and energies calculated from the meson fits,

$$\omega = v \cdot v' = \frac{E_\alpha E_\beta - \vec{p} \cdot (\vec{p} + \vec{q})}{m_\alpha m_\beta} \quad (6.24)$$

For the quark mass combinations used, there is quite a large spread of values for the recoil, as high as 1.8, so that the kinematic range is on a par with experiment. The results of the calculation of the radiative corrections,  $\beta_+(\omega)$ , are shown in tables A.1, A.2, A.3 and A.4.

The form factors obtained from the lattice calculation do not correspond to the physical processes of interest. Thus it is of prime importance to isolate the dependence on final and initial heavy quark mass. The mass dependence for  $\beta_+(\omega)$  has already been calculated and thus for small corrections,  $\beta_+(\omega)$ ,  $\gamma_+(\omega)$  an effective Isgur Wise function  $\xi(\omega)$  may be defined as,

$$\xi^{\text{eff}}(\omega) = \frac{h_+(\omega)}{1 + \beta_+(\omega)} \simeq (1 + \gamma_+(\omega))\xi(\omega) \quad (6.25)$$

where the terms proportional to the product of corrections have been ignored.

Degenerate transitions are more constrained theoretically than non-degenerate decays. There are no power corrections to  $h_+(\omega)$  and  $h_-(\omega) = 0$  for all values of  $\omega$ . Hence the data for these decays will provide the best insight into the heavy quark mass dependence of the effective Isgur Wise function.

The effective Isgur Wise function,  $\xi^{\text{eff}}(\omega)$  is calculated for each of the 12 degenerate transitions. The data is fitted to the following parametrisation of the Isgur Wise function [52],

$$\xi^{\text{NR}}(\omega) = \frac{2}{1 + \omega} \exp \left[ (1 - 2\rho_{\text{eff}}^2) \frac{\omega - 1}{\omega + 1} \right]. \quad (6.26)$$

The results of the fits are shown in tables 6.6 and 6.7.

$\kappa_Q$	$\kappa_P=0.13344$		$\kappa_P=0.13417$	
	$\rho_{\text{eff}}^2$	$\chi^2/dof$	$\rho_{\text{eff}}^2$	$\chi^2/dof$
0.11230	1.17 $^{+11}_{-12}$	7.57 / 4	1.16 $^{+16}_{-16}$	2.65 / 4
0.11730	1.12 $^{+9}_{-8}$	3.46 / 4	1.16 $^{+12}_{-12}$	3.88 / 4
0.12230	1.16 $^{+7}_{-5}$	14.75 / 4	1.13 $^{+9}_{-8}$	4.09 / 4
0.12730	1.17 $^{+5}_{-3}$	2.57 / 4	1.15 $^{+5}_{-4}$	6.12 / 4

Table 6.6: Elastic scattering at  $\beta = 6.0$ .  $\xi^{\text{eff}}(\omega)$  is fitted to the Neubert-Rieckert parametrisation.

The individual fits are shown in figures 6.10, 6.11 and 6.12. It is clear from

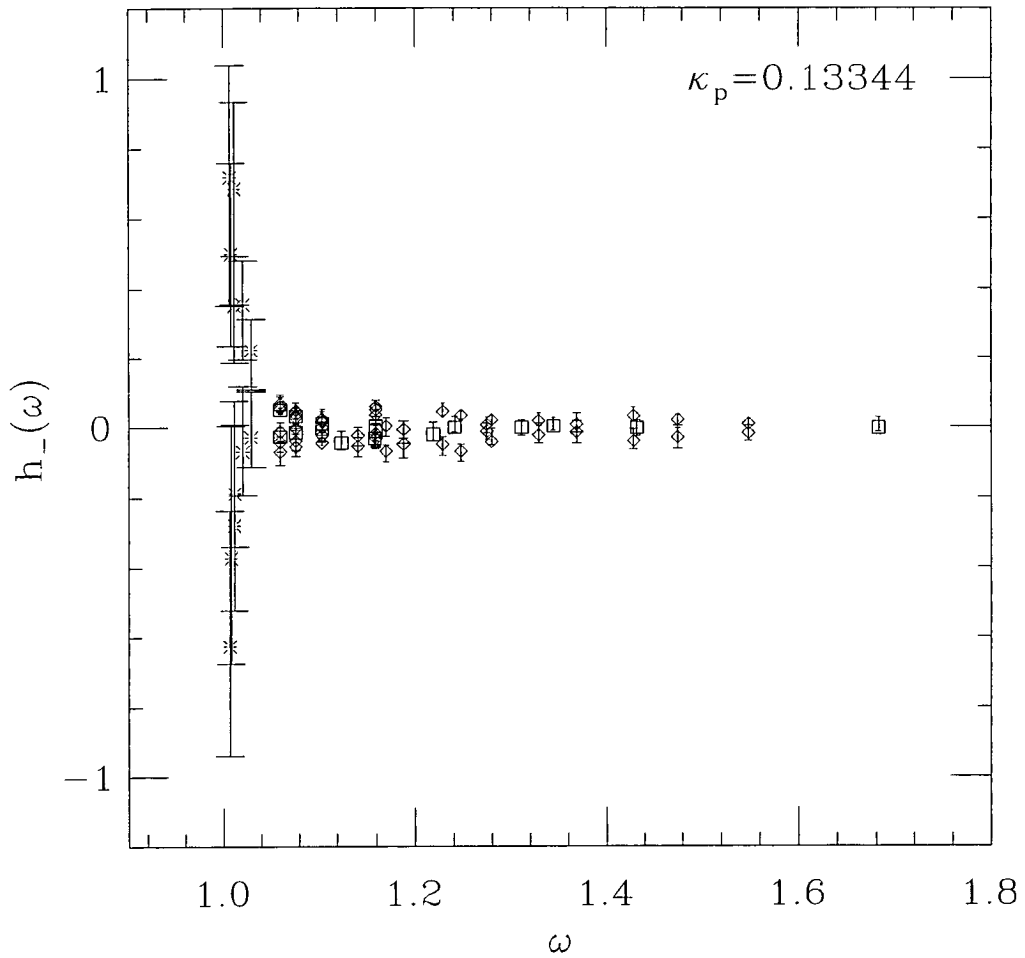


Figure 6.6:  $h_-(\omega)$  for all momentum channels excluding  $(0,0,0) \rightarrow (0,0,0)$  for  $\beta = 6.0$  at the heaviest spectator quark mass. The burst points correspond to the channel  $(1,0,0) \rightarrow (1,0,0)$ . The degenerate decays are represented by the squares. Excluding the burst points  $|h_-(\omega)| < 0.07$ .

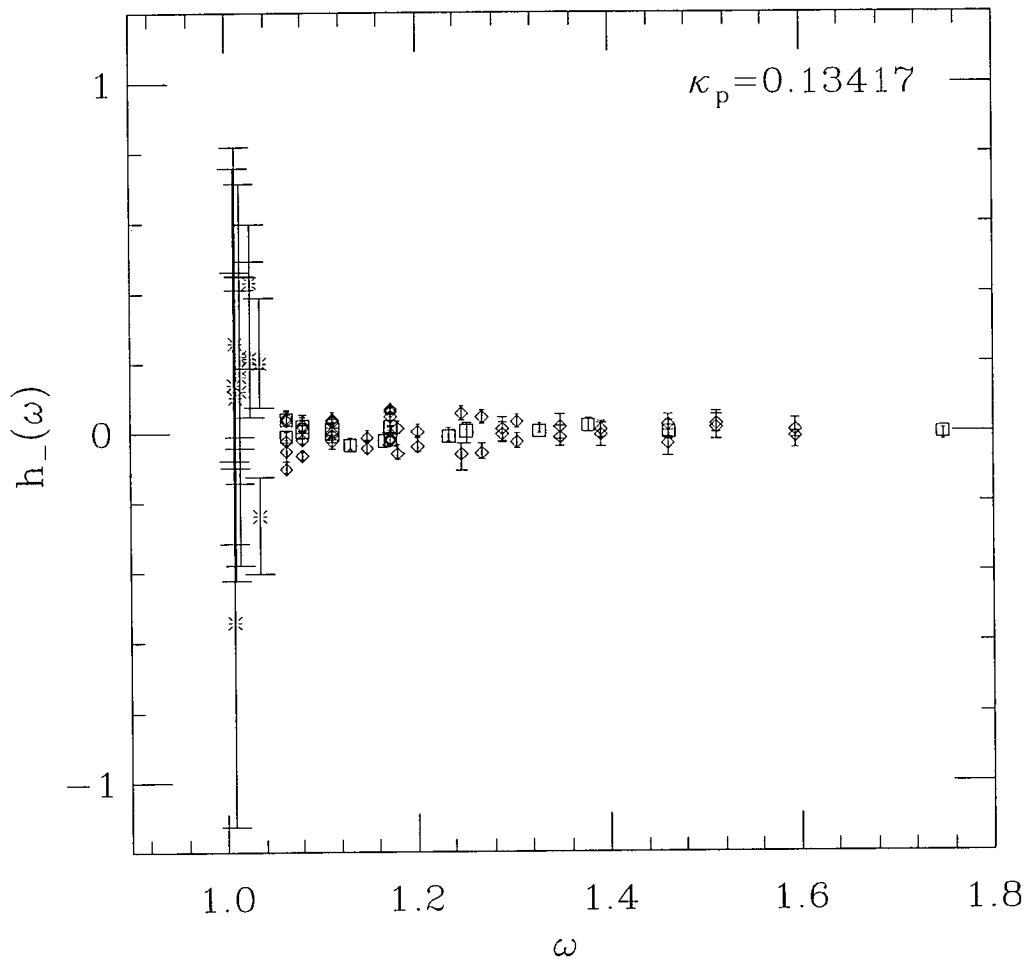


Figure 6.7: As for figure 6.6 but at the lightest spectator quark mass. Excluding the burst points  $|h_-(\omega)| < 0.08$ .

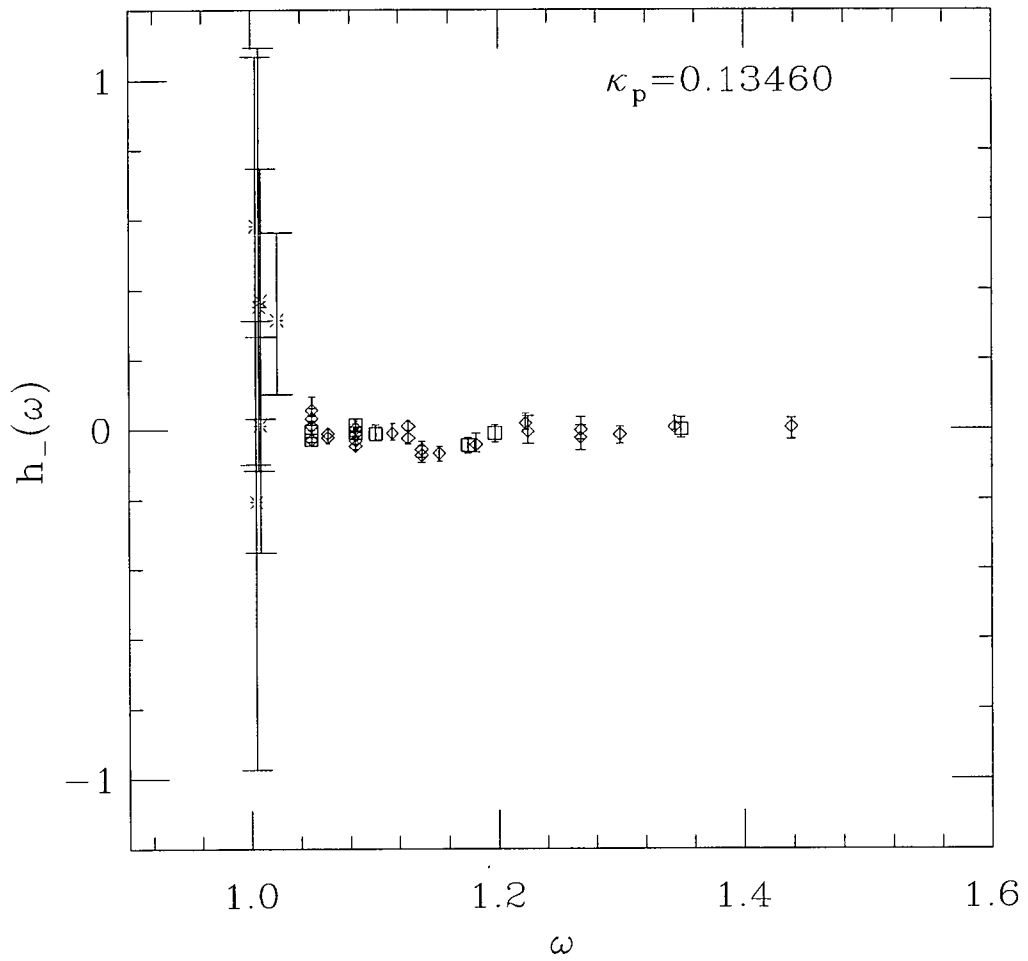


Figure 6.8: As for figure 6.6 but at  $\beta = 6.2$ . Excluding the burst points  $|h_-(\omega)| < 0.08$ .

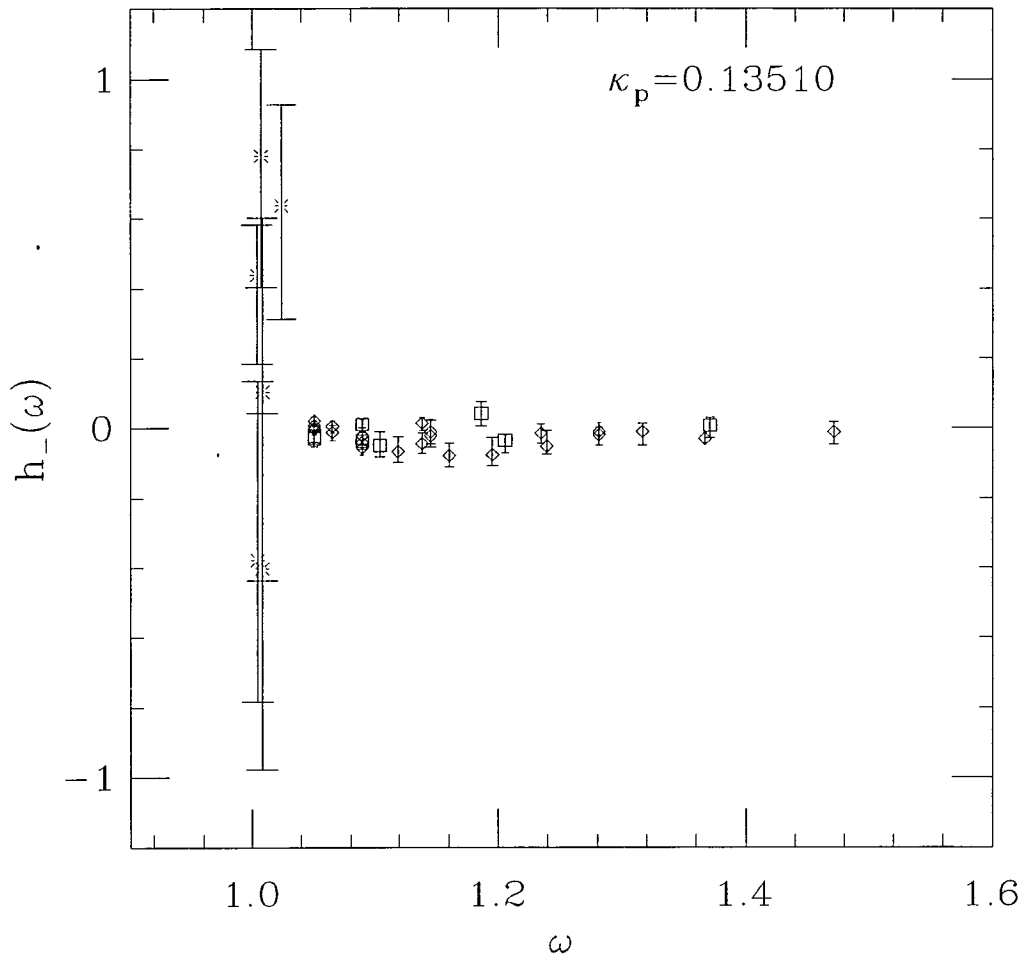


Figure 6.9: As for figure 6.6 but at  $\beta = 6.2$  and the lightest spectator quark mass. Excluding the burst points  $|h_-(\omega)| < 0.08$ .

	$\kappa_P=0.13460$		$\kappa_P=0.13510$	
$\kappa_Q$	$\rho_{\text{eff}}^2$	$\chi^2/dof$	$\rho_{\text{eff}}^2$	$\chi^2/dof$
0.1200	1.18 $^{+16}_{-21}$	3.97 / 4	1.15 $^{+21}_{-36}$	3.25 / 4
0.1266	1.19 $^{+9}_{-9}$	2.62 / 4	1.15 $^{+12}_{-15}$	0.58 / 4

Table 6.7: Elastic scattering at  $\beta = 6.2$ .  $\xi^{\text{eff}}(\omega)$  is fitted to the Neubert-Rieckert parametrisation.

these fits that the dependence on heavy quark mass is very small. The fits have been repeated with other parametrisations for the effective Isgur Wise function to verify that this is not a result of the choice of parametrisation. Tables 6.8 and 6.9 show the results when the data is fitted to

$$\xi^{\text{eff}}(\omega) = \left( \frac{2}{1 + \omega} \right)^{2\rho_{\text{eff}}^2}. \quad (6.27)$$

	$\kappa_P=0.13344$		$\kappa_P=0.13417$	
$\kappa_Q$	$\rho_{\text{eff}}^2$	$\chi^2/dof$	$\rho_{\text{eff}}^2$	$\chi^2/dof$
0.11230	1.14 $^{+10}_{-12}$	7.62 / 4	1.13 $^{+16}_{-16}$	2.88 / 4
0.11730	1.08 $^{+9}_{-8}$	4.18 / 4	1.12 $^{+11}_{-11}$	4.62 / 4
0.12230	1.12 $^{+6}_{-5}$	16.90 / 4	1.09 $^{+8}_{-7}$	5.79 / 4
0.12730	1.10 $^{+4}_{-2}$	7.11 / 4	1.08 $^{+5}_{-3}$	11.91 / 4

Table 6.8: Elastic scattering at  $\beta = 6.0$ .  $\xi^{\text{eff}}(\omega)$  is fitted to a pole ansatz for the Isgur Wise function.

	$\kappa_P=0.13460$		$\kappa_P=0.13510$	
$\kappa_Q$	$\rho_{\text{eff}}^2$	$\chi^2/dof$	$\rho_{\text{eff}}^2$	$\chi^2/dof$
0.1200	1.16 $^{+15}_{-20}$	4.04 / 4	1.13 $^{+21}_{-35}$	3.33 / 4
0.1266	1.15 $^{+9}_{-8}$	3.39 / 4	1.12 $^{+11}_{-14}$	0.40 / 4

Table 6.9: Elastic scattering at  $\beta = 6.2$ .  $\xi^{\text{eff}}(\omega)$  is fitted to a pole ansatz for the Isgur Wise function.

The results show that irrespective of the parametrisation, the degenerate transitions yield the same slope parameter. Tables 6.10 and 6.11 show the results of the elastic scattering to all data points for each spectator quark mass. The values of the slope are consistent with the individual kappa combinations shown in the previous tables.

Figure 6.13 shows a plot of all the degenerate transitions for each value of spectator quark (using the NR parametrisation), illustrating the fact that all the data lie on the same curve and that heavy quark scaling is observed. Hence if the power corrections are small enough then  $\xi^{\text{eff}}(\omega)$  can be interpreted as the physical Isgur Wise function.

$\kappa_P$	$\xi^{\text{nr}}(\omega)$	
	$\rho_{\text{eff}}^2$	$\chi^2/dof$
0.13344	$1.16 \begin{smallmatrix} +6 \\ -5 \end{smallmatrix}$	18.29 / 19
0.13417	$1.15 \begin{smallmatrix} +8 \\ -6 \end{smallmatrix}$	14.81 / 19
0.13460	$1.18 \begin{smallmatrix} +11 \\ -11 \end{smallmatrix}$	12.15 / 9
0.13510	$1.15 \begin{smallmatrix} +14 \\ -18 \end{smallmatrix}$	15.00 / 9

Table 6.10: Results for the slope of the effective Isgur Wise function for degenerate decays when fitted to the NR parametrisation.

$\kappa_P$	$\xi^{\text{pole}}(\omega)$	
	$\rho_{\text{eff}}^2$	$\chi^2/dof$
0.13344	$1.11 \begin{smallmatrix} +6 \\ -4 \end{smallmatrix}$	21.83 / 19
0.13417	$1.09 \begin{smallmatrix} +7 \\ -6 \end{smallmatrix}$	18.65 / 19
0.13460	$1.15 \begin{smallmatrix} +10 \\ -10 \end{smallmatrix}$	14.90 / 9
0.13510	$1.12 \begin{smallmatrix} +13 \\ -17 \end{smallmatrix}$	13.04 / 9

Table 6.11: Results for the slope of the effective Isgur Wise function for degenerate decays when fitted to the pole ansatz.

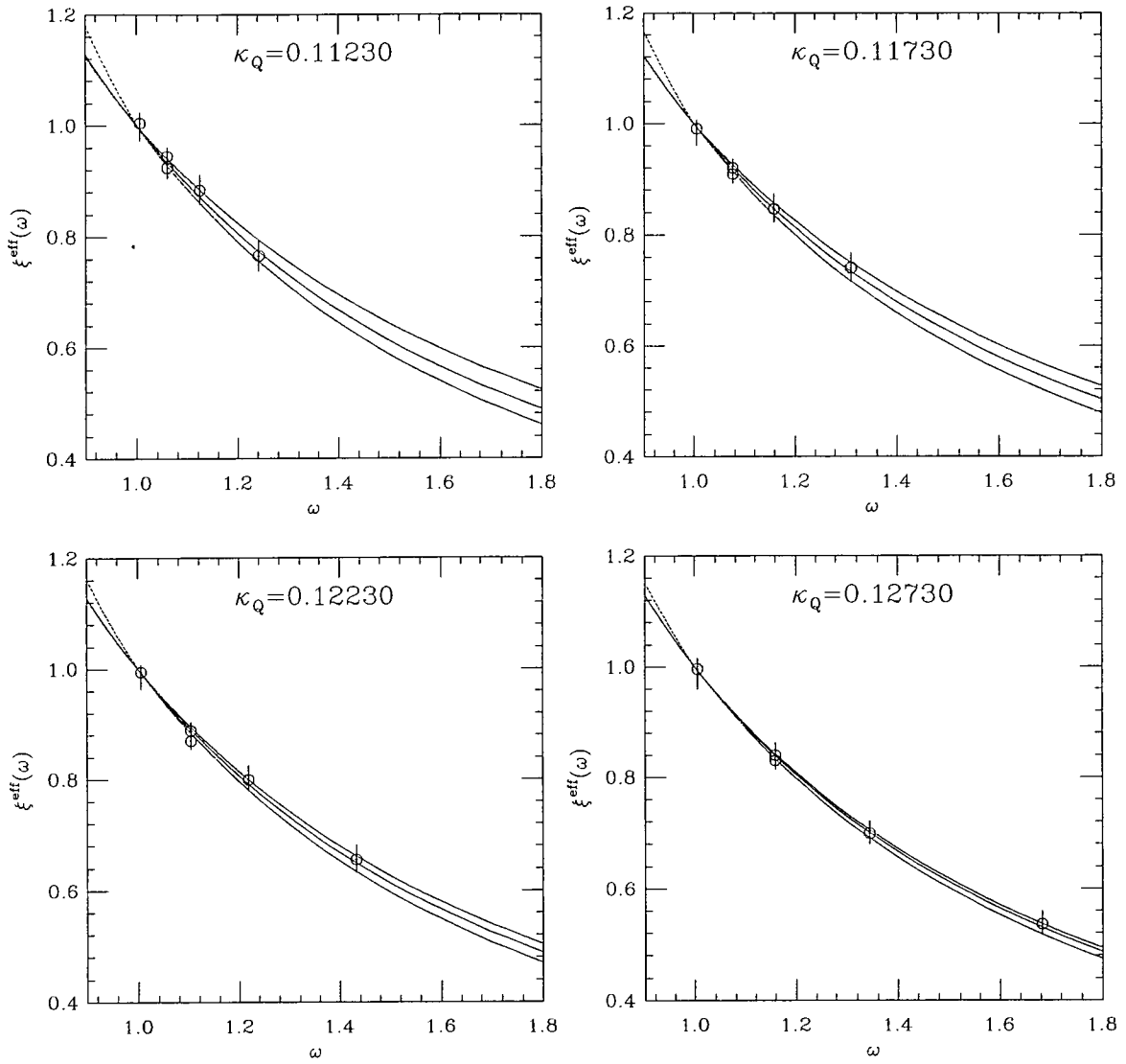


Figure 6.10: Elastic scattering for  $\beta = 6.0$ ,  $\kappa_P = 0.13344$ . Data is fitted to NR parametrisation of the Isgur Wise function.

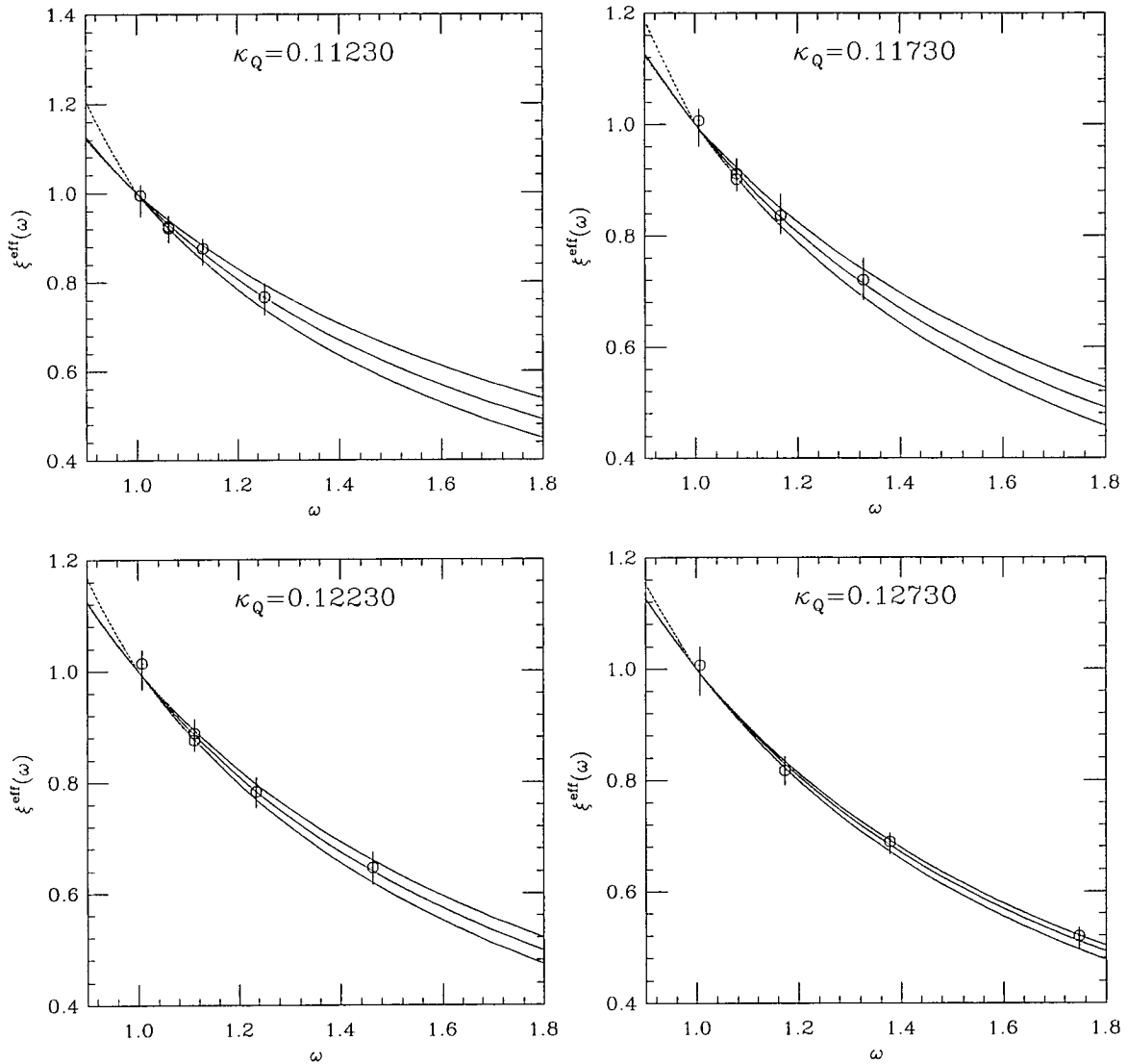


Figure 6.11: Elastic scattering for  $\beta = 6.0$ ,  $\kappa_P = 0.13417$ . Data is fitted to NR parametrisation of the Isgur Wise function.

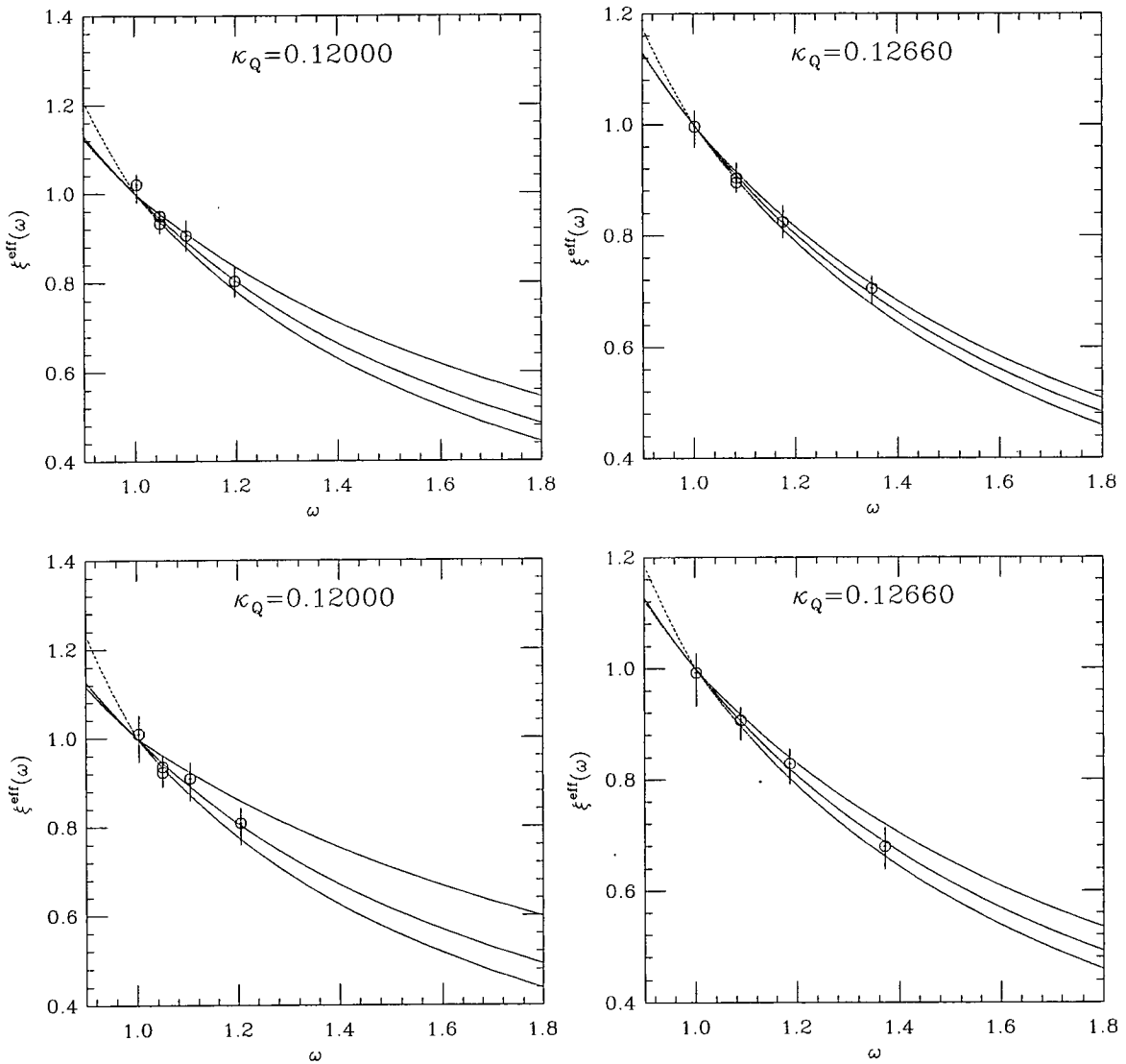


Figure 6.12: Elastic scattering for  $\beta = 6.2$ ,  $\kappa_P = 0.13460$  (top row),  $\kappa_P = 0.13510$  (bottom row). Data is fitted to NR parametrization of the Isgur Wise function.

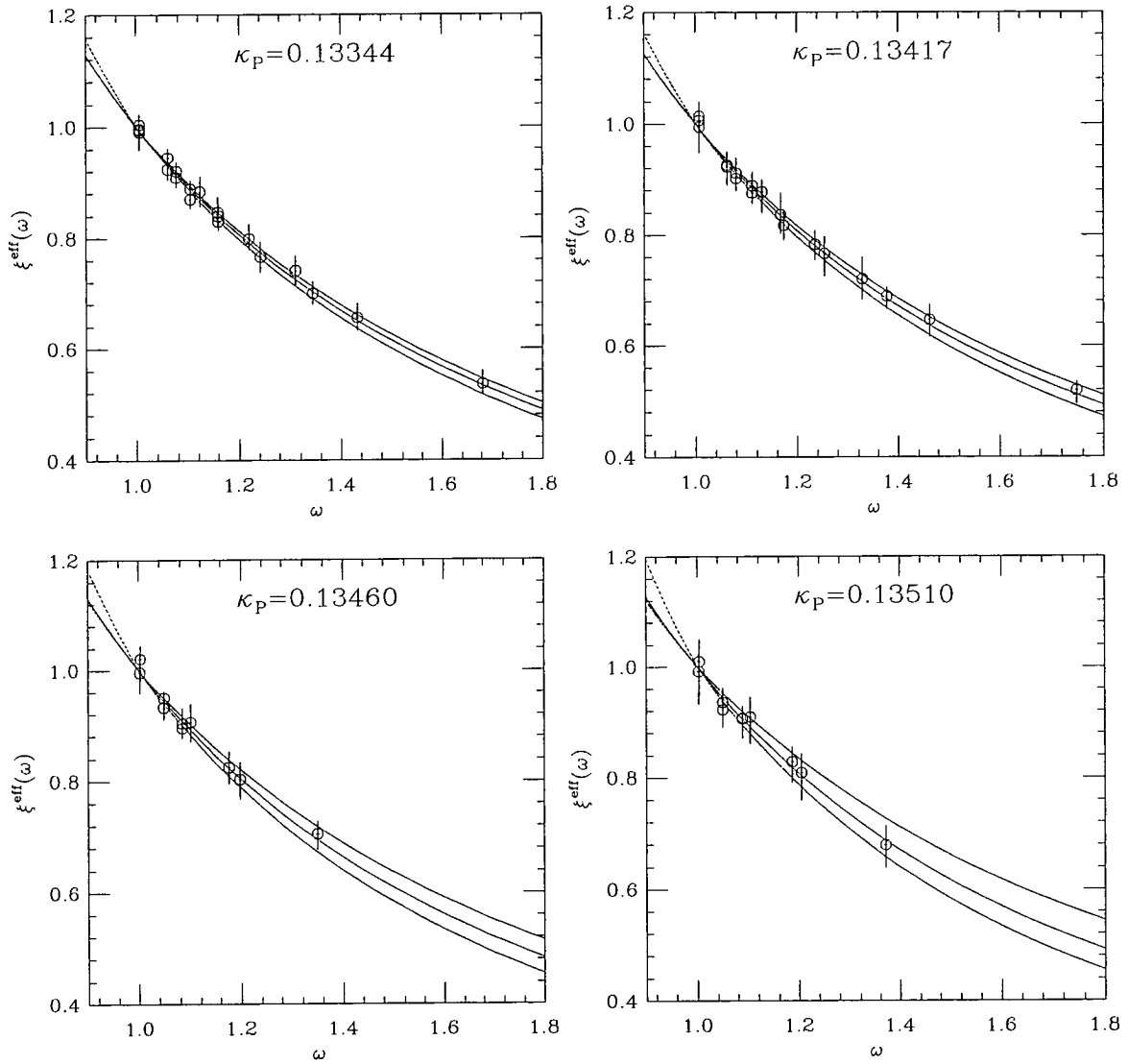


Figure 6.13: All elastic scattering data per spectator quark mass fitted to NR prescription.

## 6.5 Power Corrections

In order to determine the heavy quark mass dependence of the form factor,  $h_+(\omega)$ , it is necessary to quantify more precisely the nature of the power corrections which appear in the definition,

$$\frac{h_+(\omega)}{1 + \beta_+(\omega)} \simeq (1 + \gamma_+(\omega))\xi(\omega). \quad (6.28)$$

In the heavy quark expansion, it has been shown [74] that a mass parameter is required to parametrise the matrix elements of the higher dimensional operators. To leading order in the expansion, the power corrections can be written as,

$$\gamma_+(\omega) = \frac{\bar{\Lambda}_q}{2} \left[ \frac{g_Q(\omega, \alpha_s(m_Q), z)}{m_Q} + \frac{g_{Q'}(\omega, \alpha_s(m_{Q'}), z)}{m_{Q'}} \right] + \mathcal{O} \left( \left[ \frac{\bar{\Lambda}_q}{2m_{Q,Q'}} \right]^2 \right) \quad (6.29)$$

where

$$z = \frac{m_Q}{m_{Q'}}. \quad (6.30)$$

The quantity  $\bar{\Lambda}_q$  represents the energy carried by the light degrees of freedom. However the spectator quarks are not in the chiral limit and thus  $\bar{\Lambda}_q$  is related to  $\bar{\Lambda}$  (equation 6.19) by the difference in heavy quark mass,

$$\begin{aligned} \bar{\Lambda}_q &= m_Q^q - m_Q^x + \bar{\Lambda} \\ &= \frac{a^{-1} [3((aM_{\text{vector}}^q) - (aM_{\text{vector}}^x)) + ((aM_{\text{pseudo}}^q) - (aM_{\text{pseudo}}^x))]}{4} + \bar{\Lambda} \end{aligned} \quad (6.31)$$

The results for  $\bar{\Lambda}_q$  are shown in table 6.12.

$\kappa_Q$	0.11230		0.12000	
$\kappa_P$	0.13344	0.13417	0.13460	0.13510
$\bar{\Lambda}_q$ (GeV)	0.6117	0.5715	0.6112	0.5670

Table 6.12: Values for  $\bar{\Lambda}_q$  at heaviest quark mass.

The difference between the functions  $g_Q$  and  $g_{Q'}$  is a difference of radiative corrections and thus it is very small. Neglecting this difference, equation 6.29 reduces to

$$\gamma_+(\omega) = \frac{\bar{\Lambda}_q g(\omega)}{2} \left( \frac{1}{m_Q} + \frac{1}{m_{Q'}} \right) + \mathcal{O} \left( \left[ \frac{\bar{\Lambda}_q}{2m_{Q,Q'}} \right]^2 \right) \quad (6.32)$$

Hence a determination of the function  $g(\omega)$  amounts to a calculation of the power corrections.

It is clear from the functional dependences in the above equation that the evaluation of  $g(\omega)$  requires an exploration of the dependence on the recoil for various mass combinations. Therefore it is logical to look at the channels for which there is a vanishing spatial meson momentum for then the recoil is independent of that meson's mass (equation 6.24). Thus there are two momentum channels for which this kinematic property can be exploited,  $(0,0,0) \rightarrow (1,0,0)$  and  $(1,0,0) \rightarrow (0,0,0)$ . To extract  $g(\omega)$  the following ratios are calculated; for  $(0,0,0) \rightarrow (1,0,0)$

$$\Upsilon^{ij} \left( \omega, \frac{m_{Q^1}}{m_{Q^i}} \right) = \frac{2m_{Q^1}}{\bar{\Lambda}_q} \left[ 1 - \frac{\xi_{Q^i \rightarrow Q^j}^{\text{eff}}(\omega)}{\xi_{Q^1 \rightarrow Q^j}^{\text{eff}}(\omega)} \right] \quad (6.33)$$

For the  $(1,0,0) \rightarrow (0,0,0)$  channel, the following is calculated,

$$\Xi^{ij} \left( \omega, \frac{m_{Q^1}}{m_{Q^i}} \right) = \frac{2m_{Q^1}}{\bar{\Lambda}_q} \left[ 1 - \frac{\xi_{Q^j \rightarrow Q^i}^{\text{eff}}(\omega)}{\xi_{Q^j \rightarrow Q^1}^{\text{eff}}(\omega)} \right] \quad (6.34)$$

where  $i = 2, 3, 4$ ,  $j = 1, 2, 3, 4$  when  $\beta = 6.0$  and  $i = 2, 3, 4$ ,  $j = 1, 3$  when  $\beta = 6.2$  (and thus in this notation  $(\kappa_{Q^1}, \kappa_{Q^2}, \kappa_{Q^3}, \kappa_{Q^4}) = (0.11230, 0.11730, 0.12230, 0.12730)$  at  $\beta = 6.0$  and  $(\kappa_{Q^1}, \kappa_{Q^2}, \kappa_{Q^3}, \kappa_{Q^4}) = (0.12000, 0.12330, 0.12660, 0.12990)$  at  $\beta = 6.2$ ).

The ratio is chosen such that  $g(\omega)$  is obtained from a one parameter fit,

$$\Upsilon^{ij} \left( \omega, \frac{m_{Q^1}}{m_{Q^i}} \right) = \Xi^{ij} \left( \omega, \frac{m_{Q^1}}{m_{Q^i}} \right) = g(\omega) \left[ 1 - \frac{m_{Q^1}}{m_{Q^i}} \right] + \mathcal{O} \left( \left[ \frac{\bar{\Lambda}_q}{2m_{Q,Q'}} \right]^2 \right) \quad (6.35)$$

The results of the fits to equation 6.35 are plotted in figures 6.14, 6.15, 6.16, 6.17, 6.18 and tabulated in tables 6.13, 6.14, 6.15.

$\Upsilon^{ij}$						
	$\kappa_P = 0.13344$			$\kappa_P = 0.13417$		
$j$	$\omega$	$g(\omega)$	$\chi^2/dof$	$\omega$	$g(\omega)$	$\chi^2/dof$
1	1.0613	-0.007 $^{+19}_{-15}$	2.24/2	1.0632	0.024 $^{+29}_{-21}$	0.01/2
2	1.0763	0.016 $^{+19}_{-16}$	5.54/2	1.08047	0.025 $^{+28}_{-22}$	0.72/2
3	1.1041	-0.010 $^{+21}_{-19}$	0.15/2	1.11124	-0.008 $^{+41}_{-27}$	1.44/2
4	1.1594	0.023 $^{+19}_{-18}$	8.54/2	1.17384	-0.047 $^{+29}_{-22}$	1.74/2

Table 6.13: Form factor  $g(\omega)$  for channel  $(0,0,0) \rightarrow (1,0,0)$  at  $\beta = 6.0$ .

$\Xi^{ij}$						
	$\kappa_P = 0.13344$			$\kappa_P = 0.13417$		
$j$	$\omega$	$g(\omega)$	$\chi^2/dof$	$\omega$	$g(\omega)$	$\chi^2/dof$
1	1.0613	0.030 $^{+31}_{-24}$	0.34/2	1.0632	0.012 $^{+38}_{-33}$	0.03/2
2	1.0763	0.000 $^{+20}_{-18}$	0.88/2	1.08047	-0.01 $^{+36}_{-29}$	0.54/2
3	1.1041	-0.018 $^{+14}_{-12}$	0.46/2	1.11124	0.004 $^{+21}_{-19}$	0.14/2
4	1.1594	0.056 $^{+28}_{-21}$	9.21/2	1.17384	0.030 $^{+39}_{-28}$	7.37/2

Table 6.14: Form factor  $g(\omega)$  for channel  $(1,0,0) \rightarrow (0,0,0)$  at  $\beta = 6.0$ .

$\Upsilon^{ij}$						
	$\kappa_P = 0.13460$			$\kappa_P = 0.13510$		
$j$	$\omega$	$g(\omega)$	$\chi^2/dof$	$\omega$	$g(\omega)$	$\chi^2/dof$
1	1.04891	-0.001 $^{+15}_{-11}$	0.12/2	1.05074	0.005 $^{+16}_{-17}$	0.26/2
3	1.08438	0.015 $^{+18}_{-13}$	0.05/2	1.08934	-0.010 $^{+12}_{-9}$	0.01/2

Table 6.15: Form factor  $g(\omega)$  for channel  $(0,0,0) \rightarrow (1,0,0)$  at  $\beta = 6.2$ .

Since there are only 2 values of active quark mass at  $\beta = 6.2$ , there is no contribution to  $\Xi(\omega)$  and there are only 2 distinct values of the recoil for  $\Upsilon(\omega)$ . The figures clearly show that for all the available data,  $g(\omega)$  is consistent with zero. The results are not affected by the choice of spectator quark mass, although as

expected there is an increase in statistical noise as this mass becomes lighter. The form factor  $g(\omega)$  is plotted as a function of  $\omega$  in figure 6.19. It exhibits no trend over the range of recoils used in this analysis. Therefore the power corrections to  $h_+(\omega)$  are very small. Since there was no mass dependence on the radiatively corrected  $h_+(\omega)$  over the full range of recoils, it is assumed that the power corrections are small for the complete recoil range. Thus for  $h_+(\omega)$ , the flavour symmetry of HQET is well satisfied, and the Isgur Wise function relevant to physical processes may be obtained via an extrapolation or interpolation of the light spectator quark mass.

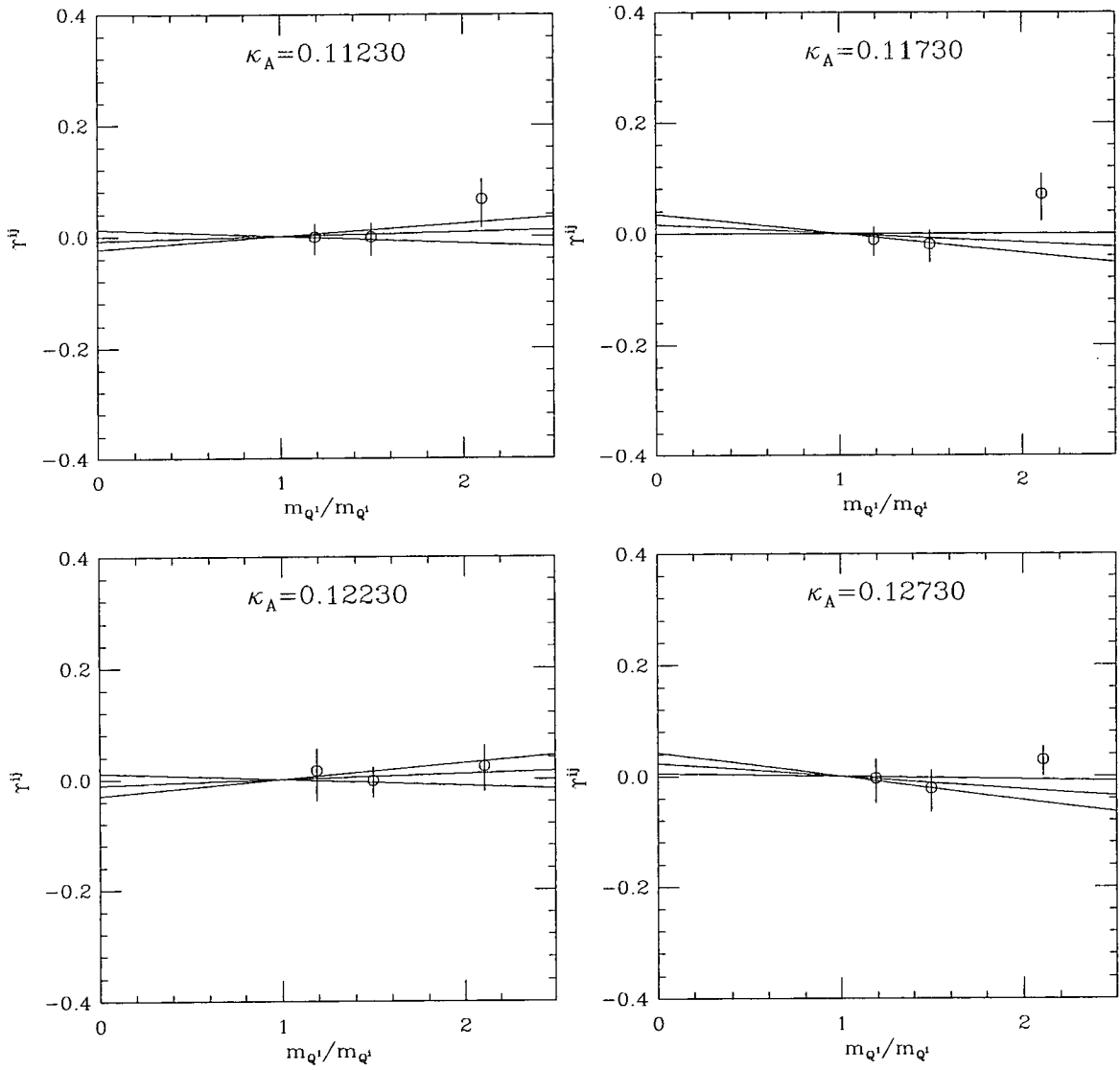
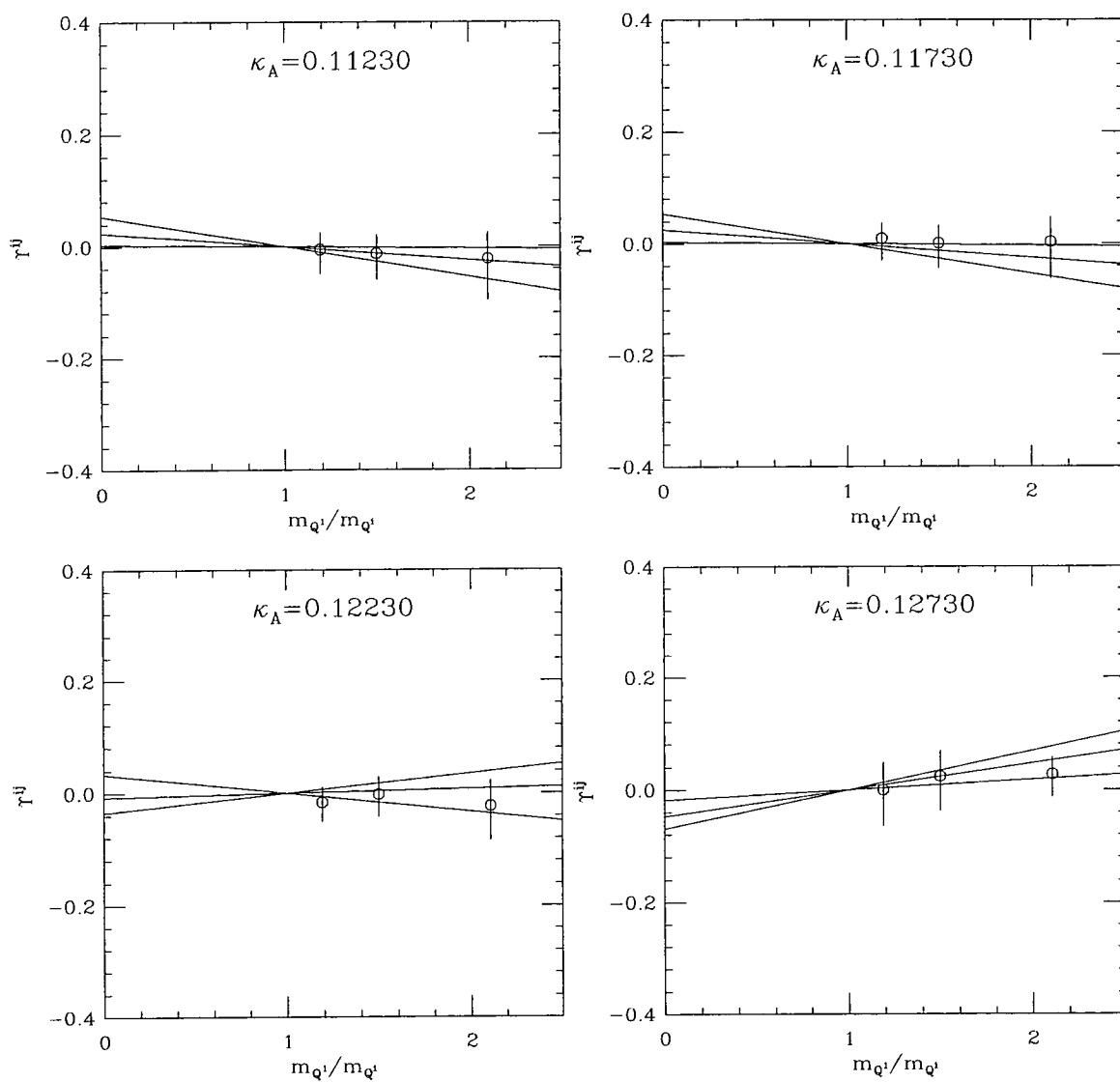
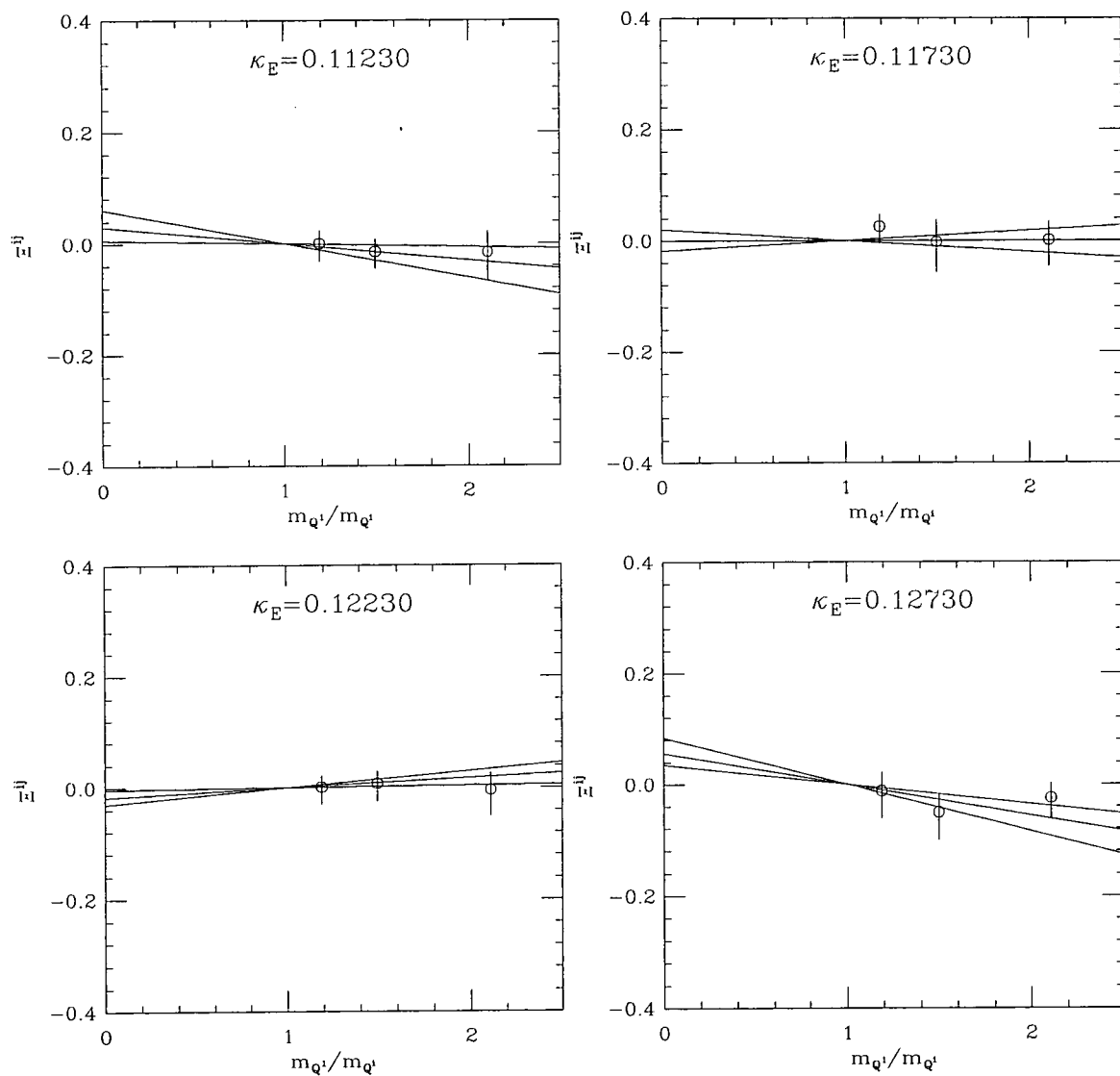
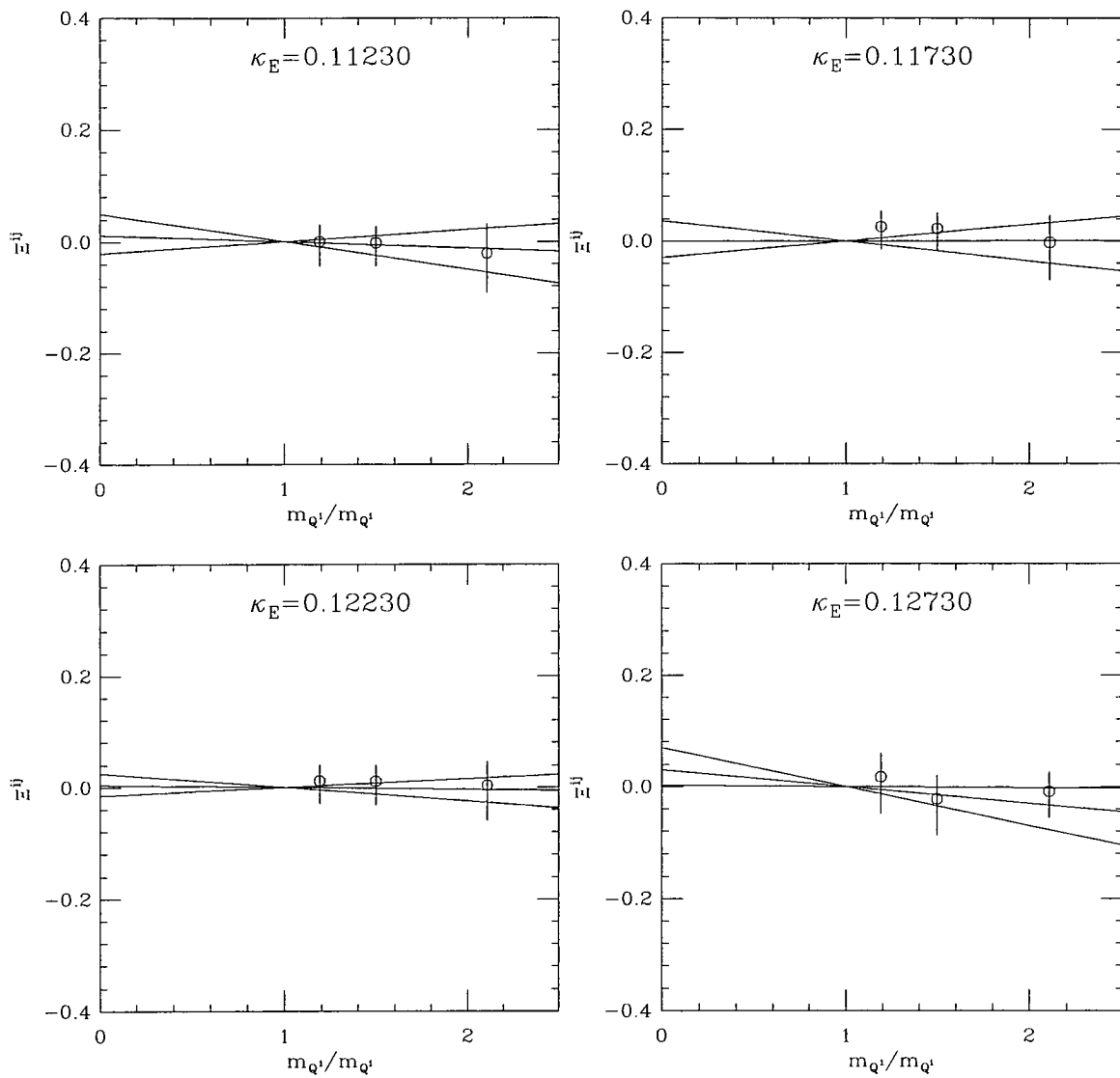


Figure 6.14: The ratio  $\Upsilon^{ij}$  for  $\kappa_P = 0.13344$ ,  $\beta = 6.0$ .

Figure 6.15: The ratio  $\Upsilon^{ij}$  for  $\kappa_P = 0.13417$ ,  $\beta = 6.0$ .

Figure 6.16: The ratio  $\Xi^{ij}$  for  $\kappa_P = 0.13344$ ,  $\beta = 6.0$ .

Figure 6.17: The ratio  $\Xi^{ij}$  for  $\kappa_P = 0.13417$ ,  $\beta = 6.0$ .

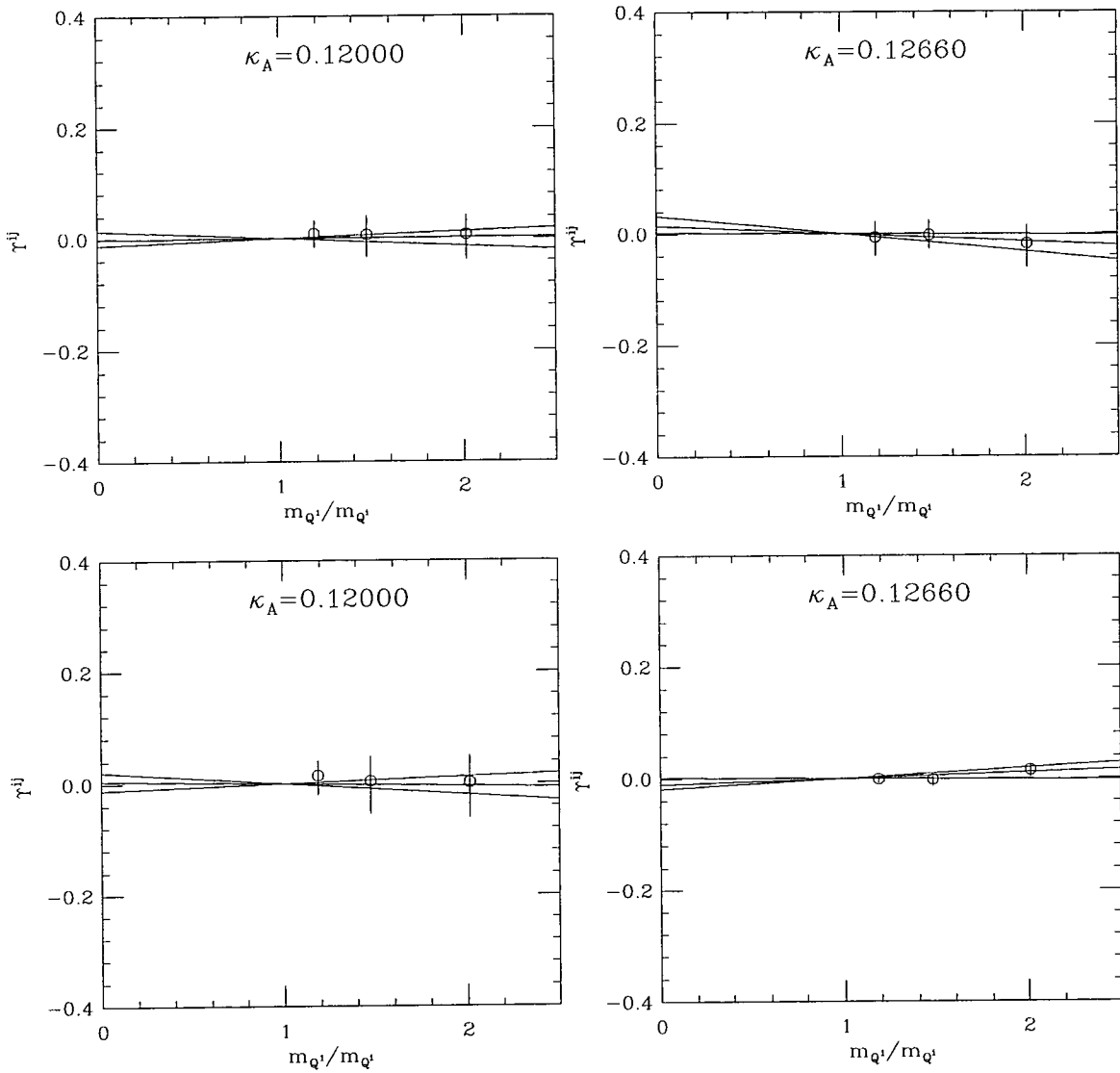
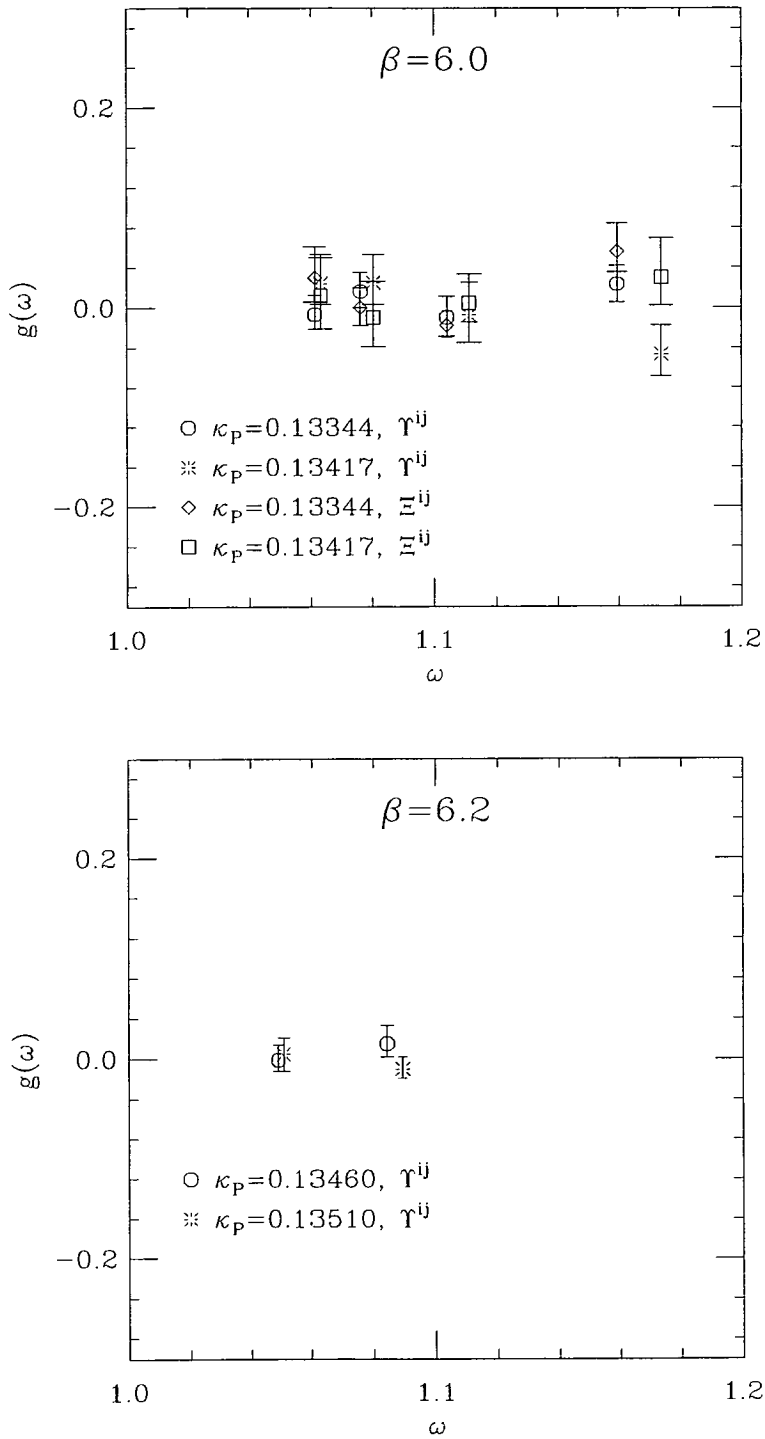


Figure 6.18: The ratio  $\Upsilon^{ij}$  for  $\kappa_P = 0.13460$  (top row),  $\kappa_P = 0.13510$  (bottom row),  $\beta = 6.2$ .

Figure 6.19: The form factor  $g(\omega)$ .

## 6.6 Lattice Isgur Wise functions

The conclusion of the preceding analysis is that for a given value of the spectator quark mass, the data for non-degenerate transitions can be reliably combined since there is no discernible heavy mass dependence on the radiatively corrected  $h_+(\omega)$ . The full data set can then be used to verify that  $\xi^{\text{eff}}(\omega)$  is an Isgur Wise function.

To check the lack of dependence on the heavy quark masses, the degenerate and non-degenerate decays are fitted to various forms of the Isgur Wise function. The four chosen parametrisations are,

$$\xi_{\text{NR}}(\omega) = \frac{2}{\omega + 1} \exp \left[ -\frac{(2\rho^2 - 1)(\omega - 1)}{\omega + 1} \right], \quad (6.36)$$

$$\xi_{\text{ISGW}}(\omega) = \exp \left[ -\rho^2(\omega - 1) \right], \quad (6.37)$$

$$\xi_{\text{POLE}}(\omega) = \left[ \frac{2}{\omega + 1} \right]^{2\rho^2}, \quad (6.38)$$

$$\xi_{\text{QUAD}}(\omega) = 1 - \rho^2(\omega - 1) + c(\omega - 1)^2. \quad (6.39)$$

The results of the fits are presented in tables 6.16-6.19 and are illustrated in figures 6.20-6.23.

$\xi^{\text{eff}}(\omega) = \xi_{\text{NR}}(\omega)$			
$\beta$	$\kappa_P$	$\rho_{\text{eff}}^2$	$\chi^2/dof$
6.0	0.13344	$1.17 \begin{smallmatrix} +6 \\ -5 \end{smallmatrix}$	53.40 / 79
6.0	0.13417	$1.15 \begin{smallmatrix} +8 \\ -7 \end{smallmatrix}$	29.38 / 79
6.2	0.13460	$1.18 \begin{smallmatrix} +10 \\ -12 \end{smallmatrix}$	10.43 / 39
6.2	0.13510	$1.15 \begin{smallmatrix} +13 \\ -15 \end{smallmatrix}$	3.88 / 39

Table 6.16: All data fitted to the Neubert Rieckert parametrisation of the Isgur Wise function.

$\xi^{\text{eff}}(\omega) = \xi_{\text{ISGW}}(\omega)$			
$\beta$	$\kappa_P$	$\rho_{\text{eff}}^2$	$\chi^2/dof$
6.0	0.13344	$1.03^{+6}_{-4}$	126.81 / 79
6.0	0.13417	$1.01^{+7}_{-6}$	84.56 / 79
6.2	0.13460	$1.08^{+9}_{-10}$	16.96 / 39
6.2	0.13510	$1.05^{+11}_{-14}$	6.00 / 39

Table 6.17: All data fitted to the ISGW parametrisation of the Isgur Wise function.

$\xi^{\text{eff}}(\omega) = \xi_{\text{POLE}}(\omega)$			
$\beta$	$\kappa_P$	$\rho_{\text{eff}}^2$	$\chi^2/dof$
6.0	0.13344	$1.12^{+6}_{-5}$	71.17 / 79
6.0	0.13417	$1.10^{+7}_{-6}$	42.51 / 79
6.2	0.13460	$1.14^{+10}_{-11}$	12.06 / 39
6.2	0.13510	$1.11^{+12}_{-14}$	4.18 / 39

Table 6.18: All data fitted to a pole ansatz for the Isgur Wise function.

$\xi^{\text{eff}}(\omega) = \xi_{\text{QUAD}}(\omega)$				
$\beta$	$\kappa_P$	$\rho_{\text{eff}}^2$	c	$\chi^2/dof$
6.0	0.13344	$1.13^{+8}_{-7}$	$0.72^{+24}_{-9}$	63.06 / 78
6.0	0.13417	$1.10^{+9}_{-10}$	$0.67^{+26}_{-9}$	37.22 / 78
6.2	0.13460	$1.17^{+14}_{-18}$	$0.89^{+66}_{-29}$	11.14 / 38
6.2	0.13510	$1.11^{+18}_{-24}$	$0.70^{+79}_{-37}$	4.40 / 38

Table 6.19: All data fitted to the quadratic expansion of the Isgur Wise function.

The results clearly show that the data is well modelled by the four chosen parametrisations of the Isgur Wise function. As can be seen from the relative  $\chi^2$ , the Neubert Rieckert parametrisation most faithfully models the data over the full range of  $\omega$ . The ISGW model provides a good fit also, but the results at  $\beta = 6.0$  where the range of recoil is larger due to the increased number of kappa combinations, suggests that this is only valid for  $\omega < 1.4$ . The pole ansatz and quadratic parametrisation show remarkable agreement to the data, although

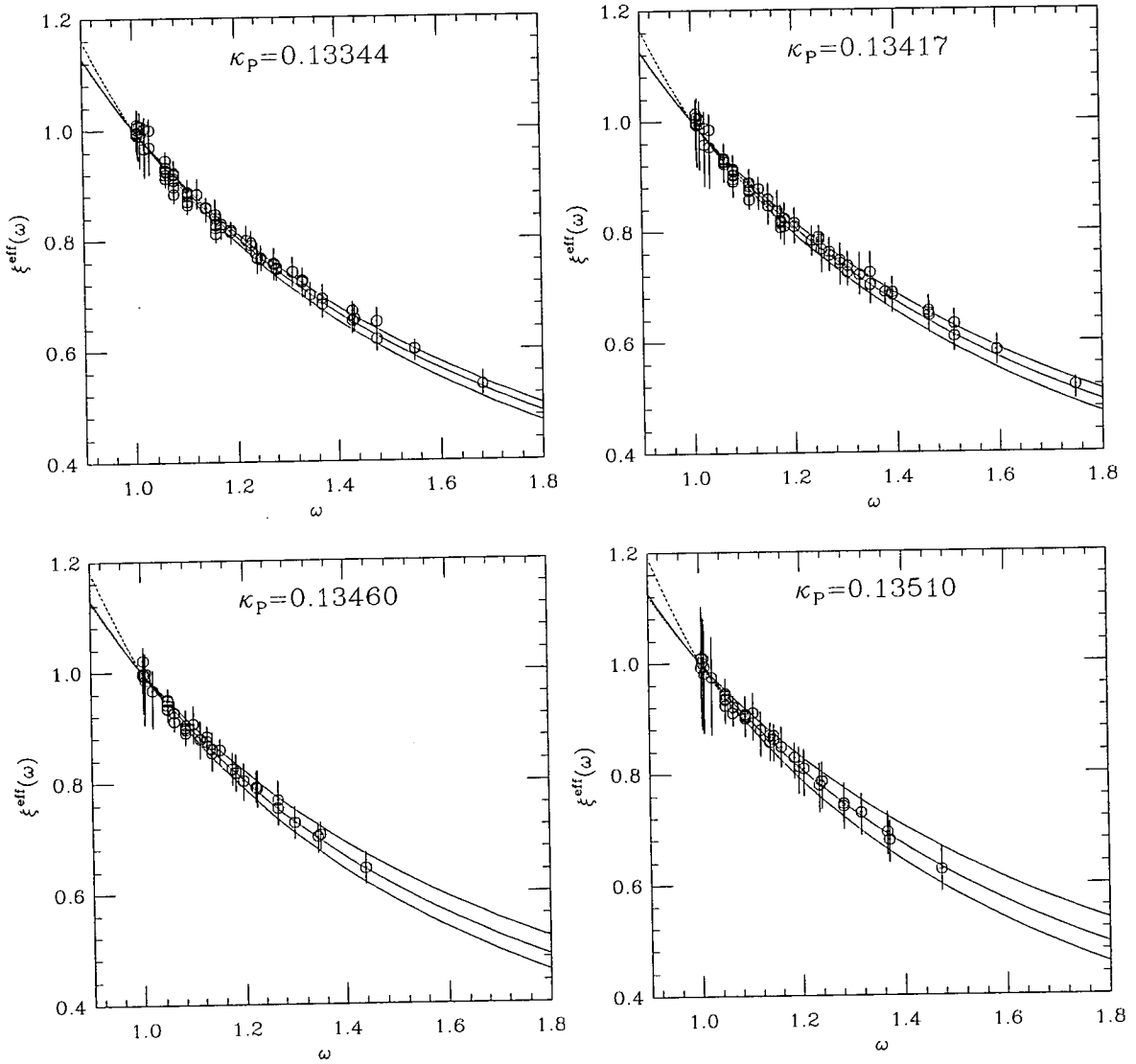


Figure 6.20: All transitions fitted to NR parametrisation. Top row  $\beta = 6.0$ , bottom row  $\beta = 6.0$ .

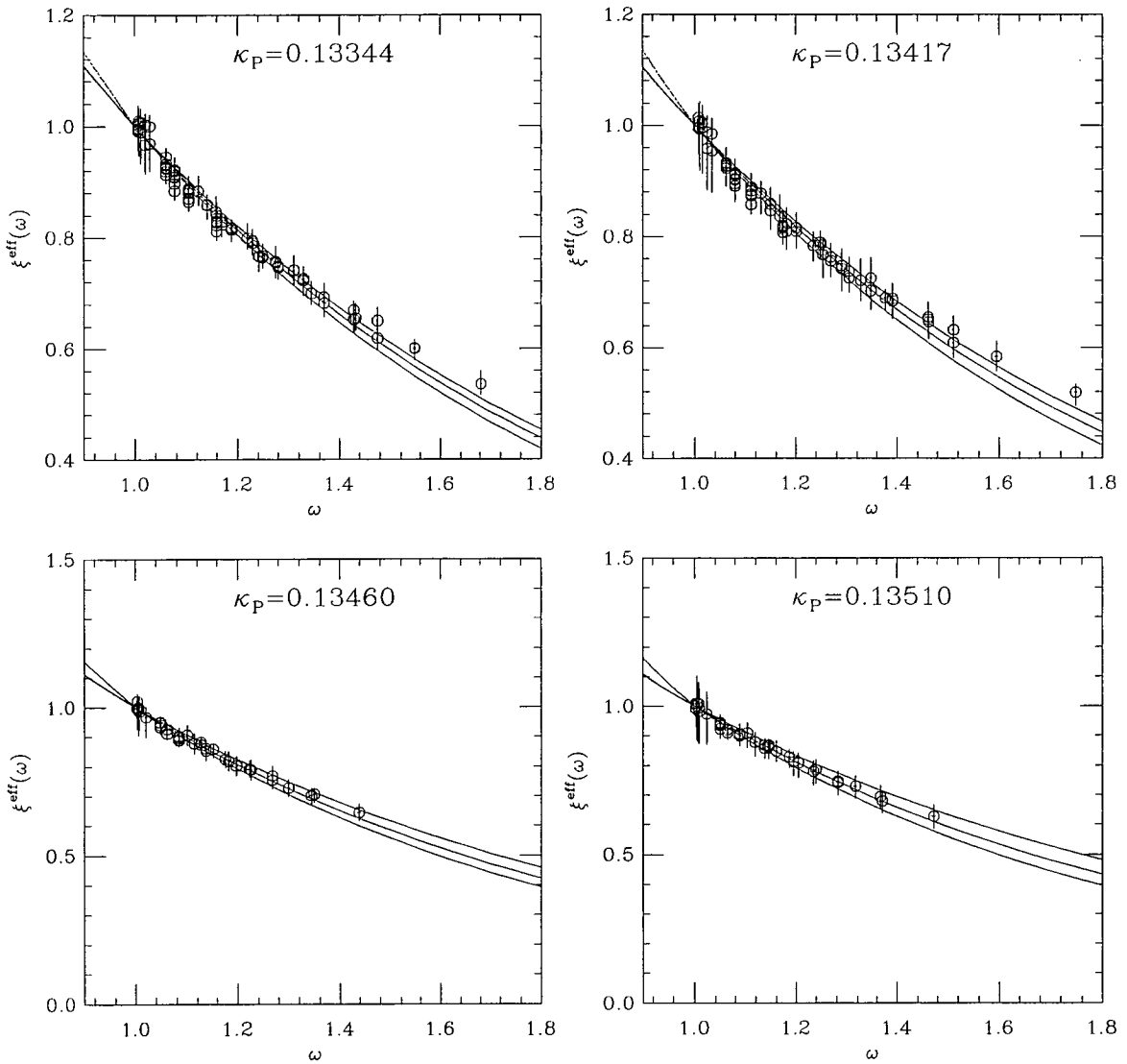


Figure 6.21: All transitions fitted to ISGW parametrisation. Top row  $\beta = 6.0$ , bottom row  $\beta = 6.0$ .

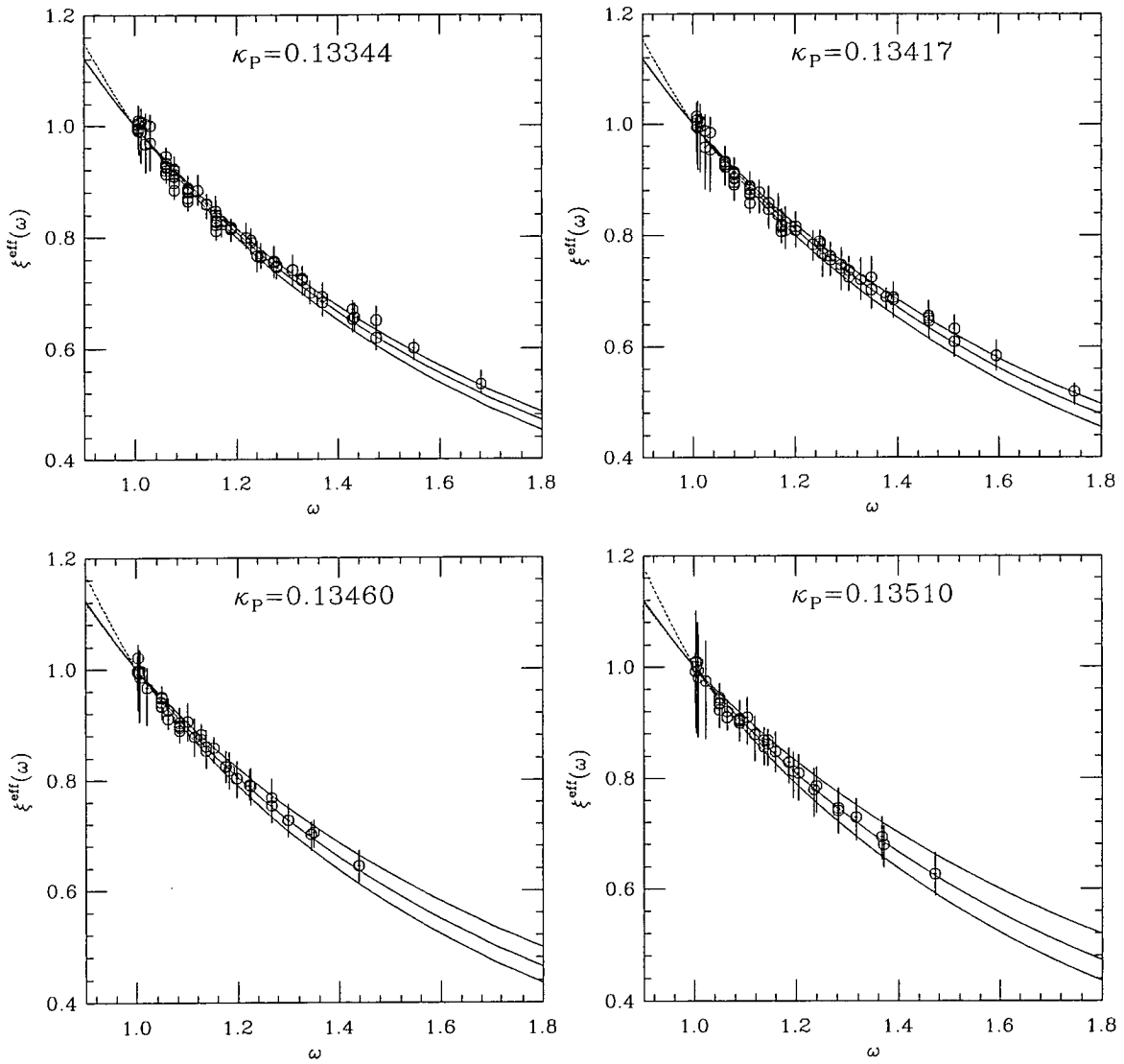


Figure 6.22: All transitions fitted to pole ansatz. Top row  $\beta = 6.0$ , bottom row  $\beta = 6.0$ .

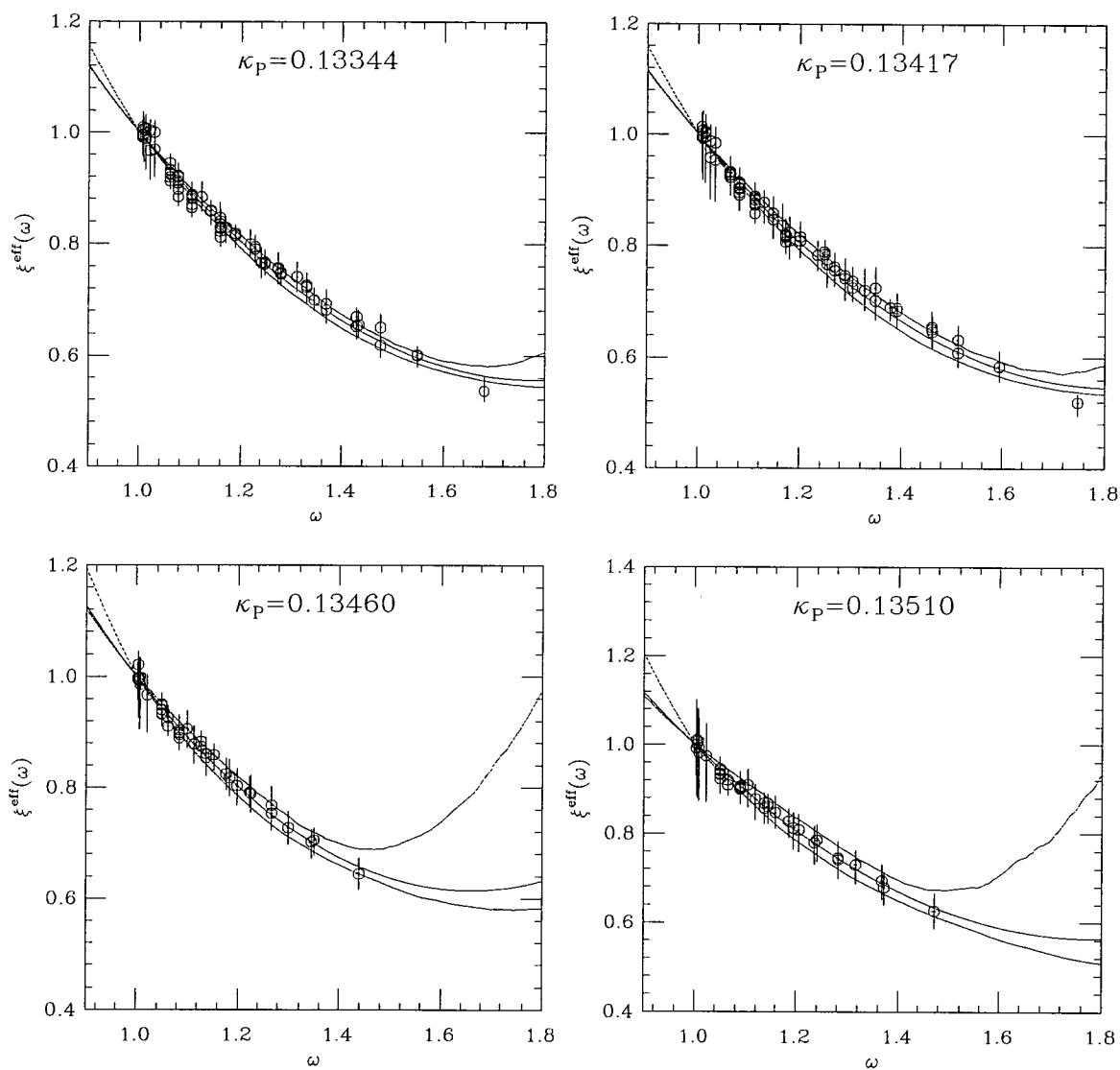


Figure 6.23: All transitions fitted to quadratic expansion. Top row  $\beta = 6.0$ , bottom row  $\beta = 6.0$ .

they exhibit a larger  $\chi^2$  than the NR parametrisation.

The plots suggest that statistical errors are very small. For the degenerate dataset, the channels  $(0,0,0) \rightarrow (1,0,0)$  and  $(1,0,0) \rightarrow (0,0,0)$  share the same velocity transfer. However the second of these channels is constructed from less raw data since for the former channel, the data is averaged over the three spatial directions for the final meson. The values of the Isgur Wise function obtained from these channels are consistent over all recoils. Also for each of these two channels, since one meson has zero spatial momentum then there is multiple data for four different values of the recoil. For example, when  $\kappa_P = 0.13344$  there are eight points for  $\omega = 1.06013$  corresponding to a non stationary heavy quark mass equivalent to  $\kappa = 0.11230$ . Reassuringly, these points are consistent providing the fits with a surprisingly low  $\chi^2/dof$ .

The channel  $(1,0,0) \rightarrow (1,0,0)$  was discussed when considering  $h_-(\omega)$ . Again it is found that this channel provides the poorest quality of data. This channel corresponds to an almost zero recoil decay and although the data over all four spectator masses is consistent with unity, the statistical errors are very large in comparison to every other channel.

## 6.7 Spectator Quark Mass Dependence

Having established that there is no discernible heavy quark mass dependence on the radiatively corrected form factor  $h_+(\omega)$ , the Isgur Wise functions corresponding to the physical processes  $\overline{B}_s \rightarrow D_s l \overline{\nu}$  and  $\overline{B} \rightarrow D l \overline{\nu}$  are then obtained by examining the dependence on the light quark mass.

Recall from section 5.4 the definition of the improved bare quark mass in the non-perturbatively improved scheme,

$$a\tilde{m}_q = am_q(1 + b_m am_q). \quad (6.40)$$

Given that for each lattice there are only two hopping parameters used in the simulation a linear extrapolation is performed in this improved quark mass.

### 6.7.1 Chiral Extrapolation

Both  $h_+(\omega)$  and  $\omega$  exhibit some dependence on the light quark mass and therefore an extrapolation is performed on both quantities. Both are fitted to a linear form,

$$\begin{aligned} h_+(\omega) &= \Theta_h(a\tilde{m}_q) + \Gamma_h, \\ \omega &= \Theta_\omega(a\tilde{m}_q) + \Gamma_\omega \end{aligned} \quad (6.41)$$

so that that  $h_+^x(\omega) = \Gamma_h$  and  $\omega^x = \Gamma_\omega$ . The results of the chiral extrapolations are given in Appendix C.

### 6.7.2 Interpolation to Strange Quark Mass

In section 5.5, the hopping parameters corresponding to the strange quark mass were found to be,

$$\begin{aligned} \kappa_s|_{\beta=6.0} &= 0.13400 \begin{array}{c} + 1 \\ - 1 \end{array} \\ \kappa_s|_{\beta=6.2} &= 0.13493 \begin{array}{c} + 1 \\ - 1 \end{array}. \end{aligned} \quad (6.42)$$

The interpolations are performed in the same way as the chiral extrapolations so that,

$$\begin{aligned} h_+^s(\omega) &= \Theta_h(a\tilde{m}_s) + h_+^x(\omega), \\ \omega^s &= \Theta_\omega(a\tilde{m}_s) + \omega^x \end{aligned} \quad (6.43)$$

where  $a\tilde{m}_s$  is the improved strange quark mass (equation 5.30). The results of the strange interpolations are given in Appendix C.

Both the chiral extrapolations and strange interpolations are fitted to the four parametrisations of  $\xi(\omega)$ . The results are presented in tables 6.20-6.23 and in figures 6.24-6.27. As expected from the results of the previous section, the most faithful parametrisation is given by the Neubert Rieckert model.

$\xi^{\text{eff}}(\omega) = \xi_{\text{NR}}(\omega)$			
$\beta$	$\kappa_P$	$\rho_{\text{eff}}^2$	$\chi^2/\text{dof}$
6.0	0.13400 (strange)	$1.15 \begin{smallmatrix} +8 \\ -6 \end{smallmatrix}$	31.42 / 79
6.0	0.13525 (chiral)	$1.13 \begin{smallmatrix} +10 \\ -11 \end{smallmatrix}$	33.25 / 79
6.2	0.13492 (strange)	$1.16 \begin{smallmatrix} +12 \\ -14 \end{smallmatrix}$	4.16 / 39
6.2	0.13583 (chiral)	$1.12 \begin{smallmatrix} +17 \\ -21 \end{smallmatrix}$	6.07 / 39

Table 6.20: Extrapolated data fitted to the Neubert Rieckert parametrisation of the Isgur Wise function.

$\xi^{\text{eff}}(\omega) = \xi_{\text{ISGW}}(\omega)$			
$\beta$	$\kappa_P$	$\rho_{\text{eff}}^2$	$\chi^2/\text{dof}$
6.0	0.13400 (strange)	$1.01 \begin{smallmatrix} +5 \\ -7 \end{smallmatrix}$	90.44 / 79
6.0	0.13525 (chiral)	$0.98 \begin{smallmatrix} +9 \\ -12 \end{smallmatrix}$	65.14 / 79
6.2	0.13492 (strange)	$1.06 \begin{smallmatrix} +13 \\ -10 \end{smallmatrix}$	7.35 / 39
6.2	0.13583 (chiral)	$1.01 \begin{smallmatrix} +19 \\ -15 \end{smallmatrix}$	7.96 / 39

Table 6.21: Extrapolated data fitted to the ISGW parametrisation of the Isgur Wise function.

$\xi^{\text{eff}}(\omega) = \xi_{\text{POLE}}(\omega)$			
$\beta$	$\kappa_P$	$\rho_{\text{eff}}^2$	$\chi^2/\text{dof}$
6.0	0.13400 (strange)	$1.10 \begin{smallmatrix} +6 \\ -7 \end{smallmatrix}$	45.55 / 79
6.0	0.13525 (chiral)	$1.07 \begin{smallmatrix} +9 \\ -10 \end{smallmatrix}$	40.43 / 79
6.2	0.13492 (strange)	$1.12 \begin{smallmatrix} +13 \\ -12 \end{smallmatrix}$	4.76 / 39
6.2	0.13583 (chiral)	$1.09 \begin{smallmatrix} +20 \\ -15 \end{smallmatrix}$	7.78 / 39

Table 6.22: Extrapolated data fitted to a pole ansatz for the Isgur Wise function.

$\xi^{\text{eff}}(\omega) = \xi_{\text{QUAD}}(\omega)$				
$\beta$	$\kappa_P$	$\rho_{\text{eff}}^2$	$c$	$\chi^2/\text{dof}$
6.0	0.13400 (strange)	$1.11 \begin{smallmatrix} +5 \\ -6 \end{smallmatrix}$	$0.68 \begin{smallmatrix} +24 \\ -34 \end{smallmatrix}$	39.64 / 78
6.0	0.13525 (chiral)	$1.06 \begin{smallmatrix} +6 \\ -7 \end{smallmatrix}$	$0.60 \begin{smallmatrix} +27 \\ -29 \end{smallmatrix}$	38.91 / 78
6.2	0.13492 (strange)	$1.13 \begin{smallmatrix} +14 \\ -28 \end{smallmatrix}$	$0.76 \begin{smallmatrix} +39 \\ -29 \end{smallmatrix}$	4.87 / 38
6.2	0.13583 (chiral)	$1.03 \begin{smallmatrix} +20 \\ -34 \end{smallmatrix}$	$0.52 \begin{smallmatrix} +42 \\ -30 \end{smallmatrix}$	11.81 / 38

Table 6.23: Extrapolated data fitted to the quadratic expansion of the Isgur Wise function.

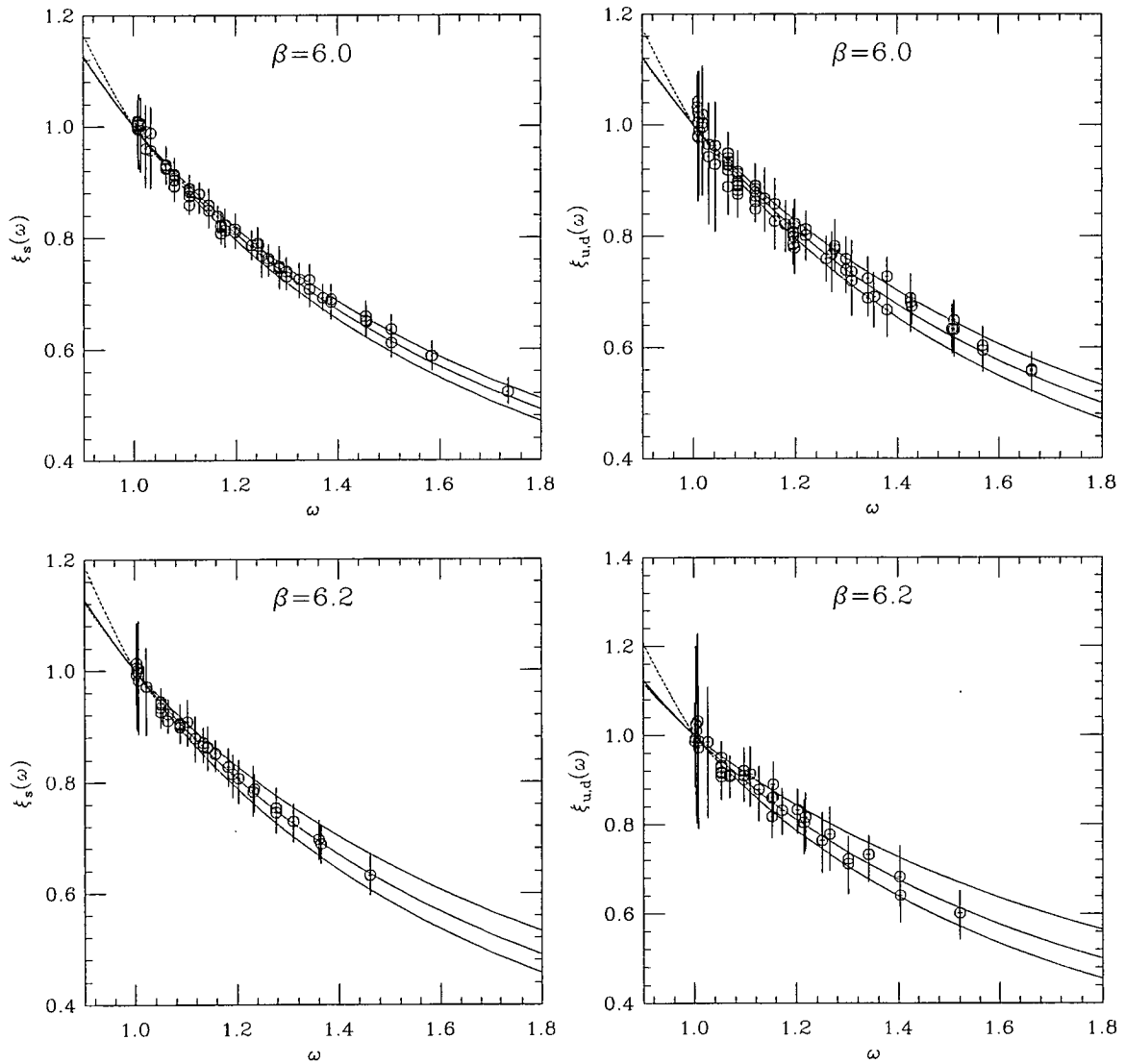


Figure 6.24: Extrapolated data fitted to Neubert Rieckert parametrisation.

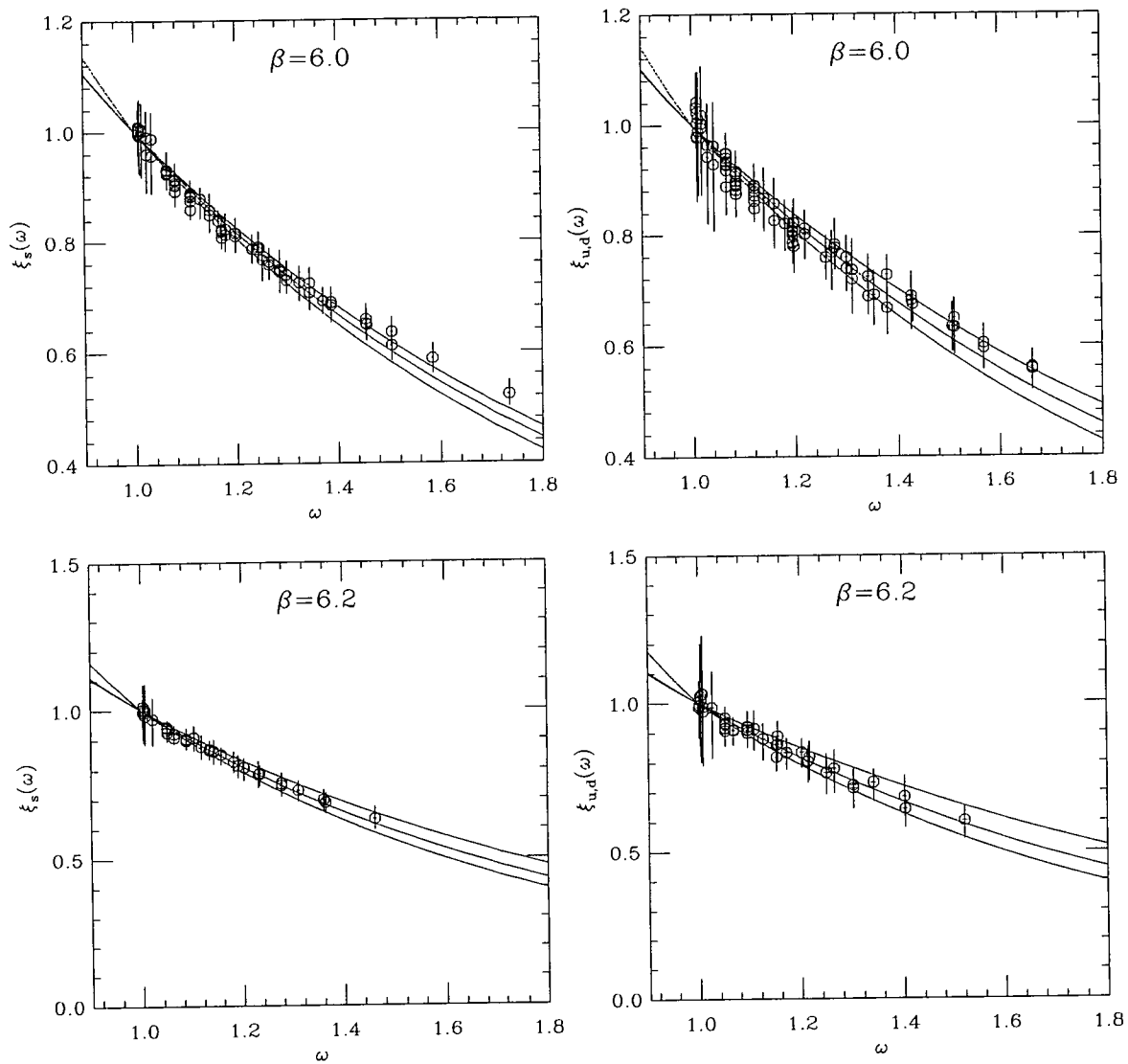


Figure 6.25: Extrapolated data fitted to ISGW model.

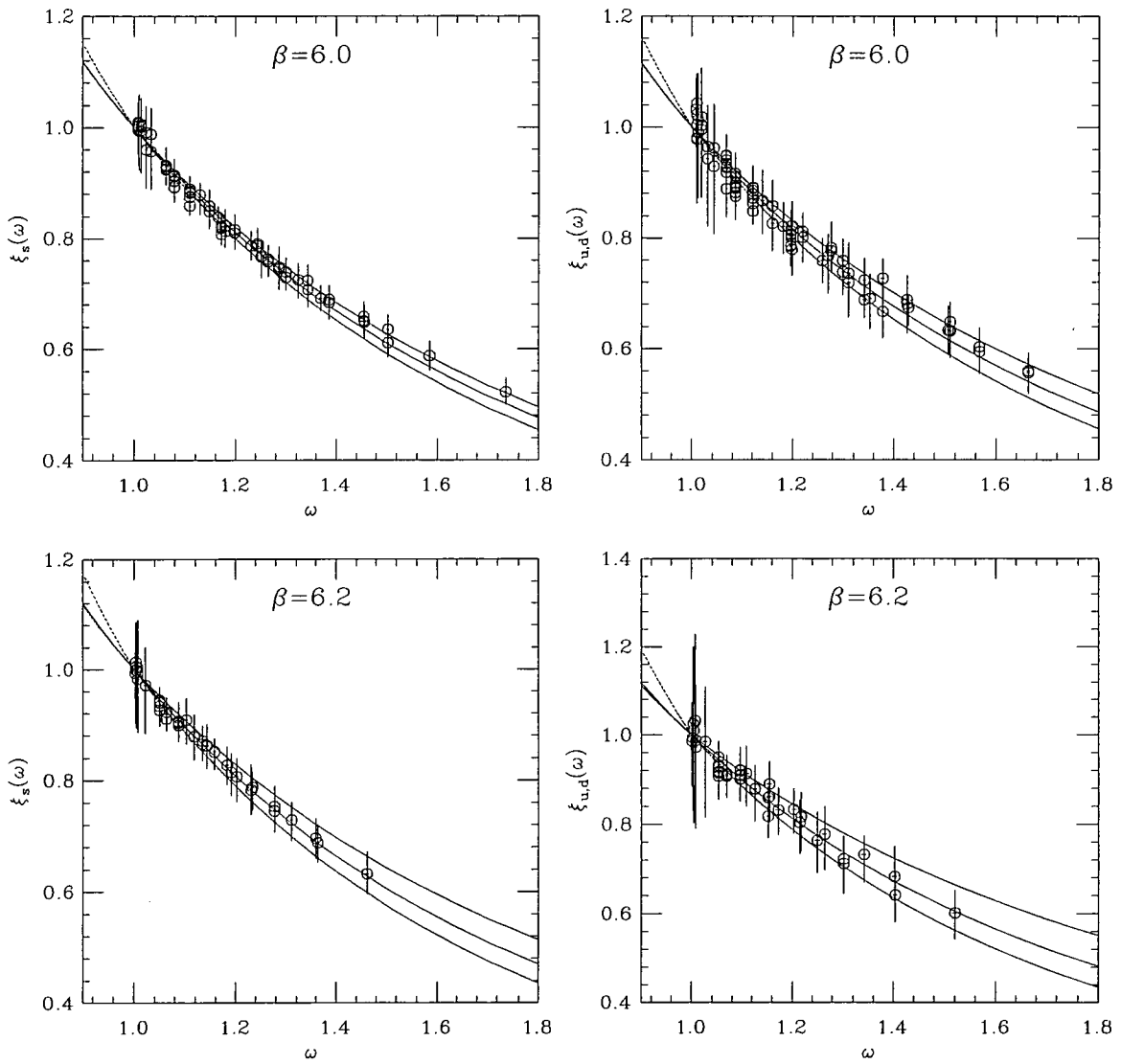


Figure 6.26: Extrapolated data fitted to pole ansatz.

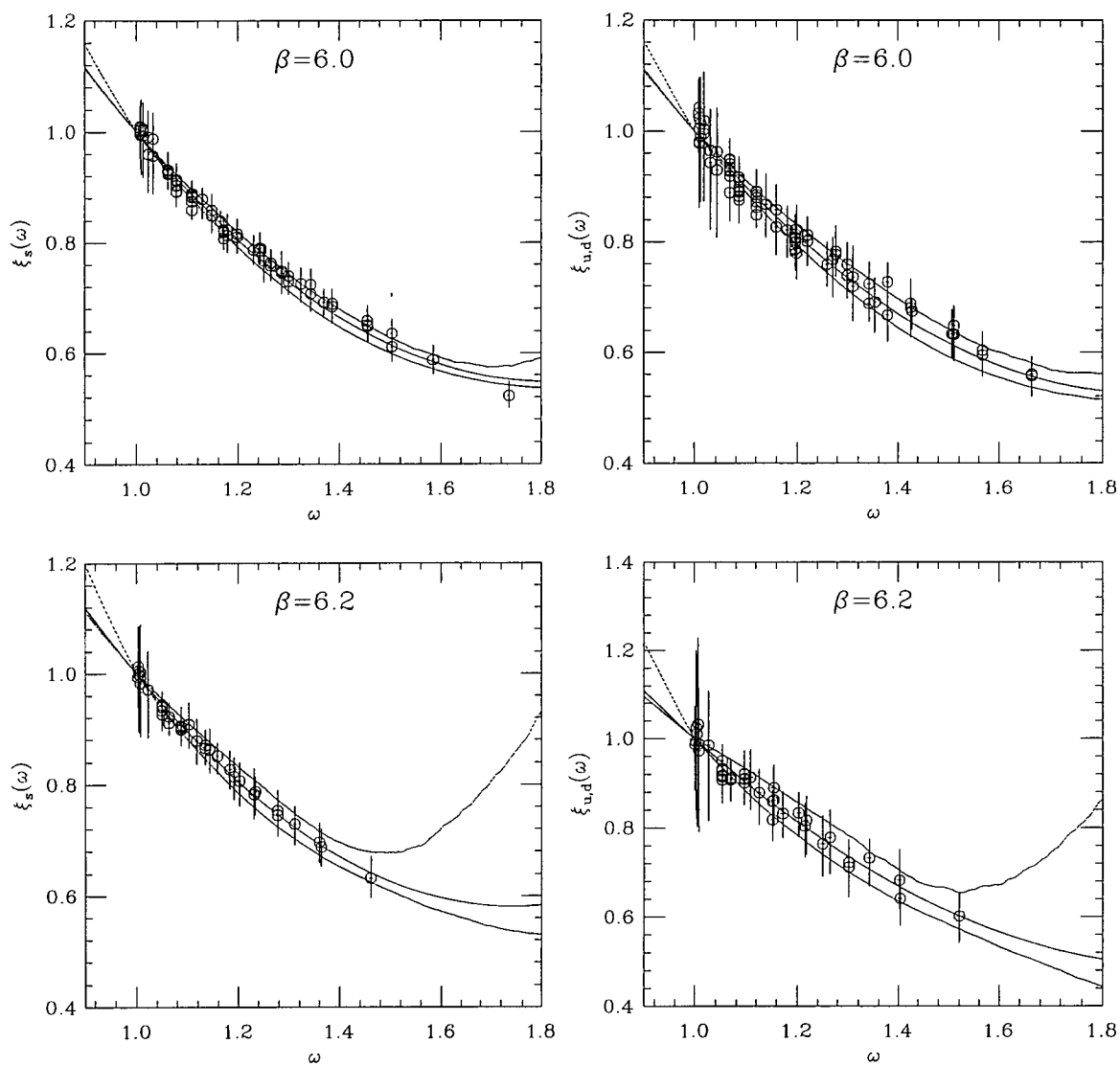


Figure 6.27: Extrapolated data fitted to quadratic expansion.

## 6.8 Extracting $\rho^2$

Since the Neubert Rieckert parametrisation yields the best fits to the data, it will be used as the standard form in the proceeding analysis, providing the central value and statistical errors for  $\rho^2$ .

### 6.8.1 Systematic error

In order to quantify the systematic error on the slope of the Isgur Wise function, the momentum dependent discretisation errors must be studied (the mass ones have been shown to be negligible). This is achieved by fitting the data to the Neubert Rieckert parametrisation independently for each of the momentum channels. The spread of central values will then provide the required systematic error. This could however be an over-estimate since in fact some of the error will be attributed to statistical uncertainty. Table 6.24 below shows the results of the fits for the individual momentum channels when the light anti-quark is  $\bar{u}$ ,  $\bar{d}$  and  $\bar{s}$ . The channel  $(1,0,0) \rightarrow (1,0,0)$  is excluded from this analysis since the data is relatively very noisy and explores only a tiny fraction of the range of recoils hence providing an unreliable estimate of the slope.

Channel	$\beta = 6.0$		$\beta = 6.2$	
	$\rho_{u,d}^2$	$\rho_s^2$	$\rho_{u,d}^2$	$\rho_s^2$
$(0,0,0) \rightarrow (1,0,0)$	1.20 $^{+16}_{-18}$	1.19 $^{+12}_{-8}$	1.10 $^{+26}_{-21}$	1.22 $^{+20}_{-14}$
$(1,0,0) \rightarrow (0,0,0)$	1.20 $^{+12}_{-18}$	1.21 $^{+10}_{-11}$	1.13 $^{+21}_{-28}$	1.19 $^{+15}_{-15}$
$(1,0,0) \rightarrow (0,1,0)$	1.10 $^{+13}_{-11}$	1.13 $^{+8}_{-6}$	1.06 $^{+24}_{-16}$	1.11 $^{+14}_{-9}$
$(1,0,0) \rightarrow (-1,0,0)$	1.08 $^{+14}_{-11}$	1.15 $^{+9}_{-6}$	1.18 $^{+15}_{-16}$	1.15 $^{+10}_{-6}$

Table 6.24: Comparison of  $\rho^2$  for different momentum channels.

There is good agreement with the central value (using all momentum channels). The channels  $(1,0,0) \rightarrow (0,1,0)$  and  $(1,0,0) \rightarrow (-1,0,0)$  provide the least statistically noisy values for the slope since those channels do not have multiple points for each value of the recoil (as discussed for the other two channels in section 6.6).

Combining these results, the final values for the slope of the Isgur Wise function are,

$$\rho_s^2|_{\beta=6.0} = 1.15 \begin{matrix} +8 & +6 \\ -6 & -2 \end{matrix}, \quad (6.44)$$

$$\rho_{u,d}^2|_{\beta=6.0} = 1.13 \begin{matrix} +10 & +7 \\ -11 & -5 \end{matrix}, \quad (6.45)$$

$$\rho_s^2|_{\beta=6.2} = 1.16 \begin{matrix} +12 & +6 \\ -14 & -5 \end{matrix}, \quad (6.46)$$

$$\rho_{u,d}^2|_{\beta=6.2} = 1.12 \begin{matrix} +17 & +6 \\ -21 & -6 \end{matrix} \quad (6.47)$$

where the first error is statistical and the second error is systematic.

As a verification of the adoption of the radiatively corrected form factor as the Isgur Wise function, the extrapolated data is fitted to the NR parametrisation for only those points for which the power corrections were explicitly shown to be negligible. Hence for  $\beta = 6.0$  only points with  $\omega < 1.2$  are fitted, and at  $\beta = 6.2$  only points with  $\omega < 1.1$  are fitted. The fits are in table 6.25 alongside the fits for the full datasets.

$\kappa_q$	$\rho^2(\omega < 1.1)$	$\rho^2(\omega < 1.2)$	$\rho^2(\text{full})$
0.13400	-	$1.18 \begin{matrix} +13 \\ -9 \end{matrix}$	$1.15 \begin{matrix} +8 \\ -6 \end{matrix}$
0.13525	-	$1.12 \begin{matrix} +15 \\ -15 \end{matrix}$	$1.13 \begin{matrix} +10 \\ -11 \end{matrix}$
0.13492	$1.17 \begin{matrix} +15 \\ -20 \end{matrix}$	-	$1.16 \begin{matrix} +6 \\ -5 \end{matrix}$
0.13583	$1.10 \begin{matrix} +23 \\ -31 \end{matrix}$	-	$1.12 \begin{matrix} +17 \\ -21 \end{matrix}$

Table 6.25: Comparison of  $-\xi'(1)$  from full and restricted data sets as described in the text.

The table shows that the obtained slopes for the full and restricted sets are consistent. Together with the previous analysis, this verifies the final results for the slope of the Isgur Wise function at zero recoil.

### 6.8.2 Discussion of results for $\rho^2$

The results of the previous section show that for both  $\rho_{rms}^2$  and  $\rho_{u,d}^2$  there is little lattice spacing dependence and scaling is observed.

The value of  $\rho^2$  is above the lower bound by Bjorken. Table 6.26 lists the results of  $\rho^2$  from various sources.

Reference	$\rho_{u,d}^2$
Voloshin [55]	$1.4^{+3}_{-3}$
Burdman [75]	$1.08^{+10}_{-10}$
Neubert [45]	$0.66^{+5}_{-5}$
Høgaasen [76]	0.98
Blok [77]	$0.70^{+25}_{-25}$
Bagan [78]	$0.84^{+2}_{-2}$
Close [79]	1.4
Morénas [80]	1.0

Table 6.26: Slope of the Isgur Wise function from various sources.

There have been several lattice calculations of the slope of the Isgur Wise function. A previous UKQCD calculation [81] in which a similar study is done, found  $\rho_{u,d}^2 = 0.9^{+2}_{-3} {}^{+4}_{-2}$ . A slightly older calculation yields  $\rho_{u,d}^2 = 1.24^{+26}_{-26} {}^{+26}_{-26}$  [82]. There have also been some lattice calculations where HQET is directly implemented into the simulation. Hashimoto et al [83] find  $\rho_{u,d}^2 = 0.70^{+17}_{-17}$ . A more recent HQET calculation [84] quotes  $\rho_{u,d}^2 = 0.64^{+13}_{-13}$ . A recent preliminary calculation using NRQCD heavy quarks finds  $\rho_{u,d}^2 = 1.5^{+3}_{-3} {}^{+4}_{-4}$  [85]. The results of this calculation are consistent with the literature.

There is a trend on both lattices for the slope  $\rho^2$  to decrease as the light quark mass is decreased. This trend was also found in a previous UKQCD calculation of these form factors [81] where it was found  $\rho_s^2 = 1.12^{+2}_{-2} {}^{+2}_{-1}$ . Similarly Close and Wambach [79] find an increased value,  $\rho_s^2 = 1.64$ . Morénas et al [80] find  $\rho_s^2 = 1.15$ . Høgaasen et al find the same trend with  $\rho_s^2 = 1.135$ . The trend observed in

this calculation is clearly much less than those found in other calculations.

The average experimental value for the slope is  $\rho_{u,d}^2 = 0.71 \begin{smallmatrix} +11 \\ -11 \end{smallmatrix} \begin{smallmatrix} +20 \\ -20 \end{smallmatrix}$  [86], where the second error is theoretical [87]. This value is somewhat low, although it is worth noting that generally, the experimental slopes are obtained using a linear fit,

$$\xi_{\text{linear}}(\omega) = 1 - \rho^2(\omega - 1). \quad (6.48)$$

This form does not have positive curvature (unlike the four parametrisations used throughout this thesis) and hence yields lower values of  $\rho^2$ .

## 6.9 Extracting $V_{cb}$

The weak decay of a meson is trivially given by the product of three quantities, kinematic factors, the relevant CKM matrix element and a non-perturbative QCD factor. This chapter has focused on the determination of this last factor and thus a knowledge of the experimental decay rate leads to a determination of  $V_{cb}$ .

The decay rate for  $\bar{B} \rightarrow D l \bar{\nu}$  is given by [88]

$$\begin{aligned} \frac{d\Gamma(\bar{B} \rightarrow D l \bar{\nu})}{d\omega} &= \frac{G_F^2}{48\pi^3} |V_{cb}|^2 (m_B + m_D)^2 m_D^3 (\omega^2 - 1)^{\frac{3}{2}} \\ &\times \left| h_+(\omega) + \frac{m_D - m_B}{m_D + m_B} h_-(\omega) \right| \end{aligned} \quad (6.49)$$

However, Luke's theorem does not protect this decay rate at zero recoil and this leads to a factor  $(\omega^2 - 1)$  in the decay rate [52], resulting in the helicity suppression of this process at zero recoil. However by exploiting the spin symmetry of HQET, the decay rates for  $\bar{B} \rightarrow D^* l \bar{\nu}$  (where there is no suppression) can be used to extract  $|V_{cb}|$ .

The differential rate for the pseudoscalar to vector decay is given by [81]

$$\begin{aligned} \frac{d\Gamma(\bar{B} \rightarrow D^* l \bar{\nu})}{d\omega} &= \frac{G_F^2}{48\pi^3} |V_{cb}|^2 (m_B - m_D)^2 m_D^3 (\omega + 1)^2 \\ &\times \sqrt{\omega^2 - 1} [1 + \beta_{A_1}(1)]^2 K(\omega) \xi_{u,d}^2(\omega) \end{aligned}$$

$$\times \left( 1 + \frac{4\omega [m_B^2 + m_D^2 - 2\omega m_D m_B]}{[\omega + 1][m_B - m_D]^2} \right) \quad (6.50)$$

where  $K(\omega)$  is a collection of radiative corrections for  $\omega \neq 1$ , power corrections to  $h_{A_1}(\omega)$ , and contributions from  $h_V(\omega)$ ,  $h_{A_2}(\omega)$  and  $h_{A_3}(\omega)$ . Neubert [45] has shown that in exact symmetry  $K(\omega) = 1 \forall \omega$ . Since  $K(\omega)$  is a function of the various radiative and power corrections it is assumed to not deviate from 1.

Assuming  $K(\omega) = 1$ ,  $|V_{cb}|$  is extracted from the decay rates for  $\bar{B} \rightarrow D^* l \bar{\nu}$ . Table 6.27 shows a one parameter fit of the experimental data from ALEPH [89] and CLEO [90] to the quantity,

$$\xi_{u,d}(\omega)[\beta_{A_1}(1) + 1]|V_{cb}|, \quad (6.51)$$

where  $\beta_{A_1} = -0.01$  from [50] and  $\xi_{u,d}$  is the lattice result. The experimental and lattice data are plotted in figure 6.28.

Experiment	$\beta = 6.0$			$\chi^2/dof$	$\beta = 6.2$			$\chi^2/dof$		
	$D V_{cb} $				$D V_{cb} $					
ALEPH	0.0379	$^{+12}_{-9}$	$^{+5}_{-4}$	$^{+17}_{-19}$	34.57/6	0.0378	$^{+13}_{-16}$	$^{+4}_{-5}$	$^{+17}_{-19}$	33.99 / 6
CLEO	0.0364	$^{+8}_{-9}$	$^{+6}_{-4}$	$^{+18}_{-4}$	4.70/6	0.0363	$^{+14}_{-17}$	$^{+5}_{-5}$	$^{+18}_{-4}$	4.77 / 6

Table 6.27: Results of fit to experimental data. The third error is the experimental uncertainty. The quantity  $D$  contains the corrections and is defined,  $D \equiv \left( \frac{1 + \beta_{A_1}(1)}{0.99} \right) (1 + \mathcal{O}(1/m_c^2))$ .

The CLEO data provides a much better fit to the lattice data as evidenced from the graph and from the  $\chi^2$  from the fits. Combined with the observation of scaling, the lattice result is taken to be the fit at  $\beta = 6.2$  to the CLEO data,

$$V_{cb}^{\text{latt}} = 0.0363 \begin{matrix} +14 & +5 & +18 \\ -17 & -5 & -4 \end{matrix} \quad (6.52)$$

The values of  $V_{cb}$  obtained are in excellent agreement with the world average [14],

$$V_{cb}^{\text{exp}} = 0.0395 \begin{matrix} +17 \\ -17 \end{matrix} \quad (6.53)$$

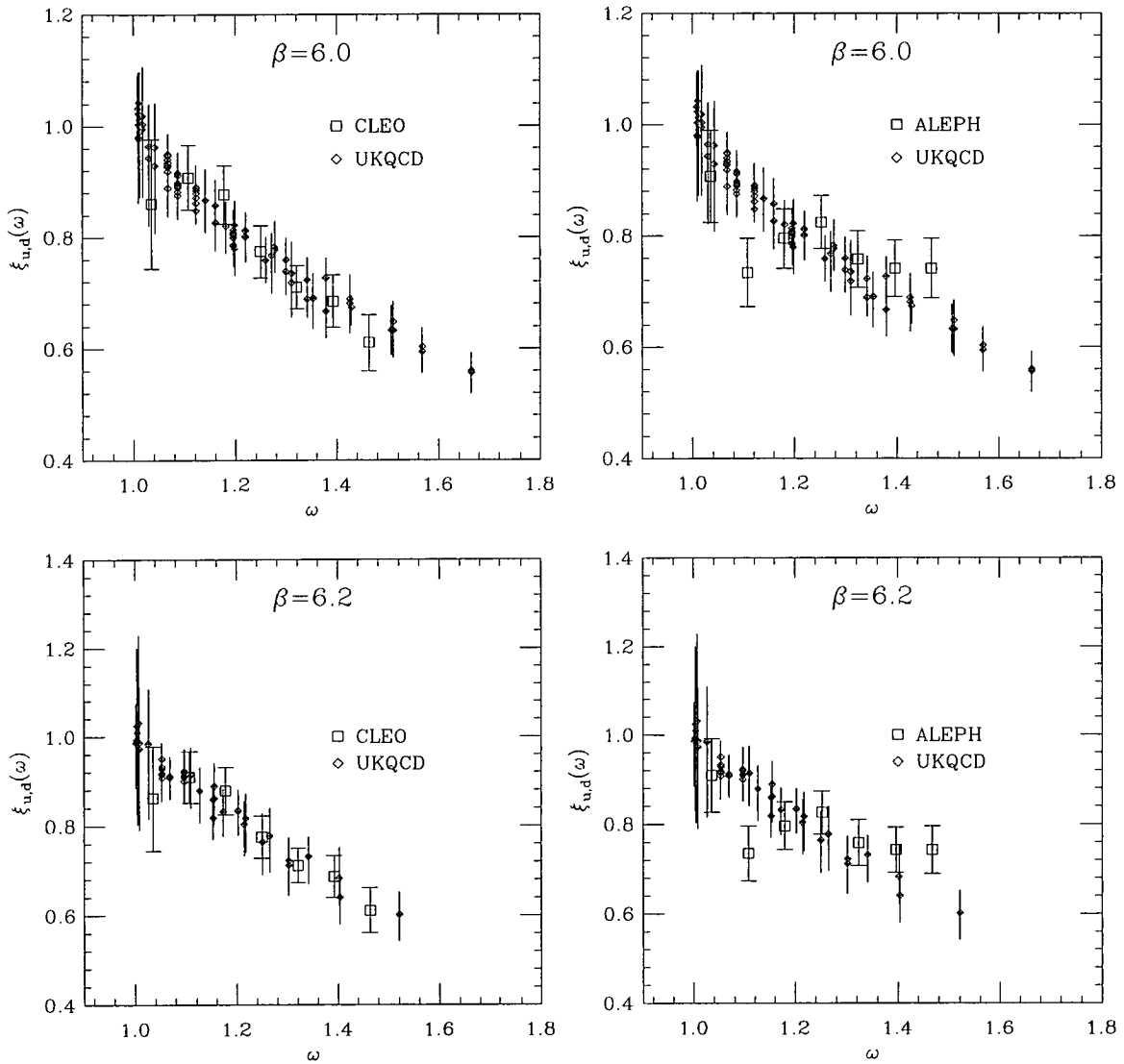


Figure 6.28: Comparison of experimental and lattice data.

## Chapter 7

### Summary and Conclusions

This thesis presents the results of a lattice QCD calculation of the matrix elements of the semi-leptonic decay  $\overline{B} \rightarrow Dl\overline{\nu}$ . The simulation was performed on a  $\beta = 6.0$  lattice with volume  $16^3 \times 48$  with an ensemble of 305 configurations and on a  $\beta = 6.2$  lattice with volume  $24^3 \times 48$  with an ensemble of 216 configurations. The simulation was performed in the quenched approximation using a non-perturbatively improved fermion action and non-perturbatively improved operators. The principle aim of the thesis was to isolate, to a greater precision, the non-perturbative hadronic matrix elements which are vital in the extraction of CKM matrix elements.

The form factors  $h_+(\omega)$  and  $h_-(\omega)$  were extracted and analysed at length. By examining the zero recoil case, a lattice determination of the renormalisation constant  $Z_V^{\text{eff}}$  was made. From this it was concluded that the discretisation errors in the lattice data were small. The results for the  $\beta = 6.0$  and  $\beta = 6.2$  lattices were consistent throughout the analysis and hence a scaling regime was observed. It was shown that the form factors were independent of the initial and final heavy quark masses and that therefore HQET could be applied safely. On comparison with previous lattice calculations, it was shown that the results were in agreement with previous studies and most importantly that the associated errors were significantly smaller. A comparison to experiment was also made and again agreement was observed.

The largest error in the simulation was the effect of quenching. It should be possible in the near future to study weak matrix elements in full QCD allowing a more confident comparison with experiment. There is expected to be much

improvement in experimental data also in the near future with new experiments such as BABAR, BELLE and CLEO III set to increase our knowledge in B physics.

## Appendix A

### Radiative Corrections

This Appendix list the radiative corrections to the form factor  $h_+(\omega)$  used in the determination of the Isgur Wise function.

	0.11230 $\rightsquigarrow$			
$\vec{p} \rightarrow \vec{p} + \vec{q}$	0.11230	0.11730	0.12230	0.12730
(0,0,0) $\rightarrow$ (0,0,0)	0.00000	0.02250	0.05166	0.09720
(0,0,0) $\rightarrow$ (1,0,0)	-0.01418	0.00490	0.02851	0.06383
(1,0,0) $\rightarrow$ (1,0,0)	-0.00143	0.02088	0.04893	0.09088
(1,0,0) $\rightarrow$ (0,0,0)	-0.01418	0.00856	0.03812	0.08434
(1,0,0) $\rightarrow$ (0,1,0)	-0.02858	-0.00935	0.01448	0.05000
(1,0,0) $\rightarrow$ (-1,0,0)	-0.05347	-0.03698	-0.01690	0.01260
	0.11730 $\rightsquigarrow$			
$\vec{p} \rightarrow \vec{p} + \vec{q}$	0.11230	0.11730	0.12230	0.12730
(0,0,0) $\rightarrow$ (0,0,0)	0.022497	0.00000	0.03596	0.09019
(0,0,0) $\rightarrow$ (1,0,0)	0.00856	-0.01682	0.01387	0.05863
(1,0,0) $\rightarrow$ (1,0,0)	0.02088	-0.00129	0.03425	0.08603
(1,0,0) $\rightarrow$ (0,0,0)	0.00489	-0.01682	0.01963	0.07481
(1,0,0) $\rightarrow$ (0,1,0)	-0.00934	-0.03398	-0.00302	0.04204
(1,0,0) $\rightarrow$ (-1,0,0)	-0.03698	-0.06336	-0.03654	0.00204
	0.12230 $\rightsquigarrow$			
$\vec{p} \rightarrow \vec{p} + \vec{q}$	0.11230	0.11730	0.12230	0.12730
(0,0,0) $\rightarrow$ (0,0,0)	0.05165	0.03596	0.00000	0.07192
(0,0,0) $\rightarrow$ (1,0,0)	0.03812	0.01963	-0.02043	0.04305
(1,0,0) $\rightarrow$ (1,0,0)	0.04893	0.03425	-0.01112	0.06986
(1,0,0) $\rightarrow$ (0,0,0)	0.02851	0.01387	-0.02043	0.05285
(1,0,0) $\rightarrow$ (0,1,0)	0.01448	-0.00302	-0.04147	0.02243
(1,0,0) $\rightarrow$ (-1,0,0)	-0.01690	-0.03654	0.01672	-0.02023
	0.12730 $\rightsquigarrow$			
$\vec{p} \rightarrow \vec{p} + \vec{q}$	0.11230	0.11730	0.12230	0.12730
(0,0,0) $\rightarrow$ (0,0,0)	0.09720	0.09019	0.07192	0.00000
(0,0,0) $\rightarrow$ (1,0,0)	0.08434	0.07481	0.05285	-0.02382
(1,0,0) $\rightarrow$ (1,0,0)	0.09088	0.08603	0.06986	-0.00074
(1,0,0) $\rightarrow$ (0,0,0)	0.06383	0.05863	0.04305	-0.02382
(1,0,0) $\rightarrow$ (0,1,0)	0.05000	0.04204	0.02243	-0.04908
(1,0,0) $\rightarrow$ (-1,0,0)	0.01260	0.00204	-0.02023	-0.08988

Table A.1:  $\beta_+(\omega)$  for  $\kappa_P = 0.13344$ ,  $\beta = 6.0$ .

0.11230 $\rightsquigarrow$				
$\vec{p} \rightarrow \vec{p} + \vec{q}$	0.11230	0.11730	0.12230	0.12730
(0,0,0) $\rightarrow$ (0,0,0)	0.00000	0.02249	0.05165	0.09720
(0,0,0) $\rightarrow$ (1,0,0)	-0.01489	0.00396	0.02698	0.06093
(1,0,0) $\rightarrow$ (1,0,0)	-0.00175	0.02057	0.04841	0.08977
(1,0,0) $\rightarrow$ (0,0,0)	-0.01489	0.00786	0.03744	0.08369
(1,0,0) $\rightarrow$ (0,1,0)	-0.0300	-0.01100	0.01221	0.04632
(1,0,0) $\rightarrow$ (-1,0,0)	-0.05583	-0.03976	-0.02062	0.00675

0.11730 $\rightsquigarrow$				
$\vec{p} \rightarrow \vec{p} + \vec{q}$	0.11230	0.11730	0.12230	0.12730
(0,0,0) $\rightarrow$ (0,0,0)	0.02249	0.00000	0.03596	0.09019
(0,0,0) $\rightarrow$ (1,0,0)	0.10786	-0.01771	0.01241	0.05588
(1,0,0) $\rightarrow$ (1,0,0)	0.02057	0.00352	0.03389	0.08524
(1,0,0) $\rightarrow$ (0,0,0)	0.00396	-0.01771	0.01877	0.07399
(1,0,0) $\rightarrow$ (0,1,0)	-0.01100	-0.03578	-0.00542	0.03830
(1,0,0) $\rightarrow$ (-1,0,0)	-0.03976	-0.06645	-0.04058	-0.00417

0.12230 $\rightsquigarrow$				
$\vec{p} \rightarrow \vec{p} + \vec{q}$	0.11230	0.11730	0.12230	0.12730
(0,0,0) $\rightarrow$ (0,0,0)	0.05165	0.03596	0.00000	0.07192
(0,0,0) $\rightarrow$ (1,0,0)	0.03744	0.01877	-0.02179	0.04052
(1,0,0) $\rightarrow$ (1,0,0)	0.04841	0.03389	-0.00148	0.06933
(1,0,0) $\rightarrow$ (0,0,0)	0.02698	0.01241	-0.02179	0.05157
(1,0,0) $\rightarrow$ (0,1,0)	0.01221	-0.00542	-0.04424	0.01839
(1,0,0) $\rightarrow$ (-1,0,0)	-0.02062	-0.04058	-0.08133	-0.02715

0.12730 $\rightsquigarrow$				
$\vec{p} \rightarrow \vec{p} + \vec{q}$	0.11230	0.11730	0.12230	0.12730
(0,0,0) $\rightarrow$ (0,0,0)	0.09720	0.09019	0.07192	0.00000
(0,0,0) $\rightarrow$ (1,0,0)	0.08369	0.05588	0.05157	-0.02589
(1,0,0) $\rightarrow$ (1,0,0)	0.08977	0.08317	0.06933	-0.00103
(1,0,0) $\rightarrow$ (0,0,0)	0.06093	0.07743	0.04052	-0.02589
(1,0,0) $\rightarrow$ (0,1,0)	0.04632	0.04201	0.01839	-0.05345
(1,0,0) $\rightarrow$ (-1,0,0)	0.00675	0.00435	-0.02715	-0.09709

Table A.2:  $\beta_+(\omega)$  for  $\kappa_P = 0.13417$ ,  $\beta = 6.0$ .

	0.12000 $\rightsquigarrow$		0.12330 $\rightsquigarrow$	
$\vec{p} \rightarrow \vec{p} + \vec{q}$	0.12000	0.12660	0.12000	0.12660
$(0,0,0) \rightarrow (0,0,0)$	0.00000	0.04839	0.02153	0.03303
$(0,0,0) \rightarrow (1,0,0)$	-0.01170	0.02925	0.01002	0.01472
$(1,0,0) \rightarrow (1,0,0)$	-0.00067	0.04669	0.02071	0.03219
$(1,0,0) \rightarrow (0,0,0)$	-0.01170	0.03719	0.00693	0.01943
$(1,0,0) \rightarrow (0,1,0)$	-0.02356	0.01771	-0.00479	0.00072
$(1,0,0) \rightarrow (-1,0,0)$	-0.04481	0.00902	-0.02839	-0.02796
	0.12660 $\rightsquigarrow$		0.12990 $\rightsquigarrow$	
$\vec{p} \rightarrow \vec{p} + \vec{q}$	0.12000	0.12660	0.12000	0.12660
$(0,0,0) \rightarrow (0,0,0)$	0.04839	0.00000	0.08754	0.06085
$(0,0,0) \rightarrow (1,0,0)$	0.03719	-0.01707	0.07684	0.02473
$(1,0,0) \rightarrow (1,0,0)$	0.04669	-0.00032	0.08297	0.05970
$(1,0,0) \rightarrow (0,0,0)$	0.02925	-0.01707	0.06017	0.03678
$(1,0,0) \rightarrow (0,1,0)$	0.01771	-0.03456	0.04885	0.01971
$(1,0,0) \rightarrow (-1,0,0)$	0.00902	-0.06505	0.01737	-0.01644

Table A.3:  $\beta_+(\omega)$  for  $\kappa_P = 0.13460$ ,  $\beta = 6.2$ .

	0.12000 $\rightsquigarrow$		0.12330 $\rightsquigarrow$	
$\vec{p} \rightarrow \vec{p} + \vec{q}$	0.12000	0.12660	0.12000	0.12660
$(0,0,0) \rightarrow (0,0,0)$	0.00000	0.04839	0.02153	0.03303
$(0,0,0) \rightarrow (1,0,0)$	-0.01213	0.02816	0.00960	0.01367
$(1,0,0) \rightarrow (1,0,0)$	-0.00059	0.04663	0.02076	0.03221
$(1,0,0) \rightarrow (0,0,0)$	-0.01213	0.03678	0.00627	0.01881
$(1,0,0) \rightarrow (0,1,0)$	-0.02443	0.01618	-0.00589	-0.00097
$(1,0,0) \rightarrow (-1,0,0)$	0.04650	0.01181	0.03049	0.03109
	0.12660 $\rightsquigarrow$		0.12990 $\rightsquigarrow$	
$\vec{p} \rightarrow \vec{p} + \vec{q}$	0.12000	0.12660	0.12000	0.12660
$(0,0,0) \rightarrow (0,0,0)$	0.04839	0.00000	0.08754	0.06085
$(0,0,0) \rightarrow (1,0,0)$	0.03678	-0.01805	0.07644	0.02380
$(1,0,0) \rightarrow (1,0,0)$	0.04663	-0.00023	0.08245	0.05964
$(1,0,0) \rightarrow (0,0,0)$	0.02816	-0.01805	0.05803	0.03489
$(1,0,0) \rightarrow (0,1,0)$	0.01618	-0.03655	0.04624	0.01677
$(1,0,0) \rightarrow (-1,0,0)$	0.01181	-0.06868	0.01296	0.02176

Table A.4:  $\beta_+(\omega)$  for  $\kappa_P = 0.13510$ ,  $\beta = 6.2$ .

## Appendix B

### Meson Spectrum

$\beta$	$\kappa_1$	$\kappa_2$	$\alpha_{PS}$	$m_{PS}$	$\chi^2/dof$
6.0	0.13344	0.13344	0.0456 $^{+6}_{-10}$	0.3966 $^{+15}_{-10}$	15.2241 / 13
	0.13417	0.13344	0.0483 $^{+7}_{-11}$	0.3539 $^{+18}_{-10}$	15.2708 / 13
	0.13417	0.13417	0.0532 $^{+9}_{-14}$	0.3068 $^{+21}_{-10}$	13.7533 / 13
	0.13455	0.13344	0.0509 $^{+10}_{-13}$	0.3302 $^{+23}_{-12}$	16.5143 / 13
	0.13455	0.13417	0.0580 $^{+11}_{-17}$	0.2798 $^{+24}_{-12}$	13.5546 / 13
	0.13455	0.13455	0.0660 $^{+15}_{-26}$	0.2504 $^{+24}_{-16}$	12.6479 / 13
6.2	0.1346	0.1346	0.0139 $^{+2}_{-3}$	0.2808 $^{+12}_{-10}$	9.88704 / 13
	0.1351	0.1346	0.0147 $^{+3}_{-4}$	0.2509 $^{+14}_{-11}$	11.2456 / 13
	0.1351	0.1351	0.0160 $^{+3}_{-5}$	0.2168 $^{+14}_{-13}$	10.857 / 13
	0.1353	0.1346	0.0153 $^{+3}_{-5}$	0.2383 $^{+15}_{-13}$	11.775 / 13
	0.1353	0.1351	0.0170 $^{+3}_{-7}$	0.2022 $^{+15}_{-13}$	11.128 / 13
	0.1353	0.1353	0.0182 $^{+3}_{-8}$	0.1862 $^{+15}_{-14}$	10.9739 / 13

Table B.1: Amplitudes and masses for light-light pseudoscalar mesons -  $\kappa_1$  is smeared and  $\kappa_2$  is local.

$\beta$	$\kappa_1$	$\kappa_2$	$\alpha_V$	$m_V$	$\chi^2/dof$
6.0	0.13344	0.13344	0.0330 <sup>+13</sup> <sub>-11</sub>	0.5383 <sup>+49</sup> <sub>-30</sub>	13.1417 / 13
	0.13417	0.13344	0.0321 <sup>+17</sup> <sub>-12</sub>	0.5108 <sup>+65</sup> <sub>-40</sub>	10.3361 / 13
	0.13417	0.13417	0.0308 <sup>+20</sup> <sub>-15</sub>	0.4825 <sup>+82</sup> <sub>-50</sub>	11.9326 / 13
	0.13455	0.13344	0.0320 <sup>+21</sup> <sub>-15</sub>	0.4969 <sup>+80</sup> <sub>-53</sub>	8.58436 / 13
	0.13455	0.13417	0.0304 <sup>+24</sup> <sub>-18</sub>	0.4680 <sup>+00</sup> <sub>-71</sub>	10.3368 / 13
	0.13455	0.13455	0.0300 <sup>+31</sup> <sub>-10</sub>	0.4564 <sup>+26</sup> <sub>-00</sub>	11.9814 / 13
6.2	0.1346	0.1346	0.0096 <sup>+3</sup> <sub>-3</sub>	0.3868 <sup>+36</sup> <sub>-26</sub>	36.0234 / 13
	0.1351	0.1346	0.0094 <sup>+4</sup> <sub>-3</sub>	0.3693 <sup>+48</sup> <sub>-33</sub>	31.7391 / 13
	0.1351	0.1351	0.0093 <sup>+4</sup> <sub>-3</sub>	0.3546 <sup>+61</sup> <sub>-46</sub>	28.4045 / 13
	0.1353	0.1346	0.0093 <sup>+4</sup> <sub>-3</sub>	0.3623 <sup>+55</sup> <sub>-39</sub>	26.8289 / 13
	0.1353	0.1351	0.0092 <sup>+5</sup> <sub>-4</sub>	0.3477 <sup>+72</sup> <sub>-53</sub>	24.6889 / 13
	0.1353	0.1353	0.0092 <sup>+6</sup> <sub>-4</sub>	0.3432 <sup>+83</sup> <sub>-63</sub>	23.0884 / 13

Table B.2: Masses and amplitudes for light-light vector mesons -  $\kappa_1$  is smeared and  $\kappa_2$  is local.

$\beta$	$\kappa_1$	$\kappa_2$	$\alpha_{PS}$	$m_{PS}$	$\chi^2/dof$
6.0	0.1123	0.13344	22.7 $^{+5}_{-5}$	1.1449 $^{+18}_{-13}$	8.96524 / 9
	0.1123	0.13417	21.8 $^{+6}_{-6}$	1.1206 $^{+26}_{-20}$	8.66111 / 9
	0.1123	0.13455	21.7 $^{+8}_{-8}$	1.1094 $^{+32}_{-29}$	8.15847 / 9
	0.1173	0.13344	26.4 $^{+5}_{-6}$	1.0059 $^{+16}_{-13}$	11.1126 / 9
	0.1173	0.13417	25.5 $^{+6}_{-7}$	0.9806 $^{+21}_{-18}$	8.41621 / 9
	0.1173	0.13455	25.4 $^{+8}_{-9}$	0.9687 $^{+29}_{-25}$	7.41585 / 9
	0.1223	0.13344	30.3 $^{+5}_{-6}$	0.8508 $^{+14}_{-11}$	9.13135 / 9
	0.1223	0.13417	29.3 $^{+6}_{-7}$	0.8239 $^{+19}_{-16}$	8.69001 / 9
	0.1223	0.13455	29.3 $^{+8}_{-9}$	0.8110 $^{+25}_{-22}$	8.46384 / 9
	0.1273	0.13344	35.4 $^{+6}_{-7}$	0.6749 $^{+13}_{-10}$	11.3789 / 9
	0.1273	0.13417	34.6 $^{+6}_{-8}$	0.6451 $^{+17}_{-13}$	10.6667 / 9
	0.1273	0.13455	34.6 $^{+8}_{-10}$	0.6302 $^{+21}_{-17}$	10.0159 / 9
6.2	0.12	0.1346	54.0 $^{+10}_{-9}$	0.8405 $^{+13}_{-10}$	9.88187 / 9
	0.12	0.1351	50.9 $^{+10}_{-10}$	0.8231 $^{+17}_{-13}$	9.15435 / 9
	0.12	0.1353	50.0 $^{+12}_{-12}$	0.8165 $^{+19}_{-14}$	8.32226 / 9
	0.1233	0.1346	58.8 $^{+10}_{-10}$	0.7387 $^{+12}_{-9}$	9.741 / 9
	0.1233	0.1351	55.5 $^{+11}_{-11}$	0.7205 $^{+15}_{-11}$	8.40011 / 9
	0.1233	0.1353	54.5 $^{+12}_{-13}$	0.7136 $^{+18}_{-13}$	7.31061 / 9
	0.1266	0.1346	64.3 $^{+10}_{-11}$	0.6284 $^{+11}_{-8}$	10.4848 / 9
	0.1266	0.1351	70.0 $^{+11}_{-13}$	0.6091 $^{+14}_{-11}$	8.59075 / 9
	0.1266	0.1353	60.0 $^{+13}_{-15}$	0.6017 $^{+16}_{-12}$	7.11151 / 9
	0.1299	0.1346	70.4 $^{+11}_{-14}$	0.5051 $^{+10}_{-8}$	11.4833 / 9
	0.1299	0.1351	67.3 $^{+13}_{-11}$	0.4840 $^{+13}_{-11}$	9.63356 / 9
	0.1299	0.1353	66.5 $^{+12}_{-19}$	0.4758 $^{+14}_{-12}$	7.82785 / 9

Table B.3: Masses and amplitudes for heavy light pseudoscalar mesons -  $\kappa_1$  is smeared and  $\kappa_2$  is local.

$\beta$	$\kappa_1$	$\kappa_2$	$\alpha_V$	$m_V$	$\chi^2/dof$
6.0	0.1123	0.13344	18.2 $^{+6}_{-6}$	1.1878 $^{+30}_{-23}$	8.97956 / 9
	0.1123	0.13417	17.8 $^{+9}_{-8}$	1.1675 $^{+43}_{-36}$	8.1843 / 9
	0.1123	0.3455	18.3 $^{+13}_{-11}$	1.1605 $^{+62}_{-50}$	6.61479 / 9
	0.1173	0.13344	20.0 $^{+6}_{-6}$	1.0563 $^{+29}_{-22}$	9.44033 / 9
	0.1173	0.13417	19.5 $^{+9}_{-8}$	1.0350 $^{+42}_{-35}$	8.53339 / 9
	0.1173	0.13455	20.0 $^{+13}_{-12}$	1.0277 $^{+58}_{-48}$	7.15953 / 9
	0.1223	0.13344	21.7 $^{+7}_{-6}$	0.9145 $^{+29}_{-21}$	11.3401 / 9
	0.1223	0.13417	21.1 $^{+10}_{-9}$	0.8924 $^{+42}_{-32}$	11.0233 / 9
	0.1223	0.13455	21.5 $^{+14}_{-12}$	0.8842 $^{+57}_{-47}$	9.52202 / 9
	0.1273	0.13344	22.8 $^{+8}_{-7}$	0.7582 $^{+31}_{-22}$	12.8219 / 9
	0.1273	0.13417	22.0 $^{+11}_{-10}$	0.7344 $^{+46}_{-35}$	13.718 / 9
0.1273	0.13455	22.3 $^{+15}_{-14}$	0.7255 $^{+62}_{-52}$	12.1441 / 9	
6.2	0.12	0.1346	42.1 $^{+10}_{-9}$	0.8711 $^{+18}_{-16}$	13.1111 / 9
	0.12	0.1351	39.3 $^{+11}_{-10}$	0.8545 $^{+22}_{-20}$	12.5276 / 9
	0.12	0.1353	38.5 $^{+12}_{-12}$	0.8483 $^{+28}_{-24}$	12.7539 / 9
	0.1233	0.1346	44.2 $^{+10}_{-9}$	0.7753 $^{+18}_{-15}$	12.7665 / 9
	0.1233	0.1351	41.3 $^{+11}_{-10}$	0.7585 $^{+22}_{-20}$	12.4356 / 9
	0.1233	0.1353	40.5 $^{+12}_{-12}$	0.7524 $^{+27}_{-24}$	12.8754 / 9
	0.1266	0.1346	45.7 $^{+10}_{-10}$	0.6732 $^{+17}_{-16}$	13.0715 / 9
	0.1266	0.1351	42.9 $^{+11}_{-11}$	0.6563 $^{+21}_{-19}$	12.9524 / 9
	0.1266	0.1353	42.0 $^{+12}_{-12}$	0.6501 $^{+25}_{-23}$	13.4178 / 9
	0.1299	0.1346	45.9 $^{+10}_{-10}$	0.5633 $^{+17}_{-15}$	15.2283 / 9
	0.1299	0.1351	43.2 $^{+10}_{-11}$	0.5460 $^{+21}_{-20}$	14.6193 / 9
0.1299	0.1353	42.4 $^{+12}_{-12}$	0.5397 $^{+24}_{-23}$	14.3555 / 9	

Table B.4: Masses and amplitudes for heavy-light vector mesons -  $\kappa_1$  is smeared and  $\kappa_2$  is local.

$\beta$	$\kappa_1$	$\kappa_2$	$\alpha_{PS}$	$E_{PS}$
6.0	0.1123	0.13344	16.9 $^{+5}_{-5}$	1.2137 $^{+25}_{-19}$
	0.1123	0.13417	16.1 $^{+6}_{-7}$	1.1914 $^{+34}_{-30}$
	0.1123	0.13455	16.1 $^{+9}_{-9}$	1.1812 $^{+50}_{-43}$
	0.1173	0.13344	19.4 $^{+5}_{-6}$	1.0827 $^{+22}_{-17}$
	0.1173	0.13417	18.4 $^{+6}_{-7}$	1.0595 $^{+30}_{-26}$
	0.1173	0.13455	18.3 $^{+9}_{-9}$	1.0486 $^{+41}_{-36}$
	0.1223	0.13344	21.8 $^{+5}_{-6}$	0.9393 $^{+18}_{-15}$
	0.1223	0.13417	20.7 $^{+6}_{-7}$	0.9156 $^{+24}_{-20}$
	0.1223	0.13455	20.6 $^{+8}_{-9}$	0.9042 $^{+32}_{-28}$
	0.1273	0.13344	24.5 $^{+5}_{-7}$	0.7825 $^{+16}_{-12}$
	0.1273	0.13417	23.3 $^{+5}_{-7}$	0.7573 $^{+18}_{-16}$
	0.1273	0.13455	23.2 $^{+7}_{-9}$	0.7450 $^{+23}_{-21}$
6.2	0.12	0.1346	40.8 $^{+8}_{-9}$	0.8816 $^{+17}_{-14}$
	0.12	0.1351	37.8 $^{+9}_{-11}$	0.8648 $^{+22}_{-18}$
	0.12	0.1353	36.7 $^{+10}_{-12}$	0.8584 $^{+24}_{-21}$
	0.1233	0.1346	44.1 $^{+8}_{-10}$	0.7847 $^{+14}_{-13}$
	0.1233	0.1351	40.8 $^{+9}_{-11}$	0.7674 $^{+18}_{-16}$
	0.1233	0.1353	39.7 $^{+10}_{-13}$	0.7609 $^{+21}_{-20}$
	0.1266	0.1346	47.6 $^{+8}_{-10}$	0.6814 $^{+13}_{-11}$
	0.1266	0.1351	44.1 $^{+9}_{-12}$	0.6635 $^{+15}_{-14}$
	0.1266	0.1353	42.9 $^{+10}_{-13}$	0.6566 $^{+17}_{-17}$
	0.1299	0.1346	50.8 $^{+8}_{-12}$	0.5694 $^{+11}_{-10}$
	0.1299	0.1351	47.1 $^{+8}_{-12}$	0.5506 $^{+12}_{-12}$
	0.1299	0.1353	45.7 $^{+9}_{-13}$	0.5433 $^{+14}_{-14}$

Table B.5: Amplitudes and energies for heavy-light pseudoscalar mesons with  $|\vec{p}| = 1$ . Energies are obtained from the dispersion relation as described in the text.

## Appendix C

### Form Factor Results

This Appendix list the values of the forms factors  $h_+(\omega)$  and  $h_-(\omega)$  corresponding to the semi-leptonic decay  $\bar{B} \rightarrow D l \bar{\nu}$ . Also listed are the results of the extrapolation to the chiral limit and interpolation to the strange quark mass.

$\kappa_P = 0.13344$						
$\kappa_E \rightarrow \kappa_A$ 0.11230 $\rightarrow$ 0.11230						
$\vec{p}$	$\vec{p} + \vec{q}$	$\omega$	$h_+(\omega)$	$h_-(\omega)$	$\xi^{\text{eff}}(\omega)$	$\chi^2/dof$
(0,0,0)	(0,0,0)	1.0000	0.627 $^{+9}_{-14}$	0.000	1.021 $^{+15}_{-23}$	9.63/8
(0,0,0)	(1,0,0)	1.0601 $^{+6}_{-6}$	0.565 $^{+18}_{-18}$	0.050 $^{+24}_{-11}$	0.945 $^{+16}_{-26}$	19.57/8
(1,0,0)	(1,0,0)	1.0062 $^{+14}_{-12}$	0.616 $^{+12}_{-19}$	0.000	1.004 $^{+19}_{-31}$	12.53/8
(1,0,0)	(0,0,0)	1.0601 $^{+6}_{-6}$	0.559 $^{+11}_{-12}$	-0.026 $^{+26}_{-18}$	0.923 $^{+18}_{-19}$	14.20/8
(1,0,0)	(0,1,0)	1.1239 $^{+13}_{-13}$	0.527 $^{+17}_{-15}$	-0.043 $^{+34}_{-19}$	0.883 $^{+28}_{-25}$	20.35/8
(1,0,0)	(-1,0,0)	1.2415 $^{+14}_{-14}$	0.445 $^{+16}_{-16}$	-0.001 $^{+32}_{-13}$	0.765 $^{+27}_{-27}$	14.16/8
$\kappa_E \rightarrow \kappa_A$ 0.11230 $\rightarrow$ 0.11730						
$\vec{p}$	$\vec{p} + \vec{q}$	$\omega$	$h_+(\omega)$	$h_-(\omega)$	$\xi^{\text{eff}}(\omega)$	$\chi^2/dof$
(0,0,0)	(0,0,0)	1.0000	0.669 $^{+8}_{-11}$	0.000	0.995 $^{+12}_{-17}$	14.37/8
(0,0,0)	(1,0,0)	1.0763 $^{+6}_{-7}$	0.606 $^{+17}_{-17}$	0.028 $^{+15}_{-20}$	0.918 $^{+25}_{-25}$	15.3/8
(1,0,0)	(1,0,0)	1.0071 $^{+14}_{-12}$	0.677 $^{+18}_{-29}$	0.718 $^{+318}_{-366}$	1.009 $^{+27}_{-43}$	34.37/8
(1,0,0)	(0,0,0)	1.0601 $^{+6}_{-6}$	0.609 $^{+13}_{-11}$	-0.041 $^{+16}_{-27}$	0.919 $^{+19}_{-17}$	16.00/8
(1,0,0)	(0,1,0)	1.1410 $^{+13}_{-14}$	0.559 $^{+12}_{-16}$	-0.053 $^{+25}_{-29}$	0.859 $^{+18}_{-24}$	18.09/8
(1,0,0)	(-1,0,0)	1.2749 $^{+13}_{-15}$	0.477 $^{+17}_{-17}$	-0.011 $^{+22}_{-23}$	0.753 $^{+27}_{-27}$	14.05/8
$\kappa_E \rightarrow \kappa_A$ 0.11230 $\rightarrow$ 0.12230						
$\vec{p}$	$\vec{p} + \vec{q}$	$\omega$	$h_+(\omega)$	$h_-(\omega)$	$\xi^{\text{eff}}(\omega)$	$\chi^2/dof$
(0,0,0)	(0,0,0)	1.0000	0.735 $^{+8}_{-11}$	0.000	0.995 $^{+11}_{-15}$	8.00/8
(0,0,0)	(1,0,0)	1.1041 $^{+6}_{-7}$	0.641 $^{+11}_{-17}$	0.001 $^{+5}_{-39}$	0.887 $^{+15}_{-23}$	10.75/8
(1,0,0)	(1,0,0)	1.0121 $^{+13}_{-13}$	0.733 $^{+18}_{-32}$	0.352 $^{+143}_{-164}$	0.994 $^{+24}_{-43}$	30.49/8
(1,0,0)	(0,0,0)	1.0601 $^{+6}_{-6}$	0.680 $^{+14}_{-12}$	-0.069 $^{+27}_{-37}$	0.932 $^{+19}_{-17}$	17.97/8
(1,0,0)	(0,1,0)	1.1704 $^{+12}_{-13}$	0.586 $^{+12}_{-16}$	-0.067 $^{+17}_{-30}$	0.822 $^{+17}_{-22}$	14.73/8
(1,0,0)	(-1,0,0)	1.3288 $^{+13}_{-15}$	0.501 $^{+12}_{-17}$	-0.022 $^{+33}_{-23}$	0.725 $^{+17}_{-25}$	14.21/8
$\kappa_E \rightarrow \kappa_A$ 0.11230 $\rightarrow$ 0.12730						
$\vec{p}$	$\vec{p} + \vec{q}$	$\omega$	$h_+(\omega)$	$h_-(\omega)$	$\xi^{\text{eff}}(\omega)$	$\chi^2/dof$
(0,0,0)	(0,0,0)	1.0000	0.801 $^{+14}_{-18}$	0.000	0.973 $^{+17}_{-22}$	4.38/8
(0,0,0)	(1,0,0)	1.1593 $^{+5}_{-8}$	0.666 $^{+18}_{-18}$	-0.031 $^{+15}_{-29}$	0.834 $^{+23}_{-22}$	6.22/8
(1,0,0)	(1,0,0)	1.0295 $^{+12}_{-13}$	0.818 $^{+17}_{-38}$	0.223 $^{+90}_{-112}$	0.999 $^{+21}_{-46}$	19.86/8
(1,0,0)	(0,0,0)	1.0601 $^{+6}_{-6}$	0.743 $^{+15}_{-13}$	-0.012 $^{+28}_{-26}$	0.913 $^{+18}_{-16}$	20.48/8
(1,0,0)	(0,1,0)	1.2290 $^{+12}_{-13}$	0.622 $^{+20}_{-16}$	-0.048 $^{+20}_{-32}$	0.789 $^{+25}_{-20}$	9.81/8
(1,0,0)	(-1,0,0)	1.4286 $^{+12}_{-17}$	0.495 $^{+20}_{-18}$	-0.039 $^{+34}_{-23}$	0.652 $^{+26}_{-24}$	15.63/8

$\kappa_P = 0.13344$						
$\kappa_E \rightarrow \kappa_A$						0.11730 $\rightarrow$ 0.11230
$\vec{p}$	$\vec{p} + \vec{q}$	$\omega$	$h_+(\omega)$	$h_-(\omega)$	$\xi^{\text{eff}}(\omega)$	$\chi^2/dof$
(0,0,0)	(0,0,0)	1.0000	0.678 $\begin{smallmatrix} +7 \\ -11 \end{smallmatrix}$	0.000	1.008 $\begin{smallmatrix} +11 \\ -17 \end{smallmatrix}$	9.08/8
(0,0,0)	(1,0,0)	1.0601 $\begin{smallmatrix} +6 \\ -6 \end{smallmatrix}$	0.614 $\begin{smallmatrix} +17 \\ -17 \end{smallmatrix}$	0.054 $\begin{smallmatrix} +35 \\ -11 \end{smallmatrix}$	0.926 $\begin{smallmatrix} +26 \\ -25 \end{smallmatrix}$	22.85/8
(1,0,0)	(1,0,0)	1.0071 $\begin{smallmatrix} +14 \\ -13 \end{smallmatrix}$	0.672 $\begin{smallmatrix} +19 \\ -30 \end{smallmatrix}$	-0.625 $\begin{smallmatrix} +387 \\ -313 \end{smallmatrix}$	1.001 $\begin{smallmatrix} +28 \\ -45 \end{smallmatrix}$	28.22/8
(1,0,0)	(0,0,0)	1.0763 $\begin{smallmatrix} +5 \\ -5 \end{smallmatrix}$	0.603 $\begin{smallmatrix} +12 \\ -12 \end{smallmatrix}$	-0.001 $\begin{smallmatrix} +14 \\ -17 \end{smallmatrix}$	0.912 $\begin{smallmatrix} +18 \\ -18 \end{smallmatrix}$	11.03/8
(1,0,0)	(0,1,0)	1.1410 $\begin{smallmatrix} +13 \\ -14 \end{smallmatrix}$	0.558 $\begin{smallmatrix} +11 \\ -16 \end{smallmatrix}$	-0.023 $\begin{smallmatrix} +24 \\ -29 \end{smallmatrix}$	0.857 $\begin{smallmatrix} +17 \\ -25 \end{smallmatrix}$	15.03/8
(1,0,0)	(-1,0,0)	1.2749 $\begin{smallmatrix} +13 \\ -15 \end{smallmatrix}$	0.479 $\begin{smallmatrix} +17 \\ -18 \end{smallmatrix}$	0.007 $\begin{smallmatrix} +22 \\ -23 \end{smallmatrix}$	0.756 $\begin{smallmatrix} +27 \\ -28 \end{smallmatrix}$	12.18/8
$\kappa_E \rightarrow \kappa_A$						0.11730 $\rightarrow$ 0.11730
$\vec{p}$	$\vec{p} + \vec{q}$	$\omega$	$h_+(\omega)$	$h_-(\omega)$	$\xi^{\text{eff}}(\omega)$	$\chi^2/dof$
(0,0,0)	(0,0,0)	1.0000	0.721 $\begin{smallmatrix} +8 \\ -12 \end{smallmatrix}$	0.000	1.020 $\begin{smallmatrix} +11 \\ -17 \end{smallmatrix}$	11.90/8
(0,0,0)	(1,0,0)	1.0763 $\begin{smallmatrix} +6 \\ -6 \end{smallmatrix}$	0.640 $\begin{smallmatrix} +11 \\ -17 \end{smallmatrix}$	0.032 $\begin{smallmatrix} +25 \\ -21 \end{smallmatrix}$	0.920 $\begin{smallmatrix} +16 \\ -25 \end{smallmatrix}$	17.95/8
(1,0,0)	(1,0,0)	1.0060 $\begin{smallmatrix} +14 \\ -13 \end{smallmatrix}$	0.699 $\begin{smallmatrix} +11 \\ -21 \end{smallmatrix}$	0.000	0.990 $\begin{smallmatrix} +15 \\ -30 \end{smallmatrix}$	30.24/8
(1,0,0)	(0,0,0)	1.0763 $\begin{smallmatrix} +6 \\ -7 \end{smallmatrix}$	0.631 $\begin{smallmatrix} +19 \\ -12 \end{smallmatrix}$	-0.013 $\begin{smallmatrix} +6 \\ -27 \end{smallmatrix}$	0.908 $\begin{smallmatrix} +28 \\ -17 \end{smallmatrix}$	12.63/8
(1,0,0)	(0,1,0)	1.1584 $\begin{smallmatrix} +13 \\ -14 \end{smallmatrix}$	0.578 $\begin{smallmatrix} +18 \\ -16 \end{smallmatrix}$	-0.031 $\begin{smallmatrix} +14 \\ -29 \end{smallmatrix}$	0.846 $\begin{smallmatrix} +27 \\ -24 \end{smallmatrix}$	13.31/8
(1,0,0)	(-1,0,0)	1.3108 $\begin{smallmatrix} +13 \\ -15 \end{smallmatrix}$	0.490 $\begin{smallmatrix} +18 \\ -17 \end{smallmatrix}$	-0.001 $\begin{smallmatrix} +22 \\ -23 \end{smallmatrix}$	0.740 $\begin{smallmatrix} +27 \\ -25 \end{smallmatrix}$	12.65/8
$\kappa_E \rightarrow \kappa_A$						0.11730 $\rightarrow$ 0.12230
$\vec{p}$	$\vec{p} + \vec{q}$	$\omega$	$h_+(\omega)$	$h_-(\omega)$	$\xi^{\text{eff}}(\omega)$	$\chi^2/dof$
(0,0,0)	(0,0,0)	1.0000	0.789 $\begin{smallmatrix} +14 \\ -16 \end{smallmatrix}$	0.000	1.002 $\begin{smallmatrix} +18 \\ -20 \end{smallmatrix}$	5.03/8
(0,0,0)	(1,0,0)	1.1041 $\begin{smallmatrix} +6 \\ -7 \end{smallmatrix}$	0.682 $\begin{smallmatrix} +19 \\ -18 \end{smallmatrix}$	-0.021 $\begin{smallmatrix} +38 \\ -20 \end{smallmatrix}$	0.885 $\begin{smallmatrix} +25 \\ -24 \end{smallmatrix}$	12.27/8
(1,0,0)	(1,0,0)	1.0081 $\begin{smallmatrix} +12 \\ -13 \end{smallmatrix}$	0.790 $\begin{smallmatrix} +16 \\ -37 \end{smallmatrix}$	0.499 $\begin{smallmatrix} +261 \\ -266 \end{smallmatrix}$	1.005 $\begin{smallmatrix} +21 \\ -47 \end{smallmatrix}$	27.56/8
(1,0,0)	(0,0,0)	1.0763 $\begin{smallmatrix} +6 \\ -7 \end{smallmatrix}$	0.703 $\begin{smallmatrix} +14 \\ -13 \end{smallmatrix}$	-0.038 $\begin{smallmatrix} +37 \\ -27 \end{smallmatrix}$	0.908 $\begin{smallmatrix} +18 \\ -17 \end{smallmatrix}$	14.57/8
(1,0,0)	(0,1,0)	1.1883 $\begin{smallmatrix} +13 \\ -16 \end{smallmatrix}$	0.619 $\begin{smallmatrix} +11 \\ -17 \end{smallmatrix}$	-0.047 $\begin{smallmatrix} +16 \\ -39 \end{smallmatrix}$	0.817 $\begin{smallmatrix} +15 \\ -22 \end{smallmatrix}$	10.90/8
(1,0,0)	(-1,0,0)	1.3685 $\begin{smallmatrix} +13 \\ -16 \end{smallmatrix}$	0.498 $\begin{smallmatrix} +12 \\ -17 \end{smallmatrix}$	-0.013 $\begin{smallmatrix} +32 \\ -33 \end{smallmatrix}$	0.681 $\begin{smallmatrix} +16 \\ -23 \end{smallmatrix}$	13.55/8
$\kappa_E \rightarrow \kappa_A$						0.11730 $\rightarrow$ 0.12730
$\vec{p}$	$\vec{p} + \vec{q}$	$\omega$	$h_+(\omega)$	$h_-(\omega)$	$\xi^{\text{eff}}(\omega)$	$\chi^2/dof$
(0,0,0)	(0,0,0)	1.0000	0.862 $\begin{smallmatrix} +13 \\ -19 \end{smallmatrix}$	0.000	0.969 $\begin{smallmatrix} +15 \\ -21 \end{smallmatrix}$	0.38/8
(0,0,0)	(1,0,0)	1.1593 $\begin{smallmatrix} +5 \\ -8 \end{smallmatrix}$	0.714 $\begin{smallmatrix} +11 \\ -18 \end{smallmatrix}$	-0.024 $\begin{smallmatrix} +37 \\ -29 \end{smallmatrix}$	0.827 $\begin{smallmatrix} +13 \\ -21 \end{smallmatrix}$	6.44/8
(1,0,0)	(1,0,0)	1.0207 $\begin{smallmatrix} +12 \\ -13 \end{smallmatrix}$	0.888 $\begin{smallmatrix} +18 \\ -43 \end{smallmatrix}$	0.355 $\begin{smallmatrix} +126 \\ -159 \end{smallmatrix}$	1.003 $\begin{smallmatrix} +20 \\ -49 \end{smallmatrix}$	18.93/8
(1,0,0)	(0,0,0)	1.0763 $\begin{smallmatrix} +6 \\ -7 \end{smallmatrix}$	0.774 $\begin{smallmatrix} +15 \\ -14 \end{smallmatrix}$	-0.054 $\begin{smallmatrix} +38 \\ -26 \end{smallmatrix}$	0.883 $\begin{smallmatrix} +17 \\ -16 \end{smallmatrix}$	17.14/8
(1,0,0)	(0,1,0)	1.2478 $\begin{smallmatrix} +12 \\ -15 \end{smallmatrix}$	0.648 $\begin{smallmatrix} +21 \\ -17 \end{smallmatrix}$	-0.068 $\begin{smallmatrix} +19 \\ -31 \end{smallmatrix}$	0.763 $\begin{smallmatrix} +25 \\ -20 \end{smallmatrix}$	7.24/8
(1,0,0)	(-1,0,0)	1.4750 $\begin{smallmatrix} +12 \\ -18 \end{smallmatrix}$	0.505 $\begin{smallmatrix} +20 \\ -17 \end{smallmatrix}$	-0.029 $\begin{smallmatrix} +33 \\ -33 \end{smallmatrix}$	0.618 $\begin{smallmatrix} +25 \\ -21 \end{smallmatrix}$	15.22/8

$\kappa_P = 0.13344$						
$\kappa_E \rightarrow \kappa_A$						0.12230 $\rightarrow$ 0.11230
$\vec{p}$	$\vec{p} + \vec{q}$	$\omega$	$h_+(\omega)$	$h_-(\omega)$	$\xi^{\text{eff}}(\omega)$	$\chi^2/dof$
(0,0,0)	(0,0,0)	1.0000	0.727 $^{+7}_{-11}$	0.000	0.984 $^{+10}_{-15}$	6.86/8
(0,0,0)	(1,0,0)	1.0601 $^{+6}_{-6}$	0.679 $^{+12}_{-18}$	0.061 $^{+35}_{-11}$	0.931 $^{+17}_{-25}$	26.83/8
(1,0,0)	(1,0,0)	1.0121 $^{+13}_{-13}$	0.742 $^{+18}_{-33}$	-0.188 $^{+197}_{-151}$	1.006 $^{+25}_{-45}$	20.60/8
(1,0,0)	(0,0,0)	1.1041 $^{+6}_{-7}$	0.640 $^{+13}_{-13}$	0.024 $^{+7}_{-38}$	0.886 $^{+18}_{-18}$	7.32/8
(1,0,0)	(0,1,0)	1.1704 $^{+13}_{-13}$	0.590 $^{+12}_{-16}$	0.004 $^{+24}_{-29}$	0.828 $^{+17}_{-23}$	8.95/8
(1,0,0)	(-1,0,0)	1.3288 $^{+13}_{-15}$	0.499 $^{+17}_{-19}$	0.018 $^{+23}_{-14}$	0.722 $^{+25}_{-27}$	11.00/8
$\kappa_E \rightarrow \kappa_A$						0.12230 $\rightarrow$ 0.11730
$\vec{p}$	$\vec{p} + \vec{q}$	$\omega$	$h_+(\omega)$	$h_-(\omega)$	$\xi^{\text{eff}}(\omega)$	$\chi^2/dof$
(0,0,0)	(0,0,0)	1.0000	0.774 $^{+9}_{-12}$	0.000	0.984 $^{+11}_{-15}$	9.27/8
(0,0,0)	(1,0,0)	1.0763 $^{+6}_{-7}$	0.713 $^{+12}_{-19}$	0.036 $^{+35}_{-11}$	0.921 $^{+15}_{-25}$	21.09/8
(1,0,0)	(1,0,0)	1.0081 $^{+12}_{-13}$	0.781 $^{+18}_{-37}$	-0.371 $^{+376}_{-301}$	0.994 $^{+23}_{-47}$	22.07/8
(1,0,0)	(0,0,0)	1.1041 $^{+6}_{-7}$	0.678 $^{+13}_{-13}$	0.016 $^{+37}_{-7}$	0.880 $^{+17}_{-17}$	8.50/8
(1,0,0)	(0,1,0)	1.1883 $^{+13}_{-14}$	0.616 $^{+11}_{-17}$	-0.005 $^{+25}_{-39}$	0.813 $^{+15}_{-22}$	7.65/8
(1,0,0)	(-1,0,0)	1.3685 $^{+13}_{-16}$	0.506 $^{+18}_{-18}$	0.008 $^{+33}_{-23}$	0.692 $^{+25}_{-25}$	11.45/8
$\kappa_E \rightarrow \kappa_A$						0.12230 $\rightarrow$ 0.12230
$\vec{p}$	$\vec{p} + \vec{q}$	$\omega$	$h_+(\omega)$	$h_-(\omega)$	$\xi^{\text{eff}}(\omega)$	$\chi^2/dof$
(0,0,0)	(0,0,0)	1.0000	0.819 $^{+9}_{-12}$	0.000	0.998 $^{+11}_{-15}$	12.51/8
(0,0,0)	(1,0,0)	1.1041 $^{+6}_{-7}$	0.713 $^{+12}_{-18}$	0.011 $^{+5}_{-39}$	0.887 $^{+15}_{-23}$	14.25/8
(1,0,0)	(1,0,0)	1.0059 $^{+12}_{-14}$	0.807 $^{+11}_{-25}$	0.000	0.994 $^{+13}_{-31}$	23.00/8
(1,0,0)	(0,0,0)	1.1041 $^{+6}_{-7}$	0.699 $^{+22}_{-13}$	-0.003 $^{+6}_{-27}$	0.869 $^{+27}_{-16}$	10.24/8
(1,0,0)	(0,1,0)	1.2190 $^{+13}_{-15}$	0.629 $^{+20}_{-16}$	-0.019 $^{+35}_{-20}$	0.799 $^{+26}_{-20}$	6.45/8
(1,0,0)	(-1,0,0)	1.4321 $^{+13}_{-18}$	0.547 $^{+21}_{-19}$	-0.002 $^{+22}_{-22}$	0.655 $^{+25}_{-23}$	12.89/8
$\kappa_E \rightarrow \kappa_A$						0.12230 $\rightarrow$ 0.12730
$\vec{p}$	$\vec{p} + \vec{q}$	$\omega$	$h_+(\omega)$	$h_-(\omega)$	$\xi^{\text{eff}}(\omega)$	$\chi^2/dof$
(0,0,0)	(0,0,0)	1.0000	0.922 $^{+12}_{-19}$	0.000	0.970 $^{+13}_{-20}$	7.25/8
(0,0,0)	(1,0,0)	1.1593 $^{+5}_{-8}$	0.764 $^{+20}_{-19}$	-0.016 $^{+37}_{-39}$	0.826 $^{+22}_{-21}$	7.09/8
(1,0,0)	(1,0,0)	1.0114 $^{+13}_{-15}$	0.954 $^{+20}_{-14}$	0.686 $^{+248}_{-331}$	1.006 $^{+21}_{-51}$	17.14/8
(1,0,0)	(0,0,0)	1.1041 $^{+6}_{-7}$	0.805 $^{+15}_{-15}$	-0.043 $^{+7}_{-7}$	0.863 $^{+16}_{-16}$	12.63/8
(1,0,0)	(0,1,0)	1.2800 $^{+11}_{-17}$	0.677 $^{+13}_{-17}$	-0.040 $^{+38}_{-11}$	0.747 $^{+14}_{-19}$	4.86/8
(1,0,0)	(-1,0,0)	1.5486 $^{+12}_{-20}$	0.520 $^{+12}_{-18}$	-0.017 $^{+23}_{-23}$	0.599 $^{+14}_{-21}$	14.59/8

$\kappa_P = 0.13344$						
$\kappa_E \rightarrow \kappa_A$ 0.12730 $\rightarrow$ 0.11230						
$\vec{p}$	$\vec{p} + \vec{q}$	$\omega$	$h_+(\omega)$	$h_-(\omega)$	$\xi^{\text{eff}}(\omega)$	$\chi^2/dof$
(0,0,0)	(0,0,0)	1.0000	0.797 $^{+14}_{-19}$	0.000	0.968 $^{+17}_{-23}$	8.38/8
(0,0,0)	(1,0,0)	1.0601 $^{+6}_{-6}$	0.754 $^{+15}_{-20}$	0.069 $^{+16}_{-11}$	0.927 $^{+18}_{-25}$	11.78/8
(1,0,0)	(1,0,0)	1.0295 $^{+12}_{-13}$	0.793 $^{+18}_{-41}$	-0.028 $^{+132}_{-84}$	0.969 $^{+22}_{-50}$	12.35/8
(1,0,0)	(0,0,0)	1.1593 $^{+5}_{-8}$	0.655 $^{+13}_{-14}$	0.060 $^{+85}_{-99}$	0.821 $^{+16}_{-17}$	3.60/8
(1,0,0)	(0,1,0)	1.2290 $^{+12}_{-14}$	0.625 $^{+12}_{-17}$	0.045 $^{+23}_{-12}$	0.793 $^{+15}_{-21}$	4.26/8
(1,0,0)	(-1,0,0)	1.4286 $^{+12}_{-17}$	0.508 $^{+12}_{-19}$	0.032 $^{+25}_{-15}$	0.669 $^{+16}_{-25}$	12.70/8
$\kappa_E \rightarrow \kappa_A$ 0.12730 $\rightarrow$ 0.11730						
$\vec{p}$	$\vec{p} + \vec{q}$	$\omega$	$h_+(\omega)$	$h_-(\omega)$	$\xi^{\text{eff}}(\omega)$	$\chi^2/dof$
(0,0,0)	(0,0,0)	1.0000	0.860 $^{+15}_{-20}$	0.000	0.967 $^{+17}_{-22}$	5.26/8
(0,0,0)	(1,0,0)	1.0763 $^{+6}_{-7}$	0.785 $^{+14}_{-21}$	0.049 $^{+6}_{-20}$	0.896 $^{+16}_{-24}$	14.71/8
(1,0,0)	(1,0,0)	1.0207 $^{+12}_{-13}$	0.857 $^{+18}_{-46}$	-0.069 $^{+189}_{-123}$	0.967 $^{+20}_{-52}$	13.57/8
(1,0,0)	(0,0,0)	1.1593 $^{+5}_{-8}$	0.700 $^{+14}_{-14}$	0.052 $^{+27}_{-29}$	0.811 $^{+16}_{-16}$	4.14/8
(1,0,0)	(0,1,0)	1.2478 $^{+11}_{-15}$	0.651 $^{+14}_{-18}$	0.035 $^{+14}_{-12}$	0.766 $^{+16}_{-21}$	3.22/8
(1,0,0)	(-1,0,0)	1.4750 $^{+12}_{-18}$	0.531 $^{+20}_{-20}$	0.021 $^{+14}_{-24}$	0.650 $^{+25}_{-24}$	11.75/8
$\kappa_E \rightarrow \kappa_A$ 0.12730 $\rightarrow$ 0.12230						
$\vec{p}$	$\vec{p} + \vec{q}$	$\omega$	$h_+(\omega)$	$h_-(\omega)$	$\xi^{\text{eff}}(\omega)$	$\chi^2/dof$
(0,0,0)	(0,0,0)	1.0000	0.921 $^{+14}_{-20}$	0.000	0.969 $^{+15}_{-21}$	6.33/8
(0,0,0)	(1,0,0)	1.1041 $^{+6}_{-7}$	0.824 $^{+22}_{-21}$	0.019 $^{+26}_{-10}$	0.883 $^{+24}_{-23}$	16.45/8
(1,0,0)	(1,0,0)	1.0114 $^{+12}_{-15}$	0.938 $^{+19}_{-53}$	-0.279 $^{+357}_{-243}$	0.989 $^{+20}_{-56}$	14.58/8
(1,0,0)	(0,0,0)	1.1593 $^{+5}_{-8}$	0.765 $^{+14}_{-15}$	0.036 $^{+16}_{-28}$	0.827 $^{+15}_{-16}$	5.45/8
(1,0,0)	(0,1,0)	1.2800 $^{+11}_{-17}$	0.675 $^{+13}_{-18}$	0.020 $^{+15}_{-12}$	0.745 $^{+14}_{-20}$	9.18/8
(1,0,0)	(-1,0,0)	1.5486 $^{+12}_{-20}$	0.522 $^{+12}_{-18}$	0.009 $^{+13}_{-13}$	0.601 $^{+14}_{-21}$	12.22/8
$\kappa_E \rightarrow \kappa_A$ 0.12730 $\rightarrow$ 0.12730						
$\vec{p}$	$\vec{p} + \vec{q}$	$\omega$	$h_+(\omega)$	$h_-(\omega)$	$\xi^{\text{eff}}(\omega)$	$\chi^2/dof$
(0,0,0)	(0,0,0)	1.0000	0.950 $^{+9}_{-14}$	0.000	0.986 $^{+9}_{-15}$	12.71/8
(0,0,0)	(1,0,0)	1.1593 $^{+5}_{-8}$	0.789 $^{+22}_{-21}$	-0.010 $^{+17}_{-29}$	0.839 $^{+23}_{-22}$	8.12/8
(1,0,0)	(1,0,0)	1.0055 $^{+13}_{-17}$	0.958 $^{+18}_{-36}$	0.000	0.995 $^{+19}_{-37}$	14.24/8
(1,0,0)	(0,0,0)	1.1593 $^{+5}_{-8}$	0.781 $^{+14}_{-15}$	0.004 $^{+27}_{-27}$	0.830 $^{+15}_{-16}$	7.29/8
(1,0,0)	(0,1,0)	1.3441 $^{+12}_{-19}$	0.640 $^{+20}_{-17}$	0.003 $^{+25}_{-12}$	0.698 $^{+22}_{-19}$	4.05/8
(1,0,0)	(-1,0,0)	1.6827 $^{+14}_{-23}$	0.469 $^{+20}_{-17}$	-0.003 $^{+32}_{-12}$	0.535 $^{+23}_{-19}$	13.63/8

$\kappa_P = 0.13417$						
$\kappa_E \rightarrow \kappa_A$			0.11230 $\rightarrow$ 0.11230			
$\vec{p}$	$\vec{p} + \vec{q}$	$\omega$	$h_+(\omega)$	$h_-(\omega)$	$\xi^{\text{eff}}(\omega)$	$\chi^2/dof$
(0,0,0)	(0,0,0)	1.0000	0.630 $\begin{smallmatrix} +9 \\ -12 \end{smallmatrix}$	0.000	1.025 $\begin{smallmatrix} +15 \\ -20 \end{smallmatrix}$	5.69/8
(0,0,0)	(1,0,0)	1.0632 $\begin{smallmatrix} +9 \\ -9 \end{smallmatrix}$	0.558 $\begin{smallmatrix} +16 \\ -14 \end{smallmatrix}$	0.039 $\begin{smallmatrix} +27 \\ -15 \end{smallmatrix}$	0.922 $\begin{smallmatrix} +27 \\ -33 \end{smallmatrix}$	11.17/8
(1,0,0)	(1,0,0)	1.0075 $\begin{smallmatrix} +21 \\ -18 \end{smallmatrix}$	0.610 $\begin{smallmatrix} +14 \\ -28 \end{smallmatrix}$	0.000	0.994 $\begin{smallmatrix} +23 \\ -46 \end{smallmatrix}$	21.60/8
(1,0,0)	(0,0,0)	1.0632 $\begin{smallmatrix} +9 \\ -9 \end{smallmatrix}$	0.560 $\begin{smallmatrix} +7 \\ -14 \end{smallmatrix}$	-0.009 $\begin{smallmatrix} +18 \\ -11 \end{smallmatrix}$	0.925 $\begin{smallmatrix} +11 \\ -23 \end{smallmatrix}$	9.53/8
(1,0,0)	(0,1,0)	1.1303 $\begin{smallmatrix} +20 \\ -18 \end{smallmatrix}$	0.522 $\begin{smallmatrix} +13 \\ -22 \end{smallmatrix}$	-0.035 $\begin{smallmatrix} +21 \\ -12 \end{smallmatrix}$	0.876 $\begin{smallmatrix} +22 \\ -37 \end{smallmatrix}$	11.69/8
(1,0,0)	(-1,0,0)	1.2531 $\begin{smallmatrix} +19 \\ -20 \end{smallmatrix}$	0.444 $\begin{smallmatrix} +18 \\ -24 \end{smallmatrix}$	0.004 $\begin{smallmatrix} +23 \\ -34 \end{smallmatrix}$	0.766 $\begin{smallmatrix} +31 \\ -41 \end{smallmatrix}$	7.30/8
$\kappa_E \rightarrow \kappa_A$			0.11230 $\rightarrow$ 0.11730			
$\vec{p}$	$\vec{p} + \vec{q}$	$\omega$	$h_+(\omega)$	$h_-(\omega)$	$\xi^{\text{eff}}(\omega)$	$\chi^2/dof$
(0,0,0)	(0,0,0)	1.0000	0.676 $\begin{smallmatrix} +9 \\ -13 \end{smallmatrix}$	0.000	1.006 $\begin{smallmatrix} +14 \\ -20 \end{smallmatrix}$	7.83/8
(0,0,0)	(1,0,0)	1.0804 $\begin{smallmatrix} +9 \\ -9 \end{smallmatrix}$	0.600 $\begin{smallmatrix} +18 \\ -20 \end{smallmatrix}$	0.022 $\begin{smallmatrix} +17 \\ -15 \end{smallmatrix}$	0.909 $\begin{smallmatrix} +27 \\ -31 \end{smallmatrix}$	8.05/8
(1,0,0)	(1,0,0)	1.0084 $\begin{smallmatrix} +19 \\ -18 \end{smallmatrix}$	0.668 $\begin{smallmatrix} +25 \\ -46 \end{smallmatrix}$	-0.541 $\begin{smallmatrix} +462 \\ -585 \end{smallmatrix}$	0.996 $\begin{smallmatrix} +38 \\ -68 \end{smallmatrix}$	20.73/8
(1,0,0)	(0,0,0)	1.0632 $\begin{smallmatrix} +9 \\ -9 \end{smallmatrix}$	0.617 $\begin{smallmatrix} +7 \\ -15 \end{smallmatrix}$	-0.023 $\begin{smallmatrix} +28 \\ -10 \end{smallmatrix}$	0.931 $\begin{smallmatrix} +11 \\ -22 \end{smallmatrix}$	10.83/8
(1,0,0)	(0,1,0)	1.1487 $\begin{smallmatrix} +19 \\ -18 \end{smallmatrix}$	0.550 $\begin{smallmatrix} +13 \\ -22 \end{smallmatrix}$	-0.045 $\begin{smallmatrix} +24 \\ -13 \end{smallmatrix}$	0.846 $\begin{smallmatrix} +20 \\ -34 \end{smallmatrix}$	10.50/8
(1,0,0)	(-1,0,0)	1.2890 $\begin{smallmatrix} +19 \\ -19 \end{smallmatrix}$	0.471 $\begin{smallmatrix} +20 \\ -24 \end{smallmatrix}$	-0.004 $\begin{smallmatrix} +33 \\ -24 \end{smallmatrix}$	0.746 $\begin{smallmatrix} +31 \\ -38 \end{smallmatrix}$	8.62/8
$\kappa_E \rightarrow \kappa_A$			0.11230 $\rightarrow$ 0.12230			
$\vec{p}$	$\vec{p} + \vec{q}$	$\omega$	$h_+(\omega)$	$h_-(\omega)$	$\xi^{\text{eff}}(\omega)$	$\chi^2/dof$
(0,0,0)	(0,0,0)	1.0000	0.738 $\begin{smallmatrix} +10 \\ -13 \end{smallmatrix}$	0.000	0.998 $\begin{smallmatrix} +14 \\ -18 \end{smallmatrix}$	7.82/8
(0,0,0)	(1,0,0)	1.1112 $\begin{smallmatrix} +7 \\ -9 \end{smallmatrix}$	0.636 $\begin{smallmatrix} +19 \\ -20 \end{smallmatrix}$	0.001 $\begin{smallmatrix} +27 \\ -13 \end{smallmatrix}$	0.881 $\begin{smallmatrix} +26 \\ -28 \end{smallmatrix}$	5.46/8
(1,0,0)	(1,0,0)	1.0144 $\begin{smallmatrix} +19 \\ -18 \end{smallmatrix}$	0.739 $\begin{smallmatrix} +24 \\ -50 \end{smallmatrix}$	0.219 $\begin{smallmatrix} +191 \\ -263 \end{smallmatrix}$	1.003 $\begin{smallmatrix} +32 \\ -68 \end{smallmatrix}$	17.05/8
(1,0,0)	(0,0,0)	1.0632 $\begin{smallmatrix} +9 \\ -9 \end{smallmatrix}$	0.675 $\begin{smallmatrix} +8 \\ -15 \end{smallmatrix}$	-0.052 $\begin{smallmatrix} +20 \\ -30 \end{smallmatrix}$	0.926 $\begin{smallmatrix} +11 \\ -21 \end{smallmatrix}$	12.50/8
(1,0,0)	(0,1,0)	1.1814 $\begin{smallmatrix} +17 \\ -19 \end{smallmatrix}$	0.585 $\begin{smallmatrix} +21 \\ -21 \end{smallmatrix}$	-0.060 $\begin{smallmatrix} +27 \\ -15 \end{smallmatrix}$	0.822 $\begin{smallmatrix} +29 \\ -30 \end{smallmatrix}$	8.84/8
(1,0,0)	(-1,0,0)	1.3485 $\begin{smallmatrix} +17 \\ -19 \end{smallmatrix}$	0.483 $\begin{smallmatrix} +21 \\ -23 \end{smallmatrix}$	-0.015 $\begin{smallmatrix} +35 \\ -25 \end{smallmatrix}$	0.702 $\begin{smallmatrix} +30 \\ -34 \end{smallmatrix}$	10.93/8
$\kappa_E \rightarrow \kappa_A$			0.11230 $\rightarrow$ 0.12730			
$\vec{p}$	$\vec{p} + \vec{q}$	$\omega$	$h_+(\omega)$	$h_-(\omega)$	$\xi^{\text{eff}}(\omega)$	$\chi^2/dof$
(0,0,0)	(0,0,0)	1.0000	0.807 $\begin{smallmatrix} +18 \\ -23 \end{smallmatrix}$	0.000	0.980 $\begin{smallmatrix} +22 \\ -28 \end{smallmatrix}$	6.67/8
(0,0,0)	(1,0,0)	1.1738 $\begin{smallmatrix} +6 \\ -11 \end{smallmatrix}$	0.649 $\begin{smallmatrix} +20 \\ -21 \end{smallmatrix}$	-0.024 $\begin{smallmatrix} +28 \\ -13 \end{smallmatrix}$	0.815 $\begin{smallmatrix} +25 \\ -26 \end{smallmatrix}$	3.93/8
(1,0,0)	(1,0,0)	1.0346 $\begin{smallmatrix} +15 \\ -18 \end{smallmatrix}$	0.805 $\begin{smallmatrix} +23 \\ -54 \end{smallmatrix}$	-0.238 $\begin{smallmatrix} +113 \\ -163 \end{smallmatrix}$	0.984 $\begin{smallmatrix} +28 \\ -66 \end{smallmatrix}$	9.49/8
(1,0,0)	(0,0,0)	1.0632 $\begin{smallmatrix} +9 \\ -9 \end{smallmatrix}$	0.753 $\begin{smallmatrix} +15 \\ -15 \end{smallmatrix}$	-0.103 $\begin{smallmatrix} +21 \\ -10 \end{smallmatrix}$	0.926 $\begin{smallmatrix} +19 \\ -19 \end{smallmatrix}$	14.43/8
(1,0,0)	(0,1,0)	1.2480 $\begin{smallmatrix} +13 \\ -18 \end{smallmatrix}$	0.615 $\begin{smallmatrix} +13 \\ -21 \end{smallmatrix}$	-0.062 $\begin{smallmatrix} +32 \\ -47 \end{smallmatrix}$	0.784 $\begin{smallmatrix} +16 \\ -27 \end{smallmatrix}$	6.45/8
(1,0,0)	(-1,0,0)	1.4613 $\begin{smallmatrix} +15 \\ -22 \end{smallmatrix}$	0.491 $\begin{smallmatrix} +22 \\ -23 \end{smallmatrix}$	-0.032 $\begin{smallmatrix} +38 \\ -36 \end{smallmatrix}$	0.650 $\begin{smallmatrix} +29 \\ -30 \end{smallmatrix}$	13.67/8

$\kappa_P = 0.13417$						
$\kappa_E \rightarrow \kappa_A$						0.11730 $\rightarrow$ 0.11230
$\vec{p}$	$\vec{p} + \vec{q}$	$\omega$	$h_+(\omega)$	$h_-(\omega)$	$\xi^{\text{eff}}(\omega)$	$\chi^2/\text{dof}$
(0,0,0)	(0,0,0)	1.0000	0.687 $^{+9}_{-13}$	0.000	1.022 $^{+13}_{-20}$	4.49/8
(0,0,0)	(1,0,0)	1.0632 $^{+9}_{-9}$	0.616 $^{+19}_{-21}$	0.036 $^{+17}_{-15}$	0.929 $^{+28}_{-32}$	13.83/8
(1,0,0)	(1,0,0)	1.0084 $^{+19}_{-18}$	0.672 $^{+24}_{-48}$	0.138 $^{+619}_{-455}$	1.002 $^{+36}_{-71}$	17.88/8
(1,0,0)	(0,0,0)	1.0804 $^{+9}_{-9}$	0.603 $^{+13}_{-16}$	0.014 $^{+39}_{-11}$	0.913 $^{+20}_{-24}$	7.02/8
(1,0,0)	(0,1,0)	1.1487 $^{+19}_{-18}$	0.557 $^{+20}_{-23}$	-0.014 $^{+22}_{-11}$	0.857 $^{+30}_{-35}$	8.38/8
(1,0,0)	(-1,0,0)	1.2890 $^{+19}_{-20}$	0.468 $^{+13}_{-25}$	0.010 $^{+34}_{-35}$	0.741 $^{+20}_{-40}$	10.56/8
$\kappa_E \rightarrow \kappa_A$						0.11730 $\rightarrow$ 0.11730
$\vec{p}$	$\vec{p} + \vec{q}$	$\omega$	$h_+(\omega)$	$h_-(\omega)$	$\xi^{\text{eff}}(\omega)$	$\chi^2/\text{dof}$
(0,0,0)	(0,0,0)	1.0000	0.730 $^{+10}_{-16}$	0.000	1.033 $^{+14}_{-23}$	6.45/8
(0,0,0)	(1,0,0)	1.0804 $^{+9}_{-9}$	0.633 $^{+18}_{-22}$	0.019 $^{+27}_{-15}$	0.911 $^{+26}_{-31}$	10.03/8
(1,0,0)	(1,0,0)	1.0070 $^{+19}_{-17}$	0.714 $^{+14}_{-33}$	0.000	1.006 $^{+20}_{-46}$	18.17/8
(1,0,0)	(0,0,0)	1.0804 $^{+9}_{-9}$	0.626 $^{+7}_{-15}$	0.004 $^{+18}_{-21}$	0.901 $^{+10}_{-22}$	8.08/8
(1,0,0)	(0,1,0)	1.1674 $^{+19}_{-19}$	0.570 $^{+27}_{-22}$	-0.023 $^{+24}_{-11}$	0.836 $^{+39}_{-33}$	7.41/8
(1,0,0)	(-1,0,0)	1.3277 $^{+18}_{-19}$	0.475 $^{+26}_{-24}$	0.003 $^{+23}_{-38}$	0.720 $^{+39}_{-37}$	17.88/8
$\kappa_E \rightarrow \kappa_A$						0.11730 $\rightarrow$ 0.12230
$\vec{p}$	$\vec{p} + \vec{q}$	$\omega$	$h_+(\omega)$	$h_-(\omega)$	$\xi^{\text{eff}}(\omega)$	$\chi^2/\text{dof}$
(0,0,0)	(0,0,0)	1.0000	0.793 $^{+10}_{-14}$	0.000	1.008 $^{+13}_{-18}$	8.99/8
(0,0,0)	(1,0,0)	1.1112 $^{+7}_{-9}$	0.681 $^{+20}_{-23}$	0.001 $^{+27}_{-13}$	0.885 $^{+26}_{-30}$	6.31/8
(1,0,0)	(1,0,0)	1.0098 $^{+17}_{-18}$	0.792 $^{+27}_{-58}$	0.101 $^{+36}_{-53}$	1.008 $^{+34}_{-74}$	16.18/8
(1,0,0)	(0,0,0)	1.0804 $^{+9}_{-9}$	0.697 $^{+22}_{-16}$	-0.020 $^{+29}_{-11}$	0.900 $^{+29}_{-21}$	9.68/8
(1,0,0)	(0,1,0)	1.2006 $^{+17}_{-20}$	0.616 $^{+20}_{-23}$	-0.039 $^{+26}_{-14}$	0.815 $^{+27}_{-30}$	6.23/8
(1,0,0)	(-1,0,0)	1.3915 $^{+16}_{-20}$	0.499 $^{+21}_{-24}$	-0.007 $^{+33}_{-34}$	0.684 $^{+29}_{-33}$	10.54/8
$\kappa_E \rightarrow \kappa_A$						0.11730 $\rightarrow$ 0.12730
$\vec{p}$	$\vec{p} + \vec{q}$	$\omega$	$h_+(\omega)$	$h_-(\omega)$	$\xi^{\text{eff}}(\omega)$	$\chi^2/\text{dof}$
(0,0,0)	(0,0,0)	1.0000	0.868 $^{+17}_{-25}$	0.000	0.976 $^{+19}_{-28}$	10.78/8
(0,0,0)	(1,0,0)	1.1738 $^{+6}_{-11}$	0.705 $^{+20}_{-22}$	-0.019 $^{+28}_{-12}$	0.819 $^{+23}_{-26}$	3.51/8
(1,0,0)	(1,0,0)	1.0245 $^{+15}_{-18}$	0.874 $^{+26}_{-60}$	0.431 $^{+168}_{-244}$	0.987 $^{+29}_{-68}$	9.75/8
(1,0,0)	(0,0,0)	1.0804 $^{+9}_{-9}$	0.783 $^{+16}_{-16}$	-0.064 $^{+10}_{-11}$	0.894 $^{+18}_{-18}$	11.71/8
(1,0,0)	(0,1,0)	1.2683 $^{+15}_{-20}$	0.644 $^{+21}_{-22}$	-0.059 $^{+29}_{-16}$	0.761 $^{+25}_{-26}$	4.51/8
(1,0,0)	(-1,0,0)	1.5120 $^{+15}_{-23}$	0.494 $^{+23}_{-22}$	0.023 $^{+36}_{-25}$	0.608 $^{+28}_{-27}$	13.57/8

$\kappa_P = 0.13417$						
$\kappa_E \rightarrow \kappa_A$ 0.12230 $\rightarrow$ 0.11230						
$\vec{p}$	$\vec{p} + \vec{q}$	$\omega$	$h_+(\omega)$	$h_-(\omega)$	$\xi^{\text{eff}}(\omega)$	$\chi^2/\text{dof}$
(0,0,0)	(0,0,0)	1.0000	0.735 $^{+10}_{-12}$	0.000	0.994 $^{+14}_{-16}$	6.77/8
(0,0,0)	(1,0,0)	1.0632 $^{+9}_{-9}$	0.677 $^{+20}_{-24}$	0.035 $^{+28}_{-14}$	0.929 $^{+27}_{-33}$	17.23/8
(1,0,0)	(1,0,0)	1.0144 $^{+18}_{-18}$	0.738 $^{+23}_{-51}$	0.162 $^{+289}_{-173}$	1.002 $^{+31}_{-69}$	13.32/8
(1,0,0)	(0,0,0)	1.1112 $^{+7}_{-9}$	0.641 $^{+14}_{-17}$	0.037 $^{+11}_{-11}$	0.888 $^{+20}_{-23}$	4.21/8
(1,0,0)	(0,1,0)	1.1814 $^{+17}_{-19}$	0.575 $^{+20}_{-23}$	0.012 $^{+20}_{-13}$	0.808 $^{+28}_{-32}$	4.75/8
(1,0,0)	(-1,0,0)	1.3485 $^{+17}_{-19}$	0.498 $^{+26}_{-26}$	0.016 $^{+36}_{-35}$	0.724 $^{+38}_{-38}$	7.20/8
$\kappa_E \rightarrow \kappa_A$ 0.12230 $\rightarrow$ 0.11730						
$\vec{p}$	$\vec{p} + \vec{q}$	$\omega$	$h_+(\omega)$	$h_-(\omega)$	$\xi^{\text{eff}}(\omega)$	$\chi^2/\text{dof}$
(0,0,0)	(0,0,0)	1.0000	0.783 $^{+9}_{-14}$	0.000	0.995 $^{+11}_{-18}$	9.27/8
(0,0,0)	(1,0,0)	1.0804 $^{+9}_{-9}$	0.699 $^{+19}_{-24}$	0.014 $^{+38}_{-14}$	0.903 $^{+25}_{-31}$	12.63/8
(1,0,0)	(1,0,0)	1.0098 $^{+18}_{-19}$	0.779 $^{+23}_{-58}$	0.257 $^{+560}_{-358}$	0.992 $^{+29}_{-74}$	13.97/8
(1,0,0)	(0,0,0)	1.1112 $^{+7}_{-9}$	0.671 $^{+15}_{-17}$	0.031 $^{+28}_{-10}$	0.872 $^{+20}_{-22}$	4.79/8
(1,0,0)	(0,1,0)	1.2006 $^{+17}_{-20}$	0.610 $^{+20}_{-23}$	0.003 $^{+22}_{-12}$	0.808 $^{+27}_{-31}$	3.75/8
(1,0,0)	(-1,0,0)	1.3915 $^{+17}_{-20}$	0.501 $^{+20}_{-26}$	0.008 $^{+24}_{-24}$	0.687 $^{+27}_{-35}$	8.01/8
$\kappa_E \rightarrow \kappa_A$ 0.12230 $\rightarrow$ 0.12230						
$\vec{p}$	$\vec{p} + \vec{q}$	$\omega$	$h_+(\omega)$	$h_-(\omega)$	$\xi^{\text{eff}}(\omega)$	$\chi^2/\text{dof}$
(0,0,0)	(0,0,0)	1.0000	0.826 $^{+10}_{-14}$	0.000	1.006 $^{+12}_{-17}$	10.53/8
(0,0,0)	(1,0,0)	1.1112 $^{+7}_{-9}$	0.713 $^{+19}_{-23}$	-0.001 $^{+17}_{-13}$	0.888 $^{+24}_{-29}$	7.69/8
(1,0,0)	(1,0,0)	1.0076 $^{+16}_{-19}$	0.830 $^{+19}_{-38}$	0.000	1.013 $^{+23}_{-46}$	13.84/8
(1,0,0)	(0,0,0)	1.1112 $^{+7}_{-9}$	0.703 $^{+22}_{-15}$	0.013 $^{+28}_{-40}$	0.875 $^{+28}_{-19}$	6.13/8
(1,0,0)	(0,1,0)	1.2348 $^{+17}_{-21}$	0.613 $^{+20}_{-23}$	-0.010 $^{+25}_{-14}$	0.782 $^{+26}_{-29}$	3.13/8
(1,0,0)	(-1,0,0)	1.4620 $^{+15}_{-22}$	0.487 $^{+20}_{-23}$	0.001 $^{+32}_{-23}$	0.646 $^{+27}_{-30}$	10.45/8
$\kappa_E \rightarrow \kappa_A$ 0.12230 $\rightarrow$ 0.12730						
$\vec{p}$	$\vec{p} + \vec{q}$	$\omega$	$h_+(\omega)$	$h_-(\omega)$	$\xi^{\text{eff}}(\omega)$	$\chi^2/\text{dof}$
(0,0,0)	(0,0,0)	1.0000	0.929 $^{+17}_{-24}$	0.000	0.978 $^{+18}_{-25}$	10.88/8
(0,0,0)	(1,0,0)	1.1738 $^{+6}_{-11}$	0.755 $^{+21}_{-24}$	-0.017 $^{+37}_{-12}$	0.818 $^{+23}_{-26}$	3.43/8
(1,0,0)	(1,0,0)	1.0142 $^{+16}_{-20}$	0.953 $^{+28}_{-74}$	0.120 $^{+328}_{-501}$	1.005 $^{+30}_{-78}$	9.88/8
(1,0,0)	(0,0,0)	1.1112 $^{+7}_{-9}$	0.799 $^{+16}_{-17}$	-0.023 $^{+29}_{-21}$	0.857 $^{+17}_{-18}$	8.01/8
(1,0,0)	(0,1,0)	1.3044 $^{+15}_{-22}$	0.654 $^{+22}_{-23}$	-0.027 $^{+26}_{-18}$	0.724 $^{+24}_{-25}$	2.71/8
(1,0,0)	(-1,0,0)	1.5945 $^{+14}_{-26}$	0.503 $^{+23}_{-23}$	-0.013 $^{+14}_{-34}$	0.583 $^{+27}_{-27}$	13.11/8

$\kappa_P = 0.13417$						
$\kappa_E \rightarrow \kappa_A$ 0.12730 $\rightarrow$ 0.11230						
$\vec{p}$	$\vec{p} + \vec{q}$	$\omega$	$h_+(\omega)$	$h_-(\omega)$	$\xi^{\text{eff}}(\omega)$	$\chi^2/\text{dof}$
(0,0,0)	(0,0,0)	1.0000	0.822 $^{+16}_{-21}$	0.000	0.998 $^{+20}_{-26}$	7.51/8
(0,0,0)	(1,0,0)	1.0632 $^{+9}_{-9}$	0.758 $^{+22}_{-24}$	0.043 $^{+11}_{-24}$	0.932 $^{+27}_{-30}$	21.78/8
(1,0,0)	(1,0,0)	1.0346 $^{+14}_{-18}$	0.779 $^{+22}_{-61}$	0.201 $^{+188}_{-127}$	0.953 $^{+27}_{-74}$	8.43/8
(1,0,0)	(0,0,0)	1.173 $^{+6}_{-11}$	0.651 $^{+23}_{-18}$	0.067 $^{+13}_{-14}$	0.818 $^{+29}_{-22}$	2.09/8
(1,0,0)	(0,1,0)	1.2480 $^{+14}_{-18}$	0.619 $^{+16}_{-24}$	0.054 $^{+21}_{-19}$	0.789 $^{+20}_{-30}$	2.43/8
(1,0,0)	(-1,0,0)	1.4613 $^{+15}_{-22}$	0.494 $^{+20}_{-25}$	0.022 $^{+27}_{-36}$	0.654 $^{+27}_{-33}$	10.97/8
$\kappa_E \rightarrow \kappa_A$ 0.12730 $\rightarrow$ 0.11730						
$\vec{p}$	$\vec{p} + \vec{q}$	$\omega$	$h_+(\omega)$	$h_-(\omega)$	$\xi^{\text{eff}}(\omega)$	$\chi^2/\text{dof}$
(0,0,0)	(0,0,0)	1.0000	0.882 $^{+18}_{-20}$	0.000	0.992 $^{+20}_{-23}$	8.37/8
(0,0,0)	(1,0,0)	1.0804 $^{+9}_{-9}$	0.766 $^{+22}_{-25}$	0.015 $^{+30}_{-13}$	0.890 $^{+26}_{-29}$	16.20/8
(1,0,0)	(1,0,0)	1.0245 $^{+15}_{-19}$	0.845 $^{+23}_{-65}$	0.215 $^{+277}_{-168}$	0.957 $^{+26}_{-74}$	18.98/8
(1,0,0)	(0,0,0)	1.1738 $^{+6}_{-11}$	0.708 $^{+24}_{-18}$	0.060 $^{+11}_{-13}$	0.806 $^{+27}_{-20}$	2.17/8
(1,0,0)	(0,1,0)	1.2683 $^{+15}_{-21}$	0.642 $^{+24}_{-25}$	0.044 $^{+21}_{-19}$	0.755 $^{+28}_{-29}$	1.41/8
(1,0,0)	(-1,0,0)	1.512 $^{+15}_{-23}$	0.517 $^{+21}_{-25}$	0.013 $^{+36}_{-35}$	0.631 $^{+26}_{-30}$	10.45/8
$\kappa_E \rightarrow \kappa_A$ 0.12730 $\rightarrow$ 0.12230						
$\vec{p}$	$\vec{p} + \vec{q}$	$\omega$	$h_+(\omega)$	$h_-(\omega)$	$\xi^{\text{eff}}(\omega)$	$\chi^2/\text{dof}$
(0,0,0)	(0,0,0)	1.0000	0.938 $^{+18}_{-22}$	0.000	0.987 $^{+19}_{-23}$	10.86/8
(0,0,0)	(1,0,0)	1.1112 $^{+7}_{-9}$	0.821 $^{+23}_{-26}$	-0.006 $^{+39}_{-13}$	0.881 $^{+25}_{-28}$	9.95/8
(1,0,0)	(1,0,0)	1.0142 $^{+16}_{-20}$	0.942 $^{+29}_{-78}$	0.184 $^{+530}_{-327}$	0.994 $^{+31}_{-82}$	9.52/8
(1,0,0)	(0,0,0)	1.1738 $^{+7}_{-11}$	0.755 $^{+16}_{-18}$	0.046 $^{+28}_{-11}$	0.818 $^{+17}_{-19}$	3.03/8
(1,0,0)	(0,1,0)	1.3044 $^{+15}_{-22}$	0.664 $^{+23}_{-24}$	0.031 $^{+21}_{-17}$	0.736 $^{+25}_{-27}$	11.31/8
(1,0,0)	(-1,0,0)	1.5945 $^{+15}_{-27}$	0.503 $^{+22}_{-22}$	0.005 $^{+33}_{-24}$	0.583 $^{+26}_{-26}$	21.19/8
$\kappa_E \rightarrow \kappa_A$ 0.12730 $\rightarrow$ 0.12730						
$\vec{p}$	$\vec{p} + \vec{q}$	$\omega$	$h_+(\omega)$	$h_-(\omega)$	$\xi^{\text{eff}}(\omega)$	$\chi^2/\text{dof}$
(0,0,0)	(0,0,0)	1.0000	0.955 $^{+10}_{-17}$	0.000	0.991 $^{+10}_{-18}$	8.30/8
(0,0,0)	(1,0,0)	1.1738 $^{+6}_{-11}$	0.767 $^{+23}_{-24}$	-0.020 $^{+38}_{-11}$	0.817 $^{+24}_{-26}$	14.20/8
(1,0,0)	(1,0,0)	1.0073 $^{+15}_{-22}$	0.968 $^{+31}_{-52}$	0.000	1.006 $^{+32}_{-54}$	18.82/8
(1,0,0)	(0,0,0)	1.1738 $^{+6}_{-11}$	0.767 $^{+14}_{-16}$	0.018 $^{+37}_{-30}$	0.817 $^{+15}_{-17}$	4.34/8
(1,0,0)	(0,1,0)	1.3778 $^{+15}_{-27}$	0.628 $^{+14}_{-21}$	0.020 $^{+21}_{-19}$	0.689 $^{+15}_{-23}$	2.30/8
(1,0,0)	(-1,0,0)	1.7484 $^{+17}_{-33}$	0.452 $^{+13}_{-20}$	-0.001 $^{+10}_{-22}$	0.519 $^{+15}_{-23}$	22.67/8

$\kappa_P = 0.13460$						
$\kappa_E \rightarrow \kappa_A$						0.12000 $\rightarrow$ 0.12000
$\vec{p}$	$\vec{p} + \vec{q}$	$\omega$	$h_+(\omega)$	$h_-(\omega)$	$\xi^{\text{eff}}(\omega)$	$\chi^2/dof$
(0,0,0)	(0,0,0)	1.0000	0.755 $^{+10}_{-12}$	0.000	1.000 $^{+13}_{-16}$	10.88/8
(0,0,0)	(1,0,0)	1.0489 $^{+10}_{-10}$	0.708 $^{+9}_{-19}$	-0.003 $^{+28}_{-32}$	0.949 $^{+12}_{-26}$	10.29/8
(1,0,0)	(1,0,0)	1.0032 $^{+21}_{-21}$	0.770 $^{+18}_{-30}$	0.000	1.020 $^{+24}_{-40}$	26.41/8
(1,0,0)	(0,0,0)	1.0489 $^{+10}_{-10}$	0.695 $^{+18}_{-16}$	-0.029 $^{+15}_{-17}$	0.932 $^{+24}_{-22}$	17.38/8
(1,0,0)	(0,1,0)	1.1002 $^{+22}_{-21}$	0.667 $^{+24}_{-26}$	-0.012 $^{+26}_{-19}$	0.905 $^{+33}_{-35}$	27.94/8
(1,0,0)	(-1,0,0)	1.1972 $^{+21}_{-23}$	0.578 $^{+22}_{-25}$	-0.010 $^{+24}_{-26}$	0.802 $^{+31}_{-35}$	12.11/8
$\kappa_E \rightarrow \kappa_A$						0.12000 $\rightarrow$ 0.12660
$\vec{p}$	$\vec{p} + \vec{q}$	$\omega$	$h_+(\omega)$	$h_-(\omega)$	$\xi^{\text{eff}}(\omega)$	$\chi^2/dof$
(0,0,0)	(0,0,0)	1.0000	0.853 $^{+13}_{-17}$	0.000	0.981 $^{+15}_{-19}$	4.31/8
(0,0,0)	(1,0,0)	1.0843 $^{+11}_{-12}$	0.768 $^{+15}_{-21}$	-0.047 $^{+27}_{-11}$	0.899 $^{+18}_{-25}$	14.05/8
(1,0,0)	(1,0,0)	1.0076 $^{+22}_{-22}$	0.866 $^{+30}_{-52}$	0.012 $^{+254}_{-364}$	0.997 $^{+35}_{-60}$	18.86/8
(1,0,0)	(0,0,0)	1.0489 $^{+10}_{-10}$	0.809 $^{+9}_{-16}$	-0.029 $^{+17}_{-15}$	0.940 $^{+10}_{-19}$	15.08/8
(1,0,0)	(0,1,0)	1.1374 $^{+23}_{-25}$	0.727 $^{+24}_{-23}$	-0.057 $^{+22}_{-22}$	0.861 $^{+29}_{-27}$	28.65/8
(1,0,0)	(-1,0,0)	1.2671 $^{+23}_{-25}$	0.630 $^{+23}_{-26}$	-0.023 $^{+34}_{-37}$	0.753 $^{+28}_{-31}$	15.48/8
$\kappa_E \rightarrow \kappa_A$						0.12330 $\rightarrow$ 0.12000
$\vec{p}$	$\vec{p} + \vec{q}$	$\omega$	$h_+(\omega)$	$h_-(\omega)$	$\xi^{\text{eff}}(\omega)$	$\chi^2/dof$
(0,0,0)	(0,0,0)	1.0000	0.813 $^{+10}_{-11}$	0.000	1.006 $^{+12}_{-14}$	9.30/8
(0,0,0)	(1,0,0)	1.0489 $^{+10}_{-10}$	0.757 $^{+17}_{-20}$	0.010 $^{+28}_{-11}$	0.947 $^{+21}_{-25}$	13.08/8
(1,0,0)	(1,0,0)	1.0038 $^{+22}_{-21}$	0.806 $^{+38}_{-57}$	0.582 $^{+484}_{-683}$	0.997 $^{+47}_{-71}$	28.83/8
(1,0,0)	(0,0,0)	1.0622 $^{+11}_{-11}$	0.738 $^{+17}_{-18}$	-0.023 $^{+15}_{-16}$	0.926 $^{+21}_{-22}$	4.83/8
(1,0,0)	(0,1,0)	1.1142 $^{+23}_{-22}$	0.691 $^{+26}_{-27}$	-0.010 $^{+27}_{-19}$	0.877 $^{+33}_{-34}$	8.38/8
(1,0,0)	(-1,0,0)	1.2246 $^{+22}_{-24}$	0.607 $^{+25}_{-27}$	-0.006 $^{+45}_{-36}$	0.789 $^{+32}_{-35}$	14.62/8
$\kappa_E \rightarrow \kappa_A$						0.12330 $\rightarrow$ 0.12660
$\vec{p}$	$\vec{p} + \vec{q}$	$\omega$	$h_+(\omega)$	$h_-(\omega)$	$\xi^{\text{eff}}(\omega)$	$\chi^2/dof$
(0,0,0)	(0,0,0)	1.0000	0.896 $^{+13}_{-15}$	0.000	0.992 $^{+14}_{-17}$	9.15/8
(0,0,0)	(1,0,0)	1.0843 $^{+11}_{-12}$	0.796 $^{+25}_{-21}$	-0.032 $^{+37}_{-10}$	0.898 $^{+28}_{-24}$	14.79/8
(1,0,0)	(1,0,0)	1.0042 $^{+23}_{-23}$	0.897 $^{+36}_{-60}$	-0.207 $^{+519}_{-767}$	0.994 $^{+40}_{-66}$	25.95/8
(1,0,0)	(0,0,0)	1.0622 $^{+11}_{-11}$	0.811 $^{+17}_{-16}$	-0.011 $^{+14}_{-13}$	0.910 $^{+19}_{-18}$	4.35/8
(1,0,0)	(0,1,0)	1.1519 $^{+24}_{-24}$	0.750 $^{+17}_{-24}$	-0.068 $^{+21}_{-22}$	0.858 $^{+20}_{-27}$	10.03/8
(1,0,0)	(-1,0,0)	1.2995 $^{+23}_{-27}$	0.618 $^{+25}_{-25}$	-0.015 $^{+23}_{-26}$	0.727 $^{+29}_{-30}$	6.64/8

$\kappa_P = 0.13460$						
$\kappa_E \rightarrow \kappa_A$						0.12660 $\rightarrow$ 0.12000
$\vec{p}$	$\vec{p} + \vec{q}$	$\omega$	$h_+(\omega)$	$h_-(\omega)$	$\xi^{\text{eff}}(\omega)$	$\chi^2/dof$
(0,0,0)	(0,0,0)	1.0000	0.874 $^{+12}_{-17}$	0.000	1.005 $^{+14}_{-19}$	0.07/8
(0,0,0)	(1,0,0)	1.0489 $^{+10}_{-10}$	0.817 $^{+17}_{-21}$	0.032 $^{+28}_{-11}$	0.949 $^{+20}_{-24}$	13.91/8
(1,0,0)	(1,0,0)	1.0076 $^{+22}_{-22}$	0.855 $^{+36}_{-56}$	0.368 $^{+378}_{-337}$	0.985 $^{+42}_{-64}$	25.77/8
(1,0,0)	(0,0,0)	1.0843 $^{+12}_{-12}$	0.759 $^{+17}_{-18}$	-0.012 $^{+16}_{-17}$	0.889 $^{+20}_{-21}$	7.48/8
(1,0,0)	(0,1,0)	1.1374 $^{+23}_{-25}$	0.720 $^{+29}_{-27}$	-0.073 $^{+27}_{-21}$	0.853 $^{+34}_{-32}$	6.68/8
(1,0,0)	(-1,0,0)	1.2671 $^{+23}_{-25}$	0.643 $^{+28}_{-27}$	-0.001 $^{+38}_{-28}$	0.768 $^{+33}_{-32}$	31.68/8
$\kappa_E \rightarrow \kappa_A$						0.12660 $\rightarrow$ 0.12660
$\vec{p}$	$\vec{p} + \vec{q}$	$\omega$	$h_+(\omega)$	$h_-(\omega)$	$\xi^{\text{eff}}(\omega)$	$\chi^2/dof$
(0,0,0)	(0,0,0)	1.0000	0.921 $^{+13}_{-10}$	0.000	1.001 $^{+14}_{-11}$	3.02/8
(0,0,0)	(1,0,0)	1.0843 $^{+11}_{-12}$	0.817 $^{+25}_{-20}$	-0.009 $^{+27}_{-11}$	0.903 $^{+28}_{-22}$	9.33/8
(1,0,0)	(1,0,0)	1.0023 $^{+23}_{-25}$	0.917 $^{+26}_{-33}$	0.000	0.996 $^{+28}_{-36}$	27.55/8
(1,0,0)	(0,0,0)	1.0843 $^{+11}_{-12}$	0.810 $^{+25}_{-16}$	0.013 $^{+11}_{-15}$	0.895 $^{+28}_{-18}$	8.60/8
(1,0,0)	(0,1,0)	1.1758 $^{+25}_{-26}$	0.732 $^{+25}_{-26}$	-0.045 $^{+22}_{-22}$	0.824 $^{+28}_{-29}$	7.56/8
(1,0,0)	(-1,0,0)	1.3494 $^{+26}_{-29}$	0.607 $^{+18}_{-24}$	0.000 $^{+33}_{-25}$	0.705 $^{+21}_{-28}$	11.63/8
$\kappa_E \rightarrow \kappa_A$						0.12990 $\rightarrow$ 0.12000
$\vec{p}$	$\vec{p} + \vec{q}$	$\omega$	$h_+(\omega)$	$h_-(\omega)$	$\xi^{\text{eff}}(\omega)$	$\chi^2/dof$
(0,0,0)	(0,0,0)	1.0000	0.935 $^{+12}_{-16}$	0.000	0.989 $^{+13}_{-17}$	0.80/8
(0,0,0)	(1,0,0)	1.0489 $^{+10}_{-10}$	0.873 $^{+18}_{-21}$	0.055 $^{+38}_{-12}$	0.933 $^{+19}_{-22}$	11.30/8
(1,0,0)	(1,0,0)	1.0209 $^{+23}_{-24}$	0.909 $^{+34}_{-63}$	0.313 $^{+249}_{-212}$	0.966 $^{+36}_{-67}$	18.11/8
(1,0,0)	(0,0,0)	1.1272 $^{+13}_{-15}$	0.813 $^{+29}_{-30}$	-0.024 $^{+22}_{-17}$	0.882 $^{+32}_{-33}$	5.57/8
(1,0,0)	(0,1,0)	1.1824 $^{+24}_{-27}$	0.745 $^{+29}_{-30}$	-0.043 $^{+33}_{-21}$	0.817 $^{+32}_{-33}$	23.28/8
(1,0,0)	(-1,0,0)	1.3438 $^{+25}_{-30}$	0.620 $^{+20}_{-26}$	0.006 $^{+30}_{-10}$	0.701 $^{+23}_{-29}$	16.48/8
$\kappa_E \rightarrow \kappa_A$						0.12990 $\rightarrow$ 0.12660
$\vec{p}$	$\vec{p} + \vec{q}$	$\omega$	$h_+(\omega)$	$h_-(\omega)$	$\xi^{\text{eff}}(\omega)$	$\chi^2/dof$
(0,0,0)	(0,0,0)	1.0000	1.008 $^{+12}_{-16}$	0.000	0.980 $^{+12}_{-16}$	1.01/8
(0,0,0)	(1,0,0)	1.0843 $^{+11}_{-12}$	0.892 $^{+18}_{-21}$	0.002 $^{+27}_{-21}$	0.898 $^{+18}_{-21}$	9.39/8
(1,0,0)	(1,0,0)	1.0064 $^{+26}_{-25}$	1.019 $^{+40}_{-89}$	0.351 $^{+75}_{-468}$	0.992 $^{+39}_{-87}$	24.74/8
(1,0,0)	(0,0,0)	1.1272 $^{+13}_{-15}$	0.879 $^{+23}_{-24}$	0.009 $^{+15}_{-13}$	0.874 $^{+23}_{-24}$	1.78/8
(1,0,0)	(0,1,0)	1.2223 $^{+28}_{-29}$	0.781 $^{+29}_{-27}$	0.017 $^{+28}_{-20}$	0.790 $^{+29}_{-27}$	13.76/8
(1,0,0)	(-1,0,0)	1.4383 $^{+30}_{-33}$	0.613 $^{+28}_{-28}$	0.006 $^{+25}_{-35}$	0.643 $^{+29}_{-29}$	18.91/8

$\kappa_P = 0.13510$						
$\kappa_E \rightarrow \kappa_A$ 0.12000 $\rightarrow$ 0.12000						
$\vec{p}$	$\vec{p} + \vec{q}$	$\omega$	$h_+(\omega)$	$h_-(\omega)$	$\xi^{\text{eff}}(\omega)$	$\chi^2/dof$
(0,0,0)	(0,0,0)	1.0000	0.760 <sup>+11</sup> <sub>-10</sub>	0.000	1.007 <sup>+14</sup> <sub>-13</sub>	12.11/8
(0,0,0)	(1,0,0)	1.0507 <sup>+18</sup> <sub>-15</sub>	0.698 <sup>+19</sup> <sub>-19</sub>	-0.023 <sup>+13</sup> <sub>-17</sub>	0.936 <sup>+25</sup> <sub>-35</sub>	6.49/8
(1,0,0)	(1,0,0)	1.0028 <sup>+24</sup> <sub>-26</sub>	0.761 <sup>+31</sup> <sub>-47</sub>	0.000	1.009 <sup>+41</sup> <sub>-62</sub>	24.22/8
(1,0,0)	(0,0,0)	1.0507 <sup>+18</sup> <sub>-25</sub>	0.688 <sup>+16</sup> <sub>-24</sub>	-0.029 <sup>+25</sup> <sub>-23</sub>	0.922 <sup>+21</sup> <sub>-32</sub>	16.63/8
(1,0,0)	(0,1,0)	1.1040 <sup>+24</sup> <sub>-27</sub>	0.670 <sup>+27</sup> <sub>-36</sub>	-0.049 <sup>+40</sup> <sub>-31</sub>	0.909 <sup>+36</sup> <sub>-49</sub>	13.83/8
(1,0,0)	(-1,0,0)	1.2052 <sup>+25</sup> <sub>-30</sub>	0.638 <sup>+26</sup> <sub>-39</sub>	-0.034 <sup>+16</sup> <sub>-35</sub>	0.808 <sup>+33</sup> <sub>-49</sub>	9.31/8
$\kappa_E \rightarrow \kappa_A$ 0.12000 $\rightarrow$ 0.12660						
$\vec{p}$	$\vec{p} + \vec{q}$	$\omega$	$h_+(\omega)$	$h_-(\omega)$	$\xi^{\text{eff}}(\omega)$	$\chi^2/dof$
(0,0,0)	(0,0,0)	1.0000	0.851 <sup>+10</sup> <sub>-11</sub>	0.000	0.978 <sup>+12</sup> <sub>-13</sub>	7.57/8
(0,0,0)	(1,0,0)	1.0893 <sup>+13</sup> <sub>-15</sub>	0.770 <sup>+20</sup> <sub>-28</sub>	-0.055 <sup>+10</sup> <sub>-20</sub>	0.903 <sup>+23</sup> <sub>-33</sub>	7.33/8
(1,0,0)	(1,0,0)	1.0079 <sup>+27</sup> <sub>-28</sub>	0.862 <sup>+52</sup> <sub>-87</sub>	-0.402 <sup>+445</sup> <sub>-576</sub>	0.993 <sup>+60</sup> <sub>-100</sub>	15.50/8
(1,0,0)	(0,0,0)	1.0507 <sup>+12</sup> <sub>-13</sub>	0.812 <sup>+22</sup> <sub>-22</sub>	0.000 <sup>+19</sup> <sub>-20</sub>	0.944 <sup>+26</sup> <sub>-26</sub>	15.95/8
(1,0,0)	(0,1,0)	1.1446 <sup>+27</sup> <sub>-28</sub>	0.726 <sup>+22</sup> <sub>-31</sub>	-0.011 <sup>+34</sup> <sub>-33</sub>	0.861 <sup>+26</sup> <sub>-37</sub>	4.42/8
(1,0,0)	(-1,0,0)	1.2813 <sup>+27</sup> <sub>-31</sub>	0.621 <sup>+27</sup> <sub>-35</sub>	-0.010 <sup>+26</sup> <sub>-11</sub>	0.740 <sup>+32</sup> <sub>-42</sub>	8.68/8
$\kappa_E \rightarrow \kappa_A$ 0.12330 $\rightarrow$ 0.12000						
$\vec{p}$	$\vec{p} + \vec{q}$	$\omega$	$h_+(\omega)$	$h_-(\omega)$	$\xi^{\text{eff}}(\omega)$	$\chi^2/dof$
(0,0,0)	(0,0,0)	1.0000	0.820 <sup>+11</sup> <sub>-12</sub>	0.000	1.014 <sup>+13</sup> <sub>-15</sub>	10.58/8
(0,0,0)	(1,0,0)	1.0507 <sup>+11</sup> <sub>-13</sub>	0.747 <sup>+21</sup> <sub>-26</sub>	-0.003 <sup>+11</sup> <sub>-17</sub>	0.935 <sup>+26</sup> <sub>-33</sub>	7.19/8
(1,0,0)	(1,0,0)	1.0036 <sup>+26</sup> <sub>-27</sub>	0.814 <sup>+75</sup> <sub>-98</sub>	0.438 <sup>+144</sup> <sub>-256</sub>	1.008 <sup>+93</sup> <sub>-121</sub>	24.21/8
(1,0,0)	(0,0,0)	1.0651 <sup>+13</sup> <sub>-14</sub>	0.733 <sup>+16</sup> <sub>-25</sub>	-0.012 <sup>+21</sup> <sub>-24</sub>	0.920 <sup>+20</sup> <sub>-32</sub>	15.57/8
(1,0,0)	(0,1,0)	1.1192 <sup>+26</sup> <sub>-28</sub>	0.691 <sup>+26</sup> <sub>-37</sub>	-0.066 <sup>+41</sup> <sub>-32</sub>	0.878 <sup>+33</sup> <sub>-47</sub>	13.92/8
(1,0,0)	(-1,0,0)	1.2348 <sup>+26</sup> <sub>-29</sub>	0.635 <sup>+30</sup> <sub>-40</sub>	-0.015 <sup>+28</sup> <sub>-28</sub>	0.779 <sup>+37</sup> <sub>-49</sub>	15.66/8
$\kappa_E \rightarrow \kappa_A$ 0.12330 $\rightarrow$ 0.12660						
$\vec{p}$	$\vec{p} + \vec{q}$	$\omega$	$h_+(\omega)$	$h_-(\omega)$	$\xi^{\text{eff}}(\omega)$	$\chi^2/dof$
(0,0,0)	(0,0,0)	1.0000	0.894 <sup>+10</sup> <sub>-13</sub>	0.000	0.990 <sup>+11</sup> <sub>-14</sub>	0.54/8
(0,0,0)	(1,0,0)	1.0893 <sup>+13</sup> <sub>-15</sub>	0.796 <sup>+19</sup> <sub>-29</sub>	-0.041 <sup>+29</sup> <sub>-19</sub>	0.899 <sup>+21</sup> <sub>-33</sub>	8.61/8
(1,0,0)	(1,0,0)	1.0041 <sup>+28</sup> <sub>-27</sub>	0.903 <sup>+69</sup> <sub>-108</sub>	-0.377 <sup>+513</sup> <sub>-407</sub>	1.001 <sup>+77</sup> <sub>-120</sub>	21.01/8
(1,0,0)	(0,0,0)	1.0651 <sup>+13</sup> <sub>-14</sub>	0.809 <sup>+22</sup> <sub>-20</sub>	0.004 <sup>+16</sup> <sub>-18</sub>	0.909 <sup>+25</sup> <sub>-23</sub>	15.60/8
(1,0,0)	(0,1,0)	1.1603 <sup>+28</sup> <sub>-30</sub>	0.739 <sup>+31</sup> <sub>-31</sub>	-0.078 <sup>+35</sup> <sub>-32</sub>	0.847 <sup>+36</sup> <sub>-36</sub>	6.76/8
(1,0,0)	(-1,0,0)	1.3165 <sup>+29</sup> <sub>-33</sub>	0.657 <sup>+31</sup> <sub>-38</sub>	-0.010 <sup>+24</sup> <sub>-38</sub>	0.729 <sup>+34</sup> <sub>-42</sub>	7.72/8

$\kappa_P = 0.13460$						
$\kappa_E \rightarrow \kappa_A$						0.12660 $\rightarrow$ 0.12000
$\vec{p}$	$\vec{p} + \vec{q}$	$\omega$	$h_+(\omega)$	$h_-(\omega)$	$\xi^{\text{eff}}(\omega)$	$\chi^2/dof$
(0,0,0)	(0,0,0)	1.0000	0.878 $^{+16}_{-17}$	0.000	1.010 $^{+18}_{-20}$	3.29/8
(0,0,0)	(1,0,0)	1.0507 $^{+11}_{-13}$	0.809 $^{+19}_{-26}$	0.007 $^{+12}_{-16}$	0.941 $^{+22}_{-30}$	12.71/8
(1,0,0)	(1,0,0)	1.0079 $^{+27}_{-28}$	0.851 $^{+69}_{-93}$	0.103 $^{+499}_{-540}$	0.980 $^{+80}_{-107}$	20.47/8
(1,0,0)	(0,0,0)	1.0893 $^{+13}_{-15}$	0.769 $^{+32}_{-27}$	-0.022 $^{+23}_{-25}$	0.902 $^{+37}_{-32}$	12.85/8
(1,0,0)	(0,1,0)	1.1446 $^{+27}_{-29}$	0.731 $^{+17}_{-39}$	-0.021 $^{+44}_{-32}$	0.867 $^{+20}_{-46}$	11.56/8
(1,0,0)	(-1,0,0)	1.2813 $^{+28}_{-31}$	0.625 $^{+31}_{-36}$	-0.019 $^{+22}_{-29}$	0.745 $^{+37}_{-43}$	3.21/8
$\kappa_E \rightarrow \kappa_A$						0.12660 $\rightarrow$ 0.12660
$\vec{p}$	$\vec{p} + \vec{q}$	$\omega$	$h_+(\omega)$	$h_-(\omega)$	$\xi^{\text{eff}}(\omega)$	$\chi^2/dof$
(0,0,0)	(0,0,0)	1.0000	0.911 $^{+4}_{-18}$	0.000	0.99 $^{+4}_{-20}$	8.63/8
(0,0,0)	(1,0,0)	1.0893 $^{+13}_{-15}$	0.819 $^{+18}_{-32}$	-0.036 $^{+12}_{-13}$	0.906 $^{+20}_{-35}$	11.41/8
(1,0,0)	(1,0,0)	1.0019 $^{+28}_{-31}$	0.913 $^{+31}_{-55}$	0.000	0.992 $^{+34}_{-60}$	27.76/8
(1,0,0)	(0,0,0)	1.0893 $^{+13}_{-16}$	0.819 $^{+21}_{-21}$	0.010 $^{+14}_{-18}$	0.906 $^{+23}_{-23}$	15.15/8
(1,0,0)	(0,1,0)	1.1866 $^{+29}_{-33}$	0.734 $^{+23}_{-33}$	0.041 $^{+35}_{-36}$	0.828 $^{+26}_{-37}$	7.40/8
(1,0,0)	(-1,0,0)	1.3713 $^{+30}_{-36}$	0.582 $^{+28}_{-34}$	0.006 $^{+24}_{-35}$	0.679 $^{+33}_{-40}$	7.21/8
$\kappa_E \rightarrow \kappa_A$						0.12660 $\rightarrow$ 0.12000
$\vec{p}$	$\vec{p} + \vec{q}$	$\omega$	$h_+(\omega)$	$h_-(\omega)$	$\xi^{\text{eff}}(\omega)$	$\chi^2/dof$
(0,0,0)	(0,0,0)	1.0000	0.944 $^{+15}_{-19}$	0.000	0.999 $^{+16}_{-20}$	0.41/8
(0,0,0)	(1,0,0)	1.0507 $^{+11}_{-13}$	0.873 $^{+27}_{-27}$	0.020 $^{+13}_{-17}$	0.933 $^{+29}_{-29}$	12.60/8
(1,0,0)	(1,0,0)	1.0232 $^{+27}_{-30}$	0.916 $^{+69}_{-97}$	0.637 $^{+290}_{-326}$	0.974 $^{+73}_{-103}$	13.61/8
(1,0,0)	(0,0,0)	1.1376 $^{+16}_{-18}$	0.787 $^{+31}_{-30}$	-0.044 $^{+31}_{-27}$	0.856 $^{+34}_{-33}$	8.58/8
(1,0,0)	(0,1,0)	1.1953 $^{+28}_{-33}$	0.738 $^{+32}_{-44}$	-0.076 $^{+49}_{-30}$	0.812 $^{+35}_{-48}$	17.71/8
(1,0,0)	(-1,0,0)	1.3673 $^{+29}_{-36}$	0.610 $^{+32}_{-36}$	-0.030 $^{+18}_{-11}$	0.693 $^{+36}_{-41}$	26.05/8
$\kappa_E \rightarrow \kappa_A$						0.12660 $\rightarrow$ 0.12660
$\vec{p}$	$\vec{p} + \vec{q}$	$\omega$	$h_+(\omega)$	$h_-(\omega)$	$\xi^{\text{eff}}(\omega)$	$\chi^2/dof$
(0,0,0)	(0,0,0)	1.0000	1.005 $^{+15}_{-19}$	0.000	0.977 $^{+15}_{-18}$	4.02/8
(0,0,0)	(1,0,0)	1.0893 $^{+13}_{-15}$	0.899 $^{+26}_{-27}$	-0.020 $^{+10}_{-13}$	0.906 $^{+26}_{-27}$	5.97/8
(1,0,0)	(1,0,0)	1.0067 $^{+31}_{-33}$	1.036 $^{+74}_{-138}$	0.780 $^{+306}_{-376}$	1.008 $^{+72}_{-134}$	19.48/8
(1,0,0)	(0,0,0)	1.1376 $^{+16}_{-18}$	0.871 $^{+20}_{-23}$	0.013 $^{+16}_{-21}$	0.868 $^{+20}_{-23}$	5.60/8
(1,0,0)	(0,1,0)	1.2392 $^{+33}_{-37}$	0.774 $^{+34}_{-48}$	-0.051 $^{+46}_{-23}$	0.785 $^{+34}_{-49}$	11.71/8
(1,0,0)	(-1,0,0)	1.4717 $^{+35}_{-42}$	0.620 $^{+39}_{-40}$	-0.011 $^{+29}_{-35}$	0.626 $^{+39}_{-40}$	7.76/8

$\kappa_P = 0.13400$			
$\kappa_E \rightarrow \kappa_A$		0.11230 $\rightarrow$ 0.11230	
$\vec{p}$	$\vec{p} + \vec{q}$	$\omega^s$	$h_+^s(\omega)$
(0,0,0)	(1,0,0)	1.0625 $\begin{smallmatrix} +9 \\ -8 \end{smallmatrix}$	0.927 $\begin{smallmatrix} +37 \\ -32 \end{smallmatrix}$
(1,0,0)	(1,0,0)	1.0073 $\begin{smallmatrix} +20 \\ -16 \end{smallmatrix}$	0.997 $\begin{smallmatrix} +23 \\ -44 \end{smallmatrix}$
(1,0,0)	(0,0,0)	1.0625 $\begin{smallmatrix} +9 \\ -8 \end{smallmatrix}$	0.926 $\begin{smallmatrix} +21 \\ -23 \end{smallmatrix}$
(1,0,0)	(0,1,0)	1.1290 $\begin{smallmatrix} +19 \\ -18 \end{smallmatrix}$	0.878 $\begin{smallmatrix} +22 \\ -35 \end{smallmatrix}$
(1,0,0)	(-1,0,0)	1.2507 $\begin{smallmatrix} +18 \\ -18 \end{smallmatrix}$	0.766 $\begin{smallmatrix} +31 \\ -38 \end{smallmatrix}$
$\kappa_E \rightarrow \kappa_A$		0.11230 $\rightarrow$ 0.11730	
$\vec{p}$	$\vec{p} + \vec{q}$	$\omega^s$	$h_+^s(\omega)$
(0,0,0)	(1,0,0)	1.0796 $\begin{smallmatrix} +8 \\ -8 \end{smallmatrix}$	0.911 $\begin{smallmatrix} +27 \\ -30 \end{smallmatrix}$
(1,0,0)	(1,0,0)	1.0081 $\begin{smallmatrix} +19 \\ -16 \end{smallmatrix}$	1.000 $\begin{smallmatrix} +55 \\ -64 \end{smallmatrix}$
(1,0,0)	(0,0,0)	1.0625 $\begin{smallmatrix} +9 \\ -8 \end{smallmatrix}$	0.928 $\begin{smallmatrix} +21 \\ -21 \end{smallmatrix}$
(1,0,0)	(0,1,0)	1.1471 $\begin{smallmatrix} +18 \\ -17 \end{smallmatrix}$	0.849 $\begin{smallmatrix} +30 \\ -31 \end{smallmatrix}$
(1,0,0)	(-1,0,0)	1.2860 $\begin{smallmatrix} +18 \\ -19 \end{smallmatrix}$	0.748 $\begin{smallmatrix} +21 \\ -36 \end{smallmatrix}$
$\kappa_E \rightarrow \kappa_A$		0.11230 $\rightarrow$ 0.12230	
$\vec{p}$	$\vec{p} + \vec{q}$	$\omega^s$	$h_+^s(\omega)$
(0,0,0)	(1,0,0)	1.1097 $\begin{smallmatrix} +7 \\ -9 \end{smallmatrix}$	0.883 $\begin{smallmatrix} +26 \\ -27 \end{smallmatrix}$
(1,0,0)	(1,0,0)	1.0139 $\begin{smallmatrix} +17 \\ -16 \end{smallmatrix}$	1.002 $\begin{smallmatrix} +41 \\ -64 \end{smallmatrix}$
(1,0,0)	(0,0,0)	1.0625 $\begin{smallmatrix} +9 \\ -8 \end{smallmatrix}$	0.928 $\begin{smallmatrix} +20 \\ -20 \end{smallmatrix}$
(1,0,0)	(0,1,0)	1.1791 $\begin{smallmatrix} +16 \\ -18 \end{smallmatrix}$	0.823 $\begin{smallmatrix} +29 \\ -28 \end{smallmatrix}$
(1,0,0)	(-1,0,0)	1.3443 $\begin{smallmatrix} +16 \\ -19 \end{smallmatrix}$	0.707 $\begin{smallmatrix} +29 \\ -32 \end{smallmatrix}$
$\kappa_E \rightarrow \kappa_A$		0.11230 $\rightarrow$ 0.12730	
$\vec{p}$	$\vec{p} + \vec{q}$	$\omega^s$	$h_+^s(\omega)$
(0,0,0)	(1,0,0)	1.1707 $\begin{smallmatrix} +6 \\ -11 \end{smallmatrix}$	0.819 $\begin{smallmatrix} +25 \\ -25 \end{smallmatrix}$
(1,0,0)	(1,0,0)	1.0336 $\begin{smallmatrix} +14 \\ -17 \end{smallmatrix}$	0.988 $\begin{smallmatrix} +47 \\ -61 \end{smallmatrix}$
(1,0,0)	(0,0,0)	1.0625 $\begin{smallmatrix} +9 \\ -8 \end{smallmatrix}$	0.924 $\begin{smallmatrix} +19 \\ -19 \end{smallmatrix}$
(1,0,0)	(0,1,0)	1.2439 $\begin{smallmatrix} +14 \\ -18 \end{smallmatrix}$	0.786 $\begin{smallmatrix} +16 \\ -26 \end{smallmatrix}$
(1,0,0)	(-1,0,0)	1.4543 $\begin{smallmatrix} +14 \\ -20 \end{smallmatrix}$	0.651 $\begin{smallmatrix} +29 \\ -29 \end{smallmatrix}$

 Table C.13: Interpolation of  $\omega$  and  $h_+(\omega)$  to the strange quark mass.

$\kappa_P = 0.13400$			
$\kappa_E \rightarrow \kappa_A$		0.11730 $\rightarrow$ 0.11230	
$\vec{p}$	$\vec{p} + \vec{q}$	$\omega^s$	$h_+^s(\omega)$
(0,0,0)	(1,0,0)	1.0625 $\begin{smallmatrix} +9 \\ -8 \end{smallmatrix}$	0.929 $\begin{smallmatrix} +27 \\ -31 \end{smallmatrix}$
(1,0,0)	(1,0,0)	1.0081 $\begin{smallmatrix} +19 \\ -16 \end{smallmatrix}$	1.002 $\begin{smallmatrix} +44 \\ -68 \end{smallmatrix}$
(1,0,0)	(0,0,0)	1.0796 $\begin{smallmatrix} +8 \\ -8 \end{smallmatrix}$	0.914 $\begin{smallmatrix} +30 \\ -23 \end{smallmatrix}$
(1,0,0)	(0,1,0)	1.1471 $\begin{smallmatrix} +18 \\ -17 \end{smallmatrix}$	0.858 $\begin{smallmatrix} +31 \\ -33 \end{smallmatrix}$
(1,0,0)	(-1,0,0)	1.2860 $\begin{smallmatrix} +18 \\ -19 \end{smallmatrix}$	0.745 $\begin{smallmatrix} +39 \\ -37 \end{smallmatrix}$
$\kappa_E \rightarrow \kappa_A$		0.11730 $\rightarrow$ 0.11730	
$\vec{p}$	$\vec{p} + \vec{q}$	$\omega^s$	$h_+^s(\omega)$
(0,0,0)	(1,0,0)	1.0796 $\begin{smallmatrix} +8 \\ -8 \end{smallmatrix}$	0.914 $\begin{smallmatrix} +26 \\ -30 \end{smallmatrix}$
(1,0,0)	(1,0,0)	1.0068 $\begin{smallmatrix} +18 \\ -16 \end{smallmatrix}$	1.003 $\begin{smallmatrix} +38 \\ -42 \end{smallmatrix}$
(1,0,0)	(0,0,0)	1.0796 $\begin{smallmatrix} +8 \\ -8 \end{smallmatrix}$	0.903 $\begin{smallmatrix} +20 \\ -21 \end{smallmatrix}$
(1,0,0)	(0,1,0)	1.1655 $\begin{smallmatrix} +18 \\ -18 \end{smallmatrix}$	0.838 $\begin{smallmatrix} +19 \\ -31 \end{smallmatrix}$
(1,0,0)	(-1,0,0)	1.3241 $\begin{smallmatrix} +17 \\ -18 \end{smallmatrix}$	0.725 $\begin{smallmatrix} +29 \\ -34 \end{smallmatrix}$
$\kappa_E \rightarrow \kappa_A$		0.11730 $\rightarrow$ 0.12230	
$\vec{p}$	$\vec{p} + \vec{q}$	$\omega^s$	$h_+^s(\omega)$
(0,0,0)	(1,0,0)	1.1097 $\begin{smallmatrix} +7 \\ -9 \end{smallmatrix}$	0.885 $\begin{smallmatrix} +26 \\ -28 \end{smallmatrix}$
(1,0,0)	(1,0,0)	1.0094 $\begin{smallmatrix} +16 \\ -17 \end{smallmatrix}$	1.008 $\begin{smallmatrix} +51 \\ -68 \end{smallmatrix}$
(1,0,0)	(0,0,0)	1.0796 $\begin{smallmatrix} +8 \\ -8 \end{smallmatrix}$	0.903 $\begin{smallmatrix} +19 \\ -20 \end{smallmatrix}$
(1,0,0)	(0,1,0)	1.1980 $\begin{smallmatrix} +16 \\ -19 \end{smallmatrix}$	0.816 $\begin{smallmatrix} +28 \\ -29 \end{smallmatrix}$
(1,0,0)	(-1,0,0)	1.3866 $\begin{smallmatrix} +15 \\ -19 \end{smallmatrix}$	0.684 $\begin{smallmatrix} +29 \\ -31 \end{smallmatrix}$
$\kappa_E \rightarrow \kappa_A$		0.11730 $\rightarrow$ 0.12730	
$\vec{p}$	$\vec{p} + \vec{q}$	$\omega^s$	$h_+^s(\omega)$
(0,0,0)	(1,0,0)	1.1707 $\begin{smallmatrix} +6 \\ -11 \end{smallmatrix}$	0.821 $\begin{smallmatrix} +24 \\ -26 \end{smallmatrix}$
(1,0,0)	(1,0,0)	1.0237 $\begin{smallmatrix} +14 \\ -17 \end{smallmatrix}$	0.991 $\begin{smallmatrix} +47 \\ -65 \end{smallmatrix}$
(1,0,0)	(0,0,0)	1.0796 $\begin{smallmatrix} +8 \\ -8 \end{smallmatrix}$	0.892 $\begin{smallmatrix} +18 \\ -18 \end{smallmatrix}$
(1,0,0)	(0,1,0)	1.2639 $\begin{smallmatrix} +14 \\ -19 \end{smallmatrix}$	0.762 $\begin{smallmatrix} +25 \\ -25 \end{smallmatrix}$
(1,0,0)	(-1,0,0)	1.5041 $\begin{smallmatrix} +14 \\ -23 \end{smallmatrix}$	0.611 $\begin{smallmatrix} +28 \\ -26 \end{smallmatrix}$

Table C.14: Interpolation of  $\omega$  and  $h_+(\omega)$  to the strange quark mass.

$\kappa_P = 0.13400$			
$\kappa_E \rightarrow \kappa_A$		0.12230 $\rightarrow$ 0.11230	
$\vec{p}$	$\vec{p} + \vec{q}$	$\omega^s$	$h_+^s(\omega)$
(0,0,0)	(1,0,0)	1.0625 $\begin{smallmatrix} +9 \\ -8 \end{smallmatrix}$	0.930 $\begin{smallmatrix} +27 \\ -31 \end{smallmatrix}$
(1,0,0)	(1,0,0)	1.0139 $\begin{smallmatrix} +17 \\ -16 \end{smallmatrix}$	1.003 $\begin{smallmatrix} +47 \\ -64 \end{smallmatrix}$
(1,0,0)	(0,0,0)	1.1097 $\begin{smallmatrix} +7 \\ -9 \end{smallmatrix}$	0.888 $\begin{smallmatrix} +20 \\ -23 \end{smallmatrix}$
(1,0,0)	(0,1,0)	1.1791 $\begin{smallmatrix} +16 \\ -18 \end{smallmatrix}$	0.813 $\begin{smallmatrix} +28 \\ -31 \end{smallmatrix}$
(1,0,0)	(-1,0,0)	1.3443 $\begin{smallmatrix} +16 \\ -19 \end{smallmatrix}$	0.724 $\begin{smallmatrix} +28 \\ -35 \end{smallmatrix}$
$\kappa_E \rightarrow \kappa_A$		0.12230 $\rightarrow$ 0.11730	
$\vec{p}$	$\vec{p} + \vec{q}$	$\omega^s$	$h_+^s(\omega)$
(0,0,0)	(1,0,0)	1.0796 $\begin{smallmatrix} +8 \\ -8 \end{smallmatrix}$	0.907 $\begin{smallmatrix} +26 \\ -29 \end{smallmatrix}$
(1,0,0)	(1,0,0)	1.0094 $\begin{smallmatrix} +16 \\ -17 \end{smallmatrix}$	0.993 $\begin{smallmatrix} +59 \\ -69 \end{smallmatrix}$
(1,0,0)	(0,0,0)	1.1097 $\begin{smallmatrix} +7 \\ -9 \end{smallmatrix}$	0.875 $\begin{smallmatrix} +19 \\ -21 \end{smallmatrix}$
(1,0,0)	(0,1,0)	1.1980 $\begin{smallmatrix} +16 \\ -19 \end{smallmatrix}$	0.810 $\begin{smallmatrix} +17 \\ -30 \end{smallmatrix}$
(1,0,0)	(-1,0,0)	1.3866 $\begin{smallmatrix} +15 \\ -19 \end{smallmatrix}$	0.689 $\begin{smallmatrix} +27 \\ -32 \end{smallmatrix}$
$\kappa_E \rightarrow \kappa_A$		0.12230 $\rightarrow$ 0.12230	
$\vec{p}$	$\vec{p} + \vec{q}$	$\omega^s$	$h_+^s(\omega)$
(0,0,0)	(1,0,0)	1.1097 $\begin{smallmatrix} +7 \\ -9 \end{smallmatrix}$	0.888 $\begin{smallmatrix} +24 \\ -28 \end{smallmatrix}$
(1,0,0)	(1,0,0)	1.0073 $\begin{smallmatrix} +16 \\ -18 \end{smallmatrix}$	1.009 $\begin{smallmatrix} +33 \\ -42 \end{smallmatrix}$
(1,0,0)	(0,0,0)	1.1097 $\begin{smallmatrix} +7 \\ -9 \end{smallmatrix}$	0.874 $\begin{smallmatrix} +18 \\ -19 \end{smallmatrix}$
(1,0,0)	(0,1,0)	1.2315 $\begin{smallmatrix} +15 \\ -19 \end{smallmatrix}$	0.786 $\begin{smallmatrix} +26 \\ -27 \end{smallmatrix}$
(1,0,0)	(-1,0,0)	1.4556 $\begin{smallmatrix} +15 \\ -20 \end{smallmatrix}$	0.648 $\begin{smallmatrix} +27 \\ -29 \end{smallmatrix}$
$\kappa_E \rightarrow \kappa_A$		0.12230 $\rightarrow$ 0.12730	
$\vec{p}$	$\vec{p} + \vec{q}$	$\omega^s$	$h_+^s(\omega)$
(0,0,0)	(1,0,0)	1.1707 $\begin{smallmatrix} +6 \\ -11 \end{smallmatrix}$	0.820 $\begin{smallmatrix} +23 \\ -26 \end{smallmatrix}$
(1,0,0)	(1,0,0)	1.0137 $\begin{smallmatrix} +16 \\ -18 \end{smallmatrix}$	1.006 $\begin{smallmatrix} +47 \\ -74 \end{smallmatrix}$
(1,0,0)	(0,0,0)	1.1097 $\begin{smallmatrix} +7 \\ -9 \end{smallmatrix}$	0.859 $\begin{smallmatrix} +17 \\ -18 \end{smallmatrix}$
(1,0,0)	(0,1,0)	1.2992 $\begin{smallmatrix} +14 \\ -22 \end{smallmatrix}$	0.729 $\begin{smallmatrix} +24 \\ -23 \end{smallmatrix}$
(1,0,0)	(-1,0,0)	1.5847 $\begin{smallmatrix} +14 \\ -25 \end{smallmatrix}$	0.587 $\begin{smallmatrix} +27 \\ -26 \end{smallmatrix}$

 Table C.15: Interpolation of  $\omega$  and  $h_+(\omega)$  to the strange quark mass.

$\kappa_P = 0.13400$			
$\kappa_E \rightarrow \kappa_A$		0.12730 $\rightarrow$ 0.11230	
$\vec{p}$	$\vec{p} + \vec{q}$	$\omega^s$	$h_+^s(\omega)$
(0,0,0)	(1,0,0)	1.0625 $\begin{smallmatrix} +9 \\ -8 \end{smallmatrix}$	0.932 $\begin{smallmatrix} +27 \\ -29 \end{smallmatrix}$
(1,0,0)	(1,0,0)	1.0336 $\begin{smallmatrix} +14 \\ -17 \end{smallmatrix}$	0.957 $\begin{smallmatrix} +56 \\ -68 \end{smallmatrix}$
(1,0,0)	(0,0,0)	1.1707 $\begin{smallmatrix} +6 \\ -11 \end{smallmatrix}$	0.819 $\begin{smallmatrix} +19 \\ -21 \end{smallmatrix}$
(1,0,0)	(0,1,0)	1.2439 $\begin{smallmatrix} +14 \\ -18 \end{smallmatrix}$	0.790 $\begin{smallmatrix} +28 \\ -29 \end{smallmatrix}$
(1,0,0)	(-1,0,0)	1.4543 $\begin{smallmatrix} +14 \\ -20 \end{smallmatrix}$	0.658 $\begin{smallmatrix} +28 \\ -32 \end{smallmatrix}$
$\kappa_E \rightarrow \kappa_A$		0.12730 $\rightarrow$ 0.11730	
$\vec{p}$	$\vec{p} + \vec{q}$	$\omega^s$	$h_+^s(\omega)$
(0,0,0)	(1,0,0)	1.0796 $\begin{smallmatrix} +8 \\ -8 \end{smallmatrix}$	0.892 $\begin{smallmatrix} +26 \\ -27 \end{smallmatrix}$
(1,0,0)	(1,0,0)	1.0237 $\begin{smallmatrix} +14 \\ -17 \end{smallmatrix}$	0.959 $\begin{smallmatrix} +43 \\ -69 \end{smallmatrix}$
(1,0,0)	(0,0,0)	1.1707 $\begin{smallmatrix} +6 \\ -11 \end{smallmatrix}$	0.807 $\begin{smallmatrix} +17 \\ -20 \end{smallmatrix}$
(1,0,0)	(0,1,0)	1.2639 $\begin{smallmatrix} +14 \\ -19 \end{smallmatrix}$	0.758 $\begin{smallmatrix} +28 \\ -27 \end{smallmatrix}$
(1,0,0)	(-1,0,0)	1.5041 $\begin{smallmatrix} +14 \\ -23 \end{smallmatrix}$	0.635 $\begin{smallmatrix} +26 \\ -29 \end{smallmatrix}$
$\kappa_E \rightarrow \kappa_A$		0.12730 $\rightarrow$ 0.12230	
$\vec{p}$	$\vec{p} + \vec{q}$	$\omega^s$	$h_+^s(\omega)$
(0,0,0)	(1,0,0)	1.1097 $\begin{smallmatrix} +7 \\ -9 \end{smallmatrix}$	0.882 $\begin{smallmatrix} +25 \\ -27 \end{smallmatrix}$
(1,0,0)	(1,0,0)	1.0137 $\begin{smallmatrix} +16 \\ -18 \end{smallmatrix}$	0.994 $\begin{smallmatrix} +29 \\ -76 \end{smallmatrix}$
(1,0,0)	(0,0,0)	1.1707 $\begin{smallmatrix} +6 \\ -11 \end{smallmatrix}$	0.820 $\begin{smallmatrix} +16 \\ -18 \end{smallmatrix}$
(1,0,0)	(0,1,0)	1.2992 $\begin{smallmatrix} +14 \\ -22 \end{smallmatrix}$	0.739 $\begin{smallmatrix} +25 \\ -25 \end{smallmatrix}$
(1,0,0)	(-1,0,0)	1.5847 $\begin{smallmatrix} +14 \\ -25 \end{smallmatrix}$	0.587 $\begin{smallmatrix} +26 \\ -25 \end{smallmatrix}$
$\kappa_E \rightarrow \kappa_A$		0.12730 $\rightarrow$ 0.12730	
$\vec{p}$	$\vec{p} + \vec{q}$	$\omega^s$	$h_+^s(\omega)$
(0,0,0)	(1,0,0)	1.1707 $\begin{smallmatrix} +6 \\ -11 \end{smallmatrix}$	0.822 $\begin{smallmatrix} +23 \\ -26 \end{smallmatrix}$
(1,0,0)	(1,0,0)	1.0070 $\begin{smallmatrix} +15 \\ -21 \end{smallmatrix}$	1.004 $\begin{smallmatrix} +40 \\ -51 \end{smallmatrix}$
(1,0,0)	(0,0,0)	1.1707 $\begin{smallmatrix} +6 \\ -11 \end{smallmatrix}$	0.820 $\begin{smallmatrix} +16 \\ -17 \end{smallmatrix}$
(1,0,0)	(0,1,0)	1.3706 $\begin{smallmatrix} +15 \\ -25 \end{smallmatrix}$	0.691 $\begin{smallmatrix} +25 \\ -23 \end{smallmatrix}$
(1,0,0)	(-1,0,0)	1.7343 $\begin{smallmatrix} +16 \\ -31 \end{smallmatrix}$	0.523 $\begin{smallmatrix} +25 \\ -22 \end{smallmatrix}$

 Table C.16: Interpolation of  $\omega$  and  $h_+(\omega)$  to the strange quark mass.

$\kappa_P = 0.13525$			
$\kappa_E \rightarrow \kappa_A$		0.11230 $\rightarrow$ 0.11230	
$\vec{p}$	$\vec{p} + \vec{q}$	$\omega^x$	$h_+^x(\omega)$
(0,0,0)	(1,0,0)	1.0678 $\begin{smallmatrix} +15 \\ -14 \end{smallmatrix}$	0.889 $\begin{smallmatrix} +33 \\ -51 \end{smallmatrix}$
(1,0,0)	(1,0,0)	1.0096 $\begin{smallmatrix} +33 \\ -32 \end{smallmatrix}$	0.980 $\begin{smallmatrix} +48 \\ -73 \end{smallmatrix}$
(1,0,0)	(0,0,0)	1.0678 $\begin{smallmatrix} +15 \\ -14 \end{smallmatrix}$	0.929 $\begin{smallmatrix} +39 \\ -37 \end{smallmatrix}$
(1,0,0)	(0,1,0)	1.1402 $\begin{smallmatrix} +31 \\ -30 \end{smallmatrix}$	0.867 $\begin{smallmatrix} +55 \\ -60 \end{smallmatrix}$
(1,0,0)	(-1,0,0)	1.2709 $\begin{smallmatrix} +31 \\ -29 \end{smallmatrix}$	0.767 $\begin{smallmatrix} +40 \\ -68 \end{smallmatrix}$
$\kappa_E \rightarrow \kappa_A$		0.11230 $\rightarrow$ 0.11730	
$\vec{p}$	$\vec{p} + \vec{q}$	$\omega^x$	$h_+^x(\omega)$
(0,0,0)	(1,0,0)	1.0867 $\begin{smallmatrix} +13 \\ -12 \end{smallmatrix}$	0.894 $\begin{smallmatrix} +42 \\ -48 \end{smallmatrix}$
(1,0,0)	(1,0,0)	1.0103 $\begin{smallmatrix} +31 \\ -30 \end{smallmatrix}$	0.978 $\begin{smallmatrix} +82 \\ -116 \end{smallmatrix}$
(1,0,0)	(0,0,0)	1.0678 $\begin{smallmatrix} +15 \\ -14 \end{smallmatrix}$	0.949 $\begin{smallmatrix} +37 \\ -33 \end{smallmatrix}$
(1,0,0)	(0,1,0)	1.1604 $\begin{smallmatrix} +31 \\ -28 \end{smallmatrix}$	0.826 $\begin{smallmatrix} +44 \\ -51 \end{smallmatrix}$
(1,0,0)	(-1,0,0)	1.3105 $\begin{smallmatrix} +31 \\ -29 \end{smallmatrix}$	0.735 $\begin{smallmatrix} +57 \\ -57 \end{smallmatrix}$
$\kappa_E \rightarrow \kappa_A$		0.11230 $\rightarrow$ 0.12230	
$\vec{p}$	$\vec{p} + \vec{q}$	$\omega^x$	$h_+^x(\omega)$
(0,0,0)	(1,0,0)	1.1221 $\begin{smallmatrix} +11 \\ -13 \end{smallmatrix}$	0.871 $\begin{smallmatrix} +40 \\ -44 \end{smallmatrix}$
(1,0,0)	(1,0,0)	1.0179 $\begin{smallmatrix} +28 \\ -27 \end{smallmatrix}$	1.018 $\begin{smallmatrix} +89 \\ -109 \end{smallmatrix}$
(1,0,0)	(0,0,0)	1.0678 $\begin{smallmatrix} +15 \\ -14 \end{smallmatrix}$	0.918 $\begin{smallmatrix} +26 \\ -28 \end{smallmatrix}$
(1,0,0)	(0,1,0)	1.1981 $\begin{smallmatrix} +28 \\ -28 \end{smallmatrix}$	0.822 $\begin{smallmatrix} +43 \\ -44 \end{smallmatrix}$
(1,0,0)	(-1,0,0)	1.3783 $\begin{smallmatrix} +27 \\ -28 \end{smallmatrix}$	0.667 $\begin{smallmatrix} +46 \\ -48 \end{smallmatrix}$
$\kappa_E \rightarrow \kappa_A$		0.11230 $\rightarrow$ 0.12730	
$\vec{p}$	$\vec{p} + \vec{q}$	$\omega^x$	$h_+^x(\omega)$
(0,0,0)	(1,0,0)	1.1957 $\begin{smallmatrix} +10 \\ -17 \end{smallmatrix}$	0.786 $\begin{smallmatrix} +29 \\ -36 \end{smallmatrix}$
(1,0,0)	(1,0,0)	1.0425 $\begin{smallmatrix} +24 \\ -26 \end{smallmatrix}$	0.962 $\begin{smallmatrix} +79 \\ -100 \end{smallmatrix}$
(1,0,0)	(0,0,0)	1.0678 $\begin{smallmatrix} +15 \\ -14 \end{smallmatrix}$	0.947 $\begin{smallmatrix} +25 \\ -26 \end{smallmatrix}$
(1,0,0)	(0,1,0)	1.2767 $\begin{smallmatrix} +23 \\ -26 \end{smallmatrix}$	0.777 $\begin{smallmatrix} +31 \\ -40 \end{smallmatrix}$
(1,0,0)	(-1,0,0)	1.5108 $\begin{smallmatrix} +23 \\ -30 \end{smallmatrix}$	0.648 $\begin{smallmatrix} +37 \\ -42 \end{smallmatrix}$

Table C.17: Extrapolation of  $\omega$  and  $h_+(\omega)$  to the chiral limit.

$\kappa_P = 0.13525$			
$\kappa_E \rightarrow \kappa_A$		0.11730 $\rightarrow$ 0.11230	
$\vec{p}$	$\vec{p} + \vec{q}$	$\omega^x$	$h_+^x(\omega)$
(0,0,0)	(1,0,0)	1.0678 $\begin{smallmatrix} +15 \\ -14 \end{smallmatrix}$	0.934 $\begin{smallmatrix} +41 \\ -48 \end{smallmatrix}$
(1,0,0)	(1,0,0)	1.0103 $\begin{smallmatrix} +31 \\ -30 \end{smallmatrix}$	1.003 $\begin{smallmatrix} +91 \\ -119 \end{smallmatrix}$
(1,0,0)	(0,0,0)	1.0867 $\begin{smallmatrix} +13 \\ -12 \end{smallmatrix}$	0.916 $\begin{smallmatrix} +37 \\ -36 \end{smallmatrix}$
(1,0,0)	(0,1,0)	1.1604 $\begin{smallmatrix} +31 \\ -28 \end{smallmatrix}$	0.858 $\begin{smallmatrix} +46 \\ -55 \end{smallmatrix}$
(1,0,0)	(-1,0,0)	1.3105 $\begin{smallmatrix} +31 \\ -29 \end{smallmatrix}$	0.719 $\begin{smallmatrix} +57 \\ -63 \end{smallmatrix}$
$\kappa_E \rightarrow \kappa_A$		0.11730 $\rightarrow$ 0.11730	
$\vec{p}$	$\vec{p} + \vec{q}$	$\omega^x$	$h_+^x(\omega)$
(0,0,0)	(1,0,0)	1.0867 $\begin{smallmatrix} +13 \\ -12 \end{smallmatrix}$	0.898 $\begin{smallmatrix} +50 \\ -46 \end{smallmatrix}$
(1,0,0)	(1,0,0)	1.0085 $\begin{smallmatrix} +29 \\ -27 \end{smallmatrix}$	1.032 $\begin{smallmatrix} +62 \\ -72 \end{smallmatrix}$
(1,0,0)	(0,0,0)	1.0867 $\begin{smallmatrix} +13 \\ -12 \end{smallmatrix}$	0.892 $\begin{smallmatrix} +26 \\ -33 \end{smallmatrix}$
(1,0,0)	(0,1,0)	1.1809 $\begin{smallmatrix} +28 \\ -27 \end{smallmatrix}$	0.821 $\begin{smallmatrix} +44 \\ -49 \end{smallmatrix}$
(1,0,0)	(-1,0,0)	1.3533 $\begin{smallmatrix} +28 \\ -29 \end{smallmatrix}$	0.691 $\begin{smallmatrix} +44 \\ -56 \end{smallmatrix}$
$\kappa_E \rightarrow \kappa_A$		0.11730 $\rightarrow$ 0.12230	
$\vec{p}$	$\vec{p} + \vec{q}$	$\omega^x$	$h_+^x(\omega)$
(0,0,0)	(1,0,0)	1.1221 $\begin{smallmatrix} +11 \\ -13 \end{smallmatrix}$	0.885 $\begin{smallmatrix} +40 \\ -43 \end{smallmatrix}$
(1,0,0)	(1,0,0)	1.0123 $\begin{smallmatrix} +27 \\ -27 \end{smallmatrix}$	1.013 $\begin{smallmatrix} +84 \\ -118 \end{smallmatrix}$
(1,0,0)	(0,0,0)	1.0867 $\begin{smallmatrix} +13 \\ -12 \end{smallmatrix}$	0.890 $\begin{smallmatrix} +24 \\ -28 \end{smallmatrix}$
(1,0,0)	(0,1,0)	1.2193 $\begin{smallmatrix} +25 \\ -26 \end{smallmatrix}$	0.812 $\begin{smallmatrix} +33 \\ -43 \end{smallmatrix}$
(1,0,0)	(-1,0,0)	1.4263 $\begin{smallmatrix} +27 \\ -29 \end{smallmatrix}$	0.688 $\begin{smallmatrix} +44 \\ -45 \end{smallmatrix}$
$\kappa_E \rightarrow \kappa_A$		0.11730 $\rightarrow$ 0.12730	
$\vec{p}$	$\vec{p} + \vec{q}$	$\omega^x$	$h_+^x(\omega)$
(0,0,0)	(1,0,0)	1.1957 $\begin{smallmatrix} +10 \\ -17 \end{smallmatrix}$	0.808 $\begin{smallmatrix} +39 \\ -37 \end{smallmatrix}$
(1,0,0)	(1,0,0)	1.0303 $\begin{smallmatrix} +23 \\ -27 \end{smallmatrix}$	0.964 $\begin{smallmatrix} +76 \\ -108 \end{smallmatrix}$
(1,0,0)	(0,0,0)	1.0867 $\begin{smallmatrix} +13 \\ -12 \end{smallmatrix}$	0.912 $\begin{smallmatrix} +23 \\ -26 \end{smallmatrix}$
(1,0,0)	(0,1,0)	1.2992 $\begin{smallmatrix} +22 \\ -28 \end{smallmatrix}$	0.759 $\begin{smallmatrix} +40 \\ -37 \end{smallmatrix}$
(1,0,0)	(-1,0,0)	1.5681 $\begin{smallmatrix} +22 \\ -34 \end{smallmatrix}$	0.595 $\begin{smallmatrix} +35 \\ -39 \end{smallmatrix}$

Table C.18: Extrapolation of  $\omega$  and  $h_+(\omega)$  to the chiral limit.

$\kappa_P = 0.13525$			
$\kappa_E \rightarrow \kappa_A$		0.12230 $\rightarrow$ 0.11230	
$\vec{p}$	$\vec{p} + \vec{q}$	$\omega^x$	$h_+^x(\omega)$
(0,0,0)	(1,0,0)	1.0678 $\begin{smallmatrix} +15 \\ -14 \end{smallmatrix}$	0.927 $\begin{smallmatrix} +33 \\ -46 \end{smallmatrix}$
(1,0,0)	(1,0,0)	1.0179 $\begin{smallmatrix} +28 \\ -27 \end{smallmatrix}$	0.995 $\begin{smallmatrix} +71 \\ -118 \end{smallmatrix}$
(1,0,0)	(0,0,0)	1.1221 $\begin{smallmatrix} +11 \\ -13 \end{smallmatrix}$	0.891 $\begin{smallmatrix} +37 \\ -35 \end{smallmatrix}$
(1,0,0)	(0,1,0)	1.1981 $\begin{smallmatrix} +28 \\ -28 \end{smallmatrix}$	0.779 $\begin{smallmatrix} +35 \\ -48 \end{smallmatrix}$
(1,0,0)	(-1,0,0)	1.3783 $\begin{smallmatrix} +27 \\ -28 \end{smallmatrix}$	0.727 $\begin{smallmatrix} +35 \\ -59 \end{smallmatrix}$
$\kappa_E \rightarrow \kappa_A$		0.12230 $\rightarrow$ 0.11730	
$\vec{p}$	$\vec{p} + \vec{q}$	$\omega^x$	$h_+^x(\omega)$
(0,0,0)	(1,0,0)	1.0867 $\begin{smallmatrix} +13 \\ -12 \end{smallmatrix}$	0.875 $\begin{smallmatrix} +31 \\ -43 \end{smallmatrix}$
(1,0,0)	(1,0,0)	1.0123 $\begin{smallmatrix} +27 \\ -27 \end{smallmatrix}$	0.990 $\begin{smallmatrix} +65 \\ -118 \end{smallmatrix}$
(1,0,0)	(0,0,0)	1.1221 $\begin{smallmatrix} +11 \\ -13 \end{smallmatrix}$	0.862 $\begin{smallmatrix} +35 \\ -30 \end{smallmatrix}$
(1,0,0)	(0,1,0)	1.2193 $\begin{smallmatrix} +25 \\ -26 \end{smallmatrix}$	0.801 $\begin{smallmatrix} +23 \\ -46 \end{smallmatrix}$
(1,0,0)	(-1,0,0)	1.4263 $\begin{smallmatrix} +27 \\ -29 \end{smallmatrix}$	0.681 $\begin{smallmatrix} +44 \\ -54 \end{smallmatrix}$
$\kappa_E \rightarrow \kappa_A$		0.12230 $\rightarrow$ 0.12230	
$\vec{p}$	$\vec{p} + \vec{q}$	$\omega^x$	$h_+^x(\omega)$
(0,0,0)	(1,0,0)	1.1221 $\begin{smallmatrix} +11 \\ -13 \end{smallmatrix}$	0.890 $\begin{smallmatrix} +41 \\ -42 \end{smallmatrix}$
(1,0,0)	(1,0,0)	1.0103 $\begin{smallmatrix} +28 \\ -29 \end{smallmatrix}$	1.043 $\begin{smallmatrix} +54 \\ -70 \end{smallmatrix}$
(1,0,0)	(0,0,0)	1.1221 $\begin{smallmatrix} +11 \\ -13 \end{smallmatrix}$	0.884 $\begin{smallmatrix} +22 \\ -26 \end{smallmatrix}$
(1,0,0)	(0,1,0)	1.2588 $\begin{smallmatrix} +25 \\ -29 \end{smallmatrix}$	0.758 $\begin{smallmatrix} +41 \\ -40 \end{smallmatrix}$
(1,0,0)	(-1,0,0)	1.5073 $\begin{smallmatrix} +26 \\ -33 \end{smallmatrix}$	0.633 $\begin{smallmatrix} +44 \\ -44 \end{smallmatrix}$
$\kappa_E \rightarrow \kappa_A$		0.12230 $\rightarrow$ 0.12730	
$\vec{p}$	$\vec{p} + \vec{q}$	$\omega^x$	$h_+^x(\omega)$
(0,0,0)	(1,0,0)	1.1957 $\begin{smallmatrix} +10 \\ -17 \end{smallmatrix}$	0.806 $\begin{smallmatrix} +38 \\ -37 \end{smallmatrix}$
(1,0,0)	(1,0,0)	1.0185 $\begin{smallmatrix} +25 \\ -30 \end{smallmatrix}$	1.003 $\begin{smallmatrix} +44 \\ -116 \end{smallmatrix}$
(1,0,0)	(0,0,0)	1.1221 $\begin{smallmatrix} +11 \\ -13 \end{smallmatrix}$	0.848 $\begin{smallmatrix} +21 \\ -24 \end{smallmatrix}$
(1,0,0)	(0,1,0)	1.3413 $\begin{smallmatrix} +23 \\ -33 \end{smallmatrix}$	0.689 $\begin{smallmatrix} +37 \\ -33 \end{smallmatrix}$
(1,0,0)	(-1,0,0)	1.6640 $\begin{smallmatrix} +26 \\ -40 \end{smallmatrix}$	0.560 $\begin{smallmatrix} +33 \\ -35 \end{smallmatrix}$

Table C.19: Extrapolation of  $\omega$  and  $h_+(\omega)$  to the chiral limit.

$\kappa_P = 0.13525$			
$\kappa_E \rightarrow \kappa_A$		0.12730 $\rightarrow$ 0.11230	
$\vec{p}$	$\vec{p} + \vec{q}$	$\omega^x$	$h_+^x(\omega)$
(0,0,0)	(1,0,0)	1.0678 $\begin{smallmatrix} +15 \\ -14 \end{smallmatrix}$	0.940 $\begin{smallmatrix} +33 \\ -41 \end{smallmatrix}$
(1,0,0)	(1,0,0)	1.0425 $\begin{smallmatrix} +24 \\ -26 \end{smallmatrix}$	0.929 $\begin{smallmatrix} +84 \\ -121 \end{smallmatrix}$
(1,0,0)	(0,0,0)	1.1957 $\begin{smallmatrix} +10 \\ -17 \end{smallmatrix}$	0.813 $\begin{smallmatrix} +36 \\ -33 \end{smallmatrix}$
(1,0,0)	(0,1,0)	1.2767 $\begin{smallmatrix} +23 \\ -26 \end{smallmatrix}$	0.782 $\begin{smallmatrix} +47 \\ -45 \end{smallmatrix}$
(1,0,0)	(-1,0,0)	1.5108 $\begin{smallmatrix} +23 \\ -30 \end{smallmatrix}$	0.632 $\begin{smallmatrix} +46 \\ -49 \end{smallmatrix}$
$\kappa_E \rightarrow \kappa_A$		0.12730 $\rightarrow$ 0.11730	
$\vec{p}$	$\vec{p} + \vec{q}$	$\omega^x$	$h_+^x(\omega)$
(0,0,0)	(1,0,0)	1.0867 $\begin{smallmatrix} +13 \\ -12 \end{smallmatrix}$	0.882 $\begin{smallmatrix} +31 \\ -40 \end{smallmatrix}$
(1,0,0)	(1,0,0)	1.0303 $\begin{smallmatrix} +23 \\ -27 \end{smallmatrix}$	0.942 $\begin{smallmatrix} +81 \\ -121 \end{smallmatrix}$
(1,0,0)	(0,0,0)	1.1957 $\begin{smallmatrix} +10 \\ -17 \end{smallmatrix}$	0.799 $\begin{smallmatrix} +23 \\ -27 \end{smallmatrix}$
(1,0,0)	(0,1,0)	1.2992 $\begin{smallmatrix} +22 \\ -28 \end{smallmatrix}$	0.739 $\begin{smallmatrix} +34 \\ -41 \end{smallmatrix}$
(1,0,0)	(-1,0,0)	1.5681 $\begin{smallmatrix} +22 \\ -34 \end{smallmatrix}$	0.603 $\begin{smallmatrix} +35 \\ -45 \end{smallmatrix}$
$\kappa_E \rightarrow \kappa_A$		0.12730 $\rightarrow$ 0.12230	
$\vec{p}$	$\vec{p} + \vec{q}$	$\omega^x$	$h_+^x(\omega)$
(0,0,0)	(1,0,0)	1.1221 $\begin{smallmatrix} +11 \\ -13 \end{smallmatrix}$	0.879 $\begin{smallmatrix} +40 \\ -40 \end{smallmatrix}$
(1,0,0)	(1,0,0)	1.0185 $\begin{smallmatrix} +25 \\ -30 \end{smallmatrix}$	1.003 $\begin{smallmatrix} +78 \\ -131 \end{smallmatrix}$
(1,0,0)	(0,0,0)	1.1957 $\begin{smallmatrix} +10 \\ -17 \end{smallmatrix}$	0.804 $\begin{smallmatrix} +21 \\ -25 \end{smallmatrix}$
(1,0,0)	(0,1,0)	1.3413 $\begin{smallmatrix} +23 \\ -33 \end{smallmatrix}$	0.723 $\begin{smallmatrix} +40 \\ -36 \end{smallmatrix}$
(1,0,0)	(-1,0,0)	1.6640 $\begin{smallmatrix} +26 \\ -40 \end{smallmatrix}$	0.557 $\begin{smallmatrix} +32 \\ -38 \end{smallmatrix}$
$\kappa_E \rightarrow \kappa_A$		0.12730 $\rightarrow$ 0.12730	
$\vec{p}$	$\vec{p} + \vec{q}$	$\omega^x$	$h_+^x(\omega)$
(0,0,0)	(1,0,0)	1.1957 $\begin{smallmatrix} +10 \\ -17 \end{smallmatrix}$	0.785 $\begin{smallmatrix} +39 \\ -36 \end{smallmatrix}$
(1,0,0)	(1,0,0)	1.0100 $\begin{smallmatrix} +25 \\ -34 \end{smallmatrix}$	1.023 $\begin{smallmatrix} +59 \\ -79 \end{smallmatrix}$
(1,0,0)	(0,0,0)	1.1957 $\begin{smallmatrix} +10 \\ -17 \end{smallmatrix}$	0.799 $\begin{smallmatrix} +28 \\ -22 \end{smallmatrix}$
(1,0,0)	(0,1,0)	1.4290 $\begin{smallmatrix} +23 \\ -39 \end{smallmatrix}$	0.674 $\begin{smallmatrix} +21 \\ -33 \end{smallmatrix}$
(1,0,0)	(-1,0,0)	1.8479 $\begin{smallmatrix} +26 \\ -48 \end{smallmatrix}$	0.494 $\begin{smallmatrix} +29 \\ -33 \end{smallmatrix}$

Table C.20: Extrapolation of  $\omega$  and  $h_+(\omega)$  to the chiral limit.

$\kappa_P = 0.13493$			
$\kappa_E \rightarrow \kappa_A$		0.12000 $\rightarrow$ 0.12000	
$\vec{p}$	$\vec{p} + \vec{q}$	$\omega^s$	$h_+^s(\omega)$
(0,0,0)	(1,0,0)	1.0501 $\begin{smallmatrix} +12 \\ -12 \end{smallmatrix}$	0.941 $\begin{smallmatrix} +24 \\ -33 \end{smallmatrix}$
(1,0,0)	(1,0,0)	1.0030 $\begin{smallmatrix} +24 \\ -24 \end{smallmatrix}$	1.013 $\begin{smallmatrix} +34 \\ -54 \end{smallmatrix}$
(1,0,0)	(0,0,0)	1.0501 $\begin{smallmatrix} +12 \\ -12 \end{smallmatrix}$	0.926 $\begin{smallmatrix} +27 \\ -29 \end{smallmatrix}$
(1,0,0)	(0,1,0)	1.1028 $\begin{smallmatrix} +25 \\ -25 \end{smallmatrix}$	0.908 $\begin{smallmatrix} +40 \\ -43 \end{smallmatrix}$
(1,0,0)	(-1,0,0)	1.2026 $\begin{smallmatrix} +25 \\ -27 \end{smallmatrix}$	0.807 $\begin{smallmatrix} +33 \\ -45 \end{smallmatrix}$
$\kappa_E \rightarrow \kappa_A$		0.12000 $\rightarrow$ 0.12660	
$\vec{p}$	$\vec{p} + \vec{q}$	$\omega^s$	$h_+^s(\omega)$
(0,0,0)	(1,0,0)	1.0877 $\begin{smallmatrix} +13 \\ -14 \end{smallmatrix}$	0.902 $\begin{smallmatrix} +22 \\ -30 \end{smallmatrix}$
(1,0,0)	(1,0,0)	1.0078 $\begin{smallmatrix} +25 \\ -26 \end{smallmatrix}$	0.995 $\begin{smallmatrix} +60 \\ -89 \end{smallmatrix}$
(1,0,0)	(0,0,0)	1.0501 $\begin{smallmatrix} +12 \\ -12 \end{smallmatrix}$	0.943 $\begin{smallmatrix} +24 \\ -23 \end{smallmatrix}$
(1,0,0)	(0,1,0)	1.1422 $\begin{smallmatrix} +25 \\ -28 \end{smallmatrix}$	0.861 $\begin{smallmatrix} +35 \\ -34 \end{smallmatrix}$
(1,0,0)	(-1,0,0)	1.2767 $\begin{smallmatrix} +25 \\ -30 \end{smallmatrix}$	0.745 $\begin{smallmatrix} +31 \\ -37 \end{smallmatrix}$
$\kappa_E \rightarrow \kappa_A$		0.12330 $\rightarrow$ 0.12000	
$\vec{p}$	$\vec{p} + \vec{q}$	$\omega^s$	$h_+^s(\omega)$
(0,0,0)	(1,0,0)	1.0501 $\begin{smallmatrix} +12 \\ -12 \end{smallmatrix}$	0.940 $\begin{smallmatrix} +23 \\ -31 \end{smallmatrix}$
(1,0,0)	(1,0,0)	1.0037 $\begin{smallmatrix} +25 \\ -25 \end{smallmatrix}$	1.005 $\begin{smallmatrix} +81 \\ -108 \end{smallmatrix}$
(1,0,0)	(0,0,0)	1.0642 $\begin{smallmatrix} +12 \\ -13 \end{smallmatrix}$	0.922 $\begin{smallmatrix} +27 \\ -29 \end{smallmatrix}$
(1,0,0)	(0,1,0)	1.1176 $\begin{smallmatrix} +26 \\ -26 \end{smallmatrix}$	0.878 $\begin{smallmatrix} +40 \\ -42 \end{smallmatrix}$
(1,0,0)	(-1,0,0)	1.2314 $\begin{smallmatrix} +26 \\ -28 \end{smallmatrix}$	0.783 $\begin{smallmatrix} +46 \\ -44 \end{smallmatrix}$
$\kappa_E \rightarrow \kappa_A$		0.12330 $\rightarrow$ 0.12660	
$\vec{p}$	$\vec{p} + \vec{q}$	$\omega^s$	$h_+^s(\omega)$
(0,0,0)	(1,0,0)	1.0877 $\begin{smallmatrix} +13 \\ -14 \end{smallmatrix}$	0.899 $\begin{smallmatrix} +21 \\ -30 \end{smallmatrix}$
(1,0,0)	(1,0,0)	1.0042 $\begin{smallmatrix} +27 \\ -28 \end{smallmatrix}$	0.999 $\begin{smallmatrix} +86 \\ -107 \end{smallmatrix}$
(1,0,0)	(0,0,0)	1.0642 $\begin{smallmatrix} +12 \\ -13 \end{smallmatrix}$	0.910 $\begin{smallmatrix} +24 \\ -22 \end{smallmatrix}$
(1,0,0)	(0,1,0)	1.1576 $\begin{smallmatrix} +26 \\ -28 \end{smallmatrix}$	0.851 $\begin{smallmatrix} +24 \\ -33 \end{smallmatrix}$
(1,0,0)	(-1,0,0)	1.3109 $\begin{smallmatrix} +26 \\ -30 \end{smallmatrix}$	0.729 $\begin{smallmatrix} +32 \\ -37 \end{smallmatrix}$

Table C.21: Interpolation of  $\omega$  and  $h_+(\omega)$  to the strange quark mass.

$\kappa_P = 0.13493$			
$\kappa_E \rightarrow \kappa_A$		0.12660 $\rightarrow$ 0.12000	
$\vec{p}$	$\vec{p} + \vec{q}$	$\omega^s$	$h_+^s(\omega)$
(0,0,0)	(1,0,0)	1.0501 $^{+12}_{-12}$	0.944 $^{+21}_{-29}$
(1,0,0)	(1,0,0)	1.0078 $^{+25}_{-26}$	0.982 $^{+67}_{-90}$
(1,0,0)	(0,0,0)	1.0877 $^{+13}_{-14}$	0.898 $^{+26}_{-29}$
(1,0,0)	(0,1,0)	1.1422 $^{+25}_{-28}$	0.863 $^{+37}_{-42}$
(1,0,0)	(-1,0,0)	1.2767 $^{+25}_{-30}$	0.753 $^{+37}_{-40}$
$\kappa_E \rightarrow \kappa_A$		0.12660 $\rightarrow$ 0.12660	
$\vec{p}$	$\vec{p} + \vec{q}$	$\omega^s$	$h_+^s(\omega)$
(0,0,0)	(1,0,0)	1.0877 $^{+13}_{-14}$	0.905 $^{+35}_{-31}$
(1,0,0)	(1,0,0)	1.0021 $^{+27}_{-30}$	0.993 $^{+41}_{-53}$
(1,0,0)	(0,0,0)	1.0877 $^{+13}_{-14}$	0.903 $^{+22}_{-22}$
(1,0,0)	(0,1,0)	1.1831 $^{+27}_{-31}$	0.827 $^{+34}_{-35}$
(1,0,0)	(-1,0,0)	1.3642 $^{+28}_{-34}$	0.688 $^{+32}_{-35}$
$\kappa_E \rightarrow \kappa_A$		0.12990 $\rightarrow$ 0.12000	
$\vec{p}$	$\vec{p} + \vec{q}$	$\omega^s$	$h_+^s(\omega)$
(0,0,0)	(1,0,0)	1.0501 $^{+12}_{-12}$	0.933 $^{+29}_{-27}$
(1,0,0)	(1,0,0)	1.0225 $^{+25}_{-28}$	0.972 $^{+69}_{-87}$
(1,0,0)	(0,0,0)	1.1342 $^{+15}_{-17}$	0.865 $^{+24}_{-30}$
(1,0,0)	(0,1,0)	1.1911 $^{+26}_{-31}$	0.814 $^{+35}_{-42}$
(1,0,0)	(-1,0,0)	1.3596 $^{+27}_{-32}$	0.696 $^{+35}_{-37}$
$\kappa_E \rightarrow \kappa_A$		0.12990 $\rightarrow$ 0.12660	
$\vec{p}$	$\vec{p} + \vec{q}$	$\omega^s$	$h_+^s(\omega)$
(0,0,0)	(1,0,0)	1.0877 $^{+13}_{-14}$	0.904 $^{+26}_{-25}$
(1,0,0)	(1,0,0)	1.0067 $^{+29}_{-31}$	1.003 $^{+86}_{-117}$
(1,0,0)	(0,0,0)	1.1342 $^{+15}_{-17}$	0.870 $^{+28}_{-24}$
(1,0,0)	(0,1,0)	1.2337 $^{+30}_{-34}$	0.787 $^{+27}_{-41}$
(1,0,0)	(-1,0,0)	1.4607 $^{+32}_{-40}$	0.632 $^{+40}_{-36}$

Table C.22: Interpolation of  $\omega$  and  $h_+(\omega)$  to the strange quark mass.

$\kappa_P = 0.13583$			
$\kappa_E \rightarrow \kappa_A$		0.12000 $\rightarrow$ 0.12000	
$\vec{p}$	$\vec{p} + \vec{q}$	$\omega^x$	$h_+^x(\omega)$
(0,0,0)	(1,0,0)	1.0534 $\begin{smallmatrix} +18 \\ -20 \end{smallmatrix}$	0.915 $\begin{smallmatrix} +37 \\ -52 \end{smallmatrix}$
(1,0,0)	(1,0,0)	1.0024 $\begin{smallmatrix} +36 \\ -38 \end{smallmatrix}$	0.993 $\begin{smallmatrix} +63 \\ -93 \end{smallmatrix}$
(1,0,0)	(0,0,0)	1.0534 $\begin{smallmatrix} +18 \\ -20 \end{smallmatrix}$	0.908 $\begin{smallmatrix} +48 \\ -52 \end{smallmatrix}$
(1,0,0)	(0,1,0)	1.1097 $\begin{smallmatrix} +38 \\ -43 \end{smallmatrix}$	0.914 $\begin{smallmatrix} +61 \\ -74 \end{smallmatrix}$
(1,0,0)	(-1,0,0)	1.2170 $\begin{smallmatrix} +39 \\ -45 \end{smallmatrix}$	0.817 $\begin{smallmatrix} +55 \\ -77 \end{smallmatrix}$
$\kappa_E \rightarrow \kappa_A$		0.12000 $\rightarrow$ 0.12660	
$\vec{p}$	$\vec{p} + \vec{q}$	$\omega^x$	$h_+^x(\omega)$
(0,0,0)	(1,0,0)	1.0966 $\begin{smallmatrix} +19 \\ -20 \end{smallmatrix}$	0.909 $\begin{smallmatrix} +45 \\ -49 \end{smallmatrix}$
(1,0,0)	(1,0,0)	1.0083 $\begin{smallmatrix} +38 \\ -41 \end{smallmatrix}$	0.988 $\begin{smallmatrix} +112 \\ -160 \end{smallmatrix}$
(1,0,0)	(0,0,0)	1.0534 $\begin{smallmatrix} +18 \\ -20 \end{smallmatrix}$	0.951 $\begin{smallmatrix} +37 \\ -38 \end{smallmatrix}$
(1,0,0)	(0,1,0)	1.1552 $\begin{smallmatrix} +40 \\ -44 \end{smallmatrix}$	0.862 $\begin{smallmatrix} +40 \\ -58 \end{smallmatrix}$
(1,0,0)	(-1,0,0)	1.3021 $\begin{smallmatrix} +41 \\ -47 \end{smallmatrix}$	0.723 $\begin{smallmatrix} +43 \\ -61 \end{smallmatrix}$
$\kappa_E \rightarrow \kappa_A$		0.12330 $\rightarrow$ 0.12000	
$\vec{p}$	$\vec{p} + \vec{q}$	$\omega^x$	$h_+^x(\omega)$
(0,0,0)	(1,0,0)	1.0534 $\begin{smallmatrix} +18 \\ -20 \end{smallmatrix}$	0.918 $\begin{smallmatrix} +43 \\ -48 \end{smallmatrix}$
(1,0,0)	(1,0,0)	1.0034 $\begin{smallmatrix} +39 \\ -39 \end{smallmatrix}$	1.025 $\begin{smallmatrix} +174 \\ -199 \end{smallmatrix}$
(1,0,0)	(0,0,0)	1.0694 $\begin{smallmatrix} +19 \\ -21 \end{smallmatrix}$	0.912 $\begin{smallmatrix} +44 \\ -51 \end{smallmatrix}$
(1,0,0)	(0,1,0)	1.1265 $\begin{smallmatrix} +40 \\ -43 \end{smallmatrix}$	0.879 $\begin{smallmatrix} +52 \\ -72 \end{smallmatrix}$
(1,0,0)	(-1,0,0)	1.2498 $\begin{smallmatrix} +41 \\ -47 \end{smallmatrix}$	0.765 $\begin{smallmatrix} +63 \\ -73 \end{smallmatrix}$
$\kappa_E \rightarrow \kappa_A$		0.12330 $\rightarrow$ 0.12660	
$\vec{p}$	$\vec{p} + \vec{q}$	$\omega^x$	$h_+^x(\omega)$
(0,0,0)	(1,0,0)	1.0966 $\begin{smallmatrix} +19 \\ -20 \end{smallmatrix}$	0.901 $\begin{smallmatrix} +42 \\ -48 \end{smallmatrix}$
(1,0,0)	(1,0,0)	1.0040 $\begin{smallmatrix} +40 \\ -42 \end{smallmatrix}$	1.010 $\begin{smallmatrix} +182 \\ -207 \end{smallmatrix}$
(1,0,0)	(0,0,0)	1.0694 $\begin{smallmatrix} +19 \\ -21 \end{smallmatrix}$	0.908 $\begin{smallmatrix} +33 \\ -36 \end{smallmatrix}$
(1,0,0)	(0,1,0)	1.1727 $\begin{smallmatrix} +42 \\ -46 \end{smallmatrix}$	0.832 $\begin{smallmatrix} +49 \\ -55 \end{smallmatrix}$
(1,0,0)	(-1,0,0)	1.3414 $\begin{smallmatrix} +44 \\ -49 \end{smallmatrix}$	0.732 $\begin{smallmatrix} +43 \\ -62 \end{smallmatrix}$

 Table C.23: Extrapolation of  $\omega$  and  $h_+(\omega)$  to the chiral limit.

$\kappa_P = 0.13583$			
$\kappa_E \rightarrow \kappa_A$		0.12660 $\rightarrow$ 0.12000	
$\vec{p}$	$\vec{p} + \vec{q}$	$\omega^x$	$h_+^x(\omega)$
(0,0,0)	(1,0,0)	1.0534 $\begin{smallmatrix} +18 \\ -20 \end{smallmatrix}$	0.929 $\begin{smallmatrix} +49 \\ -43 \end{smallmatrix}$
(1,0,0)	(1,0,0)	1.0083 $\begin{smallmatrix} +38 \\ -41 \end{smallmatrix}$	0.974 $\begin{smallmatrix} +138 \\ -183 \end{smallmatrix}$
(1,0,0)	(0,0,0)	1.0966 $\begin{smallmatrix} +19 \\ -20 \end{smallmatrix}$	0.921 $\begin{smallmatrix} +48 \\ -49 \end{smallmatrix}$
(1,0,0)	(0,1,0)	1.1552 $\begin{smallmatrix} +40 \\ -44 \end{smallmatrix}$	0.890 $\begin{smallmatrix} +52 \\ -75 \end{smallmatrix}$
(1,0,0)	(-1,0,0)	1.3021 $\begin{smallmatrix} +41 \\ -47 \end{smallmatrix}$	0.712 $\begin{smallmatrix} +62 \\ -67 \end{smallmatrix}$
$\kappa_E \rightarrow \kappa_A$		0.12660 $\rightarrow$ 0.12660	
$\vec{p}$	$\vec{p} + \vec{q}$	$\omega^x$	$h_+^x(\omega)$
(0,0,0)	(1,0,0)	1.0966 $\begin{smallmatrix} +19 \\ -20 \end{smallmatrix}$	0.911 $\begin{smallmatrix} +61 \\ -61 \end{smallmatrix}$
(1,0,0)	(1,0,0)	1.0013 $\begin{smallmatrix} +41 \\ -42 \end{smallmatrix}$	0.987 $\begin{smallmatrix} +88 \\ -101 \end{smallmatrix}$
(1,0,0)	(0,0,0)	1.0966 $\begin{smallmatrix} +19 \\ -20 \end{smallmatrix}$	0.922 $\begin{smallmatrix} +23 \\ -34 \end{smallmatrix}$
(1,0,0)	(0,1,0)	1.2025 $\begin{smallmatrix} +43 \\ -44 \end{smallmatrix}$	0.834 $\begin{smallmatrix} +47 \\ -54 \end{smallmatrix}$
(1,0,0)	(-1,0,0)	1.4036 $\begin{smallmatrix} +44 \\ -51 \end{smallmatrix}$	0.641 $\begin{smallmatrix} +51 \\ -61 \end{smallmatrix}$
$\kappa_E \rightarrow \kappa_A$		0.12990 $\rightarrow$ 0.12000	
$\vec{p}$	$\vec{p} + \vec{q}$	$\omega^x$	$h_+^x(\omega)$
(0,0,0)	(1,0,0)	1.0534 $\begin{smallmatrix} +18 \\ -20 \end{smallmatrix}$	0.933 $\begin{smallmatrix} +43 \\ -42 \end{smallmatrix}$
(1,0,0)	(1,0,0)	1.0267 $\begin{smallmatrix} +40 \\ -41 \end{smallmatrix}$	0.985 $\begin{smallmatrix} +123 \\ -169 \end{smallmatrix}$
(1,0,0)	(0,0,0)	1.1528 $\begin{smallmatrix} +23 \\ -25 \end{smallmatrix}$	0.818 $\begin{smallmatrix} +46 \\ -48 \end{smallmatrix}$
(1,0,0)	(0,1,0)	1.2143 $\begin{smallmatrix} +41 \\ -46 \end{smallmatrix}$	0.804 $\begin{smallmatrix} +51 \\ -70 \end{smallmatrix}$
(1,0,0)	(-1,0,0)	1.4020 $\begin{smallmatrix} +44 \\ -49 \end{smallmatrix}$	0.683 $\begin{smallmatrix} +70 \\ -64 \end{smallmatrix}$
$\kappa_E \rightarrow \kappa_A$		0.12990 $\rightarrow$ 0.12660	
$\vec{p}$	$\vec{p} + \vec{q}$	$\omega^x$	$h_+^x(\omega)$
(0,0,0)	(1,0,0)	1.0966 $\begin{smallmatrix} +19 \\ -20 \end{smallmatrix}$	0.920 $\begin{smallmatrix} +49 \\ -41 \end{smallmatrix}$
(1,0,0)	(1,0,0)	1.0072 $\begin{smallmatrix} +41 \\ -47 \end{smallmatrix}$	1.032 $\begin{smallmatrix} +196 \\ -225 \end{smallmatrix}$
(1,0,0)	(0,0,0)	1.1528 $\begin{smallmatrix} +23 \\ -25 \end{smallmatrix}$	0.860 $\begin{smallmatrix} +25 \\ -30 \end{smallmatrix}$
(1,0,0)	(0,1,0)	1.2640 $\begin{smallmatrix} +46 \\ -51 \end{smallmatrix}$	0.778 $\begin{smallmatrix} +62 \\ -82 \end{smallmatrix}$
(1,0,0)	(-1,0,0)	1.5208 $\begin{smallmatrix} +49 \\ -58 \end{smallmatrix}$	0.602 $\begin{smallmatrix} +51 \\ -60 \end{smallmatrix}$

 Table C.24: Extrapolation of  $\omega$  and  $h_+(\omega)$  to the chiral limit.

## References

- [1] T. Cheng and L. Li, *Gauge Theory of Elementary Particle Physics* (Clarendon Press, Oxford, 1984).
- [2] L. H. Ryder, *Quantum Field Theory* (Cambridge University Press, Cambridge, 1985).
- [3] J. Donoghue, E. Golowich, and B. Holstein, *Dynamics of the Standard Model* (Cambridge University Press, Cambridge, 1992).
- [4] L. Chang and C. Soo, *Phys. Rev. D* **53**, 5682 (1996).
- [5] D. Gross and F. Wilczek, *Phys. Rev. D* **8**, 3688 (1973).
- [6] H. Politzer, *Phys. Rev. Lett* **30**, 1346 (1973).
- [7] M. Shifman, A. Vainshtein, and V. Zakharov, *Nucl. Phys. B* **147**, 385 (1979).
- [8] H. Rothe, *Lattice Gauge Theories* (World Scientific, Singapore, 1992).
- [9] M. Creutz, *Quarks, gluons and lattices* (Cambridge University Press, Cambridge, 1983).
- [10] I. Montvay and G. Münster, *Quantum Fields on a Lattice* (Cambridge University Press, Cambridge, 1994).
- [11] N. Cabibbo, *Phys. Lett* **10**, 531 (1963).
- [12] M. Kobayashi and K. Maskawa, *Prog. Theor. Phys* **49**, 652 (1973).
- [13] L. Wolfenstein, *Phys. Rev. Lett* **51**, 1945 (1983).
- [14] P. D. Group, *Eur. Phys. J. C* **3**, 1 (1998).

- [15] A. Buras, M. Lautenbacher, and G. Ostermaier, *Phys. Rev. D* **50**, 3433 (1994).
- [16] G. Branco, F. Cagarrinho and F. Krüger, [hep-ph/9904379](#).
- [17] P. Checcia, E. Poggio, and F. Simonetto, [hep-ph/9901418](#).
- [18] H. Georgi and S. Glashow, *Phys. Lett. B* **451**, 372 (1999).
- [19] S. Mele, *Phys. Rev. D* **59**, 1130 (1999).
- [20] R. Feynman and A. Hibbs, *Quantum Mechanics and Path Integrals* (McGraw Hill, Oxford, 1965).
- [21] K. Wilson, in *New Phenomena in Subnuclear Physics*, edited by A. Zichichi (Plenum, New York, 1975).
- [22] K. Wilson, *Phys. Rev. D* **10**, 2445 (1974).
- [23] M. Lüscher and P. Weisz, *Comm. Math. Phys* **97**, 59 (1985).
- [24] H. Nielsen and M. Ninomiya, *Nucl. Phys. B* **185**, 20 (1981).
- [25] L. Susskind, *Phys. Rev. D* **16**, 3031 (1977).
- [26] D. Kaplan, *Phys. Lett. B* **288**, 342 (1992).
- [27] G. Heatlie *et al.*, *Nucl. Phys. B* **352**, 266 (1991).
- [28] B. Sheikholeslami and R. Wohlert, *Nucl. Phys. B* **259**, 572 (1985).
- [29] K. Symanzik, in *Mathematical Problems in Theoretical Physics*, edited by R. Schrader *et al.* (Springer, New York, 1982).
- [30] K. Symanzik, *Nucl. Phys. B* **226**, 187 (1983).
- [31] M. Lüscher *et al.*, *Nucl. Phys. B* **478**, 365 (1996).
- [32] M. Lüscher *et al.*, *Nucl. Phys. B* **491**, 323 (1997).
- [33] K. Symanzik, *Nucl. Phys. B* **190**, 187 (1981).

- [34] S. Sint, Nucl. Phys. B **421**, 135 (1994).
- [35] J. Cornwell, *Group Theory in Physics, Vols. 1,2* (Academic Press, London, 1984).
- [36] N. Metropolis *et al.*, J. Chem. Phys. **21**, 1087 (1953).
- [37] H. Hamber and G. Parisi, Phys. Rev. Lett **47**, 1792 (1981).
- [38] D. Weingarten, Phys. Lett. B **109**, 57 (1982).
- [39] M. Fukugita *et al.*, Phys. Lett. B **294**, 350 (1992).
- [40] R. Ellis, W. Stirling, and B. Webber, *QCD and Collider Physics* (Cambridge University Press, Cambridge, 1996).
- [41] J. Gasser and H. Leutwyler, Ann. Phys **158**, 142 (1984).
- [42] H. Politzer and M. Wise, Phys. Lett. B **208**, 504 (1988).
- [43] H. Georgi, Phys. Lett. B **240**, 447 (1990).
- [44] N. Isgur and M. Wise, Phys. Lett. B **232**, 113 (1989).
- [45] M. Neubert, Phys. Rept **245**, 259 (1994).
- [46] N. Isgur and M. Wise, Phys. Lett. B **237**, 527 (1990).
- [47] E. Eichten and F. Fienberg, Phys. Rev. D **23**, 2724 (1981).
- [48] A. Falk, H. Georgi, B. Grinstein, and M. Wise, Nucl. Phys. B **343**, 1 (1990).
- [49] A. Falk, B. Grinstein, and M. Luke, Nucl. Phys. B **357**, 185 (1991).
- [50] M. Neubert, Phys. Rev. D **46**, 2212 (1992).
- [51] M. Neubert, Phys. Rev. D **46**, 3914 (1992).
- [52] M. Neubert and V. Rieckert, Nucl. Phys. B **382**, 97 (1992).
- [53] N. Isgur, D. Scora, B. Grinstein, and M. Wise, Phys. Rev. D **39**, 799 (1989).

- [54] J. Bjorken, in *Gauge Bosons and Heavy Quarks, Proceedings of the 18th SLAC Summer Institute on Particle Physics*, edited by J. Hawthorne (SLAC-pub-5389, California, 1990), Vol. 1, p. 532.
- [55] M. Voloshin, *Phys. Rev. D* **46**, 3062 (1992).
- [56] P. Rossi, C. Davies, and G. Lepage, *Nucl. Phys. B* **297**, 287 (1988).
- [57] A. Frommer *et al.*, *J. Mod. Phys. C* **5**, 1073 (1992).
- [58] C. Allton *et al.*, *Phys. Rev. D* **47**, 5128 (1993).
- [59] P. Lacey *et al.*, *Phys. Rev. D* **51**, 6403 (1995).
- [60] P. Boyle, hep-lat/[9903033] (1999).
- [61] B. Efron, Society for Industrial and Applied Mathematics (1982).
- [62] W. Press *et al.*, *Numerical Recipes in C* (Cambridge University Press, Cambridge, 1992).
- [63] N. Cabibbo and E. Marinari, *Phys. Lett. B* **119**, 387 (1982).
- [64] M. Creutz, *Phys. Rev. D* **36**, 2394 (1987).
- [65] P. Rowland, Ph.D. thesis, University of Edinburgh, 1997.
- [66] S. Sharpe, *Phys. Rev. D* **41**, 3233 (1990).
- [67] C. Bernard and M. Golterman, *Phys. Rev. D* **46**, 853 (1992).
- [68] G. de Divitiis and R. Petronzio, *Phys. Lett. B* **419**, 311 (1998).
- [69] S. Sint and P. Weisz, *Nucl. Phys. B* **502**, 251 (1997).
- [70] M. Guagnelli, R. Sommer, and H. Wittig, *Nucl. Phys. B* **535**, 389 (1998).
- [71] K. Jansen *et al.*, *Phys. Lett. B* **372**, 275 (1996).
- [72] M. Guagnelli and R. Sommer, *Nucl. Phys. B (Proc. Suppl.)* **63A-C**, 886 (1998).

- [73] M. Lüscher, S. Sint, R. Sommer and H. Wittig, Nucl. Phys. B **491**, 344 (1997).
- [74] M. Luke, Phys. Lett. B **B**, 447 (1990).
- [75] G. Burdman, Phys. Lett. B **284**, 133 (1992).
- [76] H. Hogaasen and M. Sadzikowski, Z. Phys. C **64**, 427 (1994).
- [77] B. Blok and M. Shifman, Phys. Rev. D **47**, 2949 (1993).
- [78] E. Bagan, P. Ball, and P. Gosdzinsky, Phys. Lett. B **301**, 249 (1993).
- [79] F. Close and A. Wambach, Phys. Lett. B **348**, 207 (1995).
- [80] V. Morenas *et al.*, Phys. Lett. B **408**, 357 (1997).
- [81] K. Bowler *et al.*, Phys. Rev. D **52**, 5067 (1995).
- [82] C. Bernard, Y. Shen, and A. Soni, Phys. Lett. B **317**, 164 (1993).
- [83] S. Hashimoto and H. Matsufuru, Phys. Rev. D **54**, 4578 (1996).
- [84] J. Christensen, T. Draper, and C. McNeile, Nucl. Phys. B (Proc. Suppl.) **63**, 377 (1998).
- [85] J. Hein *et al.*, Semi-leptonic decays heavy-light to heavy-light, hep-lat/9908058.
- [86] P. Drell, Heavy Quark Decays, hep-ex/9711020.
- [87] M. Neubert, Phys. Lett. B **338**, 84 (1994).
- [88] F. Gilman and R. Singleton, Phys. Rev. D **41**, 142 (1990).
- [89] ALEPH Collaboration (D. Buskelic *et al.*), Phys. Lett. B **395**, 373 (1997).
- [90] CLEO Collaboration (B. Barish *et al.*), Phys. Rev. D **51**, 1014 (1995).